BULLETIN OF RUSSIAN STATE MEDICAL UNIVERSITY

BIOMEDICAL JOURNAL OF PIROGOV RUSSIAN NATIONAL RESEARCH MEDICAL UNIVERSITY

SUBMISSION http://vestnikrgmu.ru/login?lang=en
CORRESPONDENCE editor@vestnikrgmu.ru
COLLABORATION manager@vestnikrgmu.ru
ADDRESS ul. Ostrovityanova, d. 1, Moscow, Russia, 117997

Indexed in Scopus. CiteScore 2018: 0.16

Indexed in WoS. JCR 2018: 0.13

Five-year h-index is 4

Indexed in RSCI. IF 2018: 0,321

Listed in HAC 31.01.2020 (№ 507)

Open access to archive

Issue DOI: 10.24075/brsmu.2020-02
The mass media registration certificate no. 012769 issued on July 29, 1994
Founder and publisher is Pirogov Russian National Research Medical University (Moscow, Russia)

Approved for print 30.04.2020
Circulation: 100 copies. Printed by Print.Formula
www.print-formula.ru

ВЕСТНИК РОССИЙСКОГО ГОСУДАРСТВЕННОГО МЕДИЦИНСКОГО УНИВЕРСИТЕТА

НАУЧНЫЙ МЕДИЦИНСКИЙ ЖУРНАЛ РНИМУ ИМ. Н. И. ПИРОГОВА

ПОДАЧА РУКОПИСЕЙ http://vestnikrgmu.ru/login
ПЕРЕПИСКА С РЕДАКЦИЕЙ editor@vestnikrgmu.ru
СОТРУДНИЧЕСТВО manager@vestnikrgmu.ru
АДРЕС РЕДАКЦИИ ул. Островитянова, д. 1, г. Москва, 117997

Журнал включен в Scopus. CiteScore 2018: 0,16

Журнал включен в WoS. JCR 2018: 0,13

Индекс Хирша (h^5) журнала по оценке Google Scholar: 4

Журнал включен в РИНЦ. IF 2018: 0,321

Журнал включен в Перечень 31.01.2020 (№ 507)

Здесь находится открытый архив журнала

DOI выпуска: 10.24075/vrgmu.2020-02
Свидетельство о регистрации средства массовой информации № 012769 от 29 июля 1994 г.
Учредитель и издатель — Российский национальный исследовательский медицинский университет имени Н. И. Пирогова (Москва, Россия)

Подписано в печать 30.04.2020
Тираж 100 экз. Отпечатано в типографии Print.Formula
www.print-formula.ru

BULLETIN OF RSMU **2, 2020**
ВЕСТНИК РГМУ

Contents
Содержание

POSSIBLE EFFECTS OF CORONAVURUS INFECTION (COVID-19) ON THE CARDIOVASCULAR SYSTEM

Larina VN ✉, Golovko MG, Larin VG

Pirogov Russian National Research Medical University, Moscow, Russia

Acute viral respiratory infections can increase the risk of progression of a pre-existing condition, including a cardiovascular pathology. Life-threatening complications of Coronavirus disease 2019 (COVID-19) caused by severe acute respiratory syndrome coronavirus 2 (SARS-CoV-2) necessitate research into the cardiovascular effects of COVID-19 crucial for developing adequate treatment strategy for infected patients, especially those of advanced age. This article reviews the literature on the clinical and functional characteristics of patients with COVID-19, including those with poor outcomes. The article looks at the pathophysiological processes occurring in the cardiovascular system in the setting of SARS-CoV-2 infection, risk factors and death predictors. It also discusses continuation of therapy with angiotensin-converting enzyme inhibitors and angiotensin II receptor blockers in patients with COVID-19.

Keywords: coronavirus, cardiovascular diseases, infection, severe acute respiratory syndrome, coronavirus infection 2019, angiotensin-converting enzyme, SARS-CoV-2, COVID-19

Acknowledgements: the authors thank Gennady V. Poryadin, Professor at the Department of Pathophysiology and Clinical Pathophysiology (the Faculty of General Medicine, Pirogov Russian National Research Medical University), DMSc and the correspondent member of RAS, for his invaluable critical comments on this paper.

Author contribution: Larina VN conceived and planned the study, analyzed the literature, interpreted the literature data, and revised the manuscript; Golovko MG and Larin VG planned the study, analyzed the literature, interpreted the literature data, and wrote the draft of the manuscript.

✉ **Correspondence should be addressed:** Vera N. Larina
Ostrovityanova, 1, Moscow, 117997; larinav@mail.ru

Received: 03.04.2020 **Accepted:** 17.04.2020 **Published online:** 18.04.2020

DOI: 10.24075/brsmu.2020.020

ВЛИЯНИЕ КОРОНАВИРУСНОЙ ИНФЕКЦИИ (COVID-19) НА СЕРДЕЧНО-СОСУДИСТУЮ СИСТЕМУ

В. Н. Ларина ✉, М. Г. Головко, В. Г. Ларин

Российский национальный исследовательский медицинский университет имени Н. И. Пирогова, Москва, Россия

Острые вирусные инфекции дыхательных путей могут увеличить вероятность прогрессирования имеющейся сопутствующей патологии, в том числе сердечно-сосудистого происхождения. Появление жизнеугрожающих осложнений на фоне коронавируса 2 (severe acute respiratory syndrome coronavirus 2, или SARS-CoV-2), вызывающего коронавирусную болезнь 2019 (Coronavirus disease 2019, или COVID-19), обусловливает необходимость изучения кардиоваскулярных эффектов COVID-19 с целью оказания рациональной медицинской помощи пациентам, особенно старшего возраста. В статье представлен обзор литературных данных, посвященных анализу клинико-функциональных особенностей пациентов с COVID-19, в том числе имевших неблагоприятный прогноз. Уделено внимание патофизиологическим особенностям, происходящим на фоне инфекционного процесса в сердечно-сосудистой системе, факторам риска и предикторам летальности при COVID-19. Обсуждается вопрос о возможности продолжения приема ингибиторов ангиотензин-превращающего фермента или антагонистов рецепторов ангиотензина II большинством пациентов с сердечно-сосудистыми заболеваниями и COVID-19.

Ключевые слова: коронавирус, сердечно-сосудистые заболевания, инфекция, тяжелый острый респираторный синдром, коронавирусная болезнь 2019, ангиотензин-превращающий фермент, SARS-CoV-2, COVID-19

Благодарности: член-корреспонденту РАН, профессору, д. м. н., профессору кафедры патофизиологии и клинической патофизиологии лечебного факультета ФГАОУ ВО РНИМУ имени Н. И. Пирогова Минздрава России Геннадию Васильевичу Порядину за ценные критические замечания.

Вклад авторов: В. Н. Ларина — разработка концепции, планирование исследования, анализ литературы, интерпретация данных, написание текста; М. Г. Головко и В. Г. Ларин — планирование исследования, анализ литературы, интерпретация данных, подготовка черновика рукописи.

✉ **Для корреспонденции:** Вера Николаевна Ларина
ул. Островитянова, д. 1, г. Москва, 117997; larinav@mail.ru

Статья получена: 03.04.2020 **Статья принята к печати:** 17.04.2020 **Опубликована онлайн:** 18.04.2020

DOI: 10.24075/vrgmu.2020.020

Coronaviruses (CoVs) are a family of positive-sense single-stranded RNA viruses organized into two subfamilies and, as of January 2020, numbering 40 different species. CoVs infect animals and humans and are capable of rapid mutation and genetic recombination. CoVs owe their name to their appearance: their spike-like projections resemble the sun's corona. The spikes allow the virus to penetrate the cell membrane by mimicking the molecules recognized by the transmembrane receptors. Once the receptor has bound to the "impostor" molecule, the virus pushes it into the cell and the viral RNA gets inside.

Acute respiratory infections, such as influenza, respiratory syncytial virus infection and bacterial pneumonia, are widely acknowledged as triggers for cardiovascular diseases (CVD); in turn, pre-existing CVD are associated with other comorbid conditions and can increase the risk of inflammation or aggravate its progression.

The outbreak of the novel coronavirus disease 2019 (COVID-19) caused by the severe acute respiratory syndrome coronavirus 2 (SARS-CoV-2) has rapidly escalated into a pandemic; the majority of the infected patients are reported to have CVD [1].

The prospective cohort observational ARIC (atherosclerosis risk in communities) study has demonstrated that there is a higher risk of coronary heart disease (CHD) and ischemic stroke within up to 90 days after a past infection. The study looked at 1,312 CHD and 712 ischemic stroke cases with a past history of infections within one or two years preceding the cardiovascular event. The mean age of the participants was 75 years; 57.4% of the patients with CHD were male, whereas

54.1% of the patients with stroke were female. Of 1,312 individuals with CHD, 119 (9.1%) had a history of an inpatient infection, whereas 366 (27.9%) had a history of an outpatient infection. The most common were urinary tract infections (29%), pneumonia or respiratory infections (27%), skin /subcutaneous infections (11%), and blood infections (8%). Inpatient infections remained a stronger trigger of cardiovascular events throughout the entire follow-up period (day 14 OR = 12.83, day 30 OR = 8.39, day 42 OR = 6.24, day 90 OR = 4.48) than outpatient infections ($p < 0.05$). Therefore, hospitalized patients with an inpatient infection should be closely monitored in order to take timely measures to prevent CHD or stroke [2].

In light of this, pathophysiological processes triggered by coronavirus infections in the cardiovascular system certainly pose a great interest. Since our knowledge of the mechanisms underlying COVID-19 effects is scarce yet, the analysis of data collected during the outbreaks of viral pneumonia and MERS (Middle East respiratory syndrome coronavirus, MERS-CoV), as well as seasonal influenza, will provide a better understanding of how coronaviruses exert their effects on the cardiovascular system. This has important implications for the development of comprehensive strategies for the timely management of infected advanced-age patients with CVD.

Effects of coronavirus on human organism

Coronaviruses get their name from the crown-like spikes on their surface. These viruses are members of the Coronaviridae subfamily clustered into 4 phylogenetic groups: α, β, γ, and δ CoVs. Only α and β CoVs can cause infection in humans. Coronaviruses have 4 main structural proteins: the spike protein (S), which ensures attachment to the host cell receptor and subsequent fusion with the cell membrane, the nucleocapsid protein (N), the membrane protein (M), and the envelope protein (E).

Human coronaviruses (HCoVs) were discovered in 1965 when the first HCoV was isolated from the culture of human embryo tracheal tissue. By 2003, two types of HCoVs had been identified: HCoV-229E and HCoV-OC43.

Today, 7 different CoV strains are known to infect humans, including HCoV-229E, HCoV-NL63, HCoV-OC43, and HCoV-HKU that normally cause self-resolving symptoms. The virus can also cause severe acute respiratory syndrome (SARS), Middle East respiratory syndrome (MERS) and fatal acute respiratory syndrome resulting from SARS-CoV-2 infection.

Endemicity of coronavirus

Four types of HCoVs, including HCoV-229E (α-CoV), HCoV-NL63 (α-CoV), HCoV-OC43 (β-CoV), and HCoV-HKU1 (β-CoV), are endemic to humans and normally cause a mild respiratory infection with self-resolving symptoms, accounting for 15 to 30% of acute respiratory infections (ARI). As a rule, mild symptoms develop in young patients; in older patients, especially those with cardiovascular or bronchopulmonary pathology, the infection can provoke hospitalization and require emergency care [3].

Severe acute respiratory syndrome caused by coronavirus

The first SARS-CoV outbreak occurred in Guangdong province, South China, in 2002 [4]. Shortly after SARS-CoV was isolated and identified, similar SARS-like CoVs were detected in Himalayan palm civets and raccoon dogs; their nucleotide sequence was 99.8% homologous to that of SARS-CoV isolated from humans [5].

SARS-CoV is a representative of the β-CoV group; it binds to a zinc peptidase angiotensin-converting enzyme 2 (ACE2), which is a surface molecule exploited by the virus to enter the host cell. ACE is present in various organs and tissues; it is an integral plasma membrane protein found in endothelial, specialized epithelial, neuroepithelial, nerve terminal, and reproductive system cells. The role of ACE is not limited to the regulation of cardiovascular system functions. It also participates in hematopoiesis and the metabolism of some bioactive peptides [6].

ACE2 is found in arterial and venous endothelial cells, smooth muscle cells of the arterial wall, the epithelium of the respiratory tract and the small intestine, and immune system cells. It is hypothesized that the inhibition of ACE2 expression in patients infected with SARS-CoV is implicated in the pathological changes to pulmonary tissue, causing severe pneumonia and acute respiratory failure.

Research studies on wild animals proved that SARS-CoV could have originated in bats: Chinese horseshoe bats were found to harbor a SARS-like CoV with high nucleotide homology (87–92%) to SARS-CoV isolated from humans. Palm civets and raccoon dogs are putative intermediate hosts for SARS-CoV amplification preceding its transmission to other animals through contact at a market. SARS-CoV is transmitted from human to human by respiratory droplets during close contact (airborne spread).

There is a proposition about the possibility of the fecal-oral transmission route for SARS-CoV-2 predicated on the fact that patients stricken by SARS or MERS during the past outbreaks often had gastrointestinal symptoms, such as diarrhea and abdominal pain, and SARS-CoV RNA was detected in the feces of 14.6% patients with SARS or MERS [7]. Some patients presented with fever and diarrhea before developing pronounced respiratory symptoms [8]. In vitro studies have demonstrated that MERS-CoV can infect and replicate in the intestinal epithelium of humans using dipeptidyl peptidase 4 as a receptor. In vivo studies have revealed that inflammation and epithelial degeneration in the small intestine can precede pneumonia in MERS, confirming that pulmonary MERS-CoV-induced infection can be secondary to the enteric infection [9].

According to some authors, the incubation period for SARS-CoV-2 varies between 2 and 11 days, being 5.2 days on average (95% CI 4.1–7.0) [10]; other researchers report that the incubation period lasts up to 14 days [11].

SARS-CoV can be excreted into the environment and transmitted by hand contact between patients and healthcare workers; this means that surfaces must be sanitized and the nose, mouth and eyes must be protected against the virus [12].

The ability of an infected individual to spread the virus to other people is inferred from the R0 (basic reproduction number) value. For SARS-CoV, R0 is about 3, i.e. a person infected with SARS-CoV will potentially infect 3 other people in a susceptible population. The average R0 value for seasonal flu (swine flu, H1N1) is about 1.3 [13] (Table 1).

So far, no effective vaccine or medication against SARS-CoV has been developed. The clinical management of patients with SARS includes supportive symptomatic treatment and prescription of broad-spectrum antimicrobials against secondary bacterial infection. Advanced age (upwards of 60 years), multimorbidity (diabetes mellitus, CVD, cancer, chronic obstructive pulmonary disease), and elevated lactate dehydrogenase are predictors of death in patients with SARS-CoV infection. Some authors point to insignificant morbidity and mortality rates in children and adolescents in the past SARS outbreaks [14].

At the same time, preliminary data on 4,226 confirmed COVID-19 cases in the USA suggest high mortality in patients aged ≥ 85 years (10–27%). In patients aged 65–84 years, the case mortality rate ranged from 3 to 11%; in patients aged 55–64 years, it was 1–3%, whereas in patients aged 20–54 years, less than 1%. No deaths were reported in patients aged ≤ 19 years. There were young patients among the hospitalized individuals. Deaths registered in the group of patients aged 20–64 years amounted to 20% of overall case mortality; in this age group, hospitalized patients aged 20–44 years made 20% [15].

Currently, there is a paucity of published studies investigating risk factors and death predictors in patients with COVID-19. Starting on December 25,2019 through January 26,2020, a study was conducted in 201 patients with COVID-19 aged 43 to 60 years (the median age was 51), of whom 63.7% were men, revealing that 32.8% of the participants had a pre-existing condition. The median hospital stay was 13 (10–16) days; 33% of the patients required mechanical ventilation; the median interval between admission to hospital and progression to SARS was 2 (1–4) days. Blood tests revealed that the majority of the patients had elevated lactate dehydrogenase (98%), elevated C-reactive protein (85.6%), elevated interleukin 6 (48.8%), and elevated D-dimer (23.3%). Age upwards of 65 years, neutrophilia, organ dysfunction, and coagulation dysfunction were associated with progression to acute respiratory distress syndrome (ARDS) and death. In the patients who developed ARDS, administration of methylprednisolone was associated with lower mortality (46%), as compared to methylprednisolone-free treatment (61.8%) (OR 0.38) [16].

Clinical presentations of COVID-19

The most prevalent COVID-19 symptoms include fever, cough, labored breathing (shortness of breath or rapid breathing). Myalgia, anorexia, nausea, malaise, sore throat, nasal congestion, and headache are less common. The symptoms can set in as early as 2 days after contact with an infected person or by day 14 following such contact. The viral load does not differ between symptomatic and asymptomatic patients, suggesting a possibility of transmission from an asymptomatic individual or a patient with mild symptoms to another person. The highest number of viral copies is detected in nasal swabs, as compared to throat swabs. The diagnosis of COVID-19 is confirmed by PCR. Mucosal specimens for PCR are collected either from the upper or the lower respiratory tracts. A case of COVID-19 is assumed to be confirmed if the laboratory test for the presence of SARS-CoV-2 RNA returns a positive result even in the absence of clinical symptoms. Point-of-care serological tests are expected to be available in the nearest future.

Potential mechanisms underlying the effects of coronavirus infection on the cardiovascular system

The danger of ARI lies surging mortality from chronic diseases during an epidemic, especially among patients with cardiovascular pathology. According to a systematic review which included 42 publications and 39 clinical studies and was published in 2009 patients were at heightened risk of myocardial infarction (OR 4.95; 95% CI 4.4–5.5) and stroke (OR 3.2; 95% CI 2.8–3.6) in the first few days following the onset of ARI; over time, this risk was gradually decreasing [17].

The hypothesis that influenza can provoke acute cardiovascular events and death was proposed in the 1930s. It was then that a link was noticed between the seasonal activity of flu viruses and higher mortality from all causes, including bronchopulmonary pathology, pulmonary TB, diabetes mellitus, organic heart disease, and hemorrhagic stroke [18].

In 2004, another study reported a vast array of life-threatening clinical manifestations of coronavirus infection, including death from myocardial infarction (2 of 5 deaths); this unveiled the need for prompt treatment of CVD patients during a potential epidemic of a respiratory infection [19].

The lessons learnt from past epidemics caused by coronaviruses inspired a hypothesis that viral infections can provoke acute coronary syndrome, arrhythmias, heart failure, and thromboembolic complications resulting from the pronounced systemic inflammatory response combined with localized vascular inflammation.

In this respect, COVID-19 should not be an exception. It seems to affect the clinical course of pre-existing CVD and trigger development of life-threatening complications [20].

The severity of clinical manifestations, long- and short-term cardiovascular effects of COVID-19, and the effects of specific treatment are yet to be researched. It should be noted that during flu epidemics the majority of patients die of cardiovascular complications and not of virus-induced pneumonia itself. Considering the extreme inflammatory load caused by COVID-19 and the available clinical data on other coronavirus-related infections, one can expect to see serious cardiovascular complications in patients with COVID-19; their prevalence and severity will probably be lower in outpatients than in hospitalized individuals.

In a recently published study [21], 73% of 41 inpatients with laboratory-confirmed COVID-19 were men and 32% had pre-existing conditions, such as diabetes mellitus (20%), arterial hypertension (AH) (15%), and other CVD (15%). The median age of the patients was 49 (41–58) years. Among the most common symptoms of COVID-19 were fever (98%), cough (76%), sputum production (28%), myalgia or fatigue (44%), headache (8%), hemoptysis (5%), and diarrhea (3%). Lymphopenia was observed in 63% of the patients, shortness of breath, in 55%. The median time from the onset of symptoms to developing shortness of breath was 8 (5–13) days. Some of the complications included ARDS (29%) and acute cardiac injury (12%).

Another study conducted in 1,099 in- and outpatients with laboratory-confirmed COVID-19 (median age of 47 years; 42% women) found that the most common pre-existing conditions were AH (14.9%), diabetes mellitus (7.4%) and CAD (2.5%). ARDS (3.4%) and shock (1.1%) were the most severe complications [22].

In most patients with myocarditis, viral infection and the immune response to it are the root causes of inflammation. The leading mechanisms underlying myocardial injury in the acute phase of myocarditis are invasion of cardiomyocytes by viral particles that have tropism for myocardial tissue, the direct

Table 1. Characteristics of coronaviruses

Coronavirus species	Receptor	Incubation period (days)	R0	Co-existing CVD, %	Mean case fatality rate, %
SARS-CoV	ACE2	2–11	3	10	10
SARS-CoV-2	ACE2	2–14	2–3	от 3.4* до 40**	0.7–8***

Note: * — overall rates; ** — in hospitalized patients; *** — depending on time, geographical area and medical help available.

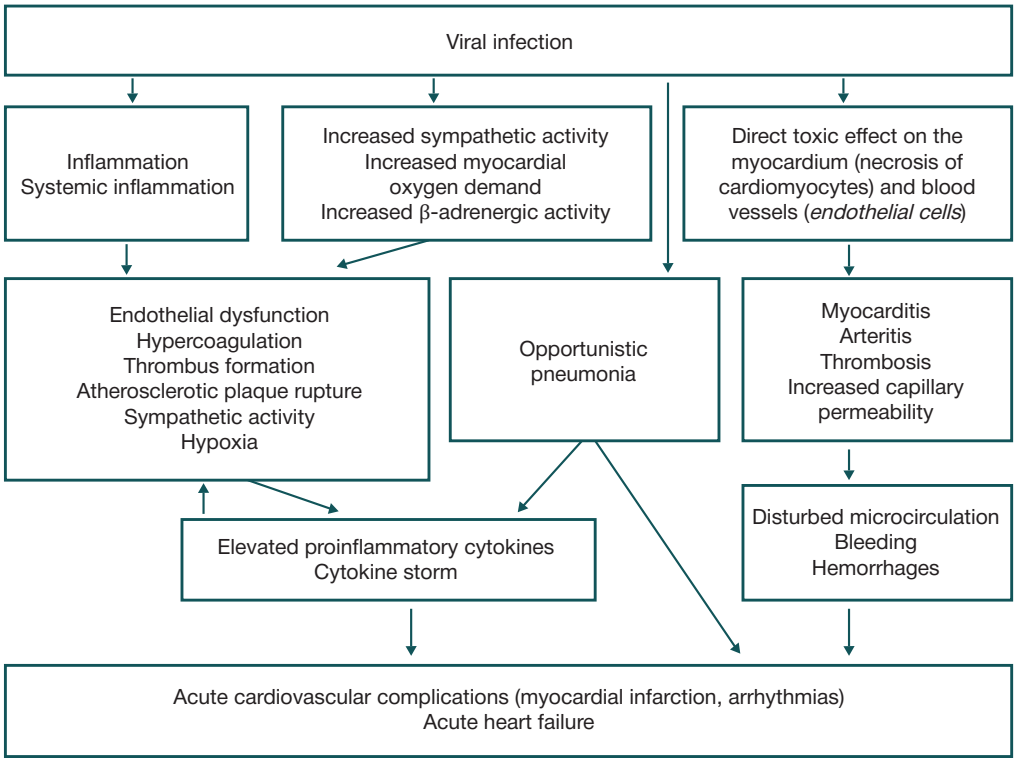

Fig. 1. Effects of viral infection on the cardiovascular system and the myocardium

cytopathic effect of the virus and the activation of nonspecific mechanisms of antiviral defense implemented by macrophages and NK cells. Activated macrophages and other immune cells start to produce chemokines and thus recruit T and B cells to the inflammation site. The recruited cells drive cell-mediated cytolysis and launch production of antiviral antibodies, thus triggering the mechanism of cardiomyocyte apoptosis, which eventually results in systolic heart failure.

The findings of sporadic autopsies and reports of severe myocarditis with left ventricular systolic dysfunction after a past COVID-19 infection suggest that the myocardium gets infiltrated by interstitial mononuclear inflammatory cells [23]. A study of cardiac biomarkers points to the high prevalence of myocardial injury in hospitalized patients; this condition is an important prognostic factor for COVID-19 [24].

Myocarditis is a polyetiological disease. It can be caused by viral or bacterial agents, as well as by non-infectious factors. Over 50% of myocarditis cases are associated with a viral infection. Parvovirus B19, Coxsackie A and B enteroviruses, ECHO-viruses, rubella virus, adenoviruses, human herpesvirus 6, Epstein-Barr virus, influenza virus, cytomegalovirus, etc. have high tropism for cardiomyocytes [25].

Clinical presentations of myocarditis are diverse and nonspecific. The diagnosis relies on a triad of medical history findings: the acute onset of the disease, the established link between the onset or exacerbation of symptoms/arrhythmias and the infection, and the time elapsed from the infection (≤ 1 year). Additional criteria include systemic immune manifestations, the combination of arrhythmia and conductivity disorders, and the positive effect of prescribed steroids [26].

In a recently published paper, researchers describe the results of observation of 416 inpatients with COVID-19; 57 (13.7%) of the patients eventually died [27]. Of them, 10.6% had CAD; 5.3%, cerebrovascular disease; 4.1%, heart failure; one in 5 patients had elevated high-sensitivity troponin levels. Patients with elevated troponin were of advanced age, had more comorbidities, lymphopenia, higher white cell count and higher levels of atrial natriuretic peptide, C-reactive protein and procalcitonin than those with normal troponin levels. Patients with acute inflammatory heart disease developed ARDS more often than those without acute cardiac condition (58.5% vs 14.7 %, respectively; $p < 0.001$); the proportion of deaths in this group was also higher (51.2% vs 4.5%, respectively; $p < 0.001$). Multivariate analysis confirmed that acute heart failure (OR 4.26) and ARDS (OR 7.89) were predictors of poor outcome in patients with COVID-19.

Similar results are reported by other authors [24], who found that 27.8% of 187 included patients with confirmed COVID-19 had developed acute cardiovascular complications resulting in cardiac dysfunction and arrhythmias; a combination of cardiovascular complications with elevated high-sensitivity troponin was associated with high mortality.

Although pathophysiological mechanisms underlying myocardial injury in patients with COVID-19 are heavily understudied, there is evidence that the SARS-CoV genome is found in the myocardium of 35% of patients with SARS. These findings increase the probability of direct damage to cardiomyocytes by the virus. SARS-CoV-2 might utilize the same mechanism of action as SARS-CoV as these two species are genetically close, although not identical. The close correlation between elevated high-sensitivity troponin and C-reactive protein levels implies the inflammatory origin of myocardial injury in the progressive disease phase. As viral particles spread along the respiratory tract and invade host cells, they may trigger a cytokine storm ensuing from the imbalance in Th1 and Th2 production and a cascade of immune reactions that lead to myocardial injury. In the setting of infection, secretion of cytokines can cause a reduction in coronary blood flow and oxygen supply, atherosclerotic plaques destabilization and formation of microclots (Fig. 1).

Myocarditis is often manifested as arrhythmias, progressive heart failure and sudden cardiac arrest that can occur at any stage of the disease.

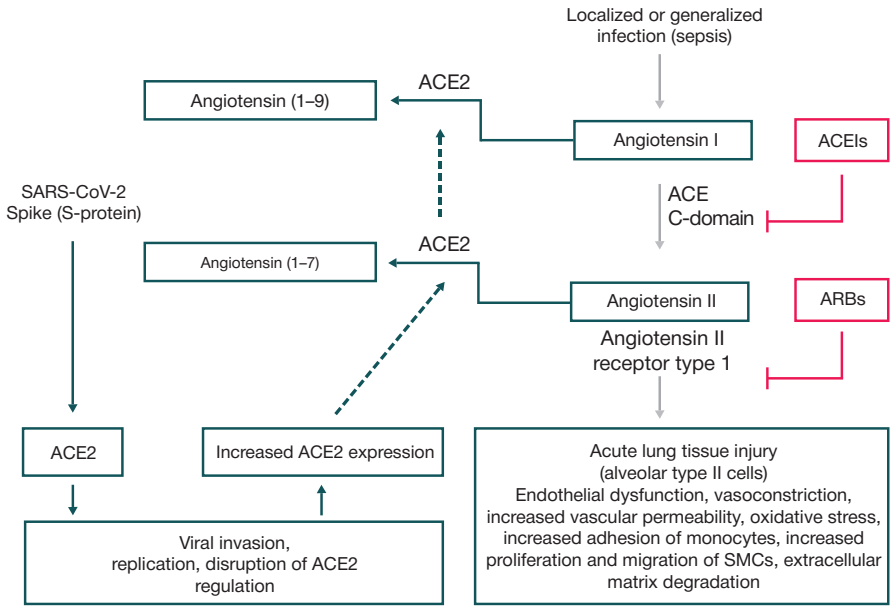

Fig. 2. Interactions between SARS-CoV-2 and the renin-angiotensin-aldosterone system. Interaction between SARS-CoV-2 and the renin-angiotensin-aldosterone system. Invasion of host cells (alveolar type II cells, in particular) by SARS-CoV-2 occurs through the binding of the virus to the functional domain of ACE2. ACE2 expression changes following endocytosis of the viral complex. This results in the accumulation of a potent vasoconstrictor angiotensin II and, possibly, mitigates the vasodilator effect of angiotensin (1–7). Local activation of the renin-angiotensin-aldosterone system can mediate damage to the lungs in response to viral infection, whereas increased ACE2 expression can aggravate pulmonary damage in patients with COVID-19. ACE2 converts angiotensin I to angiotensin (1–9) (its functions are being studied) and angiotensin II to angiotensin (1–7). This process is accompanied by inactivation of angiotensin II and synthesis of angiotensin (1–7); the latter stimulates vasodilation, reduces oxidative stress and fibrosis. ACE — angiotensin-converting enzyme; ACEI — ACE inhibitors; ARB — angiotensin II receptor blockers; SMC — smooth muscle cells. ACE — angiotensin-converting enzyme; ACEIs — ACE inhibitors; ARBs — angiotensin II receptor blockers; SMCs — smooth muscle cells

Among the first symptoms of myocarditis are malaise, fatigue, myalgia, and sometimes low-grade temperature caused by the inflammatory response to the virus but not by myocardial injury itself. Other manifestations of myocarditis include sudden cardiac arrest due to ventricular tachycardia or ventricular fibrillation following damage to the conducting system of the heart, thromboembolism, syncope, cardiogenic shock, and acute heart failure. The first clinical symptoms can set in at the onset of ARI or a few days after its onset.

There are a number of obstacles complicating the diagnosis of viral myocarditis. The primary diagnostic criterion for myocarditis is the established link between cardiac symptoms and a past infection and the signs of inflammation. The diagnosis can be facilitated by a full medical examination of the patient, which includes clinical, laboratory and instrumental tests, and by endomyocardial biopsy performed to rule out the inflammatory nature of myocardial injury [28].

Unfortunately, currently there is no substantiated evidence about the efficacy of existing antivirals and vaccines against COVID-19. Patients with pre-existing CVD are at high risk of complications, a more severe course of the disease and poor outcomes; therefore, CVD patients with COVID-19 should be stratified depending on their primary condition (CVD) and its severity in order to decide on the treatment strategy. Electrocardiography and cardiac biomarker tests (NT-proBNP) can be employed to control the condition of the patient and the course of treatment.

There is a lot of controversy over whether patients infected with a coronavirus should continue angiotensin-converting enzyme inhibitors (ACE inhibitors) and angiotensin II receptor blockers (ARBs). The fears are predicated on the fact that the protease domain of ACE2 is a potential target for SARS-CoV and SARS-CoV-2 and that increased expression of ACE2 can aggravate damage to the lungs in patients with COVID-19 (Fig. 2) (adapted from [29]).

ACE2 exists in 2 forms: as a structural transmembrane protein with an extracellular domain, which serves as a target for the S protein of SARS-CoV-2, and as a soluble circulating form. Invasion of host cells (alveolar type II cells in the first place) by SARS-CoV-2 occurs through the binding of the virus to the protease domain of ACE2. Upon endocytosis of the viral complex, ACE2 expression changes, causing increased accumulation of a potent vasoconstrictor angiotensin II. The local activation of the renin-angiotensin-aldosterone system (RAAS) can mediate damage to the lungs in response to viral infection [30].

Angiotensin (1–7) is a substrate for the N-domain of ACE; it suppresses the activity of ACE C-domain and limits pressor and vasoconstrictive effects of angiotensin II.

The role of this process in the development of COVID-19-related complications and the effects of the possible modulation of the ACE2 receptor are not fully clear and expected to be investigated in the clinical trials of human recombinant ACE2 (NCT04287686) and other therapeutic agents.

In the group of patients with COVID-19 and high troponin levels, the duration of therapy with ACEIs/ARBs prescribed for pre-existing CVD did not have any effect on mortality [22]. In another study, a positive effect of ACEIs/ARBs was observed in patients with viral pneumonias because the drugs significantly reduced inflammation and secretion of proinflammatory cytokines triggered in response to infection [31]. The beneficial effect of ACEIs/ARBs might be associated with the compensatory increase in ACE2 production. So far, there are no data on the use of ACEIs/ARBs in patients with COVID-19, which raises the need for further large-scale clinical studies.

At present, the experts from the European Society of Cardiology [32], the American Heart Association [33] and the Russian Society of Cardiology [34] recommend that patients with COVID-19 who had indications for ACEIs/ARBs and were taking these drugs before the infection should continue them because there is no evidence of their inefficacy in such patients.

Also, there are no experimental or clinical data demonstrating positive or negative effects of ACEIs/ARBs or other RAAS antagonists in patients with COVID-19, as well as in patients

Table 2. A non-exhaustive list of clinical trials of drugs for the prevention and treatment of COVID-19

Drug	Start date	Estimated completion date	Trial ID at ClinicalTrials.gov
Remdesivir	February 21, 2020	April 1, 2023	NCT04280705
Human recombinant ACE2	February 2020	April 2020	NCT04287686
Remdesivir	March 2020	May 2020	NCT04292899
Injections and infusions of the LV-SMENP-DS and antigen-specific cytotoxic T cell vaccines	February 24, 2020	December 31, 2024	NCT04276896
Fingolimod	February 22, 2020	July 1, 2020	NCT04280588
Human mesenchymal stem cells	February 24, 2020	February 1, 2021	NCT04293692
Carrimycin	February 23, 2020	February 28, 2021	NCT04286503
Methylprednisolone	February 14, 2020	May 30, 2020	NCT04273321
Washed microbiota transplantation	February 2, 2020	April 16, 2020	NCT04251767
Losartan	March 16, 2020	April 1, 2021	NCT04312009
2019-nCoV vaccine (mRNA-1273)	March 3, 2020	June 1, 2021	NCT04283461
Lopinavir / ritonavir tablets combined with xiyanping injection	March 14, 2020	April 14, 2021	NCT04295551

with COVID-19 and a history of CVD. If a patient with CVD is infected with COVID-19, the treatment strategy should account for their overall symptoms and hemodynamics.

RAAS activation plays a crucial role in the pathogenesis of many CVD. Long-term effects of increased renin and angiotensin II production and the activity of the sympathetic nervous system include left ventricular hypertrophy, dyslipidemia, arrythmias, hypercoagulation, endothelial dysfunction, insulin resistance, and metabolic syndrome. ACEIs and ARBs that have been studied and successfully used in the clinical setting for many years are first-choice drugs for treating chronic heart failure, AH, renal disorders, and diabetes mellitus [35, 36].

The ACE2-dependent entry of SARS-CoV-2 into the host cell can be blocked by camostat mesylate, the inhibitor of serine protease TMPRSS2 used by SARS-CoV-2 for S protein priming. Camostat mesylate is a promising candidate for further trials [37].

Among the antivirals for treating flu, oseltamivir does not have any effect on SARS-CoV-2 although preliminary studies have demonstrated some positive effects of favipiravir. Table 2 features a few drugs which are now in clinical trials or being considered as candidates for clinical trials in patients with COVID-19.

CONCLUSIONS

The data collected so far suggest a high prevalence of comorbidities in middle-aged and old patients with COVID-19. The most common cardiovascular conditions are AH (about 15%), diabetes mellitus (7.4–20%) and CAD (about 2.5%). Patients with COVID-19 and a pre-existing cardiovascular pathology are at high risk of developing ARDS, shock and death. Acute cardiac failure and ARDS are regarded as predictors of poor outcomes in patients with COVID-19.

It is crucial to study different aspects of screening, diagnostics, clinical manifestations, prevention and management of patients with COVID-19. As the infection spreads and more data are accumulated, risk factors for cardiovascular complications should be thoroughly investigated.

Perhaps, creating a registry of patients with COVID-19 and systemic reporting of clinical symptoms and cardiovascular and other complications will help to elucidate the characteristics of the infected patients, develop approaches to the treatment and prevention and design a risk model for predicting complications.

References

1. Fauci AS, Lane HC, Redfield RR. Covid-19: navigating the uncharted. N Engl J Med. 2020. DOI: 10.1056/NEJMe2002387.
2. Cowan LT, Lutsey PL, Pankow JS, Matsushita K, Ishigami J, Lakshminarayan K. Inpatient and outpatient infection as a trigger of cardiovascular disease: the ARIC study. J Am Heart Assoc. 2018; 7 (22): e009683-e009683. DOI: 10.1161/JAHA.118.009683.
3. Su S, Wong G, Shi W, et al. Epidemiology, genetic recombination, and pathogenesis of coronaviruses. Trends Microbiol. 2016; 24 (6): 490–502. DOI: 10.1016/j.tim.2016.03.003.
4. Song HD, Tu CC, Zhang GW, Wang SY, Zheng K, et al. Cross-host evolution of severe acute respiratory syndrome coronavirus in palm civet and human. Proceedings of the National Academy of Sciences. 2005; 102 (7) 2430–2435; DOI: 10.1073/pnas.0409608102.
5. Berry M, Gamieldien J, Fielding BC. Identification of new respiratory viruses in the new millennium. Viruses. 2015; 7 (3): 996–1019. DOI: 10.3390/v7030996.
6. Nagai T, Nitta K, Kanasaki M, Kova D, Kanasaki K. The biological significance of angiotensin-converting enzyme inhibition to combat kidney fibrosis. Clin Exp Nehrol. 2015; 19 (1): 65–74.
7. Yeo C, Kaushal S, Yeo D. Enteric involvement of coronaviruses: is faecal-oral transmission of SARS-CoV-2 possible? Lancet Gastroenterol Hepatol. 2020; 5 (4): 335–7. DOI: 10.1016/S2468-1253(20)30048-0.
8. Assiri A, Al-Tawfiq JA, Al-Rabeeah AA, et al. Epidemiological, demographic, and clinical characteristics of 47 cases of Middle East respiratory syndrome coronavirus disease from Saudi Arabia: a descriptive study. Lancet Infect Dis. 2013; (13): 752–61.
9. Zhou J, Li C, Zhao G, et al. Human intestinal tract serves as an alternative infection route for Middle East respiratory syndrome coronavirus. Sci Adv. 2017; (3): eaao4966.
10. Chan JF-W, Yuan S, Kok K-H, et al. A familial cluster of pneumonia associated with the 2019 novel coronavirus indicating person-to-person transmission: a study of a family cluster. Lancet. 2020; 395 (10223): 514–23. DOI: 10.1016/S0140-6736(20)30154-9.
11. Backer JA, Klinkenberg D, Wallinga J. Incubation period of 2019 novel coronavirus (2019-nCoV) infections among travellers from Wuhan, China, 20–28 January 2020. Euro Surveill. 2020; 25 (5): 2000062. DOI: 10.2807/1560-7917.ES.2020.25.5.2000062.
12. Otter JA, Donskey C, Yezli S, Douthwaite S, Goldenberg SD, Weber DJ. Transmission of SARS and MERS coronaviruses and

influenza virus in healthcare settings: the possible role of dry surface contamination. J Hosp Infect. 2016; 92 (3): 235–50. DOI: 10.1016/j.jhin.2015.08.027.
13. Madjid M, Safavi-Naeini P, Solomon SD, Vardeny O. Potential Effects of Coronaviruses on the Cardiovascular System: A Review. JAMA Cardiol. Published online March 27, 2020. DOI: 10.1001/jamacardio.2020.1286.
14. Berry M, Gamieldien J, Fielding BC. Identification of new respiratory viruses in the new millennium. Viruses. 2015; 7 (3): 996–1019. DOI: 10.3390/v7030996.
15. US Centers for Disease Control and Prevention COVID-19 Response Team. Severe Outcomes Among Patients with Coronavirus Disease 2019 (COVID-19): United States, February 12-March 16, 2020. MMWR Morb Mortal Wkly Rep. Published online March 18, 2020. DOI: 10.15585/mmwr.mm6912e2.
16. Wu C, Chen X, Cai Y, Xia J, Zhou X, et al. Risk factors associated with acute respiratory distress syndrome and death in patients with coronavirus disease 2019 pneumonia in Wuhan, China. JAMA Intern Med. 2020 Mar 13. https://doi.org/10.1001/jamainternmed.2020.0994.
17. C. Warren-Gash, et al. Influenza as a trigger for acute myocardial infarction or death from cardiovascular disease: a systematic review. Lancet Infect Dis. 2009; 9 (10): 601–10.
18. Collins S. Excess mortality from causes other than influenza and pneumonia during influenza epidemics. Public Health Rep. 1932; (47): 2159–89.
19. Peiris JS, Chu CM, Cheng VC, et al. HKU/UCH SARS Study Group. Clinical progression and viral load in a community outbreak of coronavirus-associated SARS pneumonia: a prospective study. Lancet. 2003; 361 (9371): 1767–72. DOI: 10.1016/S0140-6736(03)13412-5.
20. Kwong JC, Schwartz KL, Campitelli MA, et al. Acute myocardial infarction after laboratory-confirmed influenza infection. N Engl J Med. 2018; 378 (4): 345–53. DOI: 10.1056/NEJMoa1702090.
21. Huang C, Wang Y, Li X, et al. Clinical features of patients infected with 2019 novel coronavirus in Wuhan, China. Lancet. 2020; 395 (10223): 497–506. DOI: 10.1016/S0140-6736(20)30183-5.
22. Guan WJ, Ni ZY, Hu Y, et al. China Medical Treatment Expert Group for Covid-19. Clinical characteristics of coronavirus disease 2019 in China. N Engl J Med. 2020. DOI: 10.1056/NEJMoa2002032.
23. Inciardi RM, Lupi L, Zaccone G, et al. Cardiac involvement 1 with coronavirus 2019 (COVID-19) infection. JAMA Cardiol. 2020. DOI: 10.1001/jamacardio.2020.1096.
24. Guo T, Fan Y, Chen M, et al. Association of cardiovascular disease and myocardial injury with outcomes of patients hospitalized with 2019-coronavirus disease (COVID-19). JAMA Cardiol. Published online March 27, 2020. DOI: 10.1001/jamacardio.2020.1017.
25. Blagova OV, Nedostup AV. Contemporary masks of the myocarditis (from clinical signs to diagnosis. Russian Journal of Cardiology. 2014; (5): 13–22. https://doi.org/10.15829/1560-4071-2014-5-13-22. Russian.
26. Blagova OV, Nedostup AV, Kogan EA, Sedov VP, Donnikov AV, Kadochnikova VV, et al. DCMP as a clinical syndrome: results of nosological diagnostics with myocardial biopsy and differentiated treatment in virus-positive and virus-negative patiens. Russian Journal of Cardiology. 2016; (1): 7–19. https://doi.org/10.15829/1560-4071-2016-1-7-19. Russian.
27. Shi S, Qin M, Shen B, et al. Cardiac injury in patients with corona virus disease 2019. JAMA Cardiol. Published online March 25, 2020. DOI: 10.1001/jamacardio.2020.0950.
28. Cooper L, Baughman K, Feldman A, Frustaci A, Jessup M, Kuhl U, et al. The role of endomyocardial biopsy in the management of cardiovascular disease: a scientific statement from the American Heart Association, the American College of Cardiology, and the European Society of Cardiology. Endorsed by the Heart Failure Society of America and the Heart Failure Association of the European Society of Cardiology. Journal of the American College of Cardiology. 2007; 50 (19): 1914–31.
29. Vaduganathan M, Vardeny O, Michel M, McMurray J, Pfeffer M, Solomon S. Renin–Angiotensin–Aldosterone System Inhibitors in Patients with Covid-19. March 30, 2020; DOI: 10.1056/NEJMsr2005760.
30. Bavishi C, Maddox TM, Messerli FH. Coronavirus Disease 2019 (COVID-19) Infection and Renin Angiotensin System Blockers. JAMA Cardiol. Published online April 03, 2020. DOI: 10.1001/jamacardio.2020.1282
31. Henry C, Zaizafoun M, Stock E, Ghamande S, Arroliga AC, White HD. Impact of angiotensin-converting enzyme inhibitors and statins on viral pneumonia. Proc (Bayl Univ Med Cent). 2018; 31 (4): 419–23. DOI: 10.1080/08998280.2018.1499293
32. de Simone G. Position Statement of the ESC Council on Hypertension on ACE-Inhibitors and Angiotensin Receptor Blockers. https://www.escardio.org/Councils/Council-on-Hypertension-(CHT)/News/position-statement-of-the-esc-council-on-hypertension-on-ace-inhibitors-and-ang.
33. HFSA/ACC/AHA Statement Addresses Concerns Re: Using RAAS Antagonists in COVID-19. https://www.acc.org/latest-in-cardiology/articles/2020/03/17/08/59/hfsa-acc-aha-statement-addresses-concerns-re-using-raas-antagonists-in-covid-19.
34. Shlyakho EV, Konradi AO, Arutyunov GP, Arutyunov AG, Bautin AE, Boytsov SA, et al. Guidelines for the diagnosis and treatment of circulatory diseases in the context of the COVID-19 pandemic. Russian Journal of Cardiology. 2020; 25 (3): 3801. DOI: 10.15829/1560-4071-2020-3-3801. Russian.
35. Halliday BP, Wassall R, Lota AS, et al. Withdrawal of pharmacological treatment for heart failure in patients with recovered dilated cardiomyopathy (TRED-HF): an open-label, pilot, randomised trial. Lancet. 2019; (393): 61–73.
36. Thomsen M, Lewinter C, Køber L. Varying effects of recommended treatments for heart failure with reduced ejection fraction: meta-analysis of randomized controlled trials in the ESC and ACCF/AHA guidelines. ESC Heart Failure. 2016; (3): 235–44.
37. Hoffmann M, Kleine-Weber H, Schroeder S, et al. SARS-CoV-2 cell entry depends on ACE2 and TMPRSS2 and is blocked by a clinically proven protease inhibitor. Cell. 2020; (181): 1–10. DOI: 10.1016/j.cell.2020.02.052.

Литература

1. Fauci AS, Lane HC, Redfield RR. Covid-19: navigating the uncharted. N Engl J Med. 2020. DOI: 10.1056/NEJMe2002387.
2. Cowan LT, Lutsey PL, Pankow JS, Matsushita K, Ishigami J, Lakshminarayan K. Inpatient and outpatient infection as a trigger of cardiovascular disease: the ARIC study. J Am Heart Assoc. 2018; 7 (22): e009683-e009683. DOI: 10.1161/JAHA.118.009683.
3. Su S, Wong G, Shi W, et al. Epidemiology, genetic recombination, and pathogenesis of coronaviruses. Trends Microbiol. 2016; 24 (6): 490–502. DOI: 10.1016/j.tim.2016.03.003.
4. Song HD, Tu CC, Zhang GW, Wang SY, Zheng K, et al. Cross-host evolution of severe acute respiratory syndrome coronavirus in palm civet and human. Proceedings of the National Academy of Sciences. 2005; 102 (7) 2430–2435; DOI: 10.1073/pnas.0409608102.
5. Berry M, Gamieldien J, Fielding BC. Identification of new respiratory viruses in the new millennium. Viruses. 2015; 7 (3): 996–1019. DOI: 10.3390/v7030996.
6. Nagai T, Nitta K, Kanasaki M, Kova D, Kanasaki K. The biological significance of angiotensin-converting enzyme inhibition to combat kidney fibrosis. Clin Exp Nehrol. 2015; 19 (1): 65–74.
7. Yeo C, Kaushal S, Yeo D. Enteric involvement of coronaviruses: is faecal-oral transmission of SARS-CoV-2 possible? Lancet Gastroenterol Hepatol. 2020; 5 (4): 335–7. DOI: 10.1016/S2468-1253(20)30048-0.
8. Assiri A, Al-Tawfiq JA, Al-Rabeeah AA, et al. Epidemiological,

demographic, and clinical characteristics of 47 cases of Middle East respiratory syndrome coronavirus disease from Saudi Arabia: a descriptive study. Lancet Infect Dis. 2013; (13): 752–61.
9. Zhou J, Li C, Zhao G, et al. Human intestinal tract serves as an alternative infection route for Middle East respiratory syndrome coronavirus. Sci Adv. 2017; (3): eaao4966.
10. Chan JF-W, Yuan S, Kok K-H, et al. A familial cluster of pneumonia associated with the 2019 novel coronavirus indicating person-to-person transmission: a study of a family cluster. Lancet. 2020; 395 (10223): 514–23. DOI: 10.1016/S0140-6736(20)30154-9.
11. Backer JA, Klinkenberg D, Wallinga J. Incubation period of 2019 novel coronavirus (2019-nCoV) infections among travellers from Wuhan, China, 20–28 January 2020. Euro Surveill. 2020; 25 (5): 2000062. DOI: 10.2807/1560-7917.ES.2020.25.5.2000062.
12. Otter JA, Donskey C, Yezli S, Douthwaite S, Goldenberg SD, Weber DJ. Transmission of SARS and MERS coronaviruses and influenza virus in healthcare settings: the possible role of dry surface contamination. J Hosp Infect. 2016; 92 (3): 235–50. DOI: 10.1016/j.jhin.2015.08.027.
13. Madjid M, Safavi-Naeini P, Solomon SD, Vardeny O. Potential Effects of Coronaviruses on the Cardiovascular System: A Review. JAMA Cardiol. Published online March 27, 2020. DOI: 10.1001/jamacardio.2020.1286.
14. Berry M, Gamieldien J, Fielding BC. Identification of new respiratory viruses in the new millennium. Viruses. 2015; 7 (3): 996–1019. DOI: 10.3390/v7030996.
15. US Centers for Disease Control and Prevention COVID-19 Response Team. Severe Outcomes Among Patients with Coronavirus Disease 2019 (COVID-19): United States, February 12-March 16, 2020. MMWR Morb Mortal Wkly Rep. Published online March 18, 2020. DOI: 10.15585/mmwr.mm6912e2.
16. Wu C, Chen X, Cai Y, Xia J, Zhou X, et al. Risk factors associated with acute respiratory distress syndrome and death in patients with coronavirus disease 2019 pneumonia in Wuhan, China. JAMA Intern Med. 2020 Mar 13. https://doi.org/10.1001/jamainternmed.2020.0994.
17. C. Warren-Gash, et al. Influenza as a trigger for acute myocardial infarction or death from cardiovascular disease: a systematic review. Lancet Infect Dis. 2009; 9 (10): 601–10.
18. Collins S. Excess mortality from causes other than influenza and pneumonia during influenza epidemics. Public Health Rep. 1932; (47): 2159–89.
19. Peiris JS, Chu CM, Cheng VC, et al. HKU/UCH SARS Study Group. Clinical progression and viral load in a community outbreak of coronavirus-associated SARS pneumonia: a prospective study. Lancet. 2003; 361 (9371): 1767–72. DOI: 10.1016/S0140-6736(03)13412-5.
20. Kwong JC, Schwartz KL, Campitelli MA, et al. Acute myocardial infarction after laboratory-confirmed influenza infection. N Engl J Med. 2018; 378 (4): 345–53. DOI: 10.1056/NEJMoa1702090.
21. Huang C, Wang Y, Li X, et al. Clinical features of patients infected with 2019 novel coronavirus in Wuhan, China. Lancet. 2020; 395 (10223): 497–506. DOI: 10.1016/S0140-6736(20)30183-5.
22. Guan WJ, Ni ZY, Hu Y, et al. China Medical Treatment Expert Group for Covid-19. Clinical characteristics of coronavirus disease 2019 in China. N Engl J Med. 2020. DOI: 10.1056/NEJMoa2002032.
23. Inciardi RM, Lupi L, Zaccone G, et al. Cardiac involvement 1 with coronavirus 2019 (COVID-19) infection. JAMA Cardiol. 2020. DOI: 10.1001/jamacardio.2020.1096.
24. Guo T, Fan Y, Chen M, et al. Association of cardiovascular disease and myocardial injury with outcomes of patients hospitalized with 2019-coronavirus disease (COVID-19). JAMA Cardiol. Published online March 27, 2020. DOI: 10.1001/jamacardio.2020.1017.
25. Благова О. В., Недоступ А. В. Современные маски миокардита (от клинических синдромов к диагнозу). Российский кардиологический журнал. 2014; (5): 13–22. https://DOI.org/10.15829/1560-4071-2014-5-13-22.
26. Благова О. В., Недоступ А. В., Коган Е. А., Седов В. П., Донников А. Е., Кадочникова В. В., и др. ДКМП как клинический синдром: результаты нозологической диагностики с применением биопсии миокарда и дифференцированного лечения у вирус- позитивных и вирус-негативных больных. Российский кардиологический журнал. 2016; (1): 7–19. https://doi.org/10.15829/1560-4071-2016-1-7-19.
27. Shi S, Qin M, Shen B, et al. Cardiac injury in patients with corona virus disease 2019. JAMA Cardiol. Published online March 25, 2020. DOI: 10.1001/jamacardio.2020.0950.
28. Cooper L, Baughman K, Feldman A, Frustaci A, Jessup M, Kuhl U, et al. The role of endomyocardial biopsy in the management of cardiovascular disease: a scientific statement from the American Heart Association, the American College of Cardiology, and the European Society of Cardiology. Endorsed by the Heart Failure Society of America and the Heart Failure Association of the European Society of Cardiology. Journal of the American College of Cardiology. 2007; 50 (19): 1914–31.
29. Vaduganathan M, Vardeny O, Michel M, McMurray J, Pfeffer M, Solomon S. Renin–Angiotensin–Aldosterone System Inhibitors in Patients with Covid-19. March 30, 2020; DOI: 10.1056/NEJMsr2005760.
30. Bavishi C, Maddox TM, Messerli FH. Coronavirus Disease 2019 (COVID-19) Infection and Renin Angiotensin System Blockers. JAMA Cardiol. Published online April 03, 2020. DOI: 10.1001/jamacardio.2020.1282
31. Henry C, Zaizafoun M, Stock E, Ghamande S, Arroliga AC, White HD. Impact of angiotensin-converting enzyme inhibitors and statins on viral pneumonia. Proc (Bayl Univ Med Cent). 2018; 31 (4): 419–23. DOI: 10.1080/08998280.2018.1499293
32. de Simone G. Position Statement of the ESC Council on Hypertension on ACE-Inhibitors and Angiotensin Receptor Blockers. https://www.escardio.org/Councils/Council-on-Hypertension-(CHT)/News/position-statement-of-the-esc-council-on-hypertension-on-ace-inhibitors-and-ang.
33. HFSA/ACC/AHA Statement Addresses Concerns Re: Using RAAS Antagonists in COVID-19. https://www.acc.org/latest-in-cardiology/articles/2020/03/17/08/59/hfsa-acc-aha-statement-addresses-concerns-re-using-raas-antagonists-in-covid-19.
34. Шляхто Е. В., Конради А. О., Арутюнов Г. П., Арутюнов А. Г., Баутин А. Е., Бойцов С. А., и др. Руководство по диагностике и лечению болезней системы кровообращения в контексте пандемии ООУЮ-19. Российский кардиологический журнал. 2020; 25 (3): 3801. DOI: 10.15829/1560-4071-2020-3-3801.
35. Halliday BP, Wassall R, Lota AS, et al. Withdrawal of pharmacological treatment for heart failure in patients with recovered dilated cardiomyopathy (TRED-HF): an open-label, pilot, randomised trial. Lancet. 2019; (393): 61–73.
36. Thomsen M, Lewinter C, Køber L. Varying effects of recommended treatments for heart failure with reduced ejection fraction: meta-analysis of randomized controlled trials in the ESC and ACCF/AHA guidelines. ESC Heart Failure. 2016; (3): 235–44.
37. Hoffmann M, Kleine-Weber H, Schroeder S, et al. SARS-CoV-2 cell entry depends on ACE2 and TMPRSS2 and is blocked by a clinically proven protease inhibitor. Cell. 2020; (181): 1–10. DOI: 10.1016/j.cell.2020.02.052.

ON THE UNPREDICTABILITY OF OUTCOMES OF IMMUNOTHERAPY AND PREVENTIVE IMMUNIZATION AGAINST COVID-19

Chebotar IV ✉, Shagin DA

Pirogov Russian National Research Medical University, Moscow Pirogov Russian National Research Medical University, Moscow

This article analyzes the possibility of employing immunotherapy and preventive immunization to fight COVID-19. The authors think that treatment and prevention of the infection with anti-SARS-CoV-2 antibodies can have unpredictable outcomes. Although these antibodies can neutralize virus antigens (S-proteins), they also have the ability to enhance virus entry into the host cell. The article emphasizes the importance of solid evidence of efficacy and safety for candidate anti-COVID-19 therapies and protective measures.

Keywords: coronavirus, COVID-19, SARS-CoV-2, antibodies, preventive immunization, immunotherapy

Author contribution: the authors equally contributed to the manuscript

✉ **Correspondence should be addressed:** Igor V. Chebotar
Ostrovityanova, 1, Moscow, 117997; nizarnn@yandex.ru

Received: 21.04.2020 **Accepted:** 28.04.2020 **Published online:** 30.04.2020

DOI: 10.24075/brsmu.2020.025

О НЕПРЕДСКАЗУЕМОСТИ РЕЗУЛЬТАТОВ ИММУНОТЕРАПИИ И ИММУНОПРОФИЛАКТИКИ COVID-19

И. В. Чеботарь ✉, Д. А. Шагин

Российский национальный исследовательский медицинский университет имени Н. И. Пирогова, Москва, Россия

В работе проведен анализ возможности использования иммунотерапии и иммунопрофилактики в борьбе с COVID-19. Результаты, к которым может привести профилактическое или терапевтическое применение препаратов, содержащих антитела против вируса SARS-CoV-2, на наш взгляд, неоднозначны, а взаимодействие антител с коронавирусными антигенами (S-протеинами) может повлечь за собой не только нейтрализацию вируса, но и усиление его способности проникать в клетку хозяина. В работе сделан акцент на необходимости научного доказательства эффективности и безопасности планируемых к применению методов терапии и профилактики COVID-19.

Ключевые слова: коронавирус, COVID-19, SARS-CoV-2, антитела, иммунопрофилактика, иммунотерапия

Вклад авторов: авторы внесли равный вклад в написание статьи.

✉ **Для корреспонденции:** Игорь Викторович Чеботарь
ул. Островитянова, д. 1, г. Москва, 117997; nizarnn@yandex.ru

Статья получена: 21.04.2020 **Статья принята к печати:** 28.04.2020 **Опубликована онлайн:** 30.04.2020

DOI: 10.24075/vrgmu.2020.025

Finding effective treatment and developing protective measures against the novel coronavirus infection COVID-19 is a critical challenge facing medical science. Today, many candidate approaches to managing this infection are under scrutiny. Obviously, the effective treatment is expected to directly block the virus and prevent it from replicating or entering the cell. Drugs designed to inhibit HIV (ritonavir, lopinavir) and Ebola virus (remdesivir) are now being evaluated for their potential to inhibit coronavirus replication [1, 2]. However, so far there is no solid evidence of their efficacy against COVID-12; this is true for both approved drugs and those still in clinical trials [3]. The possible anticoronaviral effect of quinolines and the unclear underlying mechanism of action need further investigation.

Immunotherapy and preventive immunization might hold promise for countering COVID-19. Indeed, vaccines and passive immunization have been successful in fighting various infections, including viral infections. However, because of the features demonstrated by the causative agent of COVID-1 SARS-CoV-2, extreme caution should be exercised when using active or passive immunization approaches.

This article is an attempt to point to the unpredictability of outcomes of using anti-SARS-CoV-2 antibodies for treating and preventing COVID-19.

Interaction with viral S-proteins

Spike-glycoproteins (S-proteins) responsible for latching onto receptors of the host cell have long been identified as the primary surface target for neutralizing antibodies. Using cell and animal models of severe acute respiratory syndrome (SARS-CoV) and Middle-East respiratory syndrome (MERS-CoV), researchers have demonstrated that antibodies can bind to and neutralize S-proteins [4, 5]. It is reported that anti-S-IgG for neutralizing MERS-CoV promote survival of viral clones that carry mutations in the S-protein encoding genes; as a result, the antibodies can no longer recognize the S-protein and neutralize the virus [6].

Antibody-dependent enhancement of virus entry

Unfortunately, the emergence of clones unrecognizable to antibodies is not the only drawback of passive immunization/immunotherapy. Therapies with anticoronaviral antibodies can be devastating due to the phenomenon of antibody-dependent enhancement of virus entry. Briefly, some IgG variants can accelerate penetration of the virus into the cell because their Fab fragments can bind to the S protein of SARS-CoV, whereas other IgG domains, like Fc or unidentified sites, bind to a number of host cell receptors, including angiotensin-converting enzyme 2, dipeptidyl peptidase-4 and the FcϒR-receptor (see Figure). This phenomenon has been demonstrated in the models of some coronavirus-related infections, including SARS and MERS [7, 8]. Considering the similarity of pathogenesis between SARS, MERS and COVID-19, there is a high probability that SARS-CoV-2 will also provoke IgG-dependent enhancement of virus entry. Some authors believe that IgG-enhancement of virus entry is not limited to epithelial cells and can also occur

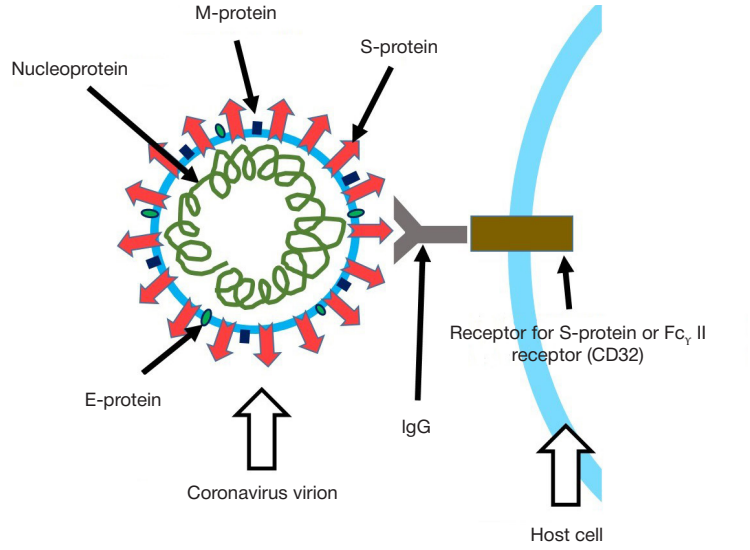

Fig. A schematic representation of antibody-dependent enhancement of virus entry

in immune cells via immunoglobulin FcϒII receptors (CD32) [9]. IgG-dependent damage to immune cells might underlie the pathogenesis of uncontrolled immune system activation and cytokine storm in patients with SARS.

It is believed that antibodies do not always enhance virus entry, depending on the antibody binding site on the S protein, the IgG subclass, IgG concentrations and expression of cell receptors. This unpredictability means that convalescent serum and synthetic anti-S antibodies should not be used in COVID-19 patients without thorough thought. The same applies to preventive immunization against COVID-19. It cannot be ruled out that vaccination will stimulate production of polyclonal antibody variants responsible for antibody-dependent virus entry.

As COVID-19 is continuing its global rampage, a worrying trend is being born: scientists are engaged in a race to develop diagnostic, therapeutic and preventive tools for the novel infection at all costs. A similar situation unfolded in the USSR shortly after HIV was discovered. In an attempt to get ahead of their foreign counterparts, some medical teams decided to treat AIDS patients with immunostimulants. The formal yet erroneous logic behind the decision dictated that a patient who developed immunodeficiency should be treated by stimulating the immune system. Dozens of patients fell victim to the ambitions of their doctors because immunostimulation provoked the irreversible progression of the disease. We hope that the story will not repeat itself with COVID-19 and that treatments for this infection will be evidence-based.

CONCLUSIONS

1. On the one hand, antibodies against coronaviral S-proteins can neutralize the virion; on the other hand, they are also capable of enhancing virus entry into the host cell. 2. Although COVID-12 is an epidemiological emergency, its treatment and prevention should be based on solid evidence of safety and efficacy.

References

1. Vremennye metodicheskie rekomendatsii Ministerstva zdravookhraneniya Rossiyskoy Federatsii «Lekarstvennaya terapiya ostrykh respiratornykh virusnykh infektsiy (ORVI) v ambulatornoy praktike v period epidemii COVID-19». Versiya 5 (08.04.2020). Available from: https://static-1.rosminzdrav.ru/system/attachments/attaches/000/049/986/original/09042020_%D0%9C%D0%A0_COVID-19_v5.pdf.
2. Cao YC, Deng QX, Dai SX. Remdesivir for severe acute respiratory syndrome coronavirus 2 causing COVID-19: an evaluation of the evidence. Travel Med Infect Dis. 2020; 2: 101647. DOI: 10.1016/j.tmaid.2020.101647.
3. Centers for Disease Control and Prevention. Information for Clinicians on Investigational Therapeutics for Patients with COVID-19. Available from: https://www.cdc.gov/coronavirus/2019-ncov.
4. Greenough TC, Babcock GJ, Roberts A, Hernandez HJ, Thomas WD Jr, Coccia JA, et al. Development and characterization of a severe acute respiratory syndrome-associated coronavirus-neutralizing human monoclonal antibody that provides effective immunoprophylaxis in mice. J Infect Dis. 2005; 191 (4): 507–14. DOI: 10.1086/427242.
5. Chen Z, Bao L, Chen C, Zou T, Xue Y, Li F, et al. Human Neutralizing Monoclonal Antibody Inhibition of Middle East Respiratory Syndrome Coronavirus Replication in the Common Marmoset. J Infect Dis. 2017; 215 (12): 1807–15. DOI: 10.1093/infdis/jix209.
6. Kleine-Weber H, Elzayat MT, Wang L, Graham BS, Müller MA, Drosten C, et al. Mutations in the Spike Protein of Middle East Respiratory Syndrome Coronavirus Transmitted in Korea Increase Resistance to Antibody-Mediated Neutralization. J Virol. 2019; 93 (2): pii: e01381-18. DOI: 10.1128/JVI.01381-18.
7. Yang ZY, Werner HC, Kong WP, Leung K, Traggiai E, Lanzavecchia A, et al. Evasion of antibody neutralization in emerging severe acute respiratory syndrome coronaviruses. Proc Natl Acad Sci USA. 2005; 102 (3): 797–01. DOI: 10.1073/pnas.0409065102.
8. Wan Y, Shang J, Sun S, Tai W, Chen J, Geng Q, et al. Molecular Mechanism for Antibody-Dependent Enhancement of Coronavirus Entry. J Virol. 2020; 94 (5): pii: e02015-19. DOI: 10.1128/JVI.02015-19 .
9. Yip MS, Leung HL, Li PH, Cheung CY, Dutry I, Li D, et al. Antibody-dependent enhancement of SARS coronavirus infection and its role in the pathogenesis of SARS. Hong Kong Med J. 2016; 22 (3 Suppl 4): 25–31.

Литература

1. Временные методические рекомендации Министерства здравоохранения Российской Федерации «Лекарственная терапия острых респираторных вирусных инфекций (ОРВИ) в амбулаторной практике в период эпидемии COVID-19». Версия 5 (08.04.2020). Доступно по ссылке: https://static-1.rosminzdrav.ru/system/attachments/attaches/000/049/986/original/09042020_%D0%9C%D0%A0_COVID-19_v5.pdf.
2. Cao YC, Deng QX, Dai SX. Remdesivir for severe acute respiratory syndrome coronavirus 2 causing COVID-19: an evaluation of the evidence. Travel Med Infect Dis. 2020; 2: 101647. DOI: 10.1016/j.tmaid.2020.101647.
3. Centers for Disease Control and Prevention. Information for Clinicians on Investigational Therapeutics for Patients with COVID-19. Available from: https://www.cdc.gov/coronavirus/2019-ncov.
4. Greenough TC, Babcock GJ, Roberts A, Hernandez HJ, Thomas WD Jr, Coccia JA, et al. Development and characterization of a severe acute respiratory syndrome-associated coronavirus-neutralizing human monoclonal antibody that provides effective immunoprophylaxis in mice. J Infect Dis. 2005; 191 (4): 507–14. DOI: 10.1086/427242.
5. Chen Z, Bao L, Chen C, Zou T, Xue Y, Li F, et al. Human Neutralizing Monoclonal Antibody Inhibition of Middle East Respiratory Syndrome Coronavirus Replication in the Common Marmoset. J Infect Dis. 2017; 215 (12): 1807–15. DOI: 10.1093/infdis/jix209.
6. Kleine-Weber H, Elzayat MT, Wang L, Graham BS, Müller MA, Drosten C, et al. Mutations in the Spike Protein of Middle East Respiratory Syndrome Coronavirus Transmitted in Korea Increase Resistance to Antibody-Mediated Neutralization. J Virol. 2019; 93 (2): pii: e01381-18. DOI: 10.1128/JVI.01381-18.
7. Yang ZY, Werner HC, Kong WP, Leung K, Traggiai E, Lanzavecchia A, et al. Evasion of antibody neutralization in emerging severe acute respiratory syndrome coronaviruses. Proc Natl Acad Sci USA. 2005; 102 (3): 797–01. DOI: 10.1073/pnas.0409065102.
8. Wan Y, Shang J, Sun S, Tai W, Chen J, Geng Q, et al. Molecular Mechanism for Antibody-Dependent Enhancement of Coronavirus Entry. J Virol. 2020; 94 (5): pii: e02015-19. DOI: 10.1128/JVI.02015-19 .
9. Yip MS, Leung HL, Li PH, Cheung CY, Dutry I, Li D, et al. Antibody-dependent enhancement of SARS coronavirus infection and its role in the pathogenesis of SARS. Hong Kong Med J. 2016; 22 (3 Suppl 4): 25–31.

ROLE OF ACE2/TMPRSS2 GENES REGULATION BY INTESTINAL microRNA ISOFORMS IN THE COVID-19 PATHOGENESIS

Nersisyan SA[1,2] ✉, Shkurnikov MYu[3], Osipyants AI[3,4], Vechorko VI[5]

[1] National Research University Higher School of Economics, Moscow, Russia

[2] Lomonosov Moscow State University, Moscow, Russia

[3] P. A. Hertsen Moscow Oncology Research Center, branch of the National Medical Research Radiology Center, Moscow, Russia

[4] Far Eastern Federal University, Vladivostok, Russia

[5] City Clinical Hospital № 15 named after O. M. Filatov, Moscow, Russia

Coronavirus SARS-CoV-2, the cause of the COVID-19 pandemic, enters the cell by binding the cell surface proteins: angiotensin-converting enzyme 2 (ACE2) and transmembrane serine protease 2 (TMPRSS2). The expression of these proteins varies significantly in individual organs and tissues of the human body. One of the proteins' expression regulation mechanisms is based on the activity of the microRNA (miRNA) molecules, small non-coding RNAs, the most important function of which is the post-transcriptional negative regulation of gene expression. The study was aimed to investigate the mechanisms of the interactions between miRNA isoforms and ACE2/TMPRSS2 genes in the colon tissues known for the high level of expression of the described enzymes. The search for interactions was performed using the correlation analysis applied to the publicly available paired mRNA/miRNA sequencing data of colon tissues. Among the others, such miRNAs as miR-30c and miR-200c were identified known for their involvement in the coronavirus infection and acute respiratory distress syndrome pathogenesis. Thus, new potential mechanisms for the ACE2 and TMPRSS2 enzymes regulation were ascertained, as well as their possible functional activity in a cell infected with coronavirus.

Keywords: COVID-19, SARS-CoV-2, ACE2, TMPRSS2, miRNA, isomiR, acute respiratory distress syndrome, coronavirus

Funding: the study was supported by the Ministry of Science and Higher Education of the Russian Federation grant (project RFMEFI61618X0092).

Author contribution: Nersisyan SA, Shkurnikov MYu, Osipyants AI, Vechorko VI — study concept; Nersisyan SA, Shkurnikov MYu — bioinformatics analysis; Nersisyan SA, Shkurnikov MYu, Osipyants AI, Vechorko VI — interpretation of results; Nersisyan SA — manuscript writing.

✉ **Correspondence should be addressed:** Stepan A. Nersisyan
Vavilova, 7, Moscow, 117312; s.a.nersisyan@gmail.com

Received: 17.04.2020 **Accepted:** 28.04.2020 **Published online:** 29.04.2020

DOI: 10.24075/brsmu.2020.024

РОЛЬ РЕГУЛЯЦИИ ГЕНОВ АПФ2/TMPRSS2 ИЗОФОРМАМИ микроРНК КИШЕЧНИКА В ПАТОГЕНЕЗЕ COVID-19

С. А. Нерсисян[1,2] ✉, М. Ю. Шкурников[3], А. И. Осипьянц[3,4], В. И. Вечорко[5]

[1] Национальный исследовательский университет «Высшая школа экономики», Москва, Россия

[2] Московский государственный университет имени М. В. Ломоносова, Москва, Россия

[3] Московский научно-исследовательский онкологический институт имени П. А. Герцена — филиал Национального медицинского исследовательского центра радиологии, Москва, Россия

[4] Дальневосточный федеральный университет, Владивосток, Россия

[5] Городская клиническая больница № 15 имени О. М. Филатова, Москва, Россия

Коронавирус SARS-CoV-2, вызвавший пандемию COVID-19, проникает в клетку, связываясь с поверхностными белками: ангиотензин-превращающим ферментом 2 (АПФ2) и сериновой протеазой 2 (TMPRSS2). Экспрессия данных белков значительно различается в отдельных органах и тканях организма человека. Одним из механизмов регуляции их экспрессии является активность молекул микроРНК — коротких некодирующих РНК, важнейшей функцией которых является посттранскрипционная негативная регуляция экспрессии генов. Целью работы было выявить механизмы взаимодействия изоформ микроРНК и генов АПФ2 / TMPRSS2 в тканях толстого кишечника, известных высоким уровнем экспрессии указанных ферментов. Поиск взаимодействий был осуществлен средствами корреляционного анализа на публично доступной выборке данных парного мРНК / микроРНК-секвенирования тканей кишечника. В числе находок оказались такие микроРНК, как miR-30c и miR-200c, известные своей ролью в патогенезе коронавирусной инфекции и острого респираторного дистресс-синдрома. Таким образом, были установлены новые потенциальные механизмы регуляции ферментов АПФ2 и TMPRSS2 и их возможная функциональная активность в клетке, инфицированной коронавирусом.

Ключевые слова: COVID-19, SARS-CoV-2, АПФ2, TMPRSS2, микроРНК, изоформа микроРНК, острый респираторный дистресс-синдром, коронавирус

Финансирование: работа выполнена при поддержке гранта Министерства образования и науки Российской Федерации (проект RFMEFI61618X0092).

Вклад авторов: С. А. Нерсисян, М. Ю. Шкурников, А. И. Осипьянц, В. И. Вечорко — разработка концепции; С. А. Нерсисян, М. Ю. Шкурников — биоинформатический анализ; С. А. Нерсисян, М. Ю. Шкурников, А. И. Осипьянц, В. И. Вечорко — интерпретация результатов; С. А. Нерсисян — написание статьи.

✉ **Для корреспонденции:** Степан Ашотович Нерсисян
ул. Вавилова, д. 7, г. Москва, 117312; s.a.nersisyan@gmail.com

Статья получена: 17.04.2020 **Статья принята к печати:** 28.04.2020 **Опубликована онлайн:** 29.04.2020

DOI: 10.24075/vrgmu.2020.024

The rapid and progressive spread of the COVID-19 infection caused by the SARS-CoV-2 coronavirus deeply affected the health of hundreds of thousands of people, which became a serious challenge to healthcare systems and global economic stability. The characteristics of SARS-CoV-2, especially distinguishing the disease from influenza, are the higher infection rate combined with the increased risk of severe course and mortality, mainly due to the acute respiratory

distress syndrome (ARDS) [1]. The mechanism of the cells infection is actively studied in many laboratories. In particular, it is known that the SARS-CoV-2 viral envelope expresses the spike protein (S protein) containing the receptor binding domain with high affinity for the extracellular domain of angiotensin-converting enzyme 2 (ACE2). The further S protein cleavage by the transmembrane serine protease 2 (TMPRSS2) aimed to produce the S1 and S2 subunits is a crucial stage for membrane fusion and virus internalization by endocytosis with ACE2 in pulmonary epithelium. It is assumed that the greater virulence of SARS-CoV-2 compared to other coronaviruses can be explained by the S1 protein's significantly higher affinity for ACE2. This mechanism of the SARS-CoV-2 entering the cell leads to the loss of ACE2 on the cell surface, thereby contributing to chronic lung function impairment and severe tissue fibrosis [2].

MicroRNAs (miRNAs) are the small non-coding single stranded RNAs containing an average of 22 nucleotides. One of the most important intracellular functions of miRNA is the negative regulation of gene expression due to complementary miRNA binding with the target mRNA, leading to mRNA degradation or translational inhibition [3]. MicroRNAs are formed from the longer hairpin molecules of pre-miRNA as a result of the hairpin cleaving Drosha and Dicer enzymes' activity [4]. The cleaving site inaccuracy leads to the emergence of various microRNA isoforms that differ in several nucleotides at the ends of the molecule. It is reported that many miRNAs of canonical types are expressed much weaker than some alternative isoforms [5]. It is of key importance that different isoforms of the same miRNA may have completely different target genes. This is because the most important role in binding to the target mRNA is played by the miRNA region between the 5' nucleotides 2–7 (seed region) [6].

It is reported that the functional impairment of miRNAs and their isoforms is associated with a large number of pathological conditions, including cancer, neurological and cardiovascular diseases [7]. A large number of papers is devoted to the study of the role of miRNAs in the pathogenesis of viral infections: some of them are aimed to study the therapeutic potential of the direct miRNA interaction with the virus [8], and the others are aimed to investigate the potential interactions of miRNAs and proteins playing a key role in the viral vital processes [9]. However, the ACE2 and TMPRSS2 expression regulation by miRNA in subjects with COVID-19 remains poorly understood. The study was aimed to reveal the mechanisms of the interactions between miRNA isoforms and ACE2/TMPRSS2 genes in the colon tissues known for the high level of expression of the described enzymes.

METHODS

To search for miRNA isoforms interacting with ACE2 and TMPRSS2 enzymes, we performed the integrated analysis of the paired mRNA and miRNA expression in the normal colon tissues' sample (the enzyme is most intensively expressed in the colon tissues). The tissue selection was also due to the fact that the gut models were often used for *in vitro* studies of viruses [10, 11]. The available for public access samples from The Cancer Genome Atlas Colon Adenocarcinoma (TCGA-COAD) collection were used. The sample analysis was carried out by the next-generation mRNA and miRNA sequencing [12]. The data were expression matrices of thousands of mRNA and miRNA isoforms in eight samples, the unit of expression was the binary logarithm of the corresponding transcript number of reads normalized to the upper quartile of the overall distribution (FPKM-UQ). To search for potential regulatory interactions between miRNA isoforms and TMPRSS2 the Spearman correlation coefficients between the expressions of 25% of the most highly expressed isoforms with the expressions of the corresponding mRNA were calculated, with subsequent filtering in accordance with the p-value (significance level 0.05).

RESULTS

The ACE2 and TMPRSS2 expression at the mRNA level turned out to be very high: TMPRSS2 was in the list of the most highly expressed genes (1%), and the ACE2 expression was between the 93rd and 94th percentiles, which was fully consistent with published data [13] (see Figure). Correlation analysis allowed us to detect the miR-21 miRNA demonstrating a significant negative correlation with the ACE2 gene expression, as well as the following miRNA families regulating TMPRSS2: let-7a/let-7d, miR-30a, miR-30c, miR-127, miR-194, miR-200c, miR-361 and miR-423. The let-7a miRNA was represented by the hsa-let-7a-5p isoform, which differed from the canonic type by adenine added at the 5' end of the molecule. The miR-194 was represented by the hsa-miR-194-3p isoform, which lacked the 5' first nucleotide. The absence of the corresponding miRNA canonical forms in the list indicates the importance of taking into account the profiles of all miRNA isoforms, not just canonical isoforms.

DISCUSSION

Some of the discovered miRNAs have already been detected during the virological studies. Thus, it was shown that the miR-30c expression in the lungs of the mouse changed significantly upon infection with SARS-CoV virus [14], which made it possible to put forward a hypothesis about the involvement of that miRNA in the development of a disease caused by the virus. The miR-200c miRNA is also of great interest. In 2017, a paper was published reporting that miR-200c miRNA played a key role in the virus-induced ARDS pathogenesis [15]. The researchers found out that the H5N1 avian influenza virus promoted the miR-200c expression, the target of which was the ACE2 receptor. Moreover, the viral proteins were detected responsible for promoting the miRNA expression. The discovery of the interaction possibility between the described miRNA and

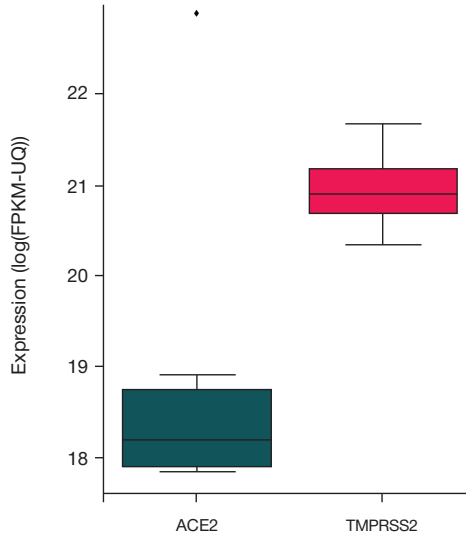

Fig. ACE2 and TMPRSS2 expression distribution in the colon tissues. Borders of the boxes correspond to the lower and upper quartiles, vertical segment inside the box represents the median value. Black rhombus shows outlier

the TMPRSS2 enzyme emphasizes the need for studying the role of miR-200c in the COVID-19 pathogenesis.

CONCLUSION

The results obtained indicate the presence of numerous regulatory interactions between miRNA isoforms and ACE2/TMPRSS2 enzymes. Such information is extremely important due to the key role of enzymes in the mechanism of cell infection with SARS-CoV-2 coronavirus. Further research is needed for refining and experimental validation of the findings. In particular, it is possible to discover new treatment options based on the ACE2 and TMPRSS2 expression regulation via microRNAs.

References

1. Munster VJ, Koopmans M, van Doremalen N, van Riel D, de Wit E. A Novel Coronavirus Emerging in China — Key Questions for Impact Assessment. N Engl J Med. 2020 Feb 20; 382 (8): 692–4.
2. Hoffmann M, Kleine-Weber H, Schroeder S, Krüger N, Herrler T, Erichsen S, et al. SARS-CoV-2 Cell Entry Depends on ACE2 and TMPRSS2 and Is Blocked by a Clinically Proven Protease Inhibitor. Cell. 2020 Mar 4. pii: S0092-8674(20)30229-4.
3. Nilsen TW. Mechanisms of microRNA-mediated gene regulation in animal cells. Trends Genet. 2007 May; 23 (5): 243–9.
4. Makarova JA, Shkurnikov MU, Turchinovich AA, Tonevitsky AG, Grigoriev AI. Circulating microRNAs. Biochemistry (Mosc). 2015 Sep; 80 (9): 1117–26.
5. Loher P, Londin ER, Rigoutsos I. IsomiR expression profiles in human lymphoblastoid cell lines exhibit population and gender dependencies. Oncotarget. 2014 Sep 30; 5 (18): 8790–802.
6. Mazière P, Enright AJ. Prediction of microRNA targets. Drug Discov Today. 2007 Jun; 12 (11–12): 452–8.
7. Osip'yants AI, Knyazev EN, Galatenko AV, Nyushko KM, Galatenko VV, Shkurnikov MY, et. al. Changes in the Level of Circulating hsa-miR-297 and hsa-miR-19b-3p miRNA Are Associated with Generalization of Prostate Cancer. Bull Exp Biol Med. 2017 Jan; 162 (3): 379–82.
8. Leon-Icaza SA, Zeng M, Rosas-Taraco AG. microRNAs in viral acute respiratory infections: immune regulation, biomarkers, therapy, and vaccines. ExRNA. 2019 Feb; 1.
9. Mallick B, Ghosh Z, Chakrabarti J. MicroRNome analysis unravels the molecular basis of SARS infection in bronchoalveolar stem cells. PLoS One. 2009 Nov 13; 4 (11): e7837.
10. Samatov TR, Senyavina NV, Galatenko VV, Trushkin EV, Tonevitskaya SA, Alexandrov DE, et al. Tumour-like druggable gene expression pattern of CaCo2 cells in microfluidic chip. BioChip J. 2016 Jul; 10: 215–20.
11. Sakharov D, Maltseva D, Knyazev E, Nikulin S, Poloznikov A, Shilin S, et. al. Towards embedding Caco-2 model of gut interface in a microfluidic device to enable multi-organ models for systems biology. BMC Syst Biol. 2019 Mar 5; 13 (Suppl 1): 19.
12. Cancer Genome Atlas Network. Comprehensive molecular characterization of human colon and rectal cancer. Nature. 2012 Jul 18; 487 (7407): 330–7.
13. Vaarala MH, Porvari KS, Kellokumpu S, Kyllönen AP, Vihko PT. Expression of transmembrane serine protease TMPRSS2 in mouse and human tissues. J Pathol. 2001 Jan; 193 (1): 134–40.
14. Peng X, Gralinski L, Ferris MT, Frieman MB, Thomas MJ, Proll S, et. al. Integrative deep sequencing of the mouse lung transcriptome reveals differential expression of diverse classes of small RNAs in response to respiratory virus infection. mBio. 2011 Nov 15; 2 (6).
15. Liu Q, Du J, Yu X, Xu J, Huang F, Li X, Zhang C, Li X, et al. miRNA-200c-3p is crucial in acute respiratory distress syndrome. Cell Discov. 2017 Jun 27; 3: 17021.

Литература

1. Munster VJ, Koopmans M, van Doremalen N, van Riel D, de Wit E. A Novel Coronavirus Emerging in China — Key Questions for Impact Assessment. N Engl J Med. 2020 Feb 20; 382 (8): 692–4.
2. Hoffmann M, Kleine-Weber H, Schroeder S, Krüger N, Herrler T, Erichsen S, et al. SARS-CoV-2 Cell Entry Depends on ACE2 and TMPRSS2 and Is Blocked by a Clinically Proven Protease Inhibitor. Cell. 2020 Mar 4. pii: S0092-8674(20)30229-4.
3. Nilsen TW. Mechanisms of microRNA-mediated gene regulation in animal cells. Trends Genet. 2007 May; 23 (5): 243–9.
4. Makarova JA, Shkurnikov MU, Turchinovich AA, Tonevitsky AG, Grigoriev AI. Circulating microRNAs. Biochemistry (Mosc). 2015 Sep; 80 (9): 1117–26.
5. Loher P, Londin ER, Rigoutsos I. IsomiR expression profiles in human lymphoblastoid cell lines exhibit population and gender dependencies. Oncotarget. 2014 Sep 30; 5 (18): 8790–802.
6. Mazière P, Enright AJ. Prediction of microRNA targets. Drug Discov Today. 2007 Jun; 12 (11–12): 452–8.
7. Osip'yants AI, Knyazev EN, Galatenko AV, Nyushko KM, Galatenko VV, Shkurnikov MY, et. al. Changes in the Level of Circulating hsa-miR-297 and hsa-miR-19b-3p miRNA Are Associated with Generalization of Prostate Cancer. Bull Exp Biol Med. 2017 Jan; 162 (3): 379–82.
8. Leon-Icaza SA, Zeng M, Rosas-Taraco AG. microRNAs in viral acute respiratory infections: immune regulation, biomarkers, therapy, and vaccines. ExRNA. 2019 Feb; 1.
9. Mallick B, Ghosh Z, Chakrabarti J. MicroRNome analysis unravels the molecular basis of SARS infection in bronchoalveolar stem cells. PLoS One. 2009 Nov 13; 4 (11): e7837.
10. Samatov TR, Senyavina NV, Galatenko VV, Trushkin EV, Tonevitskaya SA, Alexandrov DE, et al. Tumour-like druggable gene expression pattern of CaCo2 cells in microfluidic chip. BioChip J. 2016 Jul; 10: 215–20.
11. Sakharov D, Maltseva D, Knyazev E, Nikulin S, Poloznikov A, Shilin S, et. al. Towards embedding Caco-2 model of gut interface in a microfluidic device to enable multi-organ models for systems biology. BMC Syst Biol. 2019 Mar 5; 13 (Suppl 1): 19.
12. Cancer Genome Atlas Network. Comprehensive molecular characterization of human colon and rectal cancer. Nature. 2012 Jul 18; 487 (7407): 330–7.
13. Vaarala MH, Porvari KS, Kellokumpu S, Kyllönen AP, Vihko PT. Expression of transmembrane serine protease TMPRSS2 in mouse and human tissues. J Pathol. 2001 Jan; 193 (1): 134–40.
14. Peng X, Gralinski L, Ferris MT, Frieman MB, Thomas MJ, Proll S, et. al. Integrative deep sequencing of the mouse lung transcriptome reveals differential expression of diverse classes of small RNAs in response to respiratory virus infection. mBio. 2011 Nov 15; 2 (6).
15. Liu Q, Du J, Yu X, Xu J, Huang F, Li X, Zhang C, Li X, et al. miRNA-200c-3p is crucial in acute respiratory distress syndrome. Cell Discov. 2017 Jun 27; 3: 17021.

STRATEGIES OF RT-PCR-BASED ASSAY DESIGN AND SURVEILLANCE OF SARS-COV-2

Kuznetsova NA[1] ✉, Pochtovyy AA[1,2], Nikiforova MA[1], Gushchin VA[1,2]

[1] Gamaleya Research Institute of Epidemiology and Microbiology, Moscow

[2] Lomonosov Moscow State University, Moscow

High population density in the cities with bustling transportation systems and a thriving tourism industry can promote the global spread of a viral infection in a matter of days. The novel SARS-CoV-2 coronavirus has already infected over 2,000,000 people worldwide and caused upwards of 156,000 deaths. One of the factors driving the rapid unfolding of the pandemic is the absence of diagnostic tests for SARS-CoV-2 detection. Molecular techniques allow SARS-CoV-2 RNA to be quickly detected in clinical samples, aiding the differential diagnosis in severely ill patients and facilitating identification of asymptomatic carriers or presymptomatic individuals. Real-time PCR with fluorescent hybridization is the most available, highly sensitive and specific technique for SARS-CoV-2 RNA detection in biological samples. More RT-PCR assay kits are needed for mass screening, which will help to identify infected individuals and contain the current outbreak of COVID-19 in Russia.

Keywords: SARS-CoV-2, COVID-19, diagnostics, RT-PCR, assay kits, coronavirus

Author contribution: the autors equally contributed to the manuscript.

✉ **Correspondence should be addressed:** Nadezhda A. Kuznetsova
Gamalei, 16, str. 1, Moscow, 123098; nadyakuznetsova0@gmail.com

Received: 21.04.2020 **Accepted:** 28.04.2020 **Published online:** 30.04.2020

DOI: 10.24075/brsmu.2020.026

СТРАТЕГИИ ДИЗАЙНА РТ-ПЦР-СИСТЕМ И ОРГАНИЗАЦИЯ МОНИТОРИНГА SARS-COV-2

Н. А. Кузнецова[1] ✉, А. А. Почтовый[1,2], М. А. Никифорова[1], В. А. Гущин[1,2]

[1] Национальный исследовательский центр эпидемиологии и микробиологии имени Н. Ф. Гамалеи, Москва, Россия

[2] Московский государственный университет имени М. В. Ломоносова, Москва, Россия

Высокая плотность населения в городах с хорошо развитыми транспортными путями сообщения и туризмом может привести к распространению вирусных инфекций по всему миру в считаные дни. Новый коронавирус SARS-CoV-2 стал причиной заболевания COVID-19 уже более 2 000 000 человек и унес жизни более 156 000 человек по всему миру. Одной из основных причин такого стремительного развития пандемии послужило отсутствие диагностических тест-систем для выявления SARS-CoV-2. Применение молекулярно-биологических методов дает возможность быстро обнаруживать РНК вируса SARS-CoV-2 в клинических образцах, что позволяет уточнять диагноз у пациентов с тяжелыми формами течения болезни, а также выявлять людей с бессимптомным течением заболевания или находящихся в инкубационном периоде. Наиболее доступным, высокочувствительным и специфичным методом идентификации НК SARS-CoV-2 в биологических образцах является ПЦР с гибридизационно-флуоресцентной детекцией сигнала в режиме реального времени (ПЦР-РВ). Текущая вспышка COVID-19 в России требует наличия как можно большего количества ПЦР-РВ-тест-систем для проведения масштабных скрининговых исследований с целью выявления инфицированных лиц, своевременное выявление которых является крайне важным условием успешного предотвращения распространения вируса.

Ключевые слова: SARS-CoV-2, COVID-19, диагностика, РТ-ПЦР, тест-системы, коронавирус

Вклад авторов: авторы внесли равнозначный вклад в написание статьи.

✉ **Для корреспонденции:** Надежда Анатольевна Кузнецова
ул. Гамалеи, д. 16, стр. 1, г. Москва, 123098; nadyakuznetsova0@gmail.com

Статья получена: 21.04.2020 **Статья принята к печати:** 28.04.2020 **Опубликована онлайн:** 30.04.2020

DOI: 10.24075/vrgmu.2020.026

The emergence and rapid spread of the novel coronavirus SARS-CoV-2 has sparked the pandemic of COVID-19 [1]. Over 2 billion confirmed cases and more than 150, 000 deaths were reported within less than 3 months after the infection found its way out of China [2]. In the absence of specific treatments and vaccines, quarantine and lockdown are seen as the only available containment measure [3]. Since the virus is capable of presymptomatic transmission, molecular diagnostic techniques based on the amplification of nucleic acids have become the primary tool for monitoring its spread [4]. China, Singapore, South Korea, and Germany succeeded in implementing the broad testing strategy using reverse-transcription polymerase chain reaction (RT-PCR) kits and thus were able to timely identify individuals infected with SARS-CoV-2; these countries seem to have gained control of the epidemic and saved medical resources for treating critically ill patients. By contrast, Italy, Sweden and USA, who were late to adopt the broad testing strategy or initially denied its efficacy, are now facing a truly grave situation.

Molecular methods based on the amplification of nucleic acids boast high sensitivity and high specificity; they can detect viral RNA in both severely ill patients and asymptomatic individuals and thus significantly contribute to stemming the spread of the virus [5, 6]. Immediately after the first complete SARS-CoV-2 genome sequences were obtained, Chinese researchers and WHO released primer and probe sequences for PCR-based virus detection; in the months that followed, thousands of SARS-CoV-2 whole genomes were sequenced and new RT-PCR assays were developed. In this article, we talk about the main approaches to designing PCR assays and some of their specific characteristics.

In diagnostic tests, proper sample collection techniques and adequate, informative samples are essential to valid and reliable results. Knowledge of viral tropism is critical to choosing the type of the specimen to be collected. The efficacy of RT-PCR for SARS-CoV-2 detection depends on the specimen source and the applied sampling technique. It is reported that bronchoalveolar lavage fluids have the highest diagnostic value

in terms of SARS-CoV-2 detection, followed by sputum, nasal swabs, fibrobronchoscope brush biopsy, pharyngeal swabs, feces, and blood (1%) [7]. Still, nasal and oropharyngeal swabs remain the most available and informative specimen type used in screening tests for SARS-CoV-2 [8, 9]. When properly performed, swabbing allows obtaining good quality samples and is safe for the medical staff [10].

Real-time PCR with fluorescent hybridization probes (real-time PCR) is the primary molecular genetic technique for SARS-CoV-2 detection [6, 11, 12]. It is widely available, highly sensitive and specific. PCR assay kits are instrumental in implementing mass screening aimed at detecting infected individuals and quantifying viral loads in each patient.

Approaches RT-PCR assay design

So far, the oligonucleotides and real-time RT-PCR kits for SARS-CoV-2 detection have been described in a few dozens of publications by international authors. In those studies, several different approaches can be identified to designing real-time RT-PCR assays for SARS-CoV-2 detection. Singleplex PCR assays, in which oligonucleotides are selected to target only one specific gene, are the simplest and the most available. Multiplex assays are more advanced and allow targeting a number of different genes simultaneously. Primers and probes for multiplex assays can have different specificity or enable discrimination between SARS-CoV-2 and the related coronaviruses or other respiratory infections. For SARS-CoV-2 detection, primers and probes are usually selected to target the nucleocapsid genes *N1* and *N2*, the RNA-dependent RNA polymerase gene (*RdRP*) and the E protein gene of the viral envelope. For example, CDC (Centers for Disease Control and Prevention) recommends that identification of COVID-19 patients should start with a screening test for the E protein gene, whose nucleotide sequence does not differ from that of SARS, and then proceed to differentiating SARS from SARS-CoV-2 using oligonucleotides for the *RdRP* target [13]. According to the WHO protocol, the collected samples should be screened for *N* and *Orf1b*. However, the proposed oligonucleotides do not help in discriminating between SARS-CoV-2 and SARS; therefore, sequencing is advised to finalize the identification procedure [14]. Table 1 features publicly accessible primer and probe sequences for SARS-CoV-2 detection recommended by WHO and CDC.

Characteristics of existing RT-PCR assays for SARS-CoV-2 detection

Due to high demand, over 10 different commercial kits for SARS-CoV-2 detection have been launched on the Russian market; some of them have already received a medical device registration certificate (Table 2). Singleplex kits have higher sensitivity (up to 500 GE/ml) than their multiplex counterparts (1,000 to 10,000 GE/ml), whereas multiplex kits targeting several SARS-CoV-2 genes are more specific and help to avoid false-negative results associated with the variability of the virus resulting from mutations at the oligonucleotide binding site. Of note, results generated by multiplex kits are sometimes difficult to interpret due to the insufficient optimization of the oligonucleotide sequence. Nevertheless, all Russian manufacturers claim the sensitivity of their kits to be 1,000 GE/ml. Importantly, an internal control should be included in the kit, regardless of the number of specific targets. The internal control can be endogenous (human DNA) or exogenous (e.g., an RNA phage). It is used to control all stages of the protocol, from nuclear acid extraction to amplification.

Although the internal control is necessary, not every assay has it. For example, it is not found in the kits based on isothermal amplification, including loop-mediated isothermal amplification (LAMP). Such assays are advantageously fast (they take no longer than 40 min), do not require sophisticated instrumentation and can be used as point-of-care tests outside the lab, as no thermocycler is needed. LAMP-based assays boast a sensitivity of up to 1–3 RNA copies per reaction [15]. However, the actual sensitivity of currently available commercial LAMP assays is lower than claimed (Table 2).

Whole-genome sequencing

Among all techniques for molecular genetic analysis, sequencing still has the highest informative value. In the current pandemic caused by SARS-CoV-2, the number of complete

Table 1. Oligonucleotides recommended for COVID-19 diagnostics by WHO and CDC

	Target	Oligonucleotides	Detection
WHO	ORF1b-nsp14	HKU-ORF1b-nsp14F TGGGGYTTTACRGGTAACCT HKU- ORF1b-nsp14R AACRCGCTTAACAAAGCACTC HKU-ORF1b-nsp141P FAM-TAGTTGTGATGCWATCATGACTAG-BHQ1	SARS coronavirus BetaCoV/bat Bat SARS-like coronavirus SARS-CoV-2
	N gene	HKU-NF TAATCAGACAAGGAACTGATTA HKU-NR CGAAGGTGTGACTTCCATG HKU-NP FAM-GCAAATTGTGCAATTTGCGG-BHQ1	SARS coronavirus BetaCoV/bat Bat SARS-like coronavirus SARS-CoV-2
CDC	envelope protein	E_Sarbeco_F ACAGGTACGTTAATAGTTAATAGCGT E_Sarbeco_R ATATTGCAGCAGTACGCACACA E_Sarbeco_P1 FAM-ACACTAGCCATCCTTACTGCGCTTCG-BHQ1	SARS coronavirus BetaCoV/bat Bat SARS-like coronavirus SARS-CoV-2
	N gene	N_Sarbeco_F CACATTGGCACCCGCAATC N_Sarbeco_R GAGGAACGAGAAGAGGCTTG N_Sarbeco_P FAM-ACTTCCTCAAGGAACAACATTGCCA-BHQ1	SARS coronavirus BetaCoV/bat Bat SARS-like coronavirus SARS-CoV-2
	RdRP gene	RdRp_SARSr-F GTGARATGGTCATGTGTGGCGG RdRp_SARSr-R CARATGTTAAASACACTATTAGCATA RdRP_SARSr-P1 FAM-CCAGGTGGWACRTCATCMGGTGATGC-BHQ1 RdRp_SARSr-P2 FAM-CAGGTGGAACCTCATCAGGAGATGC-BHQ1	SARS coronavirus BetaCoV/bat Bat SARS-like coronavirus SARS-CoV-2 SARS-CoV-2 BetaCoV/bat

Table 2. Kits for SARS-CoV-2 RNA detection

Certificate ID and registration date (Federal Service for Surveillance in Healthcare)	Name	Manufacturer	Claimed sensitivity (GE/ml)	Amplification time
2020/10088 dated 17.04.2020	Real-time isothermal amplification kit for SARS-CoV-2 RNA detection in biological samples	Evotech Mirai Genomics LLC	10 000	25 min
2020/10064 dated 16.04.2020	*SBT-DX-SARS-CoV-2* Real-time PCR kit for SARS-CoV-2 RNA detection in biological samples (fluorescent hybridization)	SystemaBioTech LLC	1000	1 h 40 min
2020/9957 dated 02.04.2020	*Isotherm SARS-CoV-2 RNA-screen* Real-time loop-mediated isothermal amplification kit for SARS-CoV-2 RNA detection in biological samples	Generium JSC	1000	25 min
2020/9948 dated 01.04.2020	*SARS-CoV-2/SARS-CoV* Real-time RT-PCR kit for SARS-CoV-2 and SARS-CoV RNA detection	DNA-Technology TS LLC	1000	50 min
2020/10032 dated 14.04.2020	Real-time PCR kit for SARS-CoV-2 RNA detection in biological samples (fluorescent hybridization)	MediapalTech LLC	1000	1 h 20 min
2020/9904 dated 27.03.2020	*Polyvir SARS-CoV-2* RT-PCR kit for SARS-CoV-2 RNA detection	Litech LLC	1000	1 h 30 min
2020/9765 dated 27.03.2020	*AmpliTest SARS-CoV-2* PCR kit for SARS-Cov-2 RNA detection	Center for Strategic Planning, Ministry of Healthcare of the Russian Federation	1000	1 h 20 min
2020/9896 dated 27.03.2020	*Real-Best RNA SARS-CoV-2* RT-PCR kit for SARS-CoV-2 RNA detection	Vector-Best JSC	1000	1 h 20 min
41956 2014/1987 dated 25.03.2020	*AmpliSense® CoVs-Bat-FL* PCR kit for MERS-CoV and SARS-CoV/CoV-2 RNA detection in biological samples (fluorescent hybridization); technical specifications 9398-224-01897593-2013	Central Research Institute of Epidemiology, Federal Service for Surveillance in Healthcare	1000	1 h 20 min
2020/9845 dated 20.03.2020	Real-time isothermal amplification kit for SARS-CoV-2 RNA detection in biological samples	SmartLifeCare LLC	10 000	25 min
41390 2020/9700 dated 14.02.2020	*Vector-OneStepPCR-Cov-RG* Real-time PCR kit for SARS/COVID-19 RNA detection (fluorescent hybridization)	Vector, State Research Center of Virology and Biotechnology, Federal Service for Surveillance in Healthcare	n/a	n/a
41240 2020/9677 dated 11.02.2020	*Vector-real-time PCR-2019-nCoV-RG* Real-time PCR kit for 2019-nCoV RNA detection (fluorescent hybridization)	Vector, State Research Center of Virology and Biotechnology, Federal Service for Surveillance in Healthcare	n/a	n/a

genomic sequences of the virus obtained within very short time is record-breaking. Whole-genome sequencing has never been so close to adoption in the clinical setting as it is now. There are a few approaches to whole-genome sequencing of SARS-CoV-2. The classic approach consists in the extraction of nucleic acids from nasopharyngeal and/or oropharyngeal swabs, subsequent depletion of the host's ribosomal RNA for library preparation and sequencing itself carried out according to the protocols supplied by the manufacturer. However, this approach requires a fair amount of viral RNA and good read depth. With low viral loads, the virus can be replicated using cell cultures. For that, serial passages are performed in Vero V, Vero E6, LLC-MK2, and some other cell lines. This approach has been successfully used in some laboratories, including the Reference center for coronavirus infection (GISAID ID: EPI_ISL_421275).

Whole-genome amplification is an alternative to cell cultures. So far, a few panels have been designed for sequencing the entire genome of SARS-CoV-2. Among them is the Ion AmpliSeq SARS-CoV-2 Research Panel (Thermo Fisher Scientific; USA). It consists of two primer pools for the amplification of 125–275 bp-long fragments [16].

Another panel was developed by Paragon Genomics Inc (USA). It is a multiplex PCR research panel with two primer pools and an average amplicon size of 99 bp [17]. The panel can potentially detect 1.15 viral copies at 95% probability. Using two overlapping pools of primers will ensure full coverage of the entire viral genome, with a calculated detection limit of 0.29 copies at 95% probability. So far, there is no data on the actual SARS-CoV-2 detection limit for the AmpliSeq SARS-CoV-2 Research Panel.

A new protocol for sample preparation and bioinformatic analysis was proposed by the ARTIC network [18]. It was developed for Oxford Nanopore sequencing platform and generates results within 8 h.

CONCLUSIONS

Methods based on the molecular genetic analysis of nucleic acids are instrumental in the surveillance and monitoring of SARS-CoV-2 spread and help to contain the COVID-19 pandemic. Their primary advantage over thermometry or evaluation of symptoms is the ability to detect asymptomatic carriers or infected presymptomatic individuals. In spite of a plethora of designs, classic RT-PCR is still the preferred detection technique. Refinement of isothermal amplification tools will make molecular analytical techniques more accessible in the future and improve their efficacy in monitoring and controlling biological threats. Sequencing allows accumulating more data about changes occurring in the viral genome and using it for RT-PCR primer optimization, vaccine development, study of the evolution of the virus, and

reconstruction of epidemiological processes that drive the epidemic. Sequencing platforms make it possible to analyze collected samples in the clinical setting, outside the lab, thereby reducing the turnaround time.

References

1. Li Q, et al. Early transmission dynamics in Wuhan, China, of novel coronavirus-infected pneumonia. N Engl J Med. 2020; 382: 1199–207.
2. Available from: https://gisanddata.maps.arcgis.com/apps/opsdashboard/index.html#/bda7594740fd40299423467b48e9ecf6.
3. Kissler SM, Tedijanto C, Goldstein E, Grad YH, Lipsitch M. Projecting the transmission dynamics of SARS-CoV-2 through the postpandemic period. Science. 2020; eabb5793.
4. He X, Lau EHY, Wu P, et al. Temporal dynamics in viral shedding and transmissibility of COVID-19. Nat Med. 2020. Available from: https://doi.org/10.1038/s41591-020-0869-5.
5. Cheng MP, Papenburg J, Desjardins M, Kanjilal S, Quach C, Libman M, et al. Diagnostic Testing for Severe Acute Respiratory Syndrome–Related Coronavirus-2: A Narrative Review. Ann Intern Med. 2020; Apr 13: [Epub ahead of print]. DOI: 10.7326/M20-1301.
6. Shen M, Zhou Y, Ye J, Abdullah Al-Maskri AA, Kang Y, Zeng S, et al. Recent advances and perspectives of nucleic acid detection for coronavirus. J Pharm Anal. 2020 Mar 1. Available from: https://www.journals.elsevier.com/journal-of-pharmaceutical-analysis.
7. Wang W, Xu Y, Gao R, Lu R, Han K, Wu G, et al. Detection of SARS-CoV-2 in Different Types of Clinical Specimens. JAMA. 2020 Mar 11.
8. Pan Y, Zhang D, Yang P, Poon LLM, Wang Q.Viral load of SARS-CoV-2 in clinical samples. Lancet Infect Dis. 2020 Apr; 20 (4): 411–2.
9. Zou L, Ruan F, Huang M, Liang L, Huang H, Hong Z, et al. SARS-CoV-2 Viral Load in Upper Respiratory Specimens of Infected Patients. N Engl J Med. 2020 Mar 19; 382 (12): 1177–9.
10. Marty FM, Chen K, Verrill KA. How to Obtain a Nasopharyngeal Swab Specimen April 17, 2020. DOI: 10.1056/NEJMvcm2010260.
11. Cheng MP, Papenburg J, Desjardins M, Kanjilal S, Quach C, Libman M, et al. Diagnostic Testing for Severe Acute Respiratory Syndrome–Related Coronavirus-2: A Narrative Review. Ann Intern Med. 2020 Apr; 13.
12. Pang J, Wang MX, Ang IYH, Tan SHX, Lewis RF, et al. Potential Rapid Diagnostics, Vaccine and Therapeutics for 2019 Novel Coronavirus (2019-nCoV): A Systematic Review. J Clin Med. 2020 Feb 26; 9 (3): pii E623.
13. Corman VM, Landt O, Kaiser M, Molenkamp R, Meijer A, Chu DK, et al. Detection of 2019 novel coronavirus (2019-nCoV) by real-time RT-PCR. Euro Surveill. 2020 Jan; 25 (3).
14. Available from: https://www.who.int/docs/default-source/coronaviruse/peiris-protocol-16-1-20.pdf?sfvrsn=af1aac73_4.
15. R Lu, X Wu, Z Wan, Y Li, L Zuo, J Qin, et al. Development of a Novel Reverse Transcription Loop-Mediated Isothermal Amplification Method for Rapid Detection of SARS-CoV-2. Virologica Sinica. 2020; c .1.
16. Available from: https://www.thermofisher.com/ru/ru/home/life-science/sequencing/dna-sequencing/microbial-sequencing/microbial-identification-ion-torrent-next-generation-sequencing/viral-typing/coronavirus-research.html.
17. Li C, et al. High sensitivity detection of coronavirus SARS-CoV-2 using multiplex PCR and a multiplex-PCR-based metagenomic method. bioRxiv. 2020.
18. Available from: https://nanoporetech.com/about-us/news/artic-network-provides-protocol-rapid-accurate-sequencing-novel-coronavirus-ncov-2019.

Литература

1. Li Q, et al. Early transmission dynamics in Wuhan, China, of novel coronavirus-infected pneumonia. N Engl J Med. 2020; 382: 1199–207.
2. Available from: https://gisanddata.maps.arcgis.com/apps/opsdashboard/index.html#/bda7594740fd40299423467b48e9ecf6.
3. Kissler SM, Tedijanto C, Goldstein E, Grad YH, Lipsitch M. Projecting the transmission dynamics of SARS-CoV-2 through the postpandemic period. Science. 2020; eabb5793.
4. He X, Lau EHY, Wu P, et al. Temporal dynamics in viral shedding and transmissibility of COVID-19. Nat Med. 2020. Available from: https://doi.org/10.1038/s41591-020-0869-5.
5. Cheng MP, Papenburg J, Desjardins M, Kanjilal S, Quach C, Libman M, et al. Diagnostic Testing for Severe Acute Respiratory Syndrome–Related Coronavirus-2: A Narrative Review. Ann Intern Med. 2020; Apr 13: [Epub ahead of print]. DOI: 10.7326/M20-1301.
6. Shen M, Zhou Y, Ye J, Abdullah Al-Maskri AA, Kang Y, Zeng S, et al. Recent advances and perspectives of nucleic acid detection for coronavirus. J Pharm Anal. 2020 Mar 1. Available from: https://www.journals.elsevier.com/journal-of-pharmaceutical-analysis.
7. Wang W, Xu Y, Gao R, Lu R, Han K, Wu G, et al. Detection of SARS-CoV-2 in Different Types of Clinical Specimens. JAMA. 2020 Mar 11.
8. Pan Y, Zhang D, Yang P, Poon LLM, Wang Q.Viral load of SARS-CoV-2 in clinical samples. Lancet Infect Dis. 2020 Apr; 20 (4): 411–2.
9. Zou L, Ruan F, Huang M, Liang L, Huang H, Hong Z, et al. SARS-CoV-2 Viral Load in Upper Respiratory Specimens of Infected Patients. N Engl J Med. 2020 Mar 19; 382 (12): 1177–9.
10. Marty FM, Chen K, Verrill KA. How to Obtain a Nasopharyngeal Swab Specimen April 17, 2020. DOI: 10.1056/NEJMvcm2010260.
11. Cheng MP, Papenburg J, Desjardins M, Kanjilal S, Quach C, Libman M, et al. Diagnostic Testing for Severe Acute Respiratory Syndrome–Related Coronavirus-2: A Narrative Review. Ann Intern Med. 2020 Apr; 13.
12. Pang J, Wang MX, Ang IYH, Tan SHX, Lewis RF, et al. Potential Rapid Diagnostics, Vaccine and Therapeutics for 2019 Novel Coronavirus (2019-nCoV): A Systematic Review. J Clin Med. 2020 Feb 26; 9 (3): pii E623.
13. Corman VM, Landt O, Kaiser M, Molenkamp R, Meijer A, Chu DK, et al. Detection of 2019 novel coronavirus (2019-nCoV) by real-time RT-PCR. Euro Surveill. 2020 Jan; 25 (3).
14. Available from: https://www.who.int/docs/default-source/coronaviruse/peiris-protocol-16-1-20.pdf?sfvrsn=af1aac73_4.
15. R Lu, X Wu, Z Wan, Y Li, L Zuo, J Qin, et al. Development of a Novel Reverse Transcription Loop-Mediated Isothermal Amplification Method for Rapid Detection of SARS-CoV-2. Virologica Sinica. 2020; c .1.
16. Available from: https://www.thermofisher.com/ru/ru/home/life-science/sequencing/dna-sequencing/microbial-sequencing/microbial-identification-ion-torrent-next-generation-sequencing/viral-typing/coronavirus-research.html.
17. Li C, et al. High sensitivity detection of coronavirus SARS-CoV-2 using multiplex PCR and a multiplex-PCR-based metagenomic method. bioRxiv. 2020.
18. Available from: https://nanoporetech.com/about-us/news/artic-network-provides-protocol-rapid-accurate-sequencing-novel-coronavirus-ncov-2019.

CHARACTERIZATION OF THE GENOTYPE AND THE PHENOTYPE OF NONTOXIGENIC STRAINS OF *CORYNEBACTERIUM DIPHTHERIAE* SUBSP. *LAUSANNENSE* ISOLATED IN RUSSIAN RESIDENTS

Borisova OYu[1,2] ✉, Chaplin AV[1,2], Gadua NT[1], Pimenova AS[1], Alexeeva IN[3], Rakitsky GF[3], Afanasiev SS[1], Donskikh EE[2], Kafarskaya LI[2]

[1] G. N. Gabrichevsky Research Institute for Epidemiology and Microbiology, Moscow, Russia

[2] Pirogov Russian National Research Medical University, Moscow, Russia

[3] Regional Clinical Psychiatric Hospital, Khabarovsk, Russia

In 2018, a few sequencing studies were published revealing the existence of two monophyletic clusters within the *C. diphtheriae* species, meaning that this species can be divided into two subspecies: *C. diphtheriae* subsp. *diphtheriae* and *C. diphtheriae* subsp. *lausannense*. The objective of our study was to describe the genotype and the phenotype of 2 nontoxigenic *C. diphtheriae* strains isolated in Russia in 2017–2018, which were classified by us as *C. diphtheriae* subsp. *lausannense* based on the aggregated data yielded by a variety of techniques, including microbiological and molecular genetic techniques, as well as a bioinformatic search for subspecies-specific genes in the publicly available genomes of *C. diphtheriae*. The isolated strains had morphological and biochemical characteristics of *C. diphtheriae*. The strains were assigned to the MLST type ST199 included in the clonal complex associated with subsp. *lausannense*. PCR revealed that both analyzed strains of *C. diphtheriae* subsp. *lausannense* carried the ptsI gene encoding phosphoenolpyruvate-protein phosphotransferase and did not carry the *narG* gene encoding the synthesis of nitrate reductase subunits, whereas the strains of *C. diphtheriae* subsp. *diphtheriae* had the *narG* gene and did not have *ptsI*. We experimentally proved the ability of *lausannense* strains to ferment N-acetylglucosamine. Our findings expand the knowledge of the biological diversity of *C. diphtheriae* and indicate the need for estimating the spread of these microorganisms in Russia, as well as their pathogenic potential.

Keywords: diphtheria, nontoxigenic *Corynebacterium diphtheriae*, *Corynebacterium diphtheriae* subsp. *lausannense*, multilocus sequence typing, phylogenetic analysis

Author contribution: Borisova OYu carried out molecular genetic tests, analyzed the literature and the obtained data, contributed to manuscript preparation; Chaplin AV performed phylogenetic analysis, analyzed the experimental data and contributed to manuscript preparation; Gadua NT, Pimenova AS carried out microbiological tests and contributed to manuscript preparation; Alexeeva IN, Rakitsky GF examined the patients on admission and contributed to manuscript preparation; Afanasiev SS conducted molecular genetic tests and contributed to manuscript preparation; Donskikh EE analyzed the literature and the experimental data and contributed to manuscript preparation; Kafarskaya LI analyzed the experimental data and contributed to manuscript preparation.

Compliance with ethical standards: the study was approved by the Ethics Committee of G. N. Gabrichevsky Research Institute for Epidemiology and Microbiology. Informed consent was obtained from all participants.

✉ **Correspondence should be addressed:** Olga Yu. Borisova
Admirala Makarova, 10, Moscow, 125212; olgborisova@mail.ru

Received: 09.02.2020 **Accepted:** 28.02.2020 **Published online:** 18.03.2020

DOI: 10.24075/brsmu.2020.015

ХАРАКТЕРИСТИКА ГЕНОТИПА И ФЕНОТИПА НЕТОКСИГЕННЫХ ШТАММОВ *CORYNEBACTERIUM DIPHTHERIAE* SUBSP. *LAUSANNENSE*, ВЫДЕЛЕННЫХ НА ТЕРРИТОРИИ РОССИИ

О. Ю. Борисова[1,2] ✉, А. В. Чаплин[1,2], Н. Т. Гадуа[1], А. С. Пименова[1], И. Н. Алексеева[3], Г. Ф. Ракицкий[3], С. С. Афанасьев[1], Е. Е. Донских[2], Л. И. Кафарская[2]

[1] Московский научно-исследовательский институт эпидемиологии и микробиологии имени Г. Н. Габричевского, Москва, Россия

[2] Российский национальный исследовательский медицинский университет имени Н. И. Пирогова, Москва, Россия

[3] Краевая клиническая психиатрическая больница, Хабаровск, Россия

В 2018 г. на основании полногеномных данных появились публикации о наличии двух монофилетических кластеров внутри вида *C. diphtheriae*, что позволяет дифференцировать этот вид на два подвида: *C. diphtheriae* subsp. *diphtheriae* и *C. diphtheriae* subsp. *lausannense*. Целью работы было описать генотип и фенотип двух нетоксигенных штаммов *C. diphtheriae*, выделенных в 2017–2018 гг. с профилактической целью, которые на основании совокупности результатов множества методов могут быть отнесены к *C. diphtheriae* subsp. *lausannense*. В исследовании использовали микробиологические и молекулярно-генетические методы, а также биоинформатический поиск подвид-специфичных генов в публично доступных геномах *C. diphtheriae*. Выделенные штаммы имели характерные для *C. diphtheriae* морфо-культуральные свойства и биохимическую характеристику. В МЛСТ штаммы принадлежали к сиквенс-типу ST199, входящему в клональный комплекс, ассоциированный с subsp. *lausannense*. С использованием ПЦР были показаны наличие *ptsI* (гена, кодирующего фосфоенолпируват-белок фосфотрансферазы) и отсутствие *narG* (гена, кодирующего синтез субъединиц нитратредуктазы) у двух исследуемых штаммов *C. diphtheriae* subsp. *lausannense* и противоположная картина — у штаммов *C. diphtheriae* subsp. *diphtheriae*. Была экспериментально подтверждена способность выделенных штаммов подвида *lausannense* сбраживать N-ацетилглюкозамин. Полученные результаты расширяют представления о биологическом разнообразии вида *C. diphtheriae* и свидетельствуют о необходимости дальнейших исследований по оценке распространенности этих микроорганизмов и изучению их патогенного потенциала.

Ключевые слова: дифтерия, нетоксигенные *Corynebacterium diphtheriae*, *Corynebacterium diphtheriae* subsp. *lausannense*, мультилокусное секвенирование, филогенетический анализ

Вклад авторов: О. Ю. Борисова — молекулярно-генетические исследования, анализ данных, анализ литературы, подготовка рукописи; А. В. Чаплин — филогенетический анализ, анализ данных, подготовка рукописи; Н. Т. Гадуа и А. С. Пименова — микробиологические исследования, подготовка рукописи; И. Н. Алексеева и Г. Ф. Ракицкий — обследование пациентов и первичная идентификация, подготовка рукописи; С. С. Афанасьев — молекулярно-генетические исследования, подготовка рукописи; Е. Е. Донских — анализ данных, анализ литературы, подготовка рукописи; Л. И. Кафарская — анализ данных, подготовка рукописи.

Соблюдение этических стандартов: исследование одобрено этическим комитетом Московского научно-исследовательского института эпидемиологии и микробиологии имени Г. Н. Габричевского. Все пациентки подписали добровольное информированное согласие на участие в исследовании.

✉ **Для корреспонденции:** Ольга Юрьевна Борисова
ул. Адмирала Макарова, д. 10, г. Москва, 125212; olgborisova@mail.ru

Статья получена: 09.02.2020 **Статья принята к печати:** 28.02.2020 **Опубликована онлайн:** 18.03.2020

DOI: 10.24075/vrgmu.2020.015

Diphtheria is caused by toxigenic strains of *Corynebacterium diphtheriae* harboring integrated bacteriophage DNA containing the toxin gene. The infection spreads from person to person via airborne droplets and develops into classic pharyngeal or nasal diphtheria.

Over the past century, mass immunization programs have dramatically cut down the incidence of diphtheria [1]. In Russia, the incidence rate of the disease has stabilized due to good vaccination coverage (≥ 95%) [2]. In 2017, no incident cases of diphtheria and only 2 asymptomatic carriers were reported in Russia. In 2018, 4 incident cases of the disease and 3 carriers were reported, whereas in the first 9 months of 2019, there were 3 new cases of diphtheria and 2 carriers [3]. In the past few years, there have been no reports of the secondary cases or lethal infection. Most clinical forms of diphtheria are mild localized forms.

Today, diphtheria is a rare disease; therefore, it can pose a diagnostic difficulty to the clinician. This, as well as the existence of latent carriers, who act as a reservoir for the infection, and the fact that the epidemic process unfolds in the vaccinated population, still renders diphtheria a clinically important problem [3].

Recently, infections caused by nontoxigenic *C. diphtheriae* strains have been on the rise. They manifest atypically as pharyngitis, respiratory tract infections, endocarditis, osteomyelitis, septic arthritis or skin infections [4–8].

Historically, *C. diphtheriae* were classified into 4 biotypes based on their biochemical phenotypes: gravis, mitis, intermedius and belfanti [9, 10]. Representatives of the same biovar, though, can be genetically distant [11, 12]. This is why genomics does not support the use of biovars as a reliable classification tool for *C. diphtheriae* [13]. Besides, there is no correlation between the biovar and pathogenicity [14]. Multilocus sequence typing (MLST) based on the determination of allelic profiles of 7 housekeeping genes has made it possible to cluster the entire diversity of *C. diphtheriae* strains into 2 evolutionary lineages: lineage-1 (the majority of the strains) and lineage-2 (only strains of the belfanti biotype) [14].

In 2018, a paper was published describing 3 nontoxigenic strains of *C. diphtheriae* [15]. One of them had been isolated from a Swiss patient with tracheobronchitis and multiple lesions on the distal trachea and the mainstem bronchi; the 2 other strains had been isolated from nasal swabs in the UK and India. Genome comparison that used publicly available *C. diphtheriae* genomes demonstrated that average nucleotide identity between the isolated strains and the NCTC 11397 *C. diphtheriae* reference genome was lower (95.24 to 95.39%) than between the reference genome and other previously published *C. diphtheriae* genomes (> 98.15%). Phylogeny reconstruction based on whole genome sequencing data confirmed the existence of two monophyletic clusters of *C. diphtheriae* corresponding to lineage-1 and lineage-2. Consequently, it was proposed to classify *C. diphtheriae* into two subspecies: *C. diphtheriae* subsp. *diphtheriae* and *C. diphtheriae* subsp. *lausannense*.

The aim of this study was to characterize the genotype and the phenotype of nontoxigenic *C. diphtheriae* strains isolated in 2017–2018 that can be identified as *C. diphtheriae* subsp. *lausannense* based on the aggregated data yielded by a variety of different methods.

METHODS

In the experimental part of the study, we analyzed 2 nontoxigenic *C. diphtheriae* strains isolated at the bacteriological laboratory of Khabarovsk Regional Psychiatric Hospital in 2017–2018, the control toxigenic strain of *C. diphtheriae* (gravis biotype, accession number 665) from the State collection of pathogenic microorganisms (SCPM-Obolensk), freshly isolated toxigenic strains of *C. diphtheriae* (gravis biotype, strain numbers 66-19, 98-19 and mitis biotype, strain numbers 55-19, 56-19), nontoxigenic strains of *C. diphtheriae* (gravis biotype, strain numbers 57-19, 67-19 and mitis biotype, strain numbers 60-19, 91-19) that had been delivered to the Reference Center for the Surveillance of Measles, Rubella, Mumps, Pertussis, and Diphtheria (G.N. Gabrichevsky Research Institute for Epidemiology and Microbiology) from different Russian regions.

The analysis of *C. diphtheriae* strains was conducted following the guidelines № 4.2.3065-13 for laboratory diagnostics of diphtheria. The isolates were plated onto tellurite blood agar (2% fishmeal hydrolysate agar base, State Research Center for Applied Microbiology & Biotechnology; Obolensk; Russia) supplemented with 7% bovine blood (Leitran; Russia) and potassium tellurite (State Research Center for Applied Microbiology & Biotechnology; Obolensk, Russia) and kept in a temperature-controlled chamber at 37 °C for 24–48 hours. Grown colonies of *C. diphtheriae* were evaluated for their morphological, toxigenic and biochemical properties. The toxigenicity of *C. diphtheriae* strains was evaluated in a precipitation test using a Corynetoxagar medium (State Research Center for Applied Microbiology & Biotechnology; Obolensk, Russia) supplemented with 20% bovine serum (Leitran; Russia) and filter discs soaked in diphtheria antitoxin (Diagnostic Systems; Nizhny Novgorod, Russia). Each antitoxin-impregnated disc contained 5 ± 1 IU of diphtheria antitoxin (as suggested by the guidelines 4.2.3065-13). Biochemical properties of the cultures were determined from their cysteinase, urease, saccharolytic and nitrate reductase activity using the media prepared at our laboratory and a commercial DS-DIPH-CORYNE kit (Diagnostic Systems; Nizhny Novgorod, Russia).

To evaluate the ability of the analyzed strains to ferment N-acetylglucosamine, a phenol red broth was *ex tempore* supplemented with N-acetylglucosamine (Sigma-Adlrich; USA). Then, a loop full of overnight *C. diphtheriae* cultures grown on serum agar was added to 3 ml of the solution. The cultures were incubated at 37 °C for 24–48 h. Fermentation was evaluated based on the change in the color of the solution. Two toxigenic and two nontoxigenic gravis strains, as well as two toxigenic and two nontoxigenic mitis strains, were used as controls.

The sample of the analyzed published genomic sequences comprised 204 *C. diphtheriae* genomes representing diphtheriae and *lausannense* subspecies deposited in the NCBI Refseq database, 3 genomes of *C. diphtheriae* subsp. *lausannense* from the NCBI Genbank and one genome of *Corynebacterium ulcerans* BR-AD22, which served as an outgroup for phylogenetic reconstruction. In total, 208 genomes were included in the analyzed dataset.

Coding sequences retrieved from the genome annotations in the corresponding databases were clustered into ortholog groups using OrthoMCL [16] with standard settings (inflation index of 1.5; protein sequence similarity threshold of 50%; e-value of 10–5). For phylogeny reconstruction, we used the groups of orthologs that were made up of the genes present in every genome in the amount of 1 copy. Nucleotide sequences were aligned in MUSCLE software [17] and then concatenated. Phylogeny reconstruction was performed following the Maximum Likelihood algorithm implemented in FastTree software [18] using the GTR+CAT model. MLST types of the published sequences were predicted based on the

data retrieved from PubMLST. Clonal clusters were formed in Phyloviz 2 using the goeBURST algorithm at the SLV level [19].

Total DNA was isolated from overnight *C. diphtheriae* cultures grown on fishmeal hydrolysate agar (State Research Center for Applied Microbiology & Biotechnology; Obolensk, Russia) supplemented with 10% bovine serum (Leitran; Moscow) using a standard boiling extraction method with subsequent centrifugation.

Detection of *tox* gene fragments in nontoxigenic *C. diphtheriae* strains was performed in accordance with the protocol described in [20]. The PCR reaction mix contained 1.5 mM $MgCl_2$, 10 mM Tris-HCl (pH 8.3), 50 mM KCl, 0.1 μM of forward and reverse primers, 200 mM of each dNTP, and 1 unit of Taq polymerase (Thermo Fisher Scientific; USA). DNA of the control toxigenic *C. diphtheriae* strain (gravis biovar, accession number 665) was used as a positive amplification control. MLST types of *C. diphtheriae* strains were determined following the international protocol [14]; fragments of 7 housekeeping genes were Sanger-sequenced, including *atpA*, *dnaE*, *dnaK*, *fusA*, *leuA*, *odhA*, and *rpoB*. Sequencing was carried out by Evrogen JSC (Moscow). Allele identification was done using the PubMLST database.

To identify *dtxR* fragments in the sequences of *C. diphtheriae* strains, PCR was carried out with one pair of primers for the entire region of the *dtxR* gene: GGGACTACAACGCAACAAGAA and TCATCTAATTTCGCCGCCTTTA as described in [20, 21]. The following primers were used for subspecies-specific PCR: *ptsI*_F: ACTTTCCGAACCTGCCATCC and *ptsI*_R:GTGTACTCCT TCGTCTGCTC; *narG*_F: CTGACCACTGGGGCGAGG and *narG*_R: GAGTTGTCATAACGCCACTG.

RESULTS

The *C. diphtheriae* strains B-8759 and B-8760 had been isolated from the pharynx of two patients (26 and 77 years) admitted to 2 different units of a psychiatric hospital; the patients had undergone a standard preadmission test for diphtheria (see Paragraph 3.4. of the Guidelines 3.1.3018-12 on the epidemiological surveillance of diphtheria infection). The isolated strains were identified from their morphological, toxigenic and biochemical properties as recommended by the Guidelines 4.2.3065-13 on the laboratory diagnostics of diphtheria. On tellurite blood agar, the grown colonies appeared grayish-black, fuzzy, crumbly, with slightly irregular margins and a raised center. Toxigenicity of the grown colonies was determined using discs impregnated with diphtheria antitoxin (the Feldman method). After 24 and 48 hours of incubation, the isolated cultures still had not produced specific precipitation lines, unlike the control toxigenic *C. diphtheriae* strain (gravis biotype, accession number 665), suggesting the absence of toxigenicity. PCR performed to detect the fragment of the *tox* gene demonstrated that the analyzed strains did not carry the diphtheria toxin gene.

Biochemical properties of the cultures were determined from their cysteinase, urease, saccharolytic and nitrate reductase activity. The cultures exhibited cysteinase activity and formed a brown halo following inoculation into the Pisu medium; the cultures fermented glucose, maltose, fructose and galactose, did not ferment saccharose and starch, and exhibited no urease or nitrate reductase activity (Table 1). The tests allowed us to provisionally assign the analyzed *C. diphtheriae* strains to the belfanti biotype typically seen in *lausannense* subspecies.

In the next step, we analyzed the previously published genomes of *C. diphtheriae*, which was necessary to verify that the studied species can be distinctly divided into subspecies and to conduct a search for species-specific protein-encoding genes.

The constructed phylogenetic tree (Fig. 1) confirmed the results previously obtained on a smaller sample indicating that representatives of *C. diphtheriae* constituted two clades corresponding to the subspecies *diphtheriae* and *lausannense*. The tree also showed that the representatives of these subspecies belonged to non-overlapping groups of sequence types. The goeBURST clustering analysis of MLST types described in PubMLST (Fig. 2) revealed that all representatives of the *lausannense* subspecies whose genomes had been previously sequenced belonged to the sequence types ST106, ST360, or ST409, and to one previously undescribed type that differed from ST359 in just one allele. All these sequence types formed one clonal complex.

It could be hypothesized that other sequence types (such as ST35, ST37, ST69, or ST81) constituting the same clonal complex also belong to the *lausannense* subspecies. An additional argument in favor of our hypothesis is that almost all isolates representing the sequence types from this clonal complex have been described in the PubMLST database as representing the belfanti biotype typical to the *lausannense* subspecies.

The analysis of ortholog groups revealed the existence of loci specific to *C. diphtheriae* subspecies. For example, all strains of the *lausannense* subspecies had a region (presumably, an operon) harboring genes of the phosphotransferase system, for which N-acetylglucosamine is a hypothesized substrate. The following primers were selected for the gene coding

Table 1. Characteristics of the analyzed *C. diphtheriae* cultures

Characteristic	*C. diphtheriae* strains		
	Strain 665 (control)	Strain B-8759	Strain B-8760
Glucose fermentation	+	+	+
Saccharose fermentation	–	–	–
Maltose fermentation	+	+	+
Fructose fermentation	+	+	+
Galactose fermentation	+	+	+
Starch fermentation	+	–	–
Urease	–	–	–
Nitrate reductase	+	–	–
Cysteinase test	+	+	+
Toxigenicity (the Feldman method)	+	–	–
Presence of the *tox* gene	+	–	–

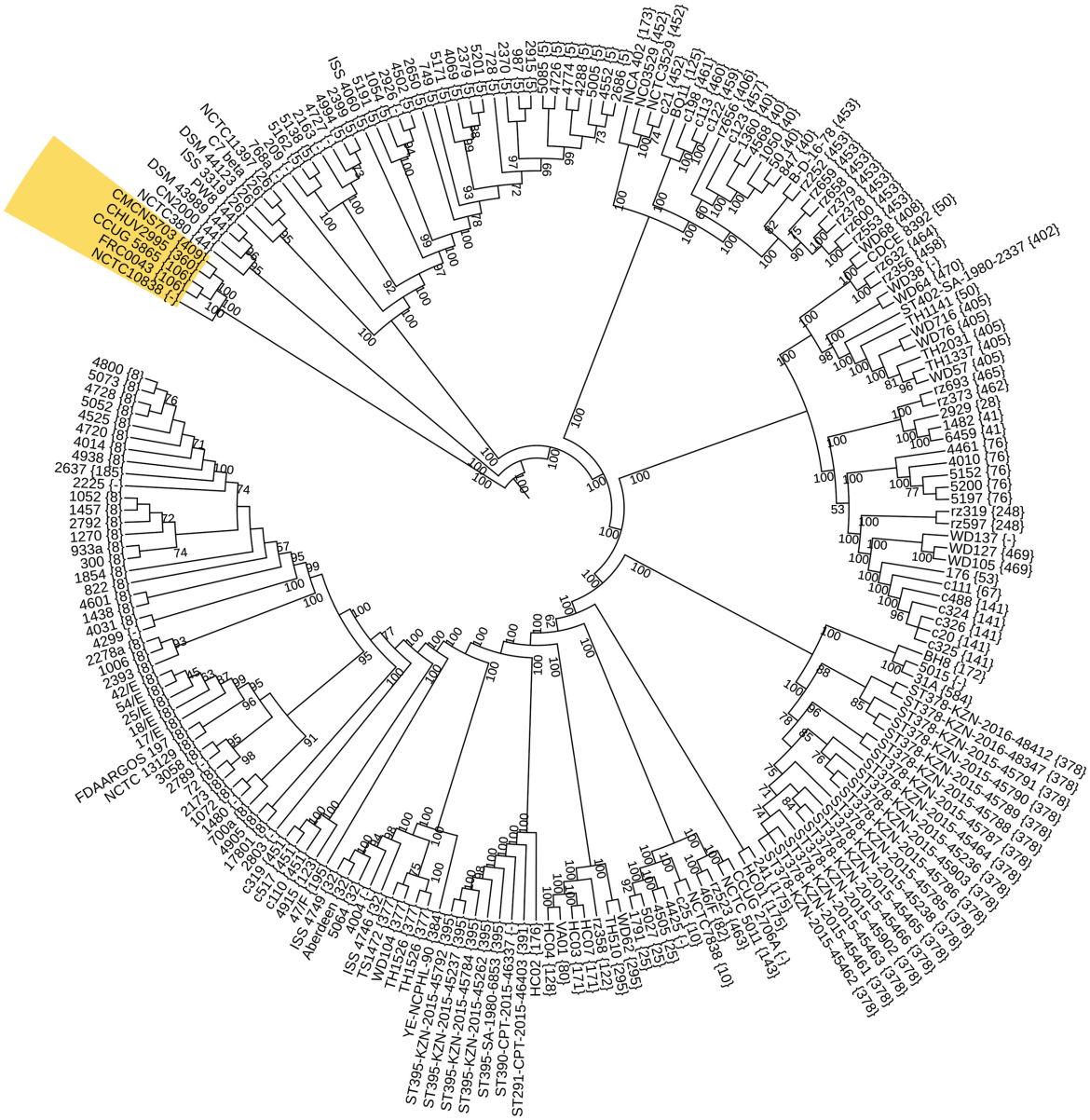

Fig. 1. A phylogenetic tree for *C. diphtheriae* strains with publicly available sequenced genomes. The length of the branches and the genome of *C. ulcerans* BR-AD22 used for rooting are not shown in the figure. The numbers on the branches represent bootstrap values. Strains of *C. diphtheriae* subsp. *lausannense* are shown in gray. The numbers in brackets refer to the predicted sequence types and follow the PubMLST nomenclature (dash marks represent yet undescribed sequence types)

for phosphoenolpyruvate-protein phosphotransferase: *ptsI*_F: ACTTTCCGAACCTGCCATCC and *ptsI*_R: GTGTACTCCTTCGTCTGCTC (the expected product length was 489 bp). At the same time, a locus encoding the synthesis of nitrate reductase subunits was detected only in the genomes of the *diphtheriae* subspecies. The following primers were selected for the gene encoding its α-subunit (the gene was present in the sequences of 201 out of 202 strains representing this subspecies in the analyzed sample): *narG*_F: CTGACCACTGGGGCGAGG and *narG*_R: GAGTTGTCATAACGCCACTG (the expected product length was 691 bp).

PCR with primers for the amplification of *ptsI* and *narG* fragments (Fig. 3) showed that the samples containing DNA of B-8759 and B-8760 strains carried the *ptsI* gene and did not carry the *narG* gene, whereas "classic" *C. diphtheriae* strains had the *narG* gene and did not have *ptsI*. There were no samples that carried either both of these genomic loci or none of them.

These findings and the results of biochemical identification allowed us to conclude that the analyzed *C. diphtheriae* strains belonged to *C. diphtheriae* subsp. *lausannense*. The conclusion was corroborated by the fact that the isolated strains represented the sequence type ST199 included in the clonal complex presumably typical to the representatives of this subspecies (Fig. 2). Another piece of evidence confirming our conclusion was the sequence of the *dtxR* gene that coincided with the sequences found in the genomes of *lausannense* subspecies.

Considering that strains of *C. diphtheriae* subsp. *lausannense* carried the gene coding for phosphoenolpyruvate-protein phosphotransferase, which is part of the phosphotransferase system for N-acetylglucosamine, we conducted a few experiments to investigate the phenotypic manifestations of this gene. The experiments showed that unlike *C. diphtheriae* subsp. *diphtheriae*, both analyzed strains, which we classified as *C. diphtheriae* subsp. *lausannense*, fermented N-acetylglucosamine (Fig. 4).

The analyzed strains, which we classified as *C. diphtheriae* subsp. *lausannense*, were deposited in the State collection of pathogenic microorganisms (SCPM-Obolensk).

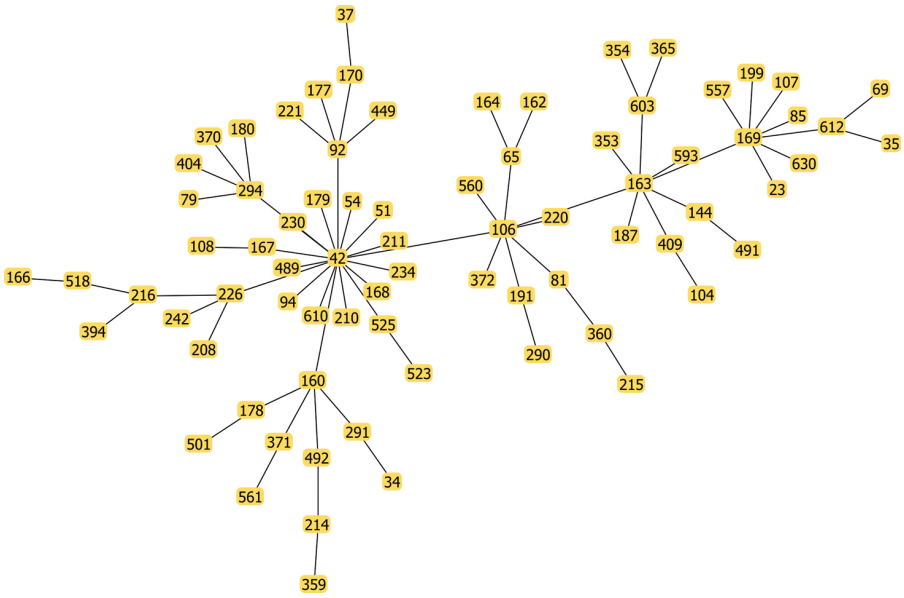

Fig. 2. The clonal complex reconstructed from PubMLST data. The complex comprises *lausannense* strains with publicly available sequenced genomes

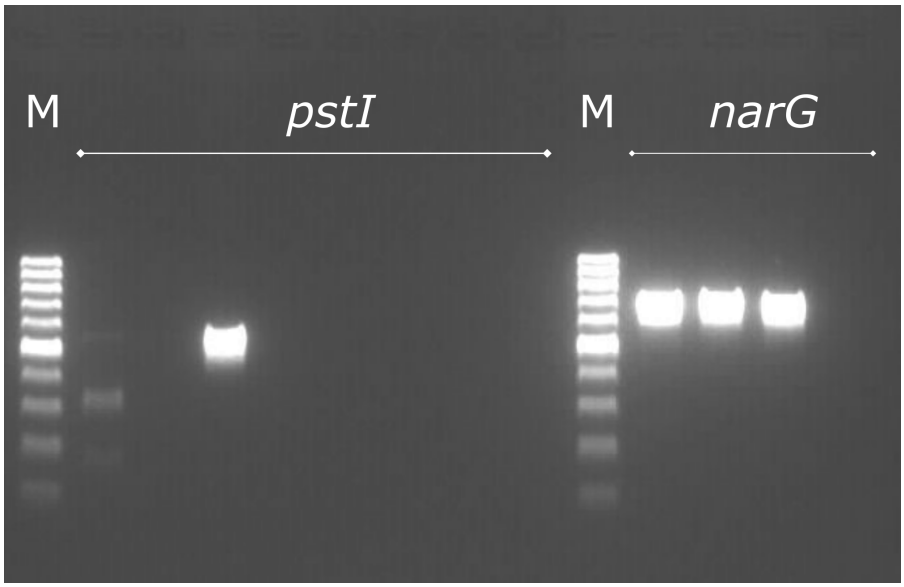

Fig. 3. Gel electrophoresis of PCR products with the following primers: *ptsI*_F — *ptsI*_R and *narG*_F — *narG*_R. M is a GeneRuler 100 bp DNA Ladder (Thermo Fisher Scientific; USA) (example)

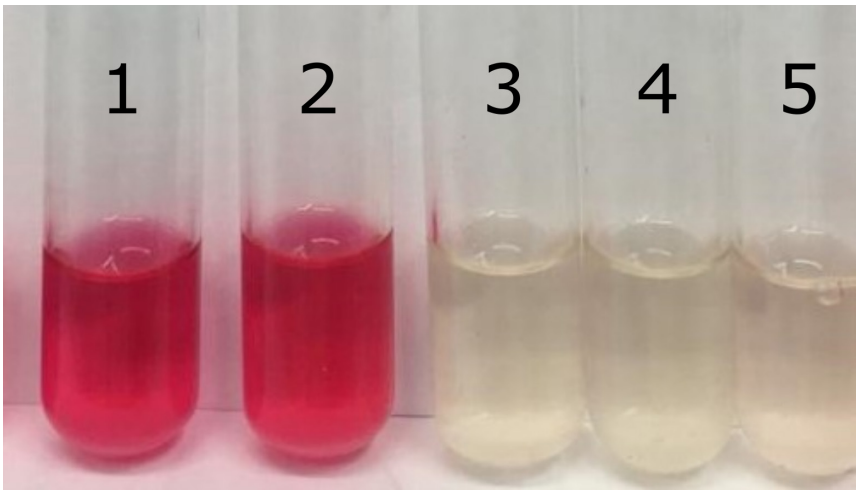

Fig. 4. Saccharolytic acivity of *C. diphtheriae* subsp. *lausannense* strains: the ability to ferment N-acetylglucosamine. The crimson color of the medium means the test results are positive. 1, 2 are isolated strains of *C. diphtheriae* subsp. *lausannense*; 3 is a strain of gravis *C. diphtheriae subsp*. *diphtheriae*; 4 is a strain of mitis *C. diphtheriae* subsp. *diphtheriae*; 5 — negative control

DISCUSSION

We were able to identify the two analyzed *C. diphtheriae* strains isolated from the samples of Russian residents as nontoxigenic representatives of subsp. *lausannense*. Our findings along with the reports of foreign researchers [14, 22] suggest that these strains are ubiquitous. They belong to the sequence type ST199, which is part of the lineage-2 cluster typical to the *lausannense* subspecies, and carry the sequence of the *dtxR* gene characteristic of *lausannense* representatives. The analysis of ortholog groups established the existence of loci specific to the subspecies of *C. diphtheriae*: the region containing the genes of the N-acetylglucosamine-phosphotransferase system (specific to the *lausannense* subspecies) and the region encoding the synthesis of nitrate reductase subunits (specific to the *diphtheriae* subspecies). Our findings are consistent with the results of earlier genomic studies of the *lausannense* subspecies [15] and the studies of the biochemical properties of the belfanti biotype [9, 10]. Primers designed for these genes and the subsequent PCR allowed us to classify the two analyzed strains as *C. diphtheriae* subsp. *lausannense*.

CONCLUSIONS

We have identified the 2 analyzed strains collected on the territory of Russia as nontoxigenic strains of *C. diphtheriae* subsp. *lausannense*. Our findings expand the knowledge of the biological diversity of *C. diphtheriae* and indicate the need for estimating the spread of these microorganisms

References

1. World Health Organization. Diphtheria reported cases. Available from: http://apps.who.int/immunization_monitoring/globalsummary/timeseries/tsincidencediphtheria.html.
2. Yakimova TN, Markina SS, Maksimova NM. Difteriya segodnya. ZNiSO. 2013; 249 (12): 18–9. Russian.
3. O zabolevaemosti difteriey i sostoyanii antitoksicheskogo protivodifteriynogo immuniteta naseleniya Rossii. Information letter № 02/14390-2019-27 from 10.10.2019. Federal Service for Surveillance on Consumer Rights Protection and Human Wellbeing (Rospotrebnadzor). Russian.
4. Romney MG, Roscoe DL, Bernard K, Lai S, Efstratiou A, Clarke AM. Emergence of an invasive clone of nontoxigenic Corynebacterium diphtheriae in the urban poor population of Vancouver, Canada. J Clin Microbiol. 2006 May; 44 (5): 1625–9.
5. Hirata J, Pereira GA, Filardy AA, Gomes DLR, Damasco PV, Rosa ACP, et al. Potential pathogenic role of aggregative-adhering Corynebacterium diphtheriae of different clonal groups in endocarditis. Brazilian J Med Biol Res. 2008; 41 (11): 986–91.
6. Gubler J, Huber-Schneider C, Gruner E, Altwegg M. An Outbreak of Nontoxigenic Corynebacterium diphtheriae Infection: Single Bacterial Clone Causing Invasive Infection Among Swiss Drug Users. Clin Infect Dis. 1998 Nov; 27 (5): 1295–8.
7. FitzGerald RP, Rosser AJ, Perera DN. Non-toxigenic penicillin-resistant cutaneous C. diphtheriae infection: A case report and review of the literature. J Infect Public Health. 2015 Jan 1; 8 (1): 98–100.
8. Edwards B, Hunt AC, Hoskisson PA. Recent cases of non-toxigenic Corynebacterium diphtheriae in Scotland: Justification for continued surveillance. Journal of Medical Microbiology. 2011; (60): 561–2.
9. Funke G, Von Graevenitz A, Clarridge JE, Bernard KA. Clinical microbiology of Coryneform bacteria. Clinical Microbiology Reviews. 1997; (10): 125–59.
10. Bernard KA, Funke G. Corynebacterium. In: Bergey's Manual of Systematics of Archaea and Bacteria. Chichester, UK: John Wiley & Sons, Ltd, 2015; p. 1–70.
11. Trost E, Blom J, de Soares SC, Huang IH, Al-Dilaimi A, Schröder J, et al. Pangenomic study of Corynebacterium diphtheriae that provides insights into the genomic diversity of pathogenic isolates from cases of classical diphtheria, endocarditis, and pneumonia. J Bacteriol. 2012; 194 (12): 3199–215.
12. Sangal V, Burkovski A, Hunt AC, Edwards B, Blom J, Hoskisson PA. A lack of genetic basis for biovar differentiation in clinically important Corynebacterium diphtheriae from whole genome sequencing. Infect Genet Evol. 2014; 21 (November): 54–7.
13. Sangal V, Hoskisson PA. Evolution, epidemiology and diversity of Corynebacterium diphtheriae: New perspectives on an old foe. Infect Genet Evol. 2016; (43): 364–70.
14. Bolt F, Cassiday P, Tondella ML, DeZoysa A, Efstratiou A, Sing A, et al. Multilocus Sequence Typing Identifies Evidence for Recombination and Two Distinct Lineages of Corynebacterium diphtheriae. J Clin Microbiol. 2010; 48 (11): 4177–85.
15. Tagini F, Pillonel T, Croxatto A, Bertelli C, Koutsokera A, Lovis A, et al. Distinct genomic features characterize two clades of Corynebacterium diphtheriae: Proposal of Corynebacterium diphtheriae Subsp. diphtheriae Subsp. nov. and Corynebacterium diphtheriae Subsp. lausannense Subsp. nov. Front Microbiol. 2018 Aug 17; (9): 1743.
16. Li L, Stoeckert CJ, Roos DS. OrthoMCL: identification of ortholog groups for eukaryotic genomes. Genome Res. 2003; 13 (9): 2178–89.
17. Edgar RC. MUSCLE: multiple sequence alignment with high accuracy and high throughput. Nucleic Acids Res. 2004; 32 (5): 1792–7.
18. Price MN, Dehal PS, Arkin AP. FastTree 2 — Approximately maximum-likelihood trees for large alignments. PLoS One. 2010 Mar 10; 5 (3).
19. Nascimento M, Sousa A, Ramirez M, Francisco AP, Carriço JA, Vaz C. PHYLOViZ 2.0: Providing scalable data integration and visualization for multiple phylogenetic inference methods. Bioinformatics. 2017; 33 (1): 128–9.
20. Nakao H, Mazurova IK, Glushkevich T, Popovic T. Analysis of heterogeneity of Corynebacterium diphtheriae toxin gene, tox, and its regulatory element, dtxR, by direct sequencing. Res Microbiol. 1997; 148 (1): 45–54.
21. Chagina IA, Perevarova YuS, Perevarov VV, Chaplin AV, Borisova OYu, Kafarskaya LI, et al. Polymorphism of the dtxR gene in the currently existing strains of Corynebacterium diphtheriae. Bulletin of RSMU. 2017; (1): 31–37.
22. Farfour E, Badell E, Dinu S, Guillot S, Guiso N. Microbiological changes and diversity in autochthonous non-toxigenic Corynebacterium diphtheriae isolated in France. Clin Microbiol Infect. 2013; 19 (10): 980–7.

Литература

1. World Health Organization. Diphtheria reported cases. Available from: http://apps.who.int/immunization_monitoring/globalsummary/timeseries/tsincidencediphtheria.html.
2. Якимова Т. Н., Маркина С. С., Максимова Н. М. Дифтерия сегодня. ЗНиСО. 2013; 249 (12): 18–9.
3. О заболеваемости дифтерией и состоянии антитоксического противодифтерийного иммунитета населения России. Информационное письмо № 02/14390-2019-27 от 10.10.2019. Федеральная служба по надзору в сфере защиты прав потребителей и благополучия человека (Роспотребнадзор).

Russian.
4. Romney MG, Roscoe DL, Bernard K, Lai S, Efstratiou A, Clarke AM. Emergence of an invasive clone of nontoxigenic Corynebacterium diphtheriae in the urban poor population of Vancouver, Canada. J Clin Microbiol. 2006 May; 44 (5): 1625–9.
5. Hirata J, Pereira GA, Filardy AA, Gomes DLR, Damasco PV, Rosa ACP, et al. Potential pathogenic role of aggregative-adhering Corynebacterium diphtheriae of different clonal groups in endocarditis. Brazilian J Med Biol Res. 2008; 41 (11): 986–91.
6. Gubler J, Huber-Schneider C, Gruner E, Altwegg M. An Outbreak of Nontoxigenic Corynebacterium diphtheriae Infection: Single Bacterial Clone Causing Invasive Infection Among Swiss Drug Users. Clin Infect Dis. 1998 Nov; 27 (5): 1295–8.
7. FitzGerald RP, Rosser AJ, Perera DN. Non-toxigenic penicillin-resistant cutaneous C. diphtheriae infection: A case report and review of the literature. J Infect Public Health. 2015 Jan 1; 8 (1): 98–100.
8. Edwards B, Hunt AC, Hoskisson PA. Recent cases of non-toxigenic Corynebacterium diphtheriae in Scotland: Justification for continued surveillance. Journal of Medical Microbiology. 2011; (60): 561–2.
9. Funke G, Von Graevenitz A, Clarridge JE, Bernard KA. Clinical microbiology of Coryneform bacteria. Clinical Microbiology Reviews. 1997; (10): 125–59.
10. Bernard KA, Funke G. Corynebacterium. In: Bergey's Manual of Systematics of Archaea and Bacteria. Chichester, UK: John Wiley & Sons, Ltd, 2015; p. 1–70.
11. Trost E, Blom J, de Soares SC, Huang IH, Al-Dilaimi A, Schröder J, et al. Pangenomic study of Corynebacterium diphtheriae that provides insights into the genomic diversity of pathogenic isolates from cases of classical diphtheria, endocarditis, and pneumonia. J Bacteriol. 2012; 194 (12): 3199–215.
12. Sangal V, Burkovski A, Hunt AC, Edwards B, Blom J, Hoskisson PA. A lack of genetic basis for biovar differentiation in clinically important Corynebacterium diphtheriae from whole genome sequencing. Infect Genet Evol. 2014; 21 (November): 54–7.
13. Sangal V, Hoskisson PA. Evolution, epidemiology and diversity of Corynebacterium diphtheriae: New perspectives on an old foe. Infect Genet Evol. 2016; (43): 364–70.
14. Bolt F, Cassiday P, Tondella ML, DeZoysa A, Efstratiou A, Sing A, et al. Multilocus Sequence Typing Identifies Evidence for Recombination and Two Distinct Lineages of Corynebacterium diphtheriae. J Clin Microbiol. 2010; 48 (11): 4177–85.
15. Tagini F, Pillonel T, Croxatto A, Bertelli C, Koutsokera A, Lovis A, et al. Distinct genomic features characterize two clades of Corynebacterium diphtheriae: Proposal of Corynebacterium diphtheriae Subsp. diphtheriae Subsp. nov. and Corynebacterium diphtheriae Subsp. lausannense Subsp. nov. Front Microbiol. 2018 Aug 17; (9): 1743.
16. Li L, Stoeckert CJ, Roos DS. OrthoMCL: identification of ortholog groups for eukaryotic genomes. Genome Res. 2003; 13 (9): 2178–89.
17. Edgar RC. MUSCLE: multiple sequence alignment with high accuracy and high throughput. Nucleic Acids Res. 2004; 32 (5): 1792–7.
18. Price MN, Dehal PS, Arkin AP. FastTree 2 — Approximately maximum-likelihood trees for large alignments. PLoS One. 2010 Mar 10; 5 (3).
19. Nascimento M, Sousa A, Ramirez M, Francisco AP, Carriço JA, Vaz C. PHYLOViZ 2.0: Providing scalable data integration and visualization for multiple phylogenetic inference methods. Bioinformatics. 2017; 33 (1): 128–9.
20. Nakao H, Mazurova IK, Glushkevich T, Popovic T. Analysis of heterogeneity of Corynebacterium diphtheriae toxin gene, tox, and its regulatory element, dtxR, by direct sequencing. Res Microbiol. 1997; 148 (1): 45–54.
21. Chagina IA, Perevarova YuS, Perevarov VV, Chaplin AV, Borisova OYu, Kafarskaya LI, et al. Polymorphism of the dtxR gene in the currently existing strains of Corynebacterium diphtheriae. Bulletin of RSMU. 2017; (1): 31–37.
22. Farfour E, Badell E, Dinu S, Guillot S, Guiso N. Microbiological changes and diversity in autochthonous non-toxigenic Corynebacterium diphtheriae isolated in France. Clin Microbiol Infect. 2013; 19 (10): 980–7.

SYNTHESIS OF ^{13}C- AND ^{14}C-LABELED LINOLEIC ACIDS FOR USE IN DIAGNOSTIC BREATH TESTS FOR HEPATOBILIARY SYSTEM DISORDERS

Tynio YY[1]✉, Morozova GV[2], Biryukova YuK[3], Sivokhin DA[4], Pozdniakova NV[5], Zylkova MV[3], Bogdanova ES[3], Smirnova MS[3], Shevelev AB[3,6]

[1] Russian State University of Physical Education, Sport, Youth and Tourism, Moscow, Russia

[2] Skryabin Moscow State Academy of Veterinary Medicine and Biotechnology, Moscow, Russia

[3] Vavilov Institute of General Genetics, Moscow, Russia

[4] Sechenov First Moscow State Medical University, Moscow, Russia

[5] Blokhin National Medical Research Center of Oncology, Moscow, Russia

[6] Plekhanov Russian University of Economics, Moscow, Russia

At present, there is a need for a simple, noninvasive, highly specific and sensitive diagnostic test for hepatobiliary system disorders. Compounds labeled with carbon isotopes are widely used in various diagnostic breath tests; they are safe and can reliably detect a metabolic disorder or enzyme deficiency. The aim of this study was to synthesize ^{13}C- and ^{14}C-labeled linoleic acids suitable for use in hepatobiliary breath tests in terms of purity. In the synthesis of ^{13}C-labeled linoleic acid, the chemical yield for 1-bromo-8,11-heptadecadien was 86.4% and the chemical yield for barium carbonate-^{13}C, 96.0%. In the synthesis of ^{14}C-labeled linoleic acid, the chemical yield for 1-bromo-8,11-heptadecadien was 87.39%; for barium carbonate-^{14}C it was 97.1%. The specific radioactivity of ^{14}C-labeled linoleic acids was 45.36 ± 0.02 mCi/g. The radiochemical yield of the reaction was 96.0%. The proposed method is suitable for batch production.

Keywords: breath test, linoleic acid, ^{13}C, ^{14}C, hepatobiliary system, liver disease

Author contribution: Tynio YY conceived and supervised the study; Morozova GV synthesized the final product by carboxylation of the Grignard reagent with ^{13}C and ^{14}C dioxides, did preparative calculations; Biryukova YuK conducted NMR-analysis of the final product; Sivokhin DA analyzed the literature and wrote the manuscript; Pozdniakova NV analyzed the literature; Zylkova MV measured the radioactivity of carbon atoms in the reagents, intermediate and final products; Bogdanova ES analyzed the NMR spectra of the final products; Smirnova MS determined the melting point of the final products; Shevelev AB provided reagents and instrumentation and revised the manuscript.

✉ **Correspondence should be addressed:** Yaroslav Y. Tynio
Sirenevyi bulvar, 4, Moscow, 105122; yytynio@mail.ru

Received: 31.03.2020 **Accepted:** 15.04.2020 **Published online:** 25.04.2020

DOI: 10.24075/brsmu.2020.022

СИНТЕЗ ЛИНОЛЕВОЙ КИСЛОТЫ, МЕЧЕННОЙ ^{13}C И ^{14}C, ДЛЯ ПРОВЕДЕНИЯ ДИАГНОСТИЧЕСКИХ ДЫХАТЕЛЬНЫХ ТЕСТОВ ЗАБОЛЕВАНИЙ ГЕПАТОБИЛИАРНОЙ СИСТЕМЫ

Я. Я. Тыньо[1] ✉, Г. В. Морозова[2], Ю. К. Бирюкова[3], Д. А. Сивохин[4], Н. В. Позднякова[5], М. В. Зылькова[3], Е. С. Богданова[3], М. С. Смирнова[3], А. Б. Шевелёв[3,6]

[1] Российский государственный университет физической культуры, спорта, молодежи и туризма, Москва, Россия

[2] Московская государственная академия ветеринарной медицины и биотехнологии имени К. И. Скрябина, Москва, Россия

[3] Институт общей генетики имени Н. И. Вавилова, Москва, Россия

[4] Первый Московский государственный медицинский университет имени И. М. Сеченова, Москва, Россия

[5] Национальный медицинский исследовательский центр онкологии имени Н. Н. Блохина, Москва, Россия

[6] Российский экономический университет имени Г. В. Плеханова, Москва, Россия

В настоящее время для диагностики заболеваний печени и билиарной системы требуется разработка простого неинвазивного теста с высокой чувствительностью и специфичностью. Соединения, меченные изотопом углерода, уже имеют широкое применение в диагностике различных заболеваний методами дыхательных тестов, безопасны и способны достоверно выявлять метаболические нарушения или дефицит специфичных ферментов в органах. Целью работы было получить линолевую кислоту, меченную ^{13}C и ^{14}C, по степени очистки пригодную для проведения дыхательных тестов в целях диагностики заболеваний гепатобилиарной системы. В предложенном способе химический выход реакции синтеза ^{13}C-линолевой кислоты по 1-бром-8,11-гептадекадиену составил 86,4%, по ^{13}C-карбонату бария — 96,0%. Химический выход реакции синтеза ^{14}C-линолевой кислоты по 1-бром-8,11-гептадекадиену составил 87,39%, по ^{14}C-карбонату бария — 97,1%. Удельная радиоактивность ^{14}C-линолевой кислоты составила 45,36 ± 0,02 мКи/г. Радиохимический выход реакции — 96,0%. Способ удобен для серийного выпуска готового продукта.

Ключевые слова: дыхательный тест, линолевая кислота, ^{13}C, ^{14}C, гепатобилиарная система, заболевания печени

Вклад авторов: Я. Я. Тыньо — идея, общее руководство; Г. В. Морозова — синтез конечных соединений путем карбоксилирования реактива Гриньяра диоксидом ^{13}C и ^{14}C, материальный баланс всей схемы синтеза; Ю. К. Бирюкова — ЯМР-анализ конечного продукта синтеза; Д. А. Сивохин — обзор литературы, подготовка рукописи к печати; Н. В. Позднякова — обзор литературы; М. В. Зылькова — определение уровня радиоактивности атомов углерода в исходных веществах, полупродуктах синтеза и конечных соединениях; Е. С. Богданова — расшифровка ЯМР-спектра конечных продуктов синтеза; М. С. Смирнова — определение температуры плавления конечного соединения; А. Б. Шевелёв — материально-техническое снабжение работы и обеспечение доступа к оборудованию, редактирование перевода рукописи.

✉ **Для корреспонденции:** Ярослав Ярославович Тыньо
Сиреневый бульвар, д. 4, г. Москва, 105122; yytynio@mail.ru

Статья получена: 31.03.2020 **Статья принята к печати:** 15.04.2020 **Опубликована онлайн:** 25.04.2020

DOI: 10.24075/vrgmu.2020.022

The prevalence of chronic liver diseases that progress to cirrhosis, including hepatitis B and C, alcoholic liver disease, toxic hepatitis, primary sclerosing cholangitis, etc., is on the rise [1].

The gold standard for evaluating the liver is a liver biopsy. However, being an invasive procedure, it is associated with the risk of complications and, therefore, cannot be used as a routine test [2]. Adoption of highly reliable, simple and safe noninvasive diagnostic tests into clinical practice [3] will allow clinicians to monitor the efficacy of treatment and estimate the functional reserve of the liver [2, 4]. Such tests have a strong advantage over elastography, as well as APRI [5] and FORNS [6] scores calculated from a patient's laboratory data.

Breath tests rely on the body's ability to metabolize ^{13}C- and ^{14}C-substrates into $^{13}CO_2$ [7] or $^{14}CO_2$ [8] that are subsequently transported in the blood to all organs and tissues and excreted through the lungs; $^{13}CO_2$ or $^{14}CO_2$ concentrations in exhaled breath can be reliably detected by mass spectrometry, nondispersive infrared spectroscopy (NDIRS) and cavity ring-down spectroscopy (CRDS), a spectroscopic technique for measuring absorption of laser light by a gaseous sample introduced into an optical cavity consisting of two high-reflectivity mirrors, where the laser pulse is reflected between them back and forth; in CRDS, absorption is calculated from the time of light decay (the ring-down time) [3, 9]. Thus, a diagnosis can be stablished by analyzing the pharmacokinetics of a radiolabeled compound, such as information about its metabolic pathways and rates and $^{14}CO_2$ concentrations in exhaled breath [10].

Currently existing clinical breath tests used to evaluate liver function measure the metabolic activity of ^{13}C-methacetin [11–13], ^{13}C-galactose, cytochrome P450 (the ^{13}C-aminophenazone test) [14], ^{13}C-phenylalanine [15, 16], ^{13}C-caffeine [17, 18], and $^{13}C3$-trioctanoin (a triglyceride of ^{13}C-labeled octanoic acid esters), which facilitates the diagnosis of exocrine pancreatic insufficiency [7, 19].

Breath tests that harness radiolabeled fatty acids, like linoleic acid, hold great promise for nuclear medicine. Linoleic acid plays an essential role in the energy metabolism of higher organisms and is a building block for a few lipid classes, including neutral fats, phosphoglycerides and cholesterol esters [20].

Linoleic acid is a long-chain water-insoluble compound. Bile secreted by the gall bladder catalyzes hydrolysis of linoleic acid in the small intestine; the reaction results in the formation of mixed micelles. The lack of bile salts in the bile caused by a hepatobiliary disorder slows absorption of a labeled fatty acid, which can be inferred from the isotopic composition of exhaled carbon dioxide [20].

The literature reports an 11-step method for stereospecific synthesis of [1-^{14}C] isomers of monounsaturated fatty acids using olefin inversion [21]. Advantageously, this method allows obtaining monounsaturated fatty acids with a C=C double bond at different positions. However, it is very labor-intensive, involves preparative separation of stereoisomers upon epoxidation and requires an expensive and toxic source of ^{14}C, such as cyanide. These factors impede adoption of the method in large-scale manufacturing.

So far, there are no published reports describing chemical synthesis of ^{13}C- and ^{14}C-labeled derivatives of most common dietary unsaturated fatty acids (linoleic and linolenic) from the most common source (CO_2) Synthesis by biological methods involving protists and fungi, like *Thraustochytrium* and *Mortierella alpina*, has a low radiochemical yield under 60% [22, 23]. The residual isotope is disposed of as waste. Given that ^{14}C is a long-lived radionuclide, this method of synthesis is a hazard to the environment. Another drawback of the method is distribution of labeled atoms along the entire carbon chain of the acyl group, which limits application of synthesized ^{13}C- and ^{14}C-labeled fatty acids in breath tests. The highest sensitivity, repeatability and safety of a liver function breath test can be achieved by using fatty acids in which 100% of labeled atoms are at position 1 (the carboxyl group). Biogenic synthesis often results in a mix of fatty acids differing in their composition. For instance, *Thraustochytrium*-based synthesis produces 10 different fatty acids with a yield range of 0.72 to 21.82%. Besides, 1.9% of the isotope is included in the structure of unidentified fatty acids [23].

This study aimed to develop a method of synthesis of linoleic acids labeled with ^{13}C- and ^{14}C-atoms at position 1 of the acyl group using CO_2 as an isotope source for use in diagnostic tests for hepatobiliary disorders.

METHODS

Equipment

Purity of intermediate and final reaction products was controlled by means of thin-layer chromatography using precoated silica gel Kieselgel 60 F254 TLC plates (Merck; Germany) and Sorbfil plates PTLC-AF-V-UF. The ethyl acetate : n-hexane (1 : 1) eluent mixture was used as a mobile phase. The separated analytes were visualized by exposing the plates to iodine vapors. The structure of the final product was confirmed using nuclear magnetic resonance spectrometers AM-300, 300 MHz (Bruker; Germany) and DRX-500, 500 MHz (Bruker; Germany). Deuterated chloroform was used as a solvent for NMR analysis; NMR spectra were recorded at 300.1 mHz.

Specific activity of tracer carbon was measured by means of a DPM 7001 liquid scintillation counter (RadEk Scientific and Technical Center; Russia) equipped with 2 photomultiplier tubes. Microcalorimetric analysis of mixtures was carried out using a Setaram C80 Calvet calorimeter (SETARAM Instrumentation; France). Potentiometric pH measurements of aqueous solutions were taken with a Sartorius PB-11 basic meter (Sartorius; Germany).

Materials

The following reagents were used in the experiment:

– 1-bromo-8,11-heptadecadien $CH_3(CH_2)_3$-$(CH_2CH{=}CH)_2$ $(CH_2)_7Br$ (AppliChem; USA); molar mass 315.332 g/mol, melting point 3.4 °C, boiling point 112 °C [24];

– the source of a stable carbon isotope: anhydrous barium carbonate-^{13}C (JSC Isotope; Russia); isotopic purity 99.32%; molecular weight 198.3359 g/mol; melting point 1,558 °C;

– the source of a radioactive carbon isotope: anhydrous barium carbonate-^{14}C (Mayak Production Association, Rosatom; Russia); isotopic purity 97.8%; molar mass 199.3359 g/mol; melting point 1,566 °C; specific activity 66.92 mCi/g;

– among other reagents were high-purity dry argon and nitrogen (M-Gas; Russia); ethyl acetate, GOST 22300-76 rev.1-3 (Chimmed; Russia); n-hexane, specifications 2631-158-44493179-13 (Lenreactiv; Russia); magnesium turnings, GOST 804-93 (Interchim; Russia); crystalline iodine, reagent grade (Lenreactiv; Russia); diethyl ether, specifications 2600-001-45682126-13 (Chimmed; Russia); sulfuric acid, pure grade, GOST 4204-77 (Chimmed; Russia); hydrochloric acid, pure grade, GOST 3118-77 (Chimmed; Russia); sodium hydroxide 98% (Fluka; Switzerland; catalog number 71695); acetonitrile, specifications 6-09-3534-87 (Chimservice; Russia).

Absolute ether was prepared as described below. Briefly, diethyl ether was washed in the saturated solution of calcium chloride (50 ml of the solution per 1 L of ether) and dried for 48 h over calcium chloride precalcined at +120 °C for 24 h (130 g of calcinated calcium chloride per 1 L of ether). The reagent was filtered through a fluted paper filter into a dry flask; then, sodium metal (1 g per 1 L of the reagent) was added to the flask. The flask was closed with a holed stopper holding a calcium chloride drying tube. Absolute ether was used to carboxylate the Grignard reagent once hydrogen was no longer released after sodium addition.

RESULTS

Linoleic acid labeled with ^{13}C and ^{14}C at position 1 was synthesized in two steps: 1) preparation of the Grignard reagent; 2) carboxylation of the Grignard reagent with ^{13}C and ^{14}C dioxides.

Preparation of the Grignard reagent

The apparatus for synthesizing the Grignard reagent was set up as shown in Fig. 1 (adopted from [25]).

A 250 ml three-necked flask was clamped on a stand; a reflux condenser with a calcium chloride drying tube and a pressure-equalizing dropping funnel were fitted into the side necks of the flask. An electric stirrer was introduced into the middle neck through an oil seal. Magnesium turnings (3.0 g) and an iodine crystal were put inside the flask. High purity grade argon was blown through the apparatus for 20 min. Then, 160 ml of absolute ether was added into the flask through the dropping funnel, the stirrer was switched on, and 3.78 g (12 mmol) of the 1-bromo-8,11-heptadecadien solution in diethyl ether (80 ml) was added under weak argon flow. To initiate the reaction, the flask was warmed over a water bath until the ether started to boil. Once the reaction started, the water bath was switched off and stirring continued until the magnesium was completely consumed.

Carboxylation of the Grignard reagent with ^{13}C and ^{14}C dioxides

Isotopically labeled acids were obtained through carboxylation of the Grignard reagent using a high vacuum manifold with ports for connecting a reaction flask, a CO_2 source, a mercury column manometer, and tubes for nitrogen inlet/outlet to the line. A cone-shaped three-necked reaction flask resistant to freezing was equipped with a magnetic stirrer that allowed carrying out reactions in vacuum at low temperatures (Fig. 2; adopted from [25]).

The source of ^{13}C and ^{14}C dioxides was represented by 5.4 mmol of isotopically labeled barium carbonate (a weighted amount of 1.071 g for the ^{13}C isotope and a weighted amount of 1.076 g for the ^{14}C isotope) placed in a round-bottom flask. The flask was connected to a pressure-equalizing dropping funnel filled with concentrated sulfuric acid. This part of the apparatus was connected to the vacuum manifold via a desiccant-containing tube.

First, the apparatus was evacuated to 0.1 mmHg using an oil pump and filled with dry nitrogen. Then, the Grignard reagent solution prepared from 6 mmol of 1-bromo-8,11-heptadecadien (half of the total synthesized amount) was taken up into a prewashed dispenser pipette filled with nitrogen and quickly injected into the flask. The free side neck of the flask was closed with a stopper. The flask was cooled in liquid nitrogen, and the apparatus was evacuated to 0.1 mmHg. Then, the solution in the reaction vessel was thawed to –77 °C in a mixture of dry ice and acetone, frozen in liquid nitrogen, and the apparatus was again evacuated to remove nitrogen.

Carboxylation of the Grignard reagent was performed at –20 °C under continuous stirring. To initiate liberation of labeled CO_2, concentrated sulfuric acid was slowly added to barium carbonate through the dropping funnel, making sure that the pressure did not exceed 500 mmHg. To finish off liberation of labeled CO_2, the reaction flask was carefully heated until barium carbonate was completely dissolved. After the Grignard reagent was depleted, manometer readings indicated that CO_2 pressure in the apparatus was no longer decreasing. For both $^{13}CO_2$ and $^{14}CO_2$ the reaction was completed in 15 minutes.

The reaction flask with the Grignard reagent was cooled in liquid nitrogen to collect the remaining labeled CO_2; the stopcock connecting the apparatus to the source of labeled CO_2, was closed and the reaction mass was stirred for 15 min at –20 °C until labeled CO_2 was fully absorbed. Then, the apparatus was filled with nitrogen and connected to the air inlet tube. The obtained complex was decomposed by diluted hydrochloric acid. The acidified mixture was extracted in ether. The resulting ether extract was treated with 100 mM NaOH,

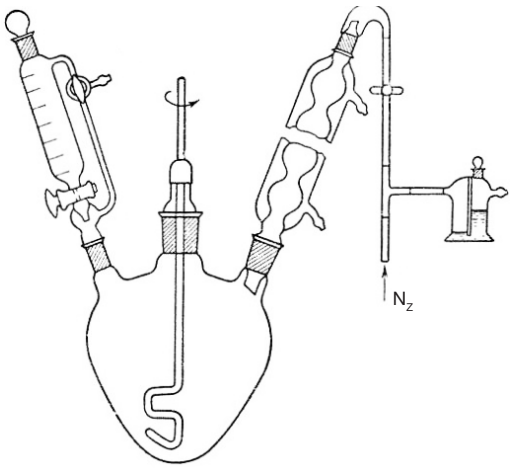

Fig. 1. The apparatus for preparing the Grignard reagent in argon atmosphere

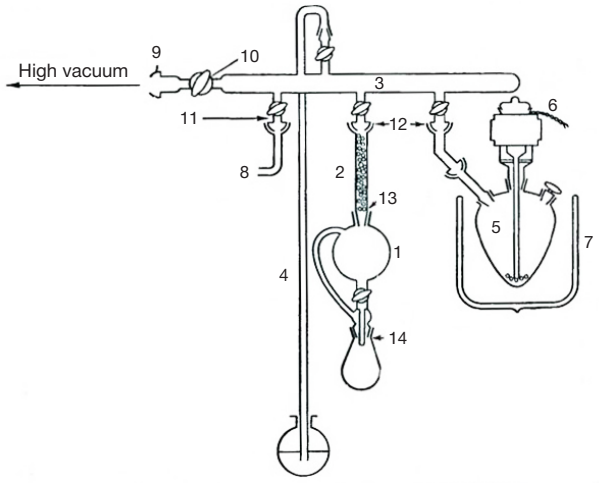

Fig. 2. The apparatus for carboxylation of the Grignard reagent. *1* — source of carbon dioxide; *2* — drierite-containing tube; *3* — high-vacuum manifold (tube diameter of 13 mm); *4* — mercury column manometer; *5* — flask; *6* — 3-phase magnetic stirrer (110 V); *7* — cooling bath; *8* — nitrogen inlet; *9* — glass joint, 28/12; *10* — stopcock, bore size 3 mm; *11* — stopcock, bore size 2 mm; *12* — ground-glass joint, 18/9; *13* — ground-glass joint, 14/35; *14* — ground-glass joint, 14/20

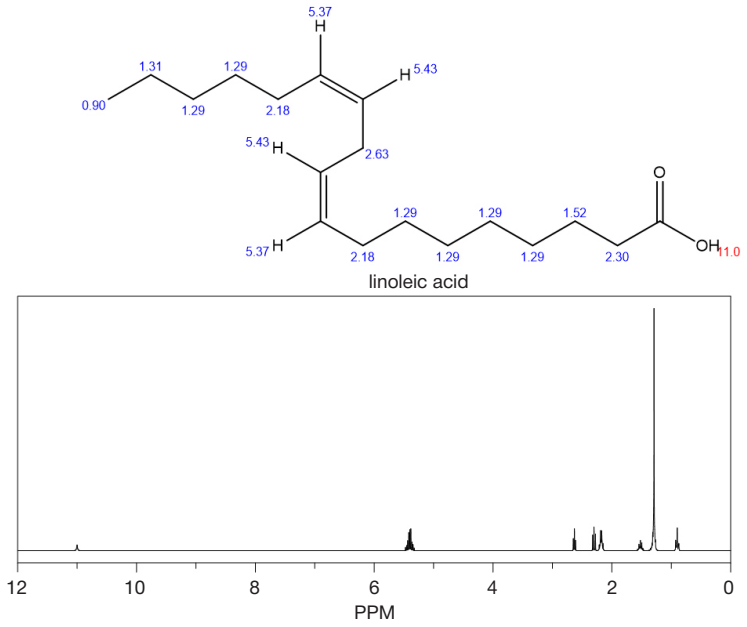

Fig. 3. The ^{1}H-NMR spectrum of ^{14}C-labeled linoleic acid

and the obtained alkaline solution was acidified to achieve pH = 7.0. The released acid was filtered. The precipitate was collected, washed in water and recrystallized from acetonitrile at –20 °C (for linoleic acid, t_{freez} was assumed to be –11 °C).

The total mass of the synthesized ^{13}C-linoleic acid equaled 1,459 mg (5.184 mmol). The final chemical yield of 1-bromo-8,11-heptadecadien was 86.4%; the $^{13}CO_2$ yield was 96.0%. For the final product, the empirically measured freezing point was –11.0 °C.

The total mass of the synthesized ^{14}C-linoleic acid was 1,480 mg (5.243 mmol). The yield of 1-bromo-8,11-heptadecadien was 87.39%; the $^{13}CO_2$ yield was 97.1%. The specific activity of ^{14}C-linoleic acid was measured using the scintillation counter and equaled 45.36 ± 0.02 mCi/g. Thus, the total radiation and chemical yield was 96.0%. The final reaction product had a freezing point at –10.7 °C.

The synthesized ^{13}C- and ^{14}C-linoleic acids were analyzed by means of thin layer chromatography using Kieselgel 60 F254 plates; the ethyl acetate : n-hexane (1 : 1) eluent mixture was used as a mobile phase (see *Methods*); the obtained linoleic acids contained admixtures. ^{13}C-linoleic acid made up 98.2% of the dry product weight after elution.

The ^{1}H NMR spectrum of ^{14}C-linoleic acid was compared to the reference spectrum of $1S/C_{18}H_{32}O_2/c1-2-3-4-5-6-7-8-9-10-11-12-13-14-15-16-17-18(19)20/h6-7, 9-10H, 2-5, 8, 11-17H_2$, $1H_3$, (H, 19, 20)/b7-6-, 10-9 described in the literature [26]; the synthesized compound matched the structure of the linoleic acid (Fig. 3).

DISCUSSION

The proposed method of synthesis of ^{13}C- and ^{14}C-labeled linoleic acids has a few strengths, including shorter reaction time, reduced loss of labeled CO_2 and increase in the total chemical and radiation yield. Importantly, the isotopically labeled atoms are not distributed along the entire carbon chain of acyl but instead occur only at position 1.

Shorter reaction time due to the optimization of reagents ratios and measurements of the CO_2 pressure in the system taken to check the completion of Grignard reagent carboxylation ensured operational simplicity and cost-effectiveness of the method. The method significantly increases the radiation and chemical yield of the product in comparison with other known techniques [21–23]. The labeled isotope is almost entirely included in the final reaction product, meaning that the amount of radioactive waste is near zero. This makes the proposed method appealing in terms of cost reduction, given that disposal of long-lived radioactive waste is difficult and expensive.

The amount and purity of the synthesized ^{13}C- and ^{14}C-linoleic acids make them suitable for use in preclinical trials of acute, subchronic, chronic and other types of toxicity [27]. Once the safety of the compounds has been confirmed, they can be recommended for clinical trials of hepatobiliary function breath tests.

CONCLUSIONS

This paper describes a method of synthesis of ^{13}C- and ^{14}C-linoleic acids with carbon isotopes occurring at position 1. The method is advantageously simple and consists of 2 steps instead of 11 reported in other works. For ^{14}C, the radiochemical yield of the method is very close to quantitative (96%), which almost rules out the issues associated with radioactive waste disposal. The method requires no sophisticated analytical and preparative instrumentation, which may facilitate its adoption to batch production.

References

1. Liou IW. Management of end-stage liver disease. Med Clin North Am. 2014; 98 (1): 119–52. DOI: 10.1016/j.mcna.2013.09.006.
2. Musialik J, Jonderko K, Kasicka-Jonderko A, Buschhaus M. $^{13}CO_2$ breath tests in non-invasive hepatological diagnosis. Prz Gastroenterol. 2015; 10 (1): 1–6.
3. Modak AS. Stable isotope breath tests in clinical medicine: A review. J Breath Res. 2007; 1 (1): R1–R13. DOI: 10.1088/1752-7155/1/1/014003.
4. Razlan H, Marzuki NM, Tai M-L S, Shamsul Tze-Zen Ong A-S, Mahadeva S. Diagnostic value of the ^{13}C-methacetin breath test in various stages of chronic liver disease. Gastroenterol Res Pract. 2011; 2011 (1): 1–6. DOI: 10.1155/2011/235796.
5. Forns X, Ampurdanès S, Llovet JM, Aponte J, Quintó L, Martínez-Bauer E, et al. Identification of chronic hepatitis C patients without hepatic fibrosis by a simple predictive model. Hepatology, 2002; 36 (4I): 986–92. DOI: 10.1053/jhep.2002.36128.
6. Wai CT, Greenson KJ, Fontana RJ, Kalbfleisch JD, Jorge AM, Hari SC, et al. A simple noninvasive index can predict both significant fibrosis and cirrhosis in patients with chronic hepatitis C. Hepatology. 2003; 38 (2): 518–26. DOI: 10.1053/jhep.2003.50346.
7. Elman AR, Rapoport SI. Stabil'no-izotopnaja diagnostika v Rossii: itogi i perspektivy. ^{13}C-preparaty, pribory, metody. Klin med. 2014; 92 (7): 5–11. Russian.
8. Balãn H, Gold CA, Dworkin HJ, McCormick VA, Freitas JE. Procedure Guideline for Carbon-14-Urea Breath Test. J Nucl Med. 2016; 39 (11): 2012–14.
9. Plavnik RG. ^{13}S-Ureaznyj dyhatel'nyj test na *Helicobacter pylori* (klinicheskie i organizacionnye aspekty). M.: MEDPRAKTIKA-M, 2017; 36 s.
10. Grattagliano I, Lauterburg BH, Palasciano G, and Portincasa P. ^{13}C-breath tests for clinical investigation of liver mitochondrial function. Eur J Clin Invest. 2010; 40 (9): 843–50. DOI: 10.1111/j.1365-2362.2010.02331.x.
11. Gorowska-Kowolik K, Chobot A, and Kwiecien J. ^{13}C-Methacetin Breath Test for Assessment of Microsomal Liver Function: Methodology and Clinical Application. Gastroenterol Res Pract. 2017; 2017 (1): 1–5.
12. Moran S, Mina A, Duque X, Ortiz-Olvera N, Rodriguez-Leal G, Sierra-Ramírez JA, et al. The utility of the ^{13}C-methacetin breath test in predicting the long-term survival of patients with decompensated cirrhosis. J Breath Res. 2017; 11 (3): 1–28. DOI: 10.1088/1752-7163/aa7b99.
13. Elman AR, Korneeva GA, Noskov YuG, Khan VN, Shishkina EYu, Negrimovski VM, Syntheses of products labeled with ^{13}C isotope for medicine diagnosis. Russian Chemical Journal. 2013; LVII (5): 3–24.
14. Giannini EG, Alberto F, Paolo B, Federica B, Federica M, et al. ^{13}C-galactose breath test and ^{13}C-aminopyrine breath test for the study of liver function in chronic liver disease. Clin Gastroenterol Hepatol. 2005; 3 (3): 279–85. DOI: 10.1016/S1542-3565(04)00720-7.
15. Moran S, Gallardo-Wong I, Rodriguez-Leal G, McCollough P, Mendez J, Castañeda B, et al. L-[1-^{13}C]phenylalanine breath test in patients with chronic liver disease of different etiologies. Isotopes Environ Health Stud. 2009; 45 (3): 192–7. DOI: 10.1080/10256010903083995.
16. Zhang GS, Bao ZJ, Zou J, Yin SM, Huang YQ, Huang H, et al. Clinical research on liver reserve function by ^{13}C-phenylalanine breath test in aged patients with chronic liver diseases. BMC Geriatr. 2010; 10 (23): 1–8 . DOI: 10.1186/1471-2318-10-23.
17. Schmilovitz-Weiss H, Niv Y, Pappo O, Halpern M, Sulkes J, Braun M, et al. The ^{13}C-caffeine breath test detects significant fibrosis in patients with nonalcoholic steatohepatitis. J Clin Gastroenterol. 2008; 42 (4): 408–12, 2008. DOI: 10.1097/MCG.0b013e318046ea65.
18. Gordon J, Park H, Wiseman E, George J, Katelaris PH, Seow F, et al. Non-invasive estimation of liver fibrosis in non-alcoholic fatty liver disease using the ^{13}C-caffeine breath test. J Gastroenterol Hepatol. 2011; 26 (9): 1411–6. DOI: 10.1111/j.1440-1746.2011.06760.x.
19. Braden B. ^{13}C breath tests for the assessment of exocrine pancreatic function. Pancreas. 2010; 39 (7): 955–9. DOI: 10.1097/MPA.0b013e3181dbf330.
20. Titov VN. Klinicheskaja biohimija zhirnyh kislot, lipidov i lipoproteinov. Gipolipidemicheskaja terapija i profilaktika ateroskleroza. Kliniko-laboratornyj konsilium. 2014; 1: 4–29. Russian.
21. Georgin D, Taran F, Mioskowski C. A divergent synthesis of [1-^{14}C]-mono-E isomers of fatty acids. Chem Phys Lipids. 2003; 125 (1): 83–91.
22. Kawashima H, Akimoto K, Tsuyoshi F, Hideo N, Kyoko K, Sakayu S. Preparation of ^{13}C-labeled polyunsaturated fatty acids by an arachidonic acid-producing fungus Mortierella alpina 1S-4. Analytical Biochemistry. 1995; 229 (2): 317–22. DOI: 10.1006/abio.1995.1419.
23. Zhao X, Qiu X. Analysis of the biosynthetic process of fatty acids in Thraustochytrium. Biochimie. 2018; 144 (1): 108–14.
24. Lide DR. CRC Handbook of Chemistry and Physics. 86th ed. CRC Press. 2006; p. 3–320.
25. Pozdeev VV, Tyño YJ, Morozova GV, Bychenko AB, Biryukova YK, Shevelev AB; LLC "GK Our World". Method of Synthesis of Linoleic and Linolenic Acids Labeled with Carbon Isotopes ^{13}C and 14C. RF Patent # 2630691. 12.09.2017.
26. Shaaban M, Abd-Alla HI, Hassan AZ, Aly HF, Ghani MA. Chemical characterization, antioxidant and inhibitory effects of some marine sponges against carbohydrate metabolizing enzymes. Org Med Chem Lett. 2012; 2 (1): 30.
27. Mironov AN. Rukovodstvo po provedeniju doklinicheskih issledovanij lekarstvennyh sredstv. M.: Grif i K, 2012; 994 s.

Литература

1. Liou IW. Management of end-stage liver disease. Med Clin North Am. 2014; 98 (1): 119–52. DOI: 10.1016/j.mcna.2013.09.006.
2. Musialik J, Jonderko K, Kasicka-Jonderko A, Buschhaus M. $^{13}CO_2$ breath tests in non-invasive hepatological diagnosis. Prz Gastroenterol. 2015; 10 (1): 1–6.
3. Modak AS. Stable isotope breath tests in clinical medicine: A review. J Breath Res. 2007; 1 (1): R1–R13. DOI: 10.1088/1752-7155/1/1/014003.
4. Razlan H, Marzuki NM, Tai M-L S, Shamsul Tze-Zen Ong A-S, Mahadeva S. Diagnostic value of the ^{13}C-methacetin breath test in various stages of chronic liver disease. Gastroenterol Res Pract. 2011; 2011 (1): 1–6. DOI: 10.1155/2011/235796.
5. Forns X, Ampurdanès S, Llovet JM, Aponte J, Quintó L, Martínez-Bauer E, et al. Identification of chronic hepatitis C patients without hepatic fibrosis by a simple predictive model. Hepatology, 2002; 36 (4I): 986–92. DOI: 10.1053/jhep.2002.36128.
6. Wai CT, Greenson KJ, Fontana RJ, Kalbfleisch JD, Jorge AM, Hari SC, et al. A simple noninvasive index can predict both significant fibrosis and cirrhosis in patients with chronic hepatitis C. Hepatology. 2003; 38 (2): 518–26. DOI: 10.1053/jhep.2003.50346.
7. Эльман А. Р., Рапопорт С. И. Стабильно-изотопная диагностика в России: итоги и перспективы. ^{13}C-препараты, приборы, методы. Клин. мед. 2014; 92 (7): 5–11.
8. Balãn H, Gold CA, Dworkin HJ, McCormick VA, Freitas JE. Procedure Guideline for Carbon-14-Urea Breath Test. J Nucl Med. 2016; 39 (11): 2012–14.
9. Плавник Р. Г. ^{13}C-Уреазный дыхательный тест на *Helicobacter pylori* (клинические и организационные аспекты). М.: МЕДПРАКТИКА-М, 2017; 36 с.
10. Grattagliano I, Lauterburg BH, Palasciano G, and Portincasa P. ^{13}C-breath tests for clinical investigation of liver mitochondrial function. Eur J Clin Invest. 2010; 40 (9): 843–50. DOI: 10.1111/j.1365-2362.2010.02331.x.
11. Gorowska-Kowolik K, Chobot A, and Kwiecien J. ^{13}C-Methacetin Breath Test for Assessment of Microsomal Liver Function:

Methodology and Clinical Application. Gastroenterol Res Pract. 2017; 2017 (1): 1–5.
12. Moran S, Mina A, Duque X, Ortiz-Olvera N, Rodriguez-Leal G, Sierra-Ramírez JA, et al. The utility of the ^{13}C-methacetin breath test in predicting the long-term survival of patients with decompensated cirrhosis. J Breath Res. 2017; 11 (3): 1–28. DOI: 10.1088/1752-7163/aa7b99.
13. Эльман А. Р., Корнеева Г. А, Носков Ю. Г, Хан В. Н., Шишкина Е. Ю., Негримовски В. М. и др. Синтез продуктов, меченных изотопом ^{13}C, для медицинской диагностики. Рос. хим. ж. (Ж. Рос. хим. об-ва им. Д. И. Менделеева). 2013; LVII (5): 3–24.
14. Giannini EG, Alberto F, Paolo B, Federica B, Federica M, et al. ^{13}C-galactose breath test and ^{13}C-aminopyrine breath test for the study of liver function in chronic liver disease. Clin Gastroenterol Hepatol. 2005; 3 (3): 279–85. DOI: 10.1016/S1542-3565(04)00720-7.
15. Moran S, Gallardo-Wong I, Rodriguez-Leal G, McCollough P, Mendez J, Castañeda B, et al. L-[1-^{13}C]phenylalanine breath test in patients with chronic liver disease of different etiologies. Isotopes Environ Health Stud. 2009; 45 (3): 192–7. DOI: 10.1080/10256010903083995.
16. Zhang GS, Bao ZJ, Zou J, Yin SM, Huang YQ, Huang H, et al. Clinical research on liver reserve function by ^{13}C-phenylalanine breath test in aged patients with chronic liver diseases. BMC Geriatr. 2010; 10 (23): 1–8 . DOI: 10.1186/1471-2318-10-23.
17. Schmilovitz-Weiss H, Niv Y, Pappo O, Halpern M, Sulkes J, Braun M, et al. The ^{13}C-caffeine breath test detects significant fibrosis in patients with nonalcoholic steatohepatitis. J Clin Gastroenterol. 2008; 42 (4): 408–12, 2008. DOI: 10.1097/MCG.0b013e318046ea65.
18. Gordon J, Park H, Wiseman E, George J, Katelaris PH, Seow F, et al. Non-invasive estimation of liver fibrosis in non-alcoholic fatty liver disease using the ^{13}C-caffeine breath test. J Gastroenterol Hepatol. 2011; 26 (9): 1411–6. DOI: 10.1111/j.1440-1746.2011.06760.x.
19. Braden B. ^{13}C breath tests for the assessment of exocrine pancreatic function. Pancreas. 2010; 39 (7): 955–9. DOI: 10.1097/MPA.0b013e3181dbf330.
20. Титов В. Н. Клиническая бихимия жирных кислот, липидов и липопротеинов. Гиполипидемическая терапия и профилактика атеросклероза. Клинико-лабораторный консилиум. 2014; 1: 4–29.
21. Georgin D, Taran F, Mioskowski C. A divergent synthesis of [1-^{14}C]-mono-E isomers of fatty acids. Chem Phys Lipids. 2003; 125 (1): 83–91.
22. Kawashima H, Akimoto K, Tsuyoshi F, Hideo N, Kyoko K, Sakayu S. Preparation of ^{13}C-labeled polyunsaturated fatty acids by an arachidonic acid-producing fungus Mortierella alpina 1S-4. Analytical Biochemistry. 1995; 229 (2): 317–22. DOI: 10.1006/abio.1995.1419.
23. Zhao X, Qiu X. Analysis of the biosynthetic process of fatty acids in Thraustochytrium. Biochimie. 2018; 144 (1): 108–14.
24. Lide DR. CRC Handbook of Chemistry and Physics. 86th ed. CRC Press. 2006; p. 3–320.
25. Поздеев В. В., Тыньо Я. Я., Морозова Г. В., Быченко А. Б., Бирюкова Ю. К., Шевелев А. Б., авторы; ООО «ГК Наш Мир», патентообладатель. Способ синтеза линолевой и линоленовой кислот, меченных изотопами углерода ^{13}C и ^{14}C. Патент РФ № 2630691. 12.09.2017.
26. Shaaban M, Abd-Alla HI, Hassan AZ, Aly HF, Ghani MA. Chemical characterization, antioxidant and inhibitory effects of some marine sponges against carbohydrate metabolizing enzymes. Org Med Chem Lett. 2012; 2 (1): 30.
27. Миронов А. Н. Руководство по проведению доклинических исследований лекарственных средств. М.: Гриф и К, 2012; 994 с.

TRANSABDOMINAL ULTRASOUND AS A SCREENING STAGE FOR THE DIAGNOSIS OF TUBERCULOUS PERITONITIS

Plotkin DV[1,2] ✉, Kirillova OV[1], Nikanorov AV[3], Reshetnikov MN[1], Shtykhno AO[1], Loshkareva EO[2], Korotkova ES[2], Sinitsyn MV[1]

[1] Moscow Research and Clinical Center for TB Control, Moscow, Russia

[2] Pirogov Russian National Research Medical University, Moscow, Russia

[3] Loginov Moscow Clinical Scientific Practical Center, Moscow, Russia

In recent years, the incidence of tuberculous peritonitis increased. Peritoneal tuberculosis is difficult to diagnose, and often the diagnosis is verified with significant delay. In clinical practice, a quick and affordable diagnostic radiology method, ultrasonography (USG), is proposed for patients with suspected tuberculous peritonitis. The study was aimed to describe the sonographic semiology of tuberculous peritonitis, to create the integrated scale for the individual peritoneal tuberculosis sonographic symptoms significance assessment, and to determine the role of ultrasound imaging in the diagnosis verification. Retrospective study of the invasive and ultrasound investigation results of 37 patients with confirmed tuberculous peritonitis was carried out in 2009–2019. Similar data obtained by investigation of 28 patients with the disorders which often mimic the tuberculous peritonitis (peritoneal carcinomatosis and sarcoidosis, non-specific ascites) were used as a comparison group. Direct and indirect signs of peritoneal lesion in patients with tuberculosis were identified. On the basis of that, an integral scale for the individual sonographic symptoms significance assessment was created. Each sonographic symptom received a 0–3 score. Assessment of those sonographic signs visualization allowed us to evaluate the probability of the disorder's tuberculous etiology. The following data were obtained: score under 4 corresponded to low probability, score 5–8 corresponded to medium probability, and score over 9 corresponded to high probability of tuberculous peritonitis based on the visualization of all described songraphic symptoms. The proposed integrated scale for the sonographic signs assessment allows the clinician to verify the tuberculous peritonitis diagnosis based on the ultrasound imaging data or to select the further tactics of diagnosis.

Keywords: ultrasonography, peritoneal tuberculosis, peritonitis, carcinomatosis, sarcoidosis

Author contribution: Plotkin DV, Reshetnikov MN, Nikanorov AV, Sinitsyn MV — study concept and design, overall management; Kirillova OV, Shtykhno AO, Loshkareva EO — sample collection; Korotkova ES, Plotkin DV — statistical analysis; Plotkin DV, Reshetnikov MN, Kirillova OV, Nikanorov AV — data analysis; Plotkin DV, Reshetnikov MN — manuscript writing; Kirillova OV, Shtykhno AO, Nikanorov AV — editing.

Compliance with ethical standards: the study was approved by the Ethics Committee of the Moscow Research and Clinical Center for TB Control (protocol №.12 dated December 9, 2019). The informed consent was submitted by all study participants.

✉ **Correspondence should be addressed:** Dmitry V. Plotkin
Ostrovityanova, 1, Moscow, 117997; kn13@list.ru

Received: 17.03.2020 **Accepted:** 04.04.2020 **Published online:** 12.04.2020

DOI: 10.24075/brsmu.2020.018

ТРАНСАБДОМИНАЛЬНОЕ УЛЬТРАЗВУКОВОЕ СКАНИРОВАНИЕ КАК СКРИНИНГОВЫЙ ЭТАП ДИАГНОСТИКИ ТУБЕРКУЛЕЗНОГО ПЕРИТОНИТА

Д. В. Плоткин[1,2] ✉, О. В. Кириллова[1], А. В. Никаноров[3], М. Н. Решетников[1], А. О. Штыхно[1], Е. О. Лошкарева[2], Е. С. Короткова[2], М. В. Синицын[1]

[1] Московский городской научно-практический центр борьбы с туберкулезом, Москва, Россия

[2] Российский национальный исследовательский медицинский университет имени Н. И. Пирогова, Москва, Россия

[3] Московский клинический научный центр имени А. С. Логинова, Москва, Россия

За последние годы отмечен рост числа случаев туберкулезного перитонита. Туберкулез брюшины — сложный объект для диагностики и нередко верификация диагноза происходит со значительными задержками. В клинической практике предложен непродолжительный и доступный метод лучевой диагностики при подозрении на туберкулезный перитонит — ультразвуковое исследование (УЗИ). Целью работы было описать эхо-семиотику туберкулезного перитонита с созданием интегральной шкалы оценки значимости отдельных эхо-симптомов туберкулеза брюшины и определить роль УЗ-сканирования в верификации диагноза. Произведен ретроспективный анализ инвазивной и УЗ-диагностики 37 пациентов с подтвержденным туберкулезным перитонитом в период с 2009 по 2019 г. В качестве группы сравнения использовали такие же данные исследований у 28 больных с заболеваниями, часто имитирующими туберкулезный перитонит (канцероматозом и саркоидозом брюшины, неспецифическим асцитом). Выделены прямые и косвенные признаки поражения брюшины при туберкулезе, на основании этого создана интегральная шкала оценки значимости отдельных эхо-симптомов. С этой целью каждому эхо-симптому присваивали от 0 до 3 баллов. При оценке визуализации описанных эхо-признаков возможно прогнозировать вероятность туберкулезной этиологии заболевания. Получены следующие статистические данные: низкая вероятность наличия туберкулезного перитонита при оценке визуализации всех описанных эхо-симптомов — до 4 баллов, средняя — от 5 до 8 баллов, высокая 9 и более баллов. Разработанная интегральная схема оценки УЗ-признаков позволяет клиницисту на основании эхографического исследования верифицировать туберкулезный перитонит или выбрать дальнейшую тактику в диагностическом поиске.

Ключевые слова: ультразвуковое исследование, туберкулез брюшины, перитонит, канцероматоз, саркоидоз

Вклад авторов: Д. В. Плоткин, М. Н. Решетников, А. В. Никаноров, М. В. Синицын — разработка концепции и дизайна исследования, общая ответственность; О. В. Кириллова, А. О. Штыхно, Е. О. Лошкарева — сбор материала; Е. С. Короткова, Д. В. Плоткин — статистическая обработка данных; Д. В. Плоткин, М. Н. Решетников, О. В. Кириллова, А. В. Никаноров — анализ полученных данных; Д. В. Плоткин, М. Н. Решетников — подготовка текста; О. В. Кириллова, А. О. Штыхно, А. В. Никаноров — редактирование.

Соблюдение этических стандартов: исследование одобрено этическим комитетом Московского научно-практического центра борьбы с туберкулезом (протокол № 12 от 9 декабря 2019 г.). Все пациенты подписали добровольное информированное согласие.

✉ **Для корреспонденции:** Дмитрий Владимирович Плоткин
ул. Островитянова, д. 1, г. Москва, 117997; kn13@list.ru

Статья получена: 17.03.2020 **Статья принята к печати:** 04.04.2020 **Опубликована онлайн:** 12.04.2020

DOI: 10.24075/vrgmu.2020.018

After the 45-year neglection, tuberculous peritonitis showed up again in European and Russian clinics. That was due to HIV pandemic, people's migration from endemic regions, emergence of extensively drug-resistant mycobacteria strains and drug-induced immunosuppression. Peritoneal tuberculosis (primary peritonitis) is a chronic inflammatory process with nonspecific clinical manifestations, which often causes significant difficulties and a delay in diagnosis [1–3]. According to the vast majority of scientists, the most accurate method of peritoneal tuberculosis verification is the diagnostic laparoscopic biopsy of the abdominal cavity serous membrane affected areas [4–5]. The growth of Mycobacterium tuberculosis (MTB) from exudates demonstrates the positive result 4–6 weeks after inoculation only in 10% of cases, and PCR analysis of effusion is informative in one-third of cases and also requires invasive intervention [5–6]. In clinical practice, short-term and affordable diagnostic radiology methods, ultrasonography and computed tomography (CT), are the first choice for patients with suspected tuberculous peritonitis [1, 7, 8], however, in most cases, they do not allow one to identify the inflammatory process in the peritoneum accurately.

Ultrasonography is the most harmless, efficient and cost-effective imaging method which can help clinicians to make decisions on the diagnosis and timely treatment of tuberculous peritonitis. Today, transabdominal ultrasound plays an important role in assessment of inflammatory, benign, and malignant diseases of the peritoneum, both in outpatient and inpatient settings. Medical literature describes different sonographic signs allowing one to suspect tuberculous peritonitis, as well as methods allowing one to distinguish between tuberculous peritonitis and peritoneal carcinomatosis or nonspecific ascites [7–11]. The accuracy of these methods depends on the qualification and experience of the doctor, as well as the class of equipment used. Over the past 10 years, most studies report the individual observations of the TB-associated peritoneal changes' visualization. However, there is no analysis of the prevalence of symptoms and their combinations [9, 11].

The study was aimed to describe the sonographic semiology of tuberculous peritonitis, to create the integrated scale for assessment of the significance of individual sonographic symptoms of peritoneal tuberculosis, and to determine the role of ultrasonography in the diagnosis verification.

METHODS

In 2009–2019, in the TB surgery department of the Hospital № 2 of the Moscow Research and Clinical Center for TB Control, Moscow, a retrospective study of the ultrasonography results of 37 patients with tuberculous peritonitis was carried out. The main clinical manifestation was a large volume of effusion in the abdominal cavity (exudative, adhesive, caseous and mixed forms of tuberculous peritonitis). Inclusion criteria: peritoneal tuberculosis diagnosed in all 37 patients via histological (100%) and bacterioscopic (81.1%) examination of peritoneal biopsies obtained using laparoscopic invasive methods. Among hospitalized patients, males predominated (22 men, 59.5%; 15 women, 40.5%) aged 20–65 (median age 37.2). Twenty three patients (62.7%) were HIV-positive, 34 patients (91.6%) had pulmonary tuberculosis, mostly the infiltrative and disseminated forms. Exclusion criteria: no histological confirmation of peritoneal tuberculosis.

For the comparison group, the patients were selected with the diseases verified using laparoscopy, histological and laboratory analysis data, which most often mimic tuberculous peritonitis, both in clinical picture and ultrasonography. The control group included 28 patients with non-specific ascites of various origin (21 patients; 75.0%), peritoneal sarcoidosis (1 patient; 3.5%) and peritoneal carcinomatosis (6 patients; 21.5%). The patients were aged 29–54 (median age 36.1). Pulmonary tuberculosis was diagnosed in all patients, 10 patients (35.7%) of the control group were HIV-positive. Exclusion criteria for the control group: tuberculous granulomas and acid resistant mycobacteria in the peritoneal biopsy; mycobacterial DNA positive effusion PCR-test.

The patients were examined using polypositional radiography, thoracic computed tomography, abdominal ultrasonography, diagnostic video-assisted laparoscopy, laboratory and morphological techniques. Diagnostic studies were expanded using histological, cytological, and molecular genetic analysis of intraoperative material (biopsies and exudate). Microbiological studies included Ziehl-Neelsen (ZN) microscopy for acid-fast bacilli examination, inoculation of solid and liquid media using the automated systems.

Abdominal ultrasonography was performed using the Toshiba Aplio 500 expert-class ultrasound system (Toshiba; Japan) and the LOGIC ER7 portable imaging system (General

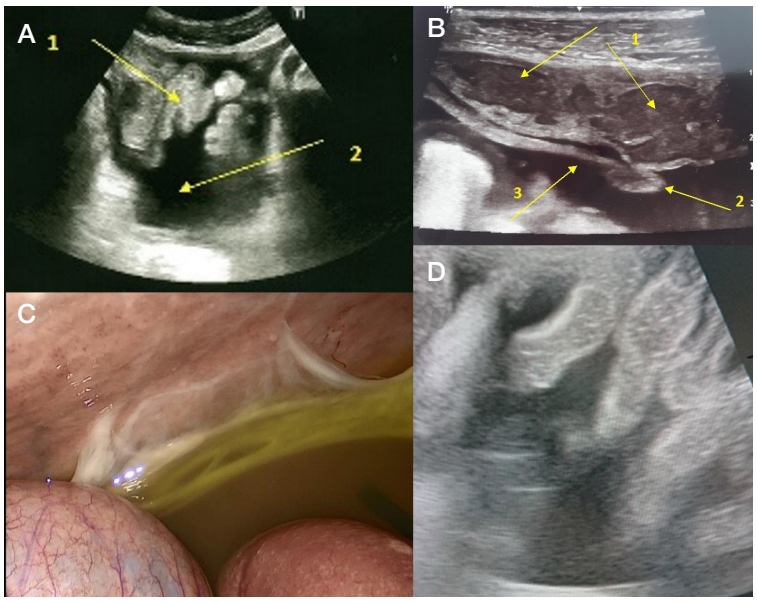

Fig. 1. Tuberculous peritonitis. **A**. Sonogram: 1 — paretic bowel loops, 2 — exudate. **B**. Sonogram: 1 — intra-peritoneal caseous abscess, 2 — tubercle, 3 — parietal peritoneum striated pattern. **C**. Laparoscopy. **D**. Sonogram: heterogeneous fibrinous effusion and paretic loops of the small intestine

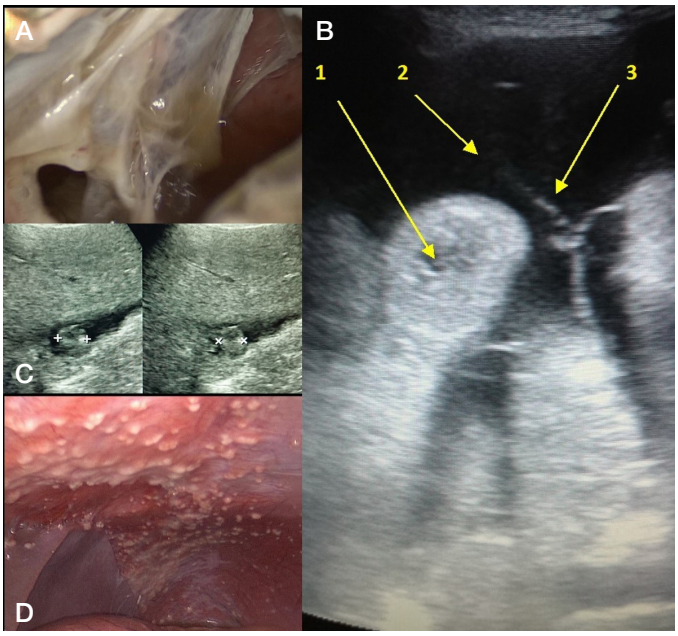

Fig. 2. Tuberculous peritonitis. **A**. Laparoscopy: fibrin overlays forming septa. **B**. Sonogram: 1 — intestinal loops, 2 — exudate, 3 — fibrin strands forming septa. **C**. Sonogram: tubercle (7 mm). **D**. Laparoscopy: tubercles on the parietal peritoneum

Electric; Republic of Korea) working in the grayscale, real-time mode. Abdominal cavity examination was carried out using the 2.5–5.0 MHz convex probe for assessment of presence and prevalence of free fluid, as well as the spleen and liver state. High-frequency linear probe (10–15 MHz) was used for evaluation of the intestinal loops, mesentery, greater and lesser omentum, lymphatic apparatus state.

Elective surgery (laparoscopic-assisted biopsy or laparotomy) was performed in patients with ascites of unknown origin or in order to clarify the nature of the pathological process detected by ultrasound imaging and computed tomography. Emergency surgery was performed in patients with clinical picture not allowing one to exclude peritonitis.

The criterion for the diagnosis verification was the detection of tuberculous granulomas in the peritoneum biopsy specimens, acid-fast bacilli during bacterioscopic examination and a positive result of PCR testing of effusion, as well as a combination of these signs.

Statistical analysis of the results was performed using standard statistical methods and the Statgraphics Centurion 18 software package (Statgraphics Technologies, Inc.; USA), Python 3.6 language (Python Software Foundation; USA) and Bayes' theorem [12]

RESULTS

To evaluate the sonographic symptoms of tuberculous peritonitis, we identified the following direct signs that were related to the inflammatory process in the serous leaflets and the associated exudation: presence of free fluid and its location in the abdominal cavity, exudate homogeneity, fibrin septa or incomplete septa in the abdominal cavity, striated pattern and heterogeneity of peritoneum and omentum, tubercles in serous leaflets.

Indirect signs of the peritoneum tuberculous lesions include the intestinal loops changes, spleen enlargement and heterogeneity, and the visualization of the enlarged mesenteric lymph nodes groups. Indirect signs do not reflect the inflammatory process in the peritoneal membranes, but may be the result of long-term ascites (thickening of the bowel walls),

Table 1. Direct and indirect signs of tuberculous peritonitis (the significance level is 0.95)

Sonographic sign	Tuberculous peritonitis $n = 37$	Ascites and carcinomatosis $n = 28$	Sign character
Free fluid in all abdominal cavity parts	51.4% ± 16.1	82.1% ± 14.1	Direct signs
Free fluid in pelvis and between intestinal loops	21.6% ± 13.2	3.6% ± 6.8	
Encysted fluid	27.0% ± 14.3	14.3% ± 12.9	
Heterogeneous effusion	75.7% ± 13. 8	3.6% ± 6.8	
Striated pattern and heterogeneity of the parietal peritoneum and omentum leaflets	37.8% ± 15.6	0	
Intra-peritoneal caseous abscesses	2.7% ± 1.6	0	
Peritoneal tubercles	24.3% ± 13.8	10.7% ± 11.5	
Bowel wall thickening	18.9% ± 12.6	21.4% ± 15.2	Indirect signs
Ileus	16.2% ± 11.9	10.7% ± 11.5	
Splenomegaly	13.5% ± 11.0	71.4% ± 16.7	
Enlarged and heterogeneous mesenteric lymph nodes	51.4% ± 16.1	14.3% ± 12.9	
Enlarged liver and vascular pattern depletion	27.0% ± 14.3	82.1% ± 14.2	
Expansion of the portal vein and diffuse changes of the liver	8.1% ± 8.8	85.7% ± 12.9	

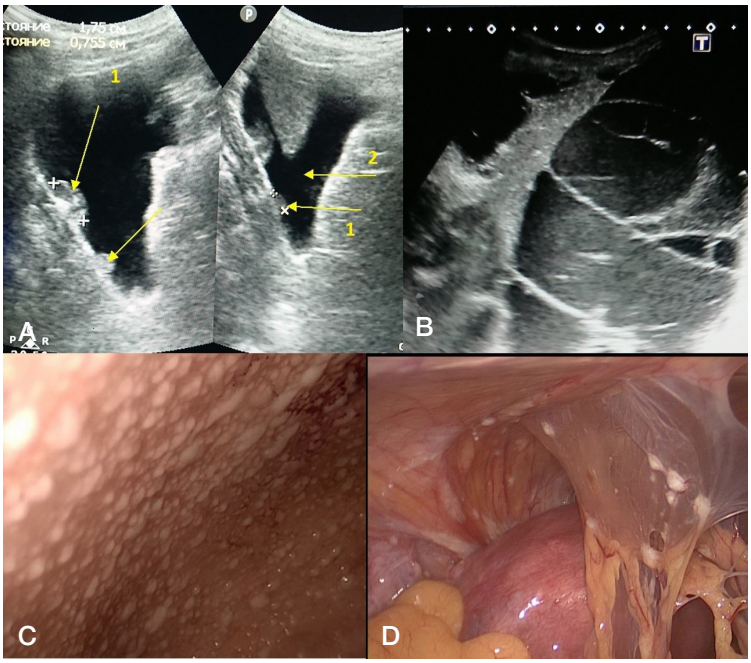

Fig. 3. Granulomatous peritonitis and carcinomatosis. **A**. Sonogram: peritoneal carcinomatosis associated with sigmoid colon cancer. 1 — disseminated tumors (17 and 8 mm), 2 — ascites. **B**. Sonogram: encysted ascites associated with ovarian cancer. **C**. Laparoscopy: parietal peritoneum carcinomatosis. **D**. Laparoscopy: peritoneal sarcoidosis

as well as the effect or specific lymphadenitis and splenitis in patients with abdominal tuberculosis.

When performing the abdominal ultrasound, various volumes of free fluid were detected in all patients with tuberculous peritonitis. The effusion in all parts of the abdominal cavity was visualized in 19 patients (51.4%). In eight patients (21.6%), free fluid was localized mainly in the pelvis and between the loops of the small intestine, and in 10 patients (27.0%) the encysted free fluid was revealed together with the formation of incomplete or complete septa from fibrin layers. The effusion heterogeneity due to freely floating layers of fibrin and small fibrin sequestra with a diameter of up to 6–8 mm was noted in the vast majority of patients (75.7%). Striated pattern and heterogeneity of certain areas of parietal peritoneum leaflets (primarily in the ileocecal region) were observed in 14 patients (37.8%), moreover, in one patient, the caseous foci were visualized inside the anterior abdominal wall (Fig. 1). Heterogeneity and striated pattern of the greater omentum were found in 9 patients (24.3%). Tubercles characteristic of tuberculous peritonitis were visualized in 9 patients (24.3%). The tubercle size varied between 5–9 mm, tubercles were described as hyperechoic avascular foci with uneven contour rising above the parietal peritoneum (Fig. 1, 2).

The other features allowing one to suspect tuberculosis as the cause of peritoneal changes included the sonographic signs of the visceral peritoneum, spleen and mesenteric lymphatic apparatus involvement in the pathological process. Bowel wall changes were registered in 7 patients (18.9%). Most comminly, there was a local thickening of the intestinal wall exceeding 3 mm with its length within 45–60 mm. In 6 patients (16.2%), the expansion of the intestinal lumen of more than 33–35 mm and the weakening or complete absence of peristalsis were revealed, which was considered a paralysis. Enlarged mesenteric lymph nodes (more than 10–16 mm in diameter) with a heterogeneous structure were detected in 19 patients (51.4%). Splenomegaly with spleen heterogeneity was observed in 5 patients (13.5%). Comparison of the control group patients' ultrasonography results is presented in Table 1.

To create an integrated scale for assessment of the tuberculous peritonitis probability using ultrasongraphy, all variants of signs (sonographic symptoms) combinations were considered. For that, each sonographic symptom received a 0–3

Table 2. Integral table of sonographic symptoms occurrence in patients with tuberculous peritonitis

Sonographic sign		Score
Free fluid in all abdominal cavity parts		1
Free fluid in pelvis and between intestinal loops		0
Encysted fluid in the abdominal cavity with septa		2
Heterogeneous effusion with fibrin fragments		2
Striated pattern and heterogeneity of the parietal peritoneum and omentum leaflets		3
Intra-peritoneal caseous abscesses		3
Peritoneal tubercles, diameter up to 9 mm		3
Peritoneal tubercles, diameter over 9 mm		0
Indirect signs: bowel wall changes and mesenteric lymphadenopathy		1
Tuberculous peritonitis probability		
High	Medium	Low
Score ≥ 9	Score 5–8	Score ≤ 4

score. The 1st three signs (free fluid distribution) determined the 1st complete event space, probability (effusion in the abdminal cavity). Tubercles of various sizes could be considered the 2nd complete event space (based on the tubercle size). The other signs (heterogenous effusion with fibrin fragments, striated pattern and heterogeneity of parietal peritoneum and omentum leaflets, intra-peritoneal caseous abscesses) were independent. Next, calculations were made for all features combinations using Python 3.6 language and Bayes' theorem, allowing one to determine the probability based on the data provided. Assumptions about the approximation of binomial distributions to normal and the conclusion on the inclusion of patients in the groups (low, medium, high probability) were made using the stats and numpy libraries (Table 2.).

DISCUSSION

Thus, it can be noted that the visual signs of tuberculous peritonitis, benign peritoneal granulomatosis (sarcoidosis), non-specific ascites, and peritoneal carcinomatosis are very similar and in most cases confront the researcher with a choice of diagnosis.

Our experience of ultrasound scanning in patients with tubercolous peritonitis, and the literature data [7–10] demonstrate that the main sonographic symptom is the presence of heterogenous free of encysted fluid in the abdominal cavity (75–80%). A characteristic feature that allows one to distinguish tuberculous peritonitis from non-specific ascites is the more frequent (about 75%) visualization of fibrin sequestrations freely floating in the exudate, which in sometimes form complete or incomplete septa causing the encysted effusion (Fig. 2). Nevertheless, similar sonographic features also occur in 50% of patients with peritoneal carcinomatosis [13]. Conversely, in patients with carcinomatosis, there is a high probability of disseminated tumors detection with a diameter of 5–18 mm (Fig. 3). Accoding to our data, similar hyperechoic foci on the peritoneum can also be detected in patients with benign granulomatosis, for example, with sarcoidosis (Fig. 3), which also does not give any reason to consider this feature specific. Tubercles in the peritoneum usually have a smaller diameter, and the maximum tubercle size is up to 9 mm (median value 4–6 mm) [11, 13–16]. A more reliable sonographic symptom of tuberculous peritonitis is the heterogeneity (striated pattern) of the parietal peritoneum and omentum areas, however, this symptom can be determined in just over one third of all cases. The most common finding is the extended hypoechoic thickening of the serous parietal leaflet (4–8 mm), which is associated with chronic inflammation. According to a number of authors, this variant of the thickened peritoneum is probably associated with tuberculosis [8, 17–20] and is less common in patients with peritoneal carcinomatosis, where the thickening of the serous membrane is most often small and nodular [20]. Various authors are equally likely to describe the involvement of the greater omentum and its changes as a characteristic sign of tuberculous omentitis or carcinomatosis, therefore we consider this symptom to be specific for both disorders, given that it is rarely possible to visualize the omental changes (less than 25% of observations) [21].

Indirect signs of peritoneal damage, such as lymphadenopathy with adenomegaly, occur in half of patients with tuberculous peritonitis, which reflects the pathogenetic charater of lymphogenous dissemination in the peritoneal leaflets. The mesenteric lymphatic apparatus changes are most often destructive, and the lymph nodes are visualized as grouped anechogenic rounded foci with a diameter exceeding 10 mm. According to the literature, the prevalence of joint lesions of intra-abdominal lymph nodes and peritoneum is 10–54% [22–24].

Thus, it is clear that tuberculous peritonitis does not have any reference or unique sonographic symptoms, which makes it extremely difficult to diagnose it using ultrasound imaging. At the same time, various combinations of some direct and indirect signs increase the probability of the ultrasound image correct interpretation in patients with peritoneal tuberculosis.

Based on the calculations and the probability distribution, the following data has been obtained: score under 4 corresponds to low probability, score 5–8 corresponds to medium probability, and the score over 9 corresponds to high probability of tuberculous peritonitis based on the visualization of all described songraphic symptoms. Based on the sum score obtained after the ultrasound scanning, a diagnostic algorithm can be proposed that clearly indicates further diagnostic and treatment strategies for each combination of sonographic symptoms, and for patients with HIV and/or pulmonary tuberculosis (Fig. 4).

CONCLUSION

The obtained integrated scale for the sonographic signs assessment is quite simple and allows the clinician to select the further tactics of diagnosis based on the ultrasound imaging results and to start the treatment in a timely manner. The proposed scheme may also complete the diagnostic search algorithm for any form of ascites or granulomatous peritonitis.

Due to the clinical symptoms non-specificity and the subacute course, the diagnosis of peritoneal tuberculosis remains a difficult task. Transabdominal ultrasound, which is affordable and commonly used in medical practice, can become a first-line screening test for verification of tuberculous peritonitis. Peritoneal tuberculosis should be taken into account in all cases of differential diagnosis of patients with unclear ascites, pulmonary tuberculosis and immunosuppression.

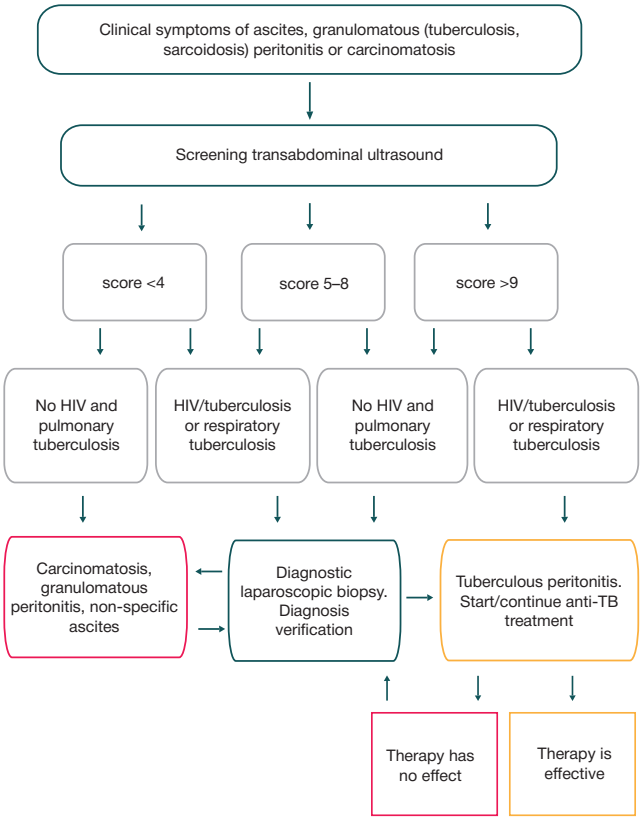

Fig. 4. Tactical algorithm for the tuberculous peritonitis diagnosis

References

1. Gupta P, Kumar S, Sharma V, Mandavdhare H, Dhaka N, Sinha SK, et al. Common and uncommon imaging features of abdominal tuberculosis. Journal of Medical Imaging and Radiation Oncology. 2019; 63 (3): 329–39. DOI: 10.1111/1754-9485.12874.
2. Sinitsyn MV, Belilovsky EM, Sokolina IA, Reshetnikov MN, Tityukhina MV, Baturin OV. Extrapulmonary tuberculosis in HIV patients. Tuberculosis and Lung Diseases. 2017; 95 (11): 19–25. DOI: 10.21292/2075-1230-2017-95-11-19-25. Russian.
3. Ködmön C, Zucs P, Van der Werf MJ. Migration-related tuberculosis: Epidemiology and characteristics of tuberculosis cases originating outside the European Union and European Economic Area, 2007 to 2013. Eurosurveillance. 2016; (21): 23–27. DOI: 10.2807/1560-7917.ES.2016.21.12.30164.
4. Chow KM, Chow VC, Szeto CC. Indication for peritoneal biopsy in tuberculous peritonitis. The American Journal of Surgery. 2003; (185): 567–73. DOI: 10.1016/s0002-9610(03)00079-5.
5. Plotkin DV, Sinitsyn MV, Reshetnikov MN, Kharitonov SV, Skopin MS, Sokolina IA. Tuberculous peritonitis. «Forgotten» disease. Khirurgiya. Zhurnal im. N.I. Pirogova. 2018; (12): 38–44. DOI: 10.17116/hirurgia20181213. Russian.
6. Vaid U, Kane GC. Tuberculous Peritonitis. Microbiology Spectrum. 2017; (5): 324–29. DOI: 10.1128/microbiolspec.TNMI7-0006-2016.
7. Demirkazik FB, Akhan O, Ozmen MN, Akata D. US and CT findings in the diagnosis of tuberculous peritonitis. Acta Radiologica. 1996; 37 (4): 517–20. DOI: 10.1177/02841851960373P217.
8. Portielje JE, van der Werf SD, Mutsaers JA, Lohle PN, Puylaert JB. Peritonitis tuberculosa echografisch te herkennen [Echographic recognition of tuberculous peritonitis]. Nederlands Tijdschrift voor Geneeskunde. 1997; 141 (2): 89–93.
9. Mojdunova NK, Turdumambetova GK. Ultrasound picture of abdominal tuberculosis. International journal of applied and fundamental research. 2017; (6): 111–3. Russian.
10. Vostrov AN, Mitina LA, Kazakevich VI, Kaprin AD, Stepanov SO, Guts OV, et al. Value of ultrasound in differential diagnosis of ovarian cancer with peritoneal carcinomatosis and peritoneal tuberculosis. Ultrasound and functional diagnostics. 2017; (3): 60–71. Russian.
11. Husain A, Firdaus H, Panday P. Study of Comparison of high resolution sonography and computed tomography in evaluation of abdominal tuberculosis among patients in Lucknow, Uttar Pradesh, India. International Journal of Surgery. 2018; (5): 1713–9. DOI: 10.18203/2349-2902.isj20181388.
12. Goodman SN. Toward Evidence-Based Medical Statistics. 2: The Bayes Factor. Annals of Internal Medicine. 1999; (130): 1005–13.
13. Smereczyński A, Kołaczyk K, Bernatowicz E. Difficulties in differentiating the nature of ascites based on ultrasound imaging. Journal of Ultrasonography. 2017; 17 (69): 96–100. DOI: 10.15557/JoU.2017.0013.
14. Atzori S, Vidili G, Delitala G. Usefulness of ultrasound in the diagnosis of peritoneal tuberculosis. The Journal of Infection in Developing Countries. 2012; 6 (12): 886–90. DOI: 10.3855/jidc.2654.
15. Weill FS, Costaz R, Guetarni S, Maltoni I, Rohmer P. Echographic diagnosis of peritoneal metastases in patients with ascites. European Journal of Radiology. 1990; (71): 365–8.
16. Stepanov SO, Mitina LA, Guts OV, Bespalov PD. Ultrasound imaging of peritoneal dissemination. Ultrasound and functional diagnostics. 2013; 3 (4): 66–70. Russian.
17. N'dri K, Gbazi GC, Konan A, Kouadio, Koffi, N'dri N, et al. Apport de l'échographie dans le diagnostic de la tuberculose péritonéale ascitique. Médecine d'Afrique Noire. 1993; (40): 503–6.
18. Dafiri R, Imani F. Tuberculose abdominale. Encycl Méd Chir (Editions Scientifiques et Médicales Elsevier SAS, Paris, tous droits réservés). Radiodiagnostic — Appareil digestif 2001; 33-010-A-30: 12.
19. Gastli H, Hassine W, Absesselem K, Gharbi HA. Echographic aspects of peritoneal tuberculosis. Apropos of 14 cases. European Journal of Radiology. 1983; (64): 325–9.
20. Mbengue A, Ndiaye AR, Amar N, Diallo M, et al. Ultrasonography of peritoneal tuberculosis. Journal of Ultrasonography. 2019; (19): 98–104. DOI: 10.15557/JoU.2019.0014.
21. Batra A, Gulati MS, Sarma D, Paul SB. Sonographic appearances in abdominal tuberculosis. Journal of Clinical Ultrasound. 2000; (28): 233–45. DOI: 10.1002/(sici)1097-0096(200006)28:5<233::aid-jcu5>3.0.co;2-c.
22. Fall F, Ndiaye AR, Ndiaye B, Gning SB, Diop Y, Fall B. Peritoneal tuberculosis: a retrospective study of 61 cases at Principal hospital in Dakar. Journal of Gastroenterology and Hepatology. 2010; (4): 38–43.
23. Darré T, Tchaou M, Sonhaye L, Patassi AA, Kanassoua K, Tchangai B. Analyse d'une série de 44 cas de tuberculose péritonéale diagnostiqués au laboratoire d'anatomie pathologique du CHU Tokoin de Lomé (1993–2014). Bulletin de la Société de Pathologie Exotique. 2015; (108): 324–7.
24. Heller T, Goblirsch S, Wallrauch C, Lessells R, Brunetti E. Abdominal tuberculosis: sonographic diagnosis and treatment response in HIV positive adults in rural South Africa. International Journal of Infectious Diseases. 2010; 14 (Suppl 3): 108–12. DOI: 10.1016/j.ijid.2009.11.030.

Литература

1. Gupta P, Kumar S, Sharma V, Mandavdhare H, Dhaka N, Sinha SK, et al. Common and uncommon imaging features of abdominal tuberculosis. Journal of Medical Imaging and Radiation Oncology. 2019; 63 (3): 329–39. DOI: 10.1111/1754-9485.12874.
2. Синицын М. В., Белиловский Е. М., Соколина И. А., Решетников М. Н., Титюхина М. В., Батурин О. В. Внелегочные локализации туберкулеза у больных ВИЧ-инфекцией. Туберкулез и болезни легких. 2017; 95 (11): 19–25. DOI: 10.21292/2075-1230-2017-95-11-19-25.
3. Ködmön C, Zucs P, Van der Werf MJ. Migration-related tuberculosis: Epidemiology and characteristics of tuberculosis cases originating outside the European Union and European Economic Area, 2007 to 2013. Eurosurveillance. 2016; (21): 23–27. DOI: 10.2807/1560-7917.ES.2016.21.12.30164.
4. Chow KM, Chow VC, Szeto CC. Indication for peritoneal biopsy in tuberculous peritonitis. The American Journal of Surgery. 2003; (185): 567–73. DOI: 10.1016/s0002-9610(03)00079-5.
5. Плоткин Д. В., Синицын М. В., Решетников М. Н., Харитонов С. В., Скопин М. С., Соколина И. А. Туберкулезный перитонит. «Забытая» болезнь. Хирургия. Журнал им. Н. И. Пирогова. 2018; (12): 38–44. DOI: 10.17116/hirurgia201812138.
6. Vaid U, Kane GC. Tuberculous Peritonitis. Microbiology Spectrum. 2017; (5): 324–29. DOI: 10.1128/microbiolspec.TNMI7-0006-2016.
7. Demirkazik FB, Akhan O, Ozmen MN, Akata D. US and CT findings in the diagnosis of tuberculous peritonitis. Acta Radiologica. 1996; 37 (4): 517–20. DOI: 10.1177/02841851960373P217.
8. Portielje JE, van der Werf SD, Mutsaers JA, Lohle PN, Puylaert JB. Peritonitis tuberculosa echografisch te herkennen [Echographic recognition of tuberculous peritonitis]. Nederlands Tijdschrift voor Geneeskunde. 1997; 141 (2): 89–93.
9. Мойдунова Н. К., Турдумамбетова Г. К. Ультразвуковая картина абдоминального туберкулеза. Международный журнал прикладных и фундаментальных исследований. 2017; (6): 111–3.
10. Востров А. Н., Митина Л. А., Казакевич В. И., Каприн А. Д., Степанов С. О., Гуц О. В. и др. Возможности ультразвуковой диагностики в дифференциации поражения брюшины при раке яичников и туберкулезе. Ультразвуковая и функциональная диагностика. 2017; (3): 60–71.
11. Husain A, Firdaus H, Panday P. Study of Comparison of high resolution sonography and computed tomography in evaluation of abdominal tuberculosis among patients in Lucknow, Uttar Pradesh, India. International Journal of Surgery. 2018; (5): 1713–9. DOI: 10.18203/2349-2902.isj20181388.

12. Goodman SN. Toward Evidence-Based Medical Statistics. 2: The Bayes Factor. Annals of Internal Medicine. 1999; (130): 1005–13.
13. Smereczyński A, Kołaczyk K, Bernatowicz E. Difficulties in differentiating the nature of ascites based on ultrasound imaging. Journal of Ultrasonography. 2017; 17 (69): 96–100. DOI: 10.15557/JoU.2017.0013.
14. Atzori S, Vidili G, Delitala G. Usefulness of ultrasound in the diagnosis of peritoneal tuberculosis. The Journal of Infection in Developing Countries. 2012; 6 (12): 886–90. DOI: 10.3855/jidc.2654.
15. Weill FS, Costaz R, Guetarni S, Maltoni I, Rohmer P. Echographic diagnosis of peritoneal metastases in patients with ascites. European Journal of Radiology. 1990; (71): 365–8.
16. Степанов С. О., Митина Л. А., Гуц О. В., Беспалов П. Д. Визуализация перитонеальной диссеминации при ультразвуковом исследовании. Ультразвуковая и функциональная диагностика. 2013; 3 (4): 66–70.
17. N'dri K, Gbazi GC, Konan A, Kouadio, Koffi, N'dri N, et al. Apport de l'échographie dans le diagnostic de la tuberculose péritonéale ascitique. Médecine d'Afrique Noire. 1993; (40): 503–6.
18. Dafiri R, Imani F. Tuberculose abdominale. Encycl Méd Chir (Editions Scientifiques et Médicales Elsevier SAS, Paris, tous droits réservés). Radiodiagnostic — Appareil digestif 2001; 33-010-A-30: 12.
19. Gastli H, Hassine W, Absesselem K, Gharbi HA. Echographic aspects of peritoneal tuberculosis. Apropos of 14 cases. European Journal of Radiology. 1983; (64): 325–9.
20. Mbengue A, Ndiaye AR, Amar N, Diallo M, et al. Ultrasonography of peritoneal tuberculosis. Journal of Ultrasonography. 2019; (19): 98–104. DOI: 10.15557/JoU.2019.0014.
21. Batra A, Gulati MS, Sarma D, Paul SB. Sonographic appearances in abdominal tuberculosis. Journal of Clinical Ultrasound. 2000; (28): 233–45. DOI: 10.1002/(sici)1097-0096(200006)28:5<233::aid-jcu5>3.0.co;2-c.
22. Fall F, Ndiaye AR, Ndiaye B, Gning SB, Diop Y, Fall B. Peritoneal tuberculosis: a retrospective study of 61 cases at Principal hospital in Dakar. Journal of Gastroenterology and Hepatology. 2010; (4): 38–43.
23. Darré T, Tchaou M, Sonhaye L, Patassi AA, Kanassoua K, Tchangai B. Analyse d'une série de 44 cas de tuberculose péritonéale diagnostiqués au laboratoire d'anatomie pathologique du CHU Tokoin de Lomé (1993–2014). Bulletin de la Société de Pathologie Exotique. 2015; (108): 324–7.
24. Heller T, Goblirsch S, Wallrauch C, Lessells R, Brunetti E. Abdominal tuberculosis: sonographic diagnosis and treatment response in HIV positive adults in rural South Africa. International Journal of Infectious Diseases. 2010; 14 (Suppl 3): 108–12. DOI: 10.1016/j.ijid.2009.11.030.

OPTIMIZATION OF A SINGLE-EMBRYO TRANSFER IN PATIENTS WITH GOOD OVARIAN RESERVE

Saraeva NV[1,2] ✉, Spiridonova NV[1], Tugushev MT[1], Shurygina OV[1], Sinitsyna AI[1], Korchagin AO[2]

[1] Samara State Medical University, Samara, Russia

[2] IDK Medical Company, the Mother and Child group, Samara, Russia

Due to refinements of assisted reproductive technology, the number of multiple pregnancies has increased substantially. Time-lapse microscopy (TLM) is a tool for selecting quality embryos for transfer. This study aimed to assess the outcomes of single-embryo transfer of autologous oocytes performed on day 5 of embryo incubation in a TLM-equipped system in patients with good ovarian reserve. The study was carried out in 208 infertile women with good ovarian reserve (over 8 oocytes retrieved). Single-embryo transfer following incubation in a TLM-equipped incubator was performed in 95 patients, who formed the main group; the control group consisted of 113 patients undergoing single-embryo transfer following a traditional culture and embryo selection procedure. We assessed the quality of transferred embryos, the rates of clinical pregnancy and pregnancy loss. Two subgroups were identified in each group of the participants: the 5SET subgroup (nonelective single-embryo transfer), which included 45 patients from the main group and 67 controls, and the 5eSET subgroup (elective single-embryo transfer), which consisted of 50 main group patients and 46 controls. The groups did not differ in terms of age, infertility factors and infertility duration. The quality of transferred embryos was excellent or good in all main group patients (100%); in the control group, the quality of transferred embryos was excellent or good in 93.8% of cases (p = 0.037). Clinical pregnancies were achieved in 64.2% of women in the main group and in 60.2% of controls (p = 0.65). Delivery rates were 54% and 51.1% in the 5eSET and 5SET subgroups of the main group, respectively (p = 0.940). For the control group, delivery rates were 54.4% and 34.3% in the 5eSET and 5SET subgroups, respectively (p = 0.052, Fisher exact test). Elective single-embryo transfer (5eSET) and the use of TLM increased the chance of pregnancy 2.17-fold (p = 0.01).

Keywords: assisted reproductive technology, single-embryo transfer, elective blastocyst transfer, time-lapse microscopy

Acknowledgements: the authors thank Komarova MV, PhD Biol., Associate Professor of Samara National Research University, for her help with the statistical analysis.

Author contribution: all authors equally contributed to the study and manuscript preparation.

Compliance with ethical standards: the study was approved by the Ethics Committee of Samara State Medical University (Protocol 194 dated September 12, 2018). Informed consent was obtained from all study participants.

✉ **Correspondence should be addressed:** Natalya V. Saraeva
Vrubelya, 15–131, Samara, 443086; kuzichkina@gmail.com

Received: 19.03.2020 **Accepted:** 07.04.2020 **Published online:** 20.04.2020

DOI: 10.24075/brsmu.2020.021

ОПТИМИЗАЦИЯ ПЕРЕНОСА ОДНОГО ЭМБРИОНА У ПАЦИЕНТОК С ХОРОШИМ ОВАРИАЛЬНЫМ РЕЗЕРВОМ

Н. В. Сараева[1,2] ✉, Н. В. Спиридонова[1], М. Т. Тугушев[1], О. В. Шурыгина[1], А. И. Синицына[1], А. О. Корчагин[2]

[1] Самарский государственный медицинский университет, Самара, Россия

[2] «Медицинская компания ИДК», группа компаний «Мать и Дитя», Самара, Россия

Совершенствование вспомогательных репродуктивных технологий привело к росту числа случаев многоплодной беременности. Один из инструментов выбора качественного эмбриона на перенос — использование time-lapse микроскопии (TLM). Целью работы было оценить исходы переноса одного эмбриона на пятые сутки культивирования у пациенток с хорошим овариальным резервом в программе ЭКО с использованием TLM. Исследовали 208 женщин с бесплодием, с хорошим овариальным резервом (при пункции фолликулов получено более восьми ооцитов): у 95 пациенток провели перенос одного эмбриона с использованием системы TLM (группа исследования); у 113 пациенток — с использованием традиционного культивирования и выбора эмбриона для переноса (группа контроля). Проведена оценка качества переносимых эмбрионов, частоты наступления клинической беременности, частоты достижения родов и случаев потери беременности. В каждой группе выделены две подгруппы: с неэлективным переносом одного эмбриона (подгруппа 5SET: 45 пациенток в группе исследования, 67 — в контрольной) и с элективным (подгруппа 5eSET: 50 пациенток в группе исследования, 46 — в контрольной). Группы не различались по среднему возрасту, фактору бесплодия, длительности бесплодия. В группе исследования в 100% случаев перенесены эмбрионы хорошего и отличного качества, в группе контроля — в 93,8% (p = 0,037). Частота наступления клинической беременности составила 64,2% в основной группе и 60,2% — в контрольной (p = 0,65). В группе исследования частота родов составила 54% в подгруппе 5eSET и 51,1% — в подгруппе 5SET (p = 0,940). В группе контроля в подгруппе 5eSET частота родов составила 54,4%, а в подгруппе 5SET — 34,3% (p = 0,052 по методу Фишера). Проведение элективного переноса эмбриона (5eSET) или использование TLM повышало вероятность родов в 2,17 раза (p = 0,01).

Ключевые слова: вспомогательные репродуктивные технологии, перенос одного эмбриона, элективный перенос бластоцисты, time-lapse микроскопия

Благодарности: к.б.н., доценту Самарского национального исследовательского университета имени академика С. П. Королева М. В. Комаровой за помощь в статистической обработке результатов исследования.

Вклад авторов: все авторы внесли равнозначный вклад в исследование и написание статьи.

Соблюдение этических стандартов: исследование одобрено этическим комитетом СамГМУ (протокол № 194 от 12 сентября 2018 г.). Всеми пациентами подписано добровольное информированное согласие на лечение методами вспомогательных репродуктивных технологий.

✉ **Для корреспонденции:** Наталья Владимировна Сараева
ул. Врубеля, 15–131, г. Самара, 443086; kuzichkina@gmail.com

Статья получена: 19.03.2020 **Статья принята к печати:** 07.04.2020 **Опубликована онлайн:** 20.04.2020

DOI: 10.24075/vrgmu.2020.021

Due to advancements in assisted reproductive technology (ART), implantation rates have significantly improved in the past 15–20 years, resulting in an increased incidence of multiple pregnancies. A multiple pregnancy is a recognized high-risk factor for obstetric and neonatal complications [1–3]. Therefore, transfer of a single embryo, as opposed to multiple embryos, is a top-priority task in ART-based infertility treatment [4, 5].

Selecting an embryo with the best developmental potential is crucial to ART success. Selection allows reducing time to pregnancy and simplifies embryo grading for cryopreservation, which, in turn, ensures that high-quality embryos are transferred first [6, 7].

Since the advent of in vitro fertilization (IVF), morphological evaluation has been the primary method exploited by embryologists to assess the development of human embryos and identify those with the highest implantation potential. Later, grading systems were proposed to estimate the viability of embryos, but their practical application was impeded by the rapid pace of embryo development in the preimplantation phase. In other words, it is possible that an embryo evaluated at 8:00 am will look very different in only a few hours [8]. So, it is very difficult to offer correct interpretation of the morphological data without analyzing the dynamicsdynamics of embryo development at a number of different time points.

Introduction of time-lapse microscopy (TLM) into IVF laboratories heralded a new age in embryology. TLM is a modern technique of embryo selection for subsequent implantation. It is used for continuous evaluation of embryo morphology in a series of images taken every few minutes [9–11].

Published reports on TLM results are conflicting. A retrospective study has demonstrated that incubation of human embryos in the EmbryoScope system can improve live birth rates whereas traditional culture techniques can negatively affect the development of embryos and their implantation potential [12]. Other retrospective and prospective studies point to the advantages of this promising technology [13–16], as well as to the absence of differences in outcomes in comparison with the conventional technique for morphological evaluation [17, 18].

The aim of our study was to assess the outcomes of single-embryo transfer following embryo incubation in a TLM-equipped incubator in patients with good ovarian reserve undergoing IVF.

METHODS

The study was conducted in 208 infertile women receiving a single-embryo transfer as part of their IVF treatment at the IDK Medical Company (Samara) in 2013–2015.

We analyzed 208 patients' clinical and embryo protocols using SPSS21 Statistics (License 20130626-3; IBM Company; USA) and Microsoft Excel (Microsoft; USA).

The following inclusion criteria were applied: participation in the IVF program, fresh autologous IVF cycles with 8 or more oocytes retrieved per cycle, embryo transfer on day 5 of incubation, and endometrial thickness of ≥ 8 mm on the day of transfer.

Exclusion criteria: participation in the ICSI program, donor oocyte cycles (with ≤ 8 oocytes), frozen-thawed embryo transfer, transfer on day 3 of incubation, multiple (2) embryo transfer, endometrial thickness of < 8 mm on the day of transfer.

There was no age limit applied. The lowest age was 20 years, whereas the highest, 42 years.

The patients were divided into two groups. The main group comprised 95 patients with good ovarian reserve undergoing a single-embryo transfer following embryo incubation in a TLM-equipped system.

The control group consisted of 113 patients with good ovarian reserve undergoing a single-embryo transfer following conventional embryo incubation and selection. The average age of the participants, infertility factors, the duration of infertility, and the number of the current IVF program did not differ between the groups. The average age was 31.40 ± 0.38 and 30.65 ± 0.37 years in the main and control groups, respectively ($p > 0.05$).

In the main group, embryo cultures were monitored using a Primo Vision time-lapse system (Vitrolife; Sweden).

In both groups, embryo quality was assessed using the alphanumeric blastocyst grading system proposed by Gardner and Schoolcraft in 1999 [19]. Grades AA, AB and BA represented excellent quality blastocysts; grade BB indicated good quality; grades AC, CA, BC, CB, and CC were considered to be satisfactory quality blastocysts.

Two subgroups were identified in each group based on the type of embryo transfer: a subgroup of nonelective single-embryo transfer on the 5th day of culture (the 5SET subgroup, which included 45 patients from the main group and 67 women from the control group) and a subgroup with elective single-embryo transfer on the 5th day of culture (the 5eSET subgroup consisting of 50 patients from the main subgroup and 46 controls). A transfer was classified as elective if there were 2 or more excellent quality embryos to choose from.

In the main group, embryos were selected for transfer based on their morphokinetic parameters. The following developmental events were assessed: time of the first cleavage division; an interval between the first and second divisions; time of the third cleavage; time of blastocyte formation. If these parameters fell within the reference range of the Primo Vision system and the embryo was of excellent or good quality, it was selected for transfer (a reference-positive embryo). The reference-positive subgroup comprised 52 patients. If one or more parameters of embryo development did not fall within the system's reference range, the standard morphological assessment technique for embryo selection was applied (a reference-negative embryo). The reference-negative subgroup included 43 patients.

In both groups, the embryos were cultured in a Continuous Single Culture medium (Irvine Scientific; USA). Embryo quality was assessed on day 5 of incubation, 116–118 h after fertilization.

RESULTS

We assessed the quality of transferred embryos and calculated the rates of successful pregnancies, delivery and pregnancy loss.

Patients of late reproductive age (≥ 35 years) made up 21.05% of women in the main group and 23.89% of women in the control group ($p > 0.05$). Because the study included only females with good ovarian reserve and a single-embryo transfer, our sample was dominated by patients of early reproductive age.

The average number of retrieved oocytes was 11.87 ± 0.32 and 12.49 ± 0.40 in the main and control groups, respectively ($p > 0.05$).

It is known that the quality of transferred embryos significantly affects the chance of pregnancy in patients undergoing IVF treatment. It is reported that transfer of excellent or good quality embryos results in much higher pregnancy rates than observed for satisfactory quality embryos [20]. In the main group, transferred embryos were of either good (16) or excellent (79) quality in 100% of cases. In the control group, good (18) or excellent (88) quality embryos were transferred in 93.8% of cases ($p = 0.037$) (Fig. 1). Satisfactory quality embryos were transferred to 7 patients in the control group (6.2%).

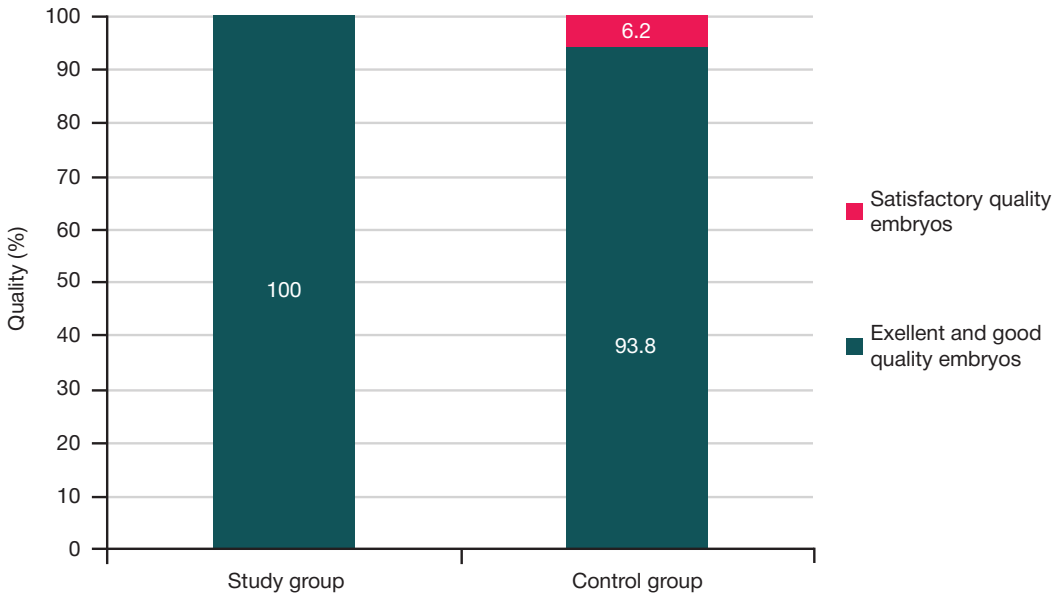

Fig. 1. Embryo quality in the main and control groups

The analysis of embryo quality did not reveal any significant differences between the reference-positive and reference-negative subgroups. In the reference-positive subgroup, 87.5% of embryo transfers were performed with excellent quality embryos, whereas in the reference-negative subgroup, the proportion of such cycles was 78.95% ($p = 0.44$).

Thus, the clinical pregnancy rate did not differ between the groups and was 64.2% in the main group and 60.2% in the control group ($p = 0.65$) (Table 1).

Live births accounted for 52.6% and 42.5% of all embryo transfer outcomes in the main and control groups, respectively ($p > 0.05$). Early pregnancy loss (biochemical pregnancy and pregnancy loss before gestational week 12) was observed in 11.6% of cases in the main group and in 17.7% of cases in the control group, but this difference was statistically insignificant.

No statistically significant differences were noted between the reference-positive and reference-negative subgroups in terms of clinical pregnancy rates (66.7% vs 60.5%, respectively) and delivery rates (50% vs 52.6%, respectively).

According to the literature, elective embryo transfer increases the probability of a positive outcome [21]; therefore, we decided to compare the delivery rate among patients who had undergone different types of transfer.

In the 5eSET subgroup (elective single-embryo transfer) of the main group, the delivery rate reached 54%; in the 5SET subgroup (nonelective single-embryo transfer), it was 51.1% ($p = 0.940$) (Fig. 2). In the control group, this parameter was significantly affected by the type of transfer: the delivery rates for the 5eSET and 5SET subgroups were 54.3% and 34.3%, respectively ($p = 0.052$, Fisher exact test). The difference in the delivery rate was 20.1 % (95%CI 1.5–37%), with OR = 2.28 (95%CI 1.06–4.91). Thus, the delivery rate was high in the TLM group, regardless of the type of transfer (54.0% and 51.1%), and did not differ significantly between the subgroups.

Considering this finding, we analyzed a possible correlation between the positive outcome of an IVF cycle (live birth) and the following factors: the absence/presence of TLM and the type of embryo transfer (elective or nonelective; Table 2).

The delivery rate was as high as 53.2% in the group with the combination of two factors (5eSET in both groups and 5SET in the main group), whereas in the control group, it was lower (34.3%) ($p = 0.01$; OR = 2.17 (1.19–3.97)). Thus, it could be hypothesized that there is a positive trend showing an increase in live births in patients undergoing IVF treatment aided by TLM regardless of the embryo transfer type.

DISCUSSION

The TLM technology minimizes exposure of the incubated embryo to environmental factors, which might be a contributor to a higher implantation potential. Continuous monitoring within short time intervals provides more information about the kinetics and morphology of embryos in comparison with traditional

Table 1. Outcomes of embryo transfer in the main and control groups

		Main group		Control group		χ^2	p
		Абс.	%	Абс.	%		
Pregnancy	No	34	35.8%	45	39.8%	0.2	0.65
	Yes	61	64.2%	68	60.2%		
Outcomes	No pregnancy	34	35.8%	45	39.8%	3.7	0.443
	Early loss of pregnancy	11	11.6%	18	15.9%		
	Late loss of pregnancy			2	1.8%		
	Preterm delivery	1	1.1%	1	0.9%		
	Delivery at term	49	51.6%	47	41.6%		
Childbirth	No	45	47.4%	65	57.5%	1.7	0.186
	Yes	50	52.6%	48	42.5%		

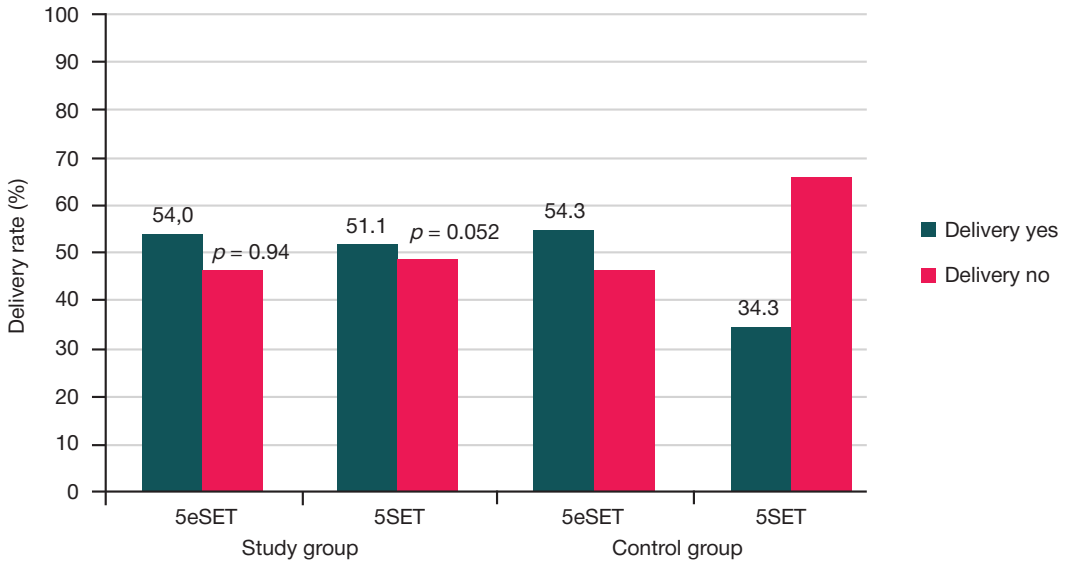

Fig. 2. Delivery rate depending on the type of the embryo transfer

morphological evaluation. So far, reports of the impact of TLM on IVF outcomes are conflicting.

We discovered that the quality of blastocytes in the TLM group was higher than in the case of traditional morphological evaluation, which is consistent with the findings of other authors [22, 23]. A study reports that in patients with good ovarian reserve, the proportion of good quality blastocytes and the number of cryopreserved embryos per patient was significantly lower in the control group than in the TLM group (50.7% and 1.72 ± 1.55 vs 60.1% and 2.64 ± 2.59, respectively; $p < 0.05$); however, no statistically significant differences were observed in the number of good quality embryos on day 3 of incubation, as well as in the rates of clinical pregnancy and implantation [23]. In our study, patients did not differ in terms of age, infertility factors and infertility duration; therefore, it could be hypothesized that the difference in the proportion of good and excellent quality embryos can be attributed to the absence of impact of environmental factors (ambient temperature, light, pH conditions) in the TLM group.

The efficacy of TLM might be determined by 2 factors: stable incubation conditions (there is no need to remove an embryo from an incubator for morphological evaluation) and the possibility of selecting an embryo for transfer using specialized software [24].

According to a recent Cochrane review that analyzed the data on 2,995 couples, there is no convincing evidence about the advantage of TLM over the conventional culture technique: no significant differences were observed in terms of clinical pregnancy rates (OR 0.95; 95%CI 0.78–1.16) and live birth rates (OR 1.12; 95%CI 0.92–1.36) [25].

By contrast, in a meta-analysis of data of 1,637 patients, TLM was shown to have an advantage over traditional incubation and morphological evaluation procedures [26]. This study reports high rates of clinical pregnancies (51.0 vs 39.9%; OR 1.54, 95%CI 1.21–1.97) and live births (44.2 vs 31.3%; OR 1.67, 95%CI 1.13–2.46) and lower rates of pregnancy loss (15.3 vs 21.3%; OR 0.66, 95%CI 0.47–0.94).

In our study, pregnancy rats were high in both groups (64.2% in the main group and 60.2% in the control group), which may suggest the absence of TLM negative effect on the incubated embryos. The use of time-lapse microscopy resulted in a reduction in the number of early pregnancy losses.

The absence of differences between the groups in terms of pregnancy rates, delivery rates and early pregnancy loss in our study might be associated with a small sample size (95 patients in the TLM group).

In another retrospective cohort study, the TLM group demonstrated an increase in clinical pregnancy rates (+15.7% per embryo transfer) [27]. However, unlike ours, that study was heterogenous in terms of patient sample (IVF cycles with donor oocytes were also included), number of transferred embryos (1–3) and time of transfer (in the majority of cases in the TLM group transfer was performed on day 3 of incubation, which decreased the overall pregnancy rate). In the TLM group, clinical pregnancies achieved after performing transfer of retrieved oocytes on the 5th day of culture were observed in 50% of cases, whereas for our patients, the pregnancy rate (embryo transfer on day 5 of incubation) was as high as 64.2%. One of the strengths of our study is a prognostic mathematical model developed by the authors of this work. The model predicted a 15.7% increase in pregnancy rates per transfer achieved through the use of TLM. Ever better outcomes can be achieved by increasing the number of IVF cycles with TLM to ≥ 200.

Like many technological advances, TLM may not ensure immediate results in every laboratory, and some standardization might be required. Indeed, TLM does not always demonstrate an advantage in terms of embryo selection [22]. However, its growing value for continuous incubation and embryo biopsy scheduling cannot be overestimated [28, 29].

At present, there are attempts to integrate artificial intelligence into TLM in order to identify the right combination of parameters predicting the potential of the embryo for implantation and live birth [24].

Table 2. Delivery rates in the absence/presence of TLM for different types of embryo transfer

Delivery	Transfer type				χ^2	p
	5eSET in both groups + 5SET in the main group		5SET in the control group			
	Abs.	%	Abs.	%		
No	66	46.8%	44	65.7%	5.75	0.01
Yes	75	53.2%	23	34.3%		

CONCLUSIONS

Our study did not reveal any differences in the rates of clinical pregnancies, delivery and early pregnancy loss between the TLM group and patients with traditional embryo incubation. This might be explained by a small number of patients in the TLM group. With TLM incubation, delivery rates were high regardless of the type of embryo transfer (selective or nonselective) and there were no differences in terms of pregnancy rates and early pregnancy losses. With traditional embryo incubation and selection, the transfer type significantly affected the delivery rate: in the elective transfer subgroup, the delivery rate was higher than in the nonelective transfer subgroup (p = 0.052; Fisher exact test). Performing elective embryo transfer on day 5 of incubation (5eSET) and the use of TLM regardless of transfer type were favorable factors and increased the chance for live birth (p = 0.01).

Our findings hold promise for exploring advantages of TLM in patients of different age groups with reduced ovarian reserve. Further accumulation of data is required to assess cumulative pregnancy rates following IVF with the use of TLM and to monitor the long-term results of this technology. There is no doubt that complex systems will soon be created for noninvasive evaluation of embryo quality (morphology, kinetics and metabolism) allowing automatization of embryo selection for transfer. They will reduce the probability of negative impact of environmental factors and thereby increase the rate of live births following embryo transfer.

References

1. Kalinkina OB, Spiridonova NV, Junusova JuR, Aravina OR. Mnogofaktornyj analiz riska razvitija akusherskih i perinatal'nyh oslozhnenij u pacientok s ozhireniem i izbytochnoj massoj tela. Izvestija Samarskogo nauchnogo centra RAN. 2015; 17 (5–3): 793–7.
2. Anderson P, Doyle LW. Victorian Infant Collaborative Study Group. Neurobehavioral outcomes of school-age children born extremely low birth weight or very preterm in the 1990s. J Am Med Assoc. 2003; 289: 3264–72.
3. Ombelet W, De Sutter P, Van der Elst J, Martens G. Multiple gestation and infertility treatment: registration, reflection and reaction-the Belgian project. Hum Reprod Update. 2005; 11: 3–14.
4. De Sutter P, Van der Elst J, Coetsier T, Dhont M. Single embryo transfer and multiple pregnancy rate reduction in IVF/ICSI: a 5-year appraisal. Reprod Biomed Online. 2003; 7: 464–9.
5. Thurin A, Hausken J, Hillensjo T, Jablonowska B, Pinborg A, Strandell A, Bergh C. Elective single-embryo transfer versus double-embryo transfer in in vitro fertilization. N Engl J Med. 2004; 351: 2392–402.
6. Bergh C. Single embryo transfer: a mini-review. Hum Reprod. 2005; 20: 323–7.
7. Gardner DK, Meseguer M, Rubio C, Treff NR. Diagnosis of human preimplantation embryo viability. Hum Reprod Update. 2015; 21: 727–47.
8. Bavister BD. Culture of preimplantation embryos: facts and artifacts. Hum Reprod Update. 1995; 1: 91–148.
9. Meseguer M. Time-lapse: the remaining questions to be answered. Fertil Steril. 2016; 105 (2): 295–6.
10. Pribenszkya C, Matyasb S, Kovacsb P, Losonczic E, Zádori J, Vajta G. Pregnancy achieved by transfer of a single blastocyst selected by time-lapse monitoring. Reprod Biomed Online. 2010; 21 (4): 533–6.
11. Wang SX. The past, present, and future of embryo selection in in vitro fertilization: Frontiers in Reproduction Conference. Yale J Biol Med. 2011; 84 (4): 487–90.
12. McEvoy K, Brison D, Roberts S, Turner C, Adeniyi T, Wood L, et al. A one year retrospective analysis comparing live birth outcomes from embryos grown and transferred from an undisturbed time-lapse culture system with a conventional culture system. Human reproduction. 2016; 31: i174–i175.
13. Shurygina OV, Saraeva NV, Tugushev MT, Pekarev VA, Bajzarova AA, Krasnova OV, et al. Otdalennye rezultaty programm VRT s ispolzovaniem sistemy nepreryvnogo videonabljudenija na jembriologichekom jetape. V sbornike: Reproduktivnye tehnologii segodnja i zavtra. Materialy XXVII mezhdunarodnoj konferencii Rossijskoj Associacii Reprodukcii Cheloveka; 6–9 centjabrja 2017 g. M.: Media Sfera, 2017; 328 s.
14. Adamson GD, Abusief ME, Palao LM, Gvakharia M. Improved implantation rates of day 3 embryo transfers with the use of an automated time-lapse–enabled test to aid in embryo selection. Fertil Steril. 2015; 105: 369–75.
15. Diamond MP, Suraj V, Behnke EJ, Yang X, Angle MJ, Lambe-Steinmiller JC, et al. Using the Eeva Test™ adjunctively to traditional day 3 morphology is informative for consistent embryo assessment within a panel of embryologists with diverse experience. J Assist Reprod Genet. 2015; 32: 61–68.
16. Ver Milyea MD, Tan Lei, Joshua TA, Conaghan J, Ivani K, Gvakharia M, et al. Computer-automated time-lapse analysis results correlate with embryo implantation and clinical pregnancy: A blinded, multi-centre study. Reprod Biomed Online. 2014; 29 (6): 729–36.
17. Kirkegaard K, Hindkjaer JJ, Grøndahl ML, Kesmodel US, Ingerslev HJ. A randomized clinical trial comparing embryo culture in a conventional incubator with a time-lapse incubator. J Assist Reprod Genet. 2012; 29 (6): 565–72.
18. Minasi MG, Colasante A, Riccio T, Ruberti A, Casciani V, Scarselli F, et al. Correlation between aneuploidy, standard morphology evaluation and morphokinetic development in 1730 biopsied blastocysts: a consecutive case series study. Hum Reprod. 2016; 31 (10): 2245–54.
19. Gardner DK, Schoolcraft WB. Culture and transfer of human blastocysts. Curr Opin Obstet Gynecol. 1999 Jun; 11 (3): 307–11.
20. Gardner DK, Lane M, Stevens J, Schlenker T, Schoolcraft WB. Blastocyst score affects implantation and pregnancy outcome: towards a single blastocyst transfer. Fertil Steril. 2000; 73: 1155–8.
21. Lee AM, Connell MT, Csokmay JM, Styer AK. Elective single embryo transfer — the power of one. Contracept Reprod Med. 2016; 1: 11.
22. Goodman LR, Goldberg J, Falcone T, Austin C, Desai N. Does the addition of time-lapse morphokinetics in the selection of embryos for transfer improve pregnancy rates? A randomized controlled trial. Fertil Steril. 2016; 105 (2): 275–85.
23. Zhang JQ, Li XL, Peng Y, Guo X, Heng BC, Tong GQ. Reduction in exposure of human embryos outside the incubator enhances embryo quality and blastulation rate. Reprod Biomed Online. 2010; 20: 510–15.
24. Apter S, Ebner T, Freour T, Guns Y, Kovacic B, Le Clef N, et al. Good practice recommendations for the use of time-lapse technology. Human Reproduction Open. 2020; 2020 (2: hoaa008. Available from: https://doi.org/10.1093/hropen/hoaa008.
25. Armstrong S, Bhide P, Jordan V, Pacey A, Marjoribanks J, Farquhar C. Time-lapse systems for embryo incubation and assessment in assisted reproduction. Cochrane Database of Systematic Reviews. 2018; 25 (5): CD011320. DOI: 10.1002/14651858.CD011320.pub4.
26. Pribenszkya C, Nilselid AM, Montag M. Time-lapse culture with morphokinetic embryo selection improves pregnancy and live birth chances and reduces early pregnancy loss: a meta-analysis. Reprod Biomed Online. 2017 Nov; 35 (5): 511–520.
27. Meseguer M, Rubio I, Cruz M, Basile N, Marcos J, Requena A. Embryo incubation and selection in a time-lapse monitoring system improves pregnancy outcome compared with a standard

incubator: a retrospective cohort study. Fertil Steril. 2012 Dec; 98 (6): 1481–9.
28. Athayde Wirka K, Chen AA, Conaghan J, Ivani K, Gvakharia M, Behr B, et al. Atypical embryo phenotypes identified by time-lapse microscopy: high prevalence and association with embryo development. Fertil Steril. 2014; 101 (6): 1637–48.
29. Liu Yanhe, Chapple V, Feenan K, Roberts P, Matson P. Time-lapse deselection model for human day 3 in vitro fertilization embryos: the combination of qualitative and quantitative measures of embryo growth. Fertil Steril. 2016; 105 (3): 656–62.

Литература

1. Калинкина О. Б., Спиридонова Н. В., Юнусова Ю. Р., Аравина О. Р. Многофакторный анализ риска развития акушерских и перинатальных осложнений у пациенток с ожирением и избыточной массой тела. Известия Самарского научного центра РАН. 2015; 17 (5–3): 793–7.
2. Anderson P, Doyle LW. Victorian Infant Collaborative Study Group. Neurobehavioral outcomes of school-age children born extremely low birth weight or very preterm in the 1990s. J Am Med Assoc. 2003; 289: 3264–72.
3. Ombelet W, De Sutter P, Van der Elst J, Martens G. Multiple gestation and infertility treatment: registration, reflection and reaction-the Belgian project. Hum Reprod Update. 2005; 11: 3–14.
4. De Sutter P, Van der Elst J, Coetsier T, Dhont M. Single embryo transfer and multiple pregnancy rate reduction in IVF/ICSI: a 5-year appraisal. Reprod Biomed Online. 2003; 7: 464–9.
5. Thurin A, Hausken J, Hillensjo T, Jablonowska B, Pinborg A, Strandell A, Bergh C. Elective single-embryo transfer versus double-embryo transfer in in vitro fertilization. N Engl J Med. 2004; 351: 2392–402.
6. Bergh C. Single embryo transfer: a mini-review. Hum Reprod. 2005; 20: 323–7.
7. Gardner DK, Meseguer M, Rubio C, Treff NR. Diagnosis of human preimplantation embryo viability. Hum Reprod Update. 2015; 21: 727–47.
8. Bavister BD. Culture of preimplantation embryos: facts and artifacts. Hum Reprod Update. 1995; 1: 91–148.
9. Meseguer M. Time-lapse: the remaining questions to be answered. Fertil Steril. 2016; 105 (2): 295–6.
10. Pribenszkya C, Matyasb S, Kovacsb P, Losonczic E, Zádori J, Vajta G. Pregnancy achieved by transfer of a single blastocyst selected by time-lapse monitoring. Reprod Biomed Online. 2010; 21 (4): 533–6.
11. Wang SX. The past, present, and future of embryo selection in in vitro fertilization: Frontiers in Reproduction Conference. Yale J Biol Med. 2011; 84 (4): 487–90.
12. McEvoy K, Brison D, Roberts S, Turner C, Adeniyi T, Wood L, et al. A one year retrospective analysis comparing live birth outcomes from embryos grown and transferred from an undisturbed time-lapse culture system with a conventional culture system. Human reproduction. 2016; 31: i174–i175.
13. Шурыгина О. В., Сараева Н. В., Тугушев М. Т., Пекарев В. А., Байзарова А. А., Краснова О. В., и др. Отдаленные результаты программ ВРТ с использованием системы непрерывного видеонаблюдения на эмбриологическом этапе. В сборнике: Репродуктивные технологии сегодня и завтра. Материалы XXVII международной конференции Российской ассоциации репродукции человека; 6–9 сентября 2017 г.; М.: Медиа Сфера, 2017; 328 с.
14. Adamson GD, Abusief ME, Palao LM, Gvakharia M. Improved implantation rates of day 3 embryo transfers with the use of an automated time-lapse–enabled test to aid in embryo selection. Fertil Steril. 2015; 105: 369–75.
15. Diamond MP, Suraj V, Behnke EJ, Yang X, Angle MJ, Lambe-Steinmiller JC, et al. Using the Eeva Test™ adjunctively to traditional day 3 morphology is informative for consistent embryo assessment within a panel of embryologists with diverse experience. J Assist Reprod Genet. 2015; 32: 61–68.
16. Ver Milyea MD, Tan Lei, Joshua TA, Conaghan J, Ivani K, Gvakharia M, et al. Computer-automated time-lapse analysis results correlate with embryo implantation and clinical pregnancy: A blinded, multi-centre study. Reprod Biomed Online. 2014; 29 (6): 729–36.
17. Kirkegaard K, Hindkjaer JJ, Grøndahl ML, Kesmodel US, Ingerslev HJ. A randomized clinical trial comparing embryo culture in a conventional incubator with a time-lapse incubator. J Assist Reprod Genet. 2012; 29 (6): 565–72.
18. Minasi MG, Colasante A, Riccio T, Ruberti A, Casciani V, Scarselli F, et al. Correlation between aneuploidy, standard morphology evaluation and morphokinetic development in 1730 biopsied blastocysts: a consecutive case series study. Hum Reprod. 2016; 31 (10): 2245–54.
19. Gardner DK, Schoolcraft WB. Culture and transfer of human blastocysts. Curr Opin Obstet Gynecol. 1999 Jun; 11 (3): 307–11.
20. Gardner DK, Lane M, Stevens J, Schlenker T, Schoolcraft WB. Blastocyst score affects implantation and pregnancy outcome: towards a single blastocyst transfer. Fertil Steril. 2000; 73: 1155–8.
21. Lee AM, Connell MT, Csokmay JM, Styer AK. Elective single embryo transfer — the power of one. Contracept Reprod Med. 2016; 1: 11.
22. Goodman LR, Goldberg J, Falcone T, Austin C, Desai N. Does the addition of time-lapse morphokinetics in the selection of embryos for transfer improve pregnancy rates? A randomized controlled trial. Fertil Steril. 2016; 105 (2): 275–85.
23. Zhang JQ, Li XL, Peng Y, Guo X, Heng BC, Tong GQ. Reduction in exposure of human embryos outside the incubator enhances embryo quality and blastulation rate. Reprod Biomed Online. 2010; 20: 510–15.
24. Apter S, Ebner T, Freour T, Guns Y, Kovacic B, Le Clef N, et al. Good practice recommendations for the use of time-lapse technology. Human Reproduction Open. 2020; 2020 (2: hoaa008. Available from: https://doi.org/10.1093/hropen/hoaa008.
25. Armstrong S, Bhide P, Jordan V, Pacey A, Marjoribanks J, Farquhar C. Time-lapse systems for embryo incubation and assessment in assisted reproduction. Cochrane Database of Systematic Reviews. 2018; 25 (5): CD011320. DOI: 10.1002/14651858.CD011320.pub4.
26. Pribenszkya C, Nilselid AM, Montag M. Time-lapse culture with morphokinetic embryo selection improves pregnancy and live birth chances and reduces early pregnancy loss: a meta-analysis. Reprod Biomed Online. 2017 Nov; 35 (5): 511–520.
27. Meseguer M, Rubio I, Cruz M, Basile N, Marcos J, Requena A. Embryo incubation and selection in a time-lapse monitoring system improves pregnancy outcome compared with a standard incubator: a retrospective cohort study. Fertil Steril. 2012 Dec; 98 (6): 1481–9.
28. Athayde Wirka K, Chen AA, Conaghan J, Ivani K, Gvakharia M, Behr B, et al. Atypical embryo phenotypes identified by time-lapse microscopy: high prevalence and association with embryo development. Fertil Steril. 2014; 101 (6): 1637–48.
29. Liu Yanhe, Chapple V, Feenan K, Roberts P, Matson P. Time-lapse deselection model for human day 3 in vitro fertilization embryos: the combination of qualitative and quantitative measures of embryo growth. Fertil Steril. 2016; 105 (3): 656–62.

BORDERLINE OVARIAN TUMORS IN PREGNANCY

Gerasimova AA[1], Shamarakova MV[1], Klimenko PA[2] ✉

[1] Center of Family Planning of Moscow Department of Health, Moscow, Russia

[2] Pirogov Russian National Research Medical University, Moscow, Russia

Borderline ovarian tumors (BOTs) are common in women in their reproductive years. In more than one-third of patients tumors are detected at the age of 15–29, the average age at initial diagnosis is 40. The study was aimed to improve methods for BOTs diagnosis in pregnancy and to determine the possibilities of organ preservation treatment. A group of 300 pregnant women with various tumor-like formations and ovarian tumors was examined. Of them, 25 patients had borderline epithelial tumors (22 patients had serous and 3 patients had mucinous tumors). Ultrasound examination together with blood serum CA-125, sFas, VEGF and IL6 level assessment were performed prior to surgery. The results obtained were compared with the results of morphological studies. Organ preservation and radical surgical treatment were carried out, and chemotherapy, if necessary. Perinatal outcomes were studied when performing the cross-comparison. It was discovered, that ultrasonography and logistic regression analysis made it possible to distinguish between benign ovarian tumors, BOTs and malignant ovarian tumors. The levels of VEGF above the 500 pg/ml, IL6 above the 8.1 pg/ml and CA-125 above the 300 U/ml indicated the high probability of malignant ovarian tumors in pregnant women. Only the morphological study of ovarian tissue, obtained regardless of surgical methods, ensured understanding of the ovarian tumor's true nature during pregnancy. At the same time, in three pregnant women with ovarian tumors, the morphological examination revealed some tissue areas common both for BOTs and malignant ovarian tumors. Thus, the predominance of the tumor early stages, relatively mild course and, favorable prognosis in patients with BOTs make it possible to use gentle surgical treatment making it possible to preserve menstrual function and fertility.

Keywords: ultrasound, morphological examination, ovarian tumors in pregnant women, CD31

Author contribution: all authors contributed to the research and manuscript preparation equally, read the approved the final version of the article before publishing.

Compliance with ethical standards: the study was approved by the Ethics Committee of Pirogov Russian National Research Medical University (protocol № 176 dates June 25, 2018). The informed consent was submitted by all study participants.

✉ **Correspondence should be addressed:** Piotr A. Klimenko
Sevastopolsky prospect, 24a, Moscow, 117209; pa.klimenko@mail.ru

Received: 07.04.2020 **Accepted:** 21.04.2020 **Published online:** 26.04.2020

DOI: 10.24075/brsmu.2020.023

ПОГРАНИЧНЫЕ ОПУХОЛИ ЯИЧНИКОВ У БЕРЕМЕННЫХ

А. А. Герасимова[1], М. В. Шамаракова[1], П. А. Клименко[2] ✉

[1] Центр планирования семьи и репродукции, Москва, Россия

[2] Российский национальный исследовательский медицинский университет имени Н. И. Пирогова, Москва, Россия

Пограничные опухоли яичников характерны для женщин репродуктивного периода, более чем у трети больных опухоли выявляют в возрасте 15–29 лет, средний возраст при первичной постановке диагноза составляет 40 лет. Целью исследования было усовершенствовать методы диагностики пограничных опухолей яичников на фоне беременности и определить возможности выполнения органосохраняющего лечения. Обследовано 300 беременных с различными опухолевидными образованиями (ООЯ) и опухолями яичников (ОЯ), из которых 25 имели пограничные эпителиальные опухоли: 22 — серозные, три — муцинозные. До операции проводили УЗИ, определяли концентрацию в сыворотке крови CA-125, sFas, VEGF и IL6. Полученные результаты сопоставляли с морфологическими исследованиями. Проводили органосохраняющее и радикальное хирургическое лечение, при необходимости — химиотерапию. При перекрестном сравнении изучали перинатальные исходы. Обнаружено, что различить доброкачественные опухоли яичников от пограничных (ПОЯ) и злокачественных (ЗОЯ) возможно с помощью УЗИ и логрегрессионных моделей. Уровни VEGF выше 500 пг/мл, IL6 выше 8,1 пг/мл и CA-125 выше 300 ЕД/мл свидетельствуют о высокой вероятности ЗОЯ у беременных. И только морфологическое исследование тканей яичников, полученных независимо от хирургических способов, давало истинное представление о характере опухоли яичников у беременных. Вместе с тем у трех беременных с ОЯ при морфологическом исследовании выявлены участки ткани, характерные как для ПОЯ, так и для ЗОЯ. Таким образом, преобладание начальных форм опухолевого процесса, относительно благоприятное течение и прогноз при ПОЯ позволяют достаточно широко использовать хирургическое лечение щадящего характера с сохранением менструальной функции и фертильности.

Ключевые слова: ультразвуковое исследование, морфологическое исследование, опухоли яичников у беременных, CD31

Вклад авторов: все авторы внесли равнозначный вклад в проведение исследования и подготовку статьи, прочли и одобрили ее финальную версию перед публикацией.

Соблюдение этических стандартов: исследование одобрено этическим комитетом РНИМУ имени Н. И. Пирогова (протокол № 176 от 25 июня 2018 г.). Все пациенты подписали информированное согласие на участие в исследовании.

✉ **Для корреспонденции:** Петр Афанасьевич Клименко
Севастопольский проспект, д. 24а, г. Москва, 117209; pa.klimenko@mail.ru

Статья получена: 07.04.2020 **Статья принята к печати:** 21.04.2020 **Опубликована онлайн:** 26.04.2020

DOI: 10.24075/vrgmu.2020.023

Borderline epithelial tumors (borderline ovarian tumors, BOTs) are ovarian neoplasms associated with cellular and nuclear atypia without destructive stromal invasion which have a favorable prognosis. BOTs account for 15–20% of all ovarian neoplasms [1–3]. However, the data of specialized oncological clinics analysis revealed a higher incidence (21–35%) due to specialized patients' selection [4–8]. In pregnant women, the incidence of malignant ovarian neoplasms, together with BOTs, does not exceed 9%. Due to no pathognomonic signs, reliable ultrasound signs and the results of marker glycoprotein CA-125 determination, BOTs are difficult to diagnose, often it is hard to distinguish between BOTs, benign and malignant ovarian neoplasms. Therefore, the borderline tumor can be diagnosed reliably only during the post-operative tumor morphology

examination [9–10]. In more than 70% of pregnant women, the tumors are detected during the ultrasound scan in the early stages of gestation (tumor early stages according to the FIGO system). Surgical treatment of malignant ovarian tumors and BOTs in pregnant women is normally performed in the first and second trimesters of pregnancy [5, 11–12], which leads to increased perinatal morbidity and early infant mortality.

The study was aimed to improve methods for BOTs diagnosis in pregnancy and to determine the possibilities of organ preservation treatment.

METHODS

In 2000–2017 a group of 300 pregnant women with various tumor-like formations and ovarian tumors was prospectively examined. Inclusion criteria: pregnant women with tumor-like formations/ovarian tumors diagnosed during I–III trimesters. Exclusion criteria: the woman's refuse to participate in the study; pregnant women with cancer diagnosed before the study; patients with threatened abortion, intrauterine infection, impairments in a fetus diagnosed before the study. The results of the study were evaluated by cross-analysis. The results' distribution in accordance with the morphological structure, tumor stage and the abnormality degree is presented in Fig. 1.

In 76 of 300 pregnant women with ovarian neoplasms, BOTs and malignant ovarian tumors were detected. Of 25 patients with BOTs, 22 patients had serous and 3 had mucinous forms. It should be noted that the study was carried out for a long time and the patients' recruitment was random, not population-based.

Ultrasonographic examination was performed with the Voluson 530 MT (Kretztechnik; Austria) and Voluson E8 (General Electric; USA) systems, and the RIC5-9-D (4–9 MHz), C1-5-D (2–5 MHz), RAB4-8-D (2–8 MHz) probes. An ultrasound scan was carried out in 2D and 3D mode, combined with color and energy Doppler mapping, as well as with three-dimensional angiography. The color Doppler mapping was used for assessment of the following features: vascularization pattern (tumor periphery, central parts of the tumor, septa, papillary features), the curve of the blood flow velocity analysis together with resistance index (RI) and peak systolic blood flow velocity (cm/s) determination. Of 30 ultrasound signs of tumor-like formations, benign ovarian tumors, BOTs and malignant ovarian tumors, 17 signs appeared to be informative. For ultrasound diagnostics the proposed model was used allowing one to distinguish between benign ovarian tumors, BOTs and malignant ovarian tumors [13]. Our previous studies [14] demonstrated that ovarian tumors in pregnant women had ultrasound signs allowing one to differentiate between benign and malignant ovarian tumors with high accuracy. During the study it was noted that the differences in the ultrasound features of various ovarian neoplasms were significant. When studying the ultrasound signs of malignant epithelial tumors of the ovaries (ovarian cancer), four types of structure, and, which in most important, unique hemodynamic parameters were identified. At the same time, the assessment scale based on the ultrasound signs analysis was created. To evaluate the accuracy of the model, in addition to the actual percentage of correct assignments, the sensitivity (Se) and specificity (Sp) parameters were taken into account.

Molecular biology techniques were applied as follows. Concentration of CA-125 was determined using the enzyme immunoassay test system (Siemens; Germany). Enzyme immunoassay method was used to determine the sFas concentration in the blood serum using monoclonal antibodies, and the VEGF concentration using the reagent kits (R@D; USA). The concentration of IL6 was evaluated by the Sandwich Enzyme-Linked ImmunoSorbent Assay (ELISA) using the reagent kits (R&D; USA).

Different pathologists examined the hematoxylin and eosin stains. The WHO Classification of Tumors of Female Reproductive Organs (2003) was used for morphological diagnosis, since that classification was adopted in the Russian Federation at the time of the study. For immunohistochemical studies, paraffin blocks of 15 pregnant women with BOTs and 10 pregnant women with malignant ovarian tumors were selected. Analysis of the angiogenesis was performed using antibodies to the vascular endothelial growth factor, VEGF, the major signal transducer for angiogenesis (VENTANA; USA), and antibodies to CD31 endothelial marker, the type 1 platelet endothelial

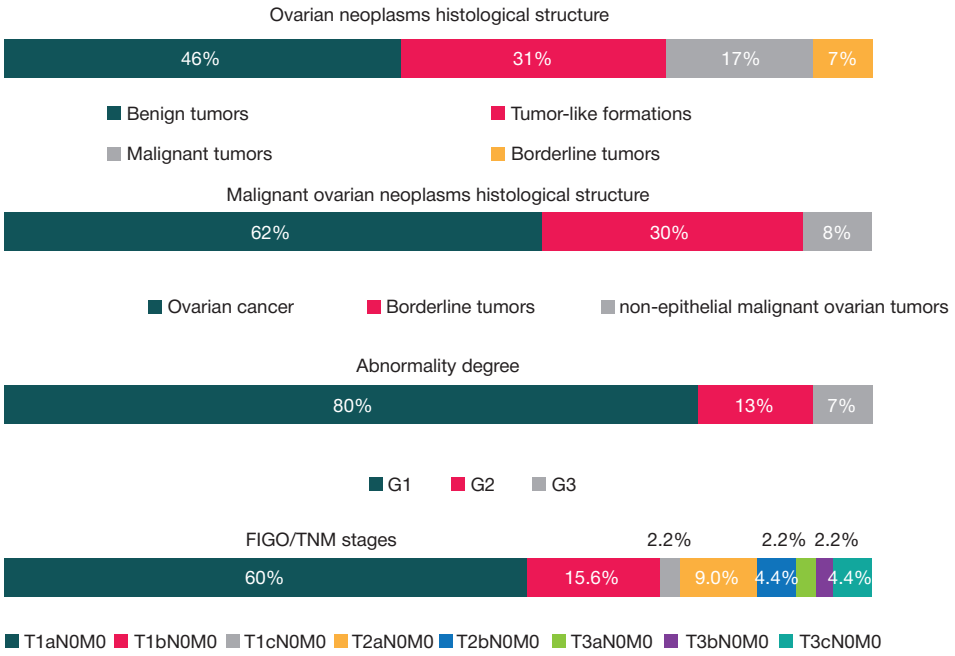

Fig. 1. Ovarian tumors/tumor-like formations distribution in accordance with the histological structure, stage (BOTs/ malignant ovarian tumors) and abnormality degree (ovarian cancer)

cell adhesion molecule (JC70 clone; VENTANA, USA). When evaluating the expression of CD31 under the microscope with small magnification, first, the areas with the largest number of microvessels were selected. Subsequently, in two separate fields of view with the increased microvasculature density, the number of all positive microvessels was calculated (200-fold magnification). The VEGF expression level was evaluated by semi-quantitative method (comparison of staining intensity and number of positive cells) in five fields of view (400-fold magnification). When measuring the staining intensity, unstained cells were assigned score 0, cells with pale yellow staining were assigned score 1, yellow-brown stained cells were assigned score 2, and brown stained cells were assigned score 3. The number of positively stained cells varied: score 0 corresponded to less than 10% of all cells, score 1 corresponded to 10–49% of stained cells, score 2 corresponded to 50–74% of stained cells, score 3 corresponded to over than 75% of stained cells. The results of both counts were added, the score over 2 was considered positive.

In addition, histories and outcomes of pregnancy and childbirth after treatment were studied in 300 patients with ovarian neoplasms.

Statistical analysis was carried out using the SPSS 15.0 software package (IBM; USA). Data were analyzed by the frequency method using the crosstabs. The differences were considered significant when $p < 0.05$.

RESULTS

The study demonstrated that the examined pregnant women's clinical characteristics did not vary significantly between the groups. Thus, the age of 76 pregnant women with BOTs and malignant ovarian tumors varied in a wide range, from 18 to 45 years. More than 60% of patients were aged 30. Pain in the lower abdomen and impaired function of neighboring organs (9% of cases), increase in abdomen size (10.9% of cases) were registered, and the history of menstruation irregularities (10.9% of cases) and infertility (2.7% of cases) was revealed in pregnant women with BOTs/malignant ovarian tumors. The structure of concomitant extragenital, gynecological pathologies and previous gynecological operations before pregnancy in patients with tumor-like formations/ovarian tumors correlated mainly with age and did not depend on the tumors' morphology.

Among the BOTs histological types the serous types prevailed (22 (88%) patients). Mucinous tumors were detected in 3 (12%) pregnant women. The 28% of patients had bilateral ovarian lesions. In most pregnant patients stage I BOTs were diagnosed (19 (76%) patients). Stage II was revealed in 5 (20%) patients, and stage III was verified only in one patient.

Ultrasonic signs in pregnant women with BOTs matched several morphological types: in 32.6% of patients, mixed tumors with the predominant solid pattern were diagnosed. About 55% of patients had tumors with the predominant cystic component, over 10% of patients had solid tumors. Doppler sonography revealed central and peripheral hypervascularization with low RI values (less than or equal to 0.4) and high values of peak systolic blood flow velocity (over 15 cm/s) obtained during the curve of the blood flow velocity analysis, as well as the mosaic vessels indicating the presence of arteriovenous shunting in the tumor vasculature.

The use of the proposed model for the differential diagnosis of ovarian tumors in pregnant women made it possible to distinguish between tumor-like formations, benign ovarian tumors, BOTs and malignant ovarian tumors (sensitivity was 100%, specificity 92.3%, with an overall accuracy of the model 92.8%). Due to the similarity of images and hemodynamic indicators during the ultrasound scan, it was impossible to distinguish BOTs from malignant ovarian tumors. At the same time, in all patients with neoplasms of the described type, blood vessels were located in the center with a branched network in the septa, solid component, and papillary components. The low-resistance blood flow was revealed.

In pregnant women with BOTs, the CA-125 concentration varied in the range from 24.4 to 361 U/ml in the I trimester, and from 24.1 to 223 U/ml in the II trimester of pregnancy. The level of sFas was 40–200 ng/ml in the I trimester, and 46–180 in the

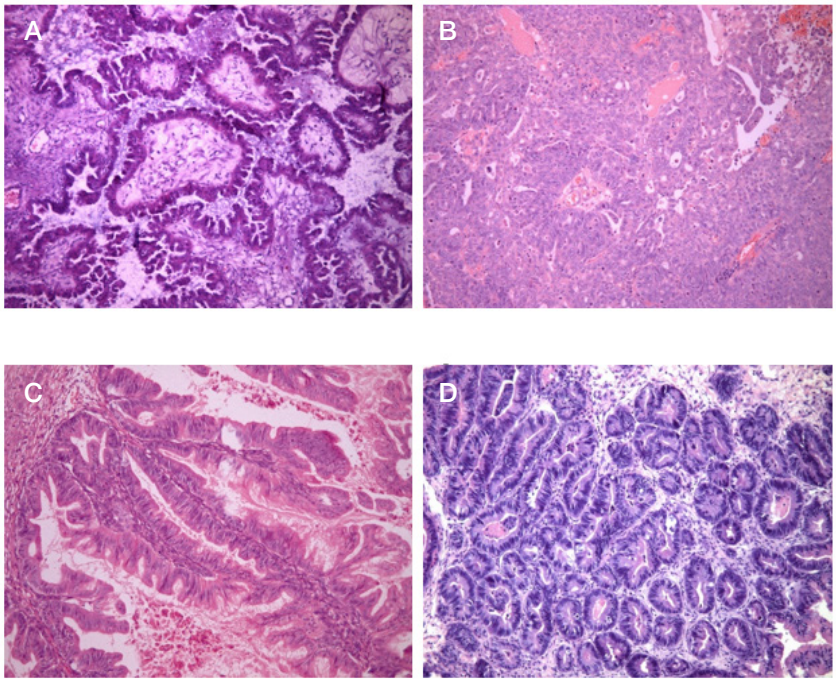

Fig. 2. Morphology of BOTs and malignant ovarian tumors in pregnant women. **A**. Borderline serous ovarian cystadenoma (×10, hematoxylin and eosin staining). **B**. Poorly differentiated serous ovarian carcinoma (×10, hematoxylin and eosin staining). **C**. Borderline mucinous ovarian cystadenoma (×10, hematoxylin and eosin staining). **D**. Mucinous ovarian carcinoma (×10, hematoxylin and eosin staining).

II trimester. The VEGF concentration varied in the range from 89 to 286 pg/ml in the I trimester, and from 92 to 480 pg/ml in the II trimester of pregnancy. IL6 reached 3.6–12 in the I trimester and 8–40.9 pg/ml in the II trimester.

In patients with malignant ovarian tumors (compared to patients with BOTs) the significant increase of CA-125 and other tumor markers (sFas, VEGF, IL6) levels in blood serum was observed at any time during pregnancy. In the blood of 3 patients with adenocarcinoma of the ovary the CA-125 level was 540–1224.6 U/ml, the sFas level was 180–312.6 ng/ml, the VEGF level was 510–1028 pg/ml, and the IL6 level was 9.8–40.9 pg/ml. The same concentration of molecular factors was observed in the blood of patients with dysgerminoma, mixed germ cell tumor and immature teratoma. In these patients, the CA-125 level exceeded 361 U/ml, the sFas level was above 240 ng/ml, the VEGF level above 490 pg/ml, and the IL6 level above 8.1 pg/ml.

When studying the BOTs morphology (Fig. 2), the features making it possible to distinguish BOTs from benign and malignant ovarian tumors were detected in 22 cases. In 3 cases, the inconsistencies were found in the final histological response of patients diagnosed with serous adenocarcinoma against the background serous borderline tumor. During the second preparations review no elements of the malignant tumor were found.

The borderline serous cystadenoma was a cystic tumor with discohesive wall and the pronounced papillary features which filled the entire inner surface and in 70% of cases were present on the outer surface. BOTs were characterized by the presence of epithelial features with the formation of cell bundles and separation of cells groups simultaneously with strictly ordered branching, in which small papilla came from large, centrally located papillae. Cells of the borderline serous tumors had some features of epithelial and mesothelial differentiation. Ciliated cells similar to cells of the fallopian tube were detected in one third of tumors. Cells with abundant eosinophilic cytoplasm and rounded nuclei resembled mesothelium, they were located on the tops of papilla. Cell nuclei were located basally, oval or round, with -slight atypia, delicate chromatin, and sometimes with pronounced nucleoli. Rare mitoses were detected (usually 4–10 in the fields of view). Psammoma (sand) bodies were revealed in a half of preparations.

Serous carcinomas reached large sizes (up to 20 cm in diameter), they consisted of cysts with serous or sanious contents, filled with soft loose papillary features. The outer surface was smooth with some papillary structures on it. The solid tumors usually had less pronounced pink gray papilla, they were soft or dense depending on the underlying stroma type. At the same time the foci of hemorrhage and necrosis were observed. Under the microscope the serous carcinomas had a papillary structure with solid foci, large round cells with polymorphic hyperchromatic nuclei, clumpy nuclear chromatin pattern and increased nuclear-cytoplasmic ratio, pseudostratified epithelium. Those were characterized by the loss of polarity, no cilia on the cell surface, increased mitotic activity.

The borderline mucinous cystadenoma of the ovary was usually multilocular with a diameter up to 30 cm, it contained the straw-colored liquid or mucus. Morphological examination of the described tumors' preparations revealed areas lined with the multi-layered mucinous epithelium of the intestinal type with the villous glandular and papillary features and- slight atypia of cell nuclei.

Mucinous carcinoma differed from the borderline mucinous cystadenoma by the foci with a glands complex arrangement lined with cells with moderate and severe nuclei atypia, mitoses, as well as by the foci of necrosis inside the tumor.

CD31 expression (Fig. 3–4) was detected in the tumor stroma in all patients. The average number of CD31-positive vessels in women with BOTs was 36 (12–48), and in women with malignant ovarian tumors it was 44 (19–56). The evaluated by the semi-quantitative method immunoreactivity for VEGF was scored 5 (4–6) in women with BOTs, and 6 (5–7) in women with malignant ovarian tumors. No significant differences in both markers' expression levels were revealed.

The medical history analysis of pregnant women with BOTs and malignant ovarian tumors showed that those of them who had disseminated tumors underwent the cytoreductive surgery with abortion. The other patients underwent the cytoreductive surgery twice: upon the detection of a tumor and after the cesarean section.

All patients demonstrating signs of ovarian tumor malignization got the midline laparotomy with the curve around the umbilicus on the left. In six patients, diagnostic laparoscopy was performed first, and after that laparotomy and primary lesion removal (due to the suspected ovarian cancer).

The volume of the surgical procedure was determined intraoperatively in accordance with the clinical picture, reproductive history, age, ultrasonography, serum tumor marker levels and express histopathological examination results. During the intervention, surgical tumor staging was performed, as well as the abdomen and pelvic organs revision, greater omentum resection/removal, multiple peritoneal biopsies, taking swabs or ascitic fluid from the abdominal cavity. In patients with mucinous tumors, an appendectomy was carried out. The patients not interested in pregnancy maintenance and fertility underwent the radical surgery (7 patients of 76). At the first stage during pregnancy, 20 patients with BOTs underwent the organ sparing intervention preserving uterus and the healthy ovary fragment. In two patients, the bilateral adnexectomy was performed. In one of them, the borderline tumor was found during the histopathological examination of the resected part of the visually unchanged contralateral ovary (stage IB).

It should be noted that during the histopathological examination of biopsy material or tumor preparations, errors and inaccuracies may occur. Thus, during our study, in three pregnant women with ovarian tumors, morphological examination revealed tissue features characteristic of both BOT and malignant ovarian tumors. The patients were diagnosed with well-differentiated adenocarcinoma of both ovaries against the background of the borderline serous cystadenoma. In one of those patients, bilateral ovarian tumors with signs of malignization and ascites were clinically defined during the weeks 11–12 of pregnancy. In the oncology hospital the

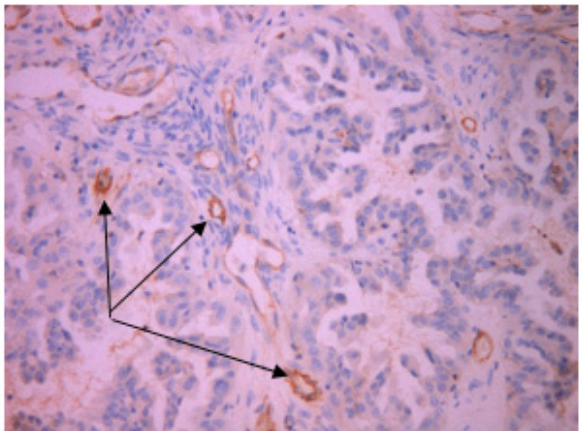

Fig. 3. CD31 expression in the malignant ovarian tumor (×20). Vessels are marked with arrows

diagnostic laparoscopy (right-sided adnexectomy with express histological examination) was performed, and the borderline cystadenoma was diagnosed. The laparoscopic entry was changed to laparotomy. A midline laparotomy was used for the left ovary biopsy, greater omentum resection and multiple peritoneal biopsies. The differentiated adenocarcinoma developed against the background of a serous borderline tumor with cancer emboli in the lumen of the greater omentum vessels was diagnosed by the morphological examination (ovarian cancer T3cN0M0). Artificial abortion and radical surgery were performed (hysterectomy with left adnexectomy and the subtotal greater omentum resection). The abdominal cavity swabs' cytological studies revealed the adenogenic cancer signs. Prior to the chemotherapy appointment, the interdisciplinary oncological consultation was held due to discrepancy in the cytological and histological studies results interpretation by different specialists. The initial diagnosis was not confirmed. The patient was diagnosed with the borderline tumor of the ovary with noninvasive implants in the greater omentum. It was decided not to use chemotherapy. The patient observed for four years demonstrates no signs of the disease progression.

The results of the patients with borderline tumors treatment were as follows: 3 pregnant women underwent abortion and surgery (panhysterectomy due to the presence of adenocarcinoma together with the serous BOT), 2 women had spontaneous abortion, 10 patients delivered on their own on time, 6 women delivered prematurely by cesarean section due to obstetric indications, in 4 patients the repeated surgery was carried out for restaging.

Later the tumor recurrence was observed in two pregnant women with BOTs. In one of them, diagnosed with serous histological type IA stage tumor in the resected ovarian tissue after the organ preservation surgery, the recurrence was detected in the 5th year of observation. The morphological examination revealed a well-differentiated adenocarcinoma, followed by a radical intervention supplemented with chemotherapy. In the 2nd patient, 2 years after the first surgery the recurrence was detected, and the tumor in its histological pattern was similar to the primary tumor (atypical proliferative serous tumor). After the recurrent neoplasm removal, the patient received combined therapy. Both patients remained alive for more than 3 years. Five patients dropped out of the observation. We tracked the long-term effect of treatment in 17 of 25 patients for 3–10 years. All patients were alive at the time of the study. The overall 5-year survival rate was 100%.

In patients with BOTs, 2–5 years after surgery 9 pregnancies occurred, the four of which ended in delivery with a favorable outcome. In three patients, pregnancy ended in spontaneous abortion.

DISCUSSION

Literature data indicate no specific clinical manifestations of BOTs during pregnancy. Doppler ultrasonography used in the model for differential diagnosis has high specificity.

Currently, no molecular factors have been identified that reliably characterize BOTs [2, 15]. The use of most tumor markers is limited due to the high variability of their values, including those depending on the gestational age. In our study, the significant increase of the carcinogenesis markers levels over the threshold (VEGF level exceeded 500 pg/ml, IL6 level was above 8.1 pg/ml) was detected in pregnant women with malignant neoplasms of the ovary. The test specificity was 91.5%, and the sensitivity was 75%. The CA-125 concentration in pregnant women with malignant ovarian tumors exceeded 300 U/ml. Our results were consistent with the other authors' data [16].

When evaluating the VEGF expression level in the paraffin blocks by the semi-quantitative method, the increased immunoreactivity for the marker (score 5–7) was detected in ovarian carcinomas. The VEGF expression association with ovarian cancer has been confirmed by many studies. An increase in VEGF immunoreactivity in ovarian carcinoma (compared to BOT) has been proven, while a high VEGF expression level indicates the disease progression [17]. Increased immunoreactivity of CD31 in the malignant ovarian tumors preparations compared to BOT preparations indicates increased blood flow in the tumor tissues due to neovascularization detected in malignant tumors [18].

The main method of the BOTs treatment is surgery (organ preservation or radical approach). Researchers of the world are actively discussing the possibility of ultra-conservative interventions as an organ preservation option leaving the affected with BOT ovarian tissue unchanged after the resection/cystectomy [2, 19]. Adnexectomy on the lesion side with a morphological study of peritoneal swabs and multiple biopsies is considered the optimal intervention volume. The final surgical staging should be performed during cesarean section or after delivery (in case of vaginal birth) [20, 21]. We did not use the ultraconservative interventions in our study, 80% of patients with BOTs underwent organ preservation surgery. The restaging surgery was performed in 16% of patients.

Approximately one-third of the patients with BOTs and well-differentiated adenocarcinoma need a final postoperative morphological study using paraffin blocks [2, 22–24]. According to some reports, the high overdiagnosis rate in patients with BOTs having the suspicious for ovarian cancer foci leads to an unreasonable overestimation of the surgical interventions volume, even when performing the final histopathological examination in the specialized institutions [3]. According to our results, the morphological response interpretation discrepancies in the differential diagnosis of BOTs and ovarian cancer have been detected in 12% of patients. The diverse BOTs structure and the need for a thorough study of multiple slices are the reason for the strict requirements for the morphologist's qualification and experience. The other researchers hold a similar opinion [3, 9, 22].

The overall recurrence rate in patients with BOTs varies from 3 to 10%, and the recurrence occurs in 25% of patients with common tumor stages. Our study has revealed recurrence in 8% of patients. According to the literature data, the 5-year survival rate of patients with I–II stage tumors is 98–99%, and

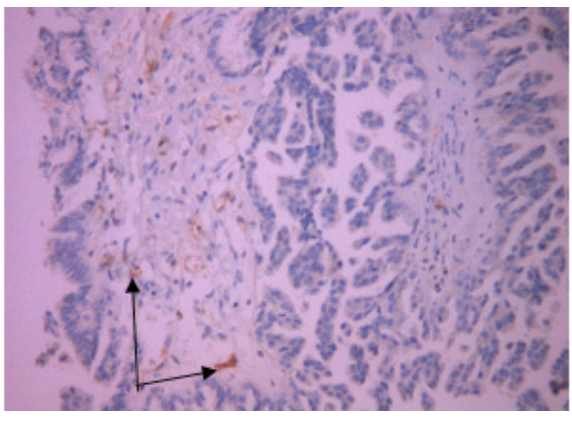

Fig. 4. CD31 expression in the borderline ovarian tumor (×20). Vessels are marked with arrows

in patients with III–IV tumors it is 82–90% [25, 26]. Possibly, the high the 5-year survival rate values are associated with the BOTs early stages detection and with the small sample size.

The papers on the study of fertility after the organ preservation treatment report that spontaneous pregnancies occur in 40–72% of patients. The effect of pregnancy on the course of the disease remains unknown [1, 2, 27, 28]. It is worth mentioning, that the reproductive results obtained during our study were pregnancies detected in more than 35% of patients with BOTs diagnosed in pregnancy after the organ preservation surgical interventions. The results obtained made it possible to highlight the following important signs complex in the diagnostic algorithm for pregnant women with suspected malignization of the ovarian tumors: mixed echographic structure with hypervascular supply pattern and low RI values, VEGF value exceeding 500 pg/ml and IL6 value over 8.1 pg/ml, CA-125 concentration exceeding 300 U/ml. However, the similarity of BOTs and malignant ovarian tumors ultrasonic signs did not allow us to distinguish between these types of neoplasms accurately. The diagnosis of BOT is confirmed during the final postoperative morphological examination. The results of the express ovarian tissue histological analysis in frozen sections not always provide true information on the ovarian tumors nature in pregnant women. High 5-year survival rate after the BOTs organ preservation surgical treatment carried out during pregnancy indicates the possibility to use the gentle approach in the treatment of the tumor's early stages.

CONCLUSION

Despite significant scientific and practical interest to BOTs, many problems related to improving the diagnosis and to the treatment of patients in pregnancy have not been resolved. The predominance of the tumor early stages, relatively mild course and favorable prognosis in patients with BOTs make it possible to use the gentle surgical treatment preserving menstrual function and fertility.

References

1. Battalova G. Ju. Pogranichnye opuholi jaichnikov (optimizacija metodov lechenija i mediko-socialnoj reabilitacii bolnyh) [dissertation]. M., 2005. Russian.
2. Novikova EG, Andreeva YuYu, Shevchuk AS. Fertility sparing treatment for patients with bilateral borderline ovarian tumors. Oncology. 2013; (1): 84–91.
3. Davydova IYu. Serous borderline ovarian tumors (clinical and morphological features, treatment, prognosis) [dissertation]. M., 2018. Russian.
4. Giuntoli RL, Vang RS, Bristow RE. Evaluation and management of adnexal masses during pregnancy. Clin Obstet Gynecol. 2006; 49 (3): 492–505.
5. Bakhidze EV. Ovarian tumors in pregnancy. Journal of Obstetrics and Women's Diseases. 2011; 3: 190–6.
6. Morice P, Uzan C, Gouy S, Verschraegen C, Haie-Meder C. Gynecological cancers in pregnancy. Lancet. 2012; 379 (9815); 558–69.
7. Aggarwal P, Kehoe S. Ovarian tumors in pregnancy a literature review. Eur J Obstet Gynecol Reprod Biol. 2011; 155 (2): 119–24.
8. Gui T, Cao D, Shen K, Yang J, Fu C, Lang J, Liu X. Management and outcome of ovarian malignancy complicating pregnancy: an analysis of 41 cases and review of the literature. Clin Transl Oncol. 2013; 15 (7): 548–54.
9. Shloma EN, Fridman MV, Shelkovich SE, Demidchik YuE. Borderline epithelial tumors of the ovaries: clinical course and problems of morphological diagnosis. Minsk: Publishing house "Bel MAPO", 2012; 80 s.
10. Davydova IYu, Kuznetsov VV, Karseladze AI, Meshcheryakova LA. Borderline ovarian tumors. Obstetrics and gynecology: news, opinions, training. 2019; 7 (1): 92–104.
11. Nadereh B, Mojgan KZ, Mitra MG, Fatemeh G, Azamsadat M, Fahimeh G. Ovarian carcinoma with pregnancy: a clinicopathologic analysis of 23 cases and review of the literature. BMC Pregnancy Childbirth. 2008; 8: 3. Available from: https://www.ncbi.nlm.nih.gov/pmc/articles/PMC2266699/.
12. Yong-Soon K, Jung-Eun M, Kyung-Taek L, In-Ho L, Tae-Jin K, Ki-Heon L, et al. Ovarian cancer during pregnancy clinical and pregnancy outcome. Korean Med Sci. 2010; 25 (2): 230–4.
13. Gerasimova AA, Gus AI, Klimenko PA, inventor; Klimenko Petr Afanasevich, assignee. A method for the differential diagnosis of tumorous formations and tumors of the ovaries in pregnant women. Russian Federation patent RF 2325118. 2007 Jun 1. Russan.
14. Gerasimova AA, Shvyrev S, Solomatina AA, Gus AI, Klimenko PA. Procedure for detecting the pattern of ovarian masses. Oncology. 2013; 1: 34–40.
15. Tinelli R, Tinelli A, Tinelli F, Cicenelli E, Malvasi A. Conservative surgery for borderline ovarian tumors: a review. Gynecol Oncol. 2006; 100 (1): 185–91.
16. Manuhin IB, Vysockij MM, Kushlinskij NE. Molekuljarno-biologicheskie faktory v patogeneze i hirurgicheskom lechenii opuholej jaichnikov. M.: Izd-vo «Dinastija», 2007; 208 s. Russian.
17. Moghaddam SM, Amini A, Morris D, Pourgholami H. Significance of vascular endothelial growth factor in growth and peritoneal dissemination of ovarian cancer. Cancer Metastasis Rev. 2012; 31 (1–2): 143–62. DOI: 10.1007/s10555-011-9337-5.
18. Viallard C, Larrivée B. Tumor angiogenesis and vascular normalization: alternative therapeutic targets. Angiogenesis. 2017; 20 (4): 409–26. DOI: 10.1007/s10456-017-9562-9.
19. Novikova EG, Shevchuk AS. Organ-preserving treatment of patients with borderline ovarian tumors. Oncology issues. 2014; 60 (3): 267–73.
20. Fauvet R, Brzakowski M, Morice P, Resch B, Marret H, Graesslin O, et al. Borderline ovarian tumors diagnosed during pregnancy exhibit a high incidence of aggressive features: results of a French multicenter study. Ann Oncol. 2012; 23 (6): 1481–7.
21. Zagouri F, Dimitrakakis C, Marinopoulos S, Tsigginou A, Dimopoulos MA. Cancer in pregnancy: disentangling treatment modalities. ESMO. 2016; 1 (3). Available from: https://www.ncbi.nlm.nih.gov/pmc/articles/PMC5070264/
22. Shevchuk AS. Repeated laparoscopic operations in patients with malignant ovarian tumors [dissertation]. M., 2005.
23. Kim JH, Kim TJ, Park YG. Clinical analysis of intra — operative frozen section proven borderline tumors of the ovary. J Gynecol Oncol. 2009; 20 (3): 176–80.
24. Brun JL, Cortez A, Rouzier R. Factors influencing the use and accuracy of frozen section diagnosis of epithelial ovarian tumors. Am J Obstet Gynecol. 2008; 199 (3): 241–7.
25. Du Bois A, Ewald-Riegler N, du Bois O, Harter P. Borderline tumors of the ovary — a systematic review. Geburtsh Frauenheilk. 2009; 69: 807–33.
26. Trope C, Davidson B, Paulsen T, Abeler VM, Kaern J. Diagnosis and treatment of borderline ovarian neoplasms «the state of the art». Eur J Gynecol Oncol. 2009; 30 (5): 471–82.
27. Fauvet R, Poncelet C, Boccara J. Fertility after conservative treatment for borderline ovarian tumors a French multicenter study. Fertil Steril. 2005; 83: 284.
28. Tinelli F, Tinelli R, La Grotta F. Pregnancy outcome and recurrence after conservative laparoscopic surgery for borderline ovarian tumors. Acta Obstet Gynecol Scand. 2007; 86: 81.

Литература

1. Батталова Г. Ю. Пограничные опухоли яичников (оптимизация методов лечения и медико-социальной реабилитации больных) [диссертация]. М., 2005.
2. Новикова Е. Г., Андреева Ю. Ю., Шевчук А. С. Пограничные опухоли яичников. Онкология. 2013; (1): 84–91.
3. Давыдова И. Ю. Серозные пограничные опухоли яичников (клинико-морфологические особенности, лечение, прогноз) [диссертация]. М., 2018.
4. Giuntoli RL, Vang RS, Bristow RE. Evaluation and management of adnexal masses during pregnancy. Clin Obstet Gynecol. 2006; 49 (3): 492–505.
5. Бахидзе Е. В. Опухоли яичника у беременных. Журнал акушерства и женских болезней. 2011; 3: 190–6.
6. Morice P, Uzan C, Gouy S, Verschraegen C, Haie-Meder C. Gynecological cancers in pregnancy. Lancet. 2012; 379 (9815); 558–69.
7. Aggarwal P, Kehoe S. Ovarian tumors in pregnancy a literature review. Eur J Obstet Gynecol Reprod Biol. 2011; 155 (2): 119–24.
8. Gui T, Cao D, Shen K, Yang J, Fu C, Lang J, Liu X. Management and outcome of ovarian malignancy complicating pregnancy: an analysis of 41 cases and review of the literature. Clin Transl Oncol. 2013; 15 (7): 548–54.
9. Шлома Е. Н., Фридман М. В., Шелкович С. Е., Демидчик Ю. Е. Пограничные эпителиальные опухоли яичников: клиническое течение и проблемы морфологической диагностики. Минск: Изд-во «Бел МАПО», 2012; 80 с.
10. Давыдова И. Ю., Кузнецов В. В., Карселадзе А. И., Мещерякова Л. А. Пограничные опухоли яичников. Акушерство и гинекология: новости, мнения, обучение. 2019; 7 (1): 92–104.
11. Nadereh B, Mojgan KZ, Mitra MG, Fatemeh G, Azamsadat M, Fahimeh G. Ovarian carcinoma with pregnancy: a clinicopathologic analysis of 23 cases and review of the literature. BMC Pregnancy Childbirth. 2008; 8: 3. Available from: https://www.ncbi.nlm.nih.gov/pmc/articles/PMC2266699/.
12. Yong-Soon K, Jung-Eun M, Kyung-Taek L, In-Ho L, Tae-Jin K, Ki-Heon L, et al. Ovarian cancer during pregnancy clinical and pregnancy outcome. Korean Med Sci. 2010; 25 (2): 230–4.
13. Герасимова А. А., Гус А. И., Клименко П. А., авторы; Клименко Петр Афанасьевич, патентообладатель. Способ дифференциальной диагностики опухолевидных образований и опухолей яичников у беременных. Патент РФ № 2325118. 05.06.2007.
14. Герасимова А. А., Швырев С. Л., Соломатина А. А., Гус А. И., Клименко П. А. Способ выявления характера яичниковых образований. Онкология. 2013; 1: 34–40.
15. Tinelli R, Tinelli A, Tinelli F, Cicenelli E, Malvasi A. Conservative surgery for borderline ovarian tumors: a review. Gynecol Oncol. 2006; 100 (1): 185–91.
16. Манухин И. Б., Высоцкий М. М., Кушлинский Н. Е. Молекулярно-биологические факторы в патогенезе и хирургическом лечении опухолей яичников. М.: Изд-во «Династия», 2007; 208 с.
17. Moghaddam SM, Amini A, Morris D, Pourgholami H. Significance of vascular endothelial growth factor in growth and peritoneal dissemination of ovarian cancer. Cancer Metastasis Rev. 2012; 31 (1–2): 143–62. DOI: 10.1007/s10555-011-9337-5.
18. Viallard C, Larrivée B. Tumor angiogenesis and vascular normalization: alternative therapeutic targets. Angiogenesis. 2017; 20 (4): 409–26. DOI: 10.1007/s10456-017-9562-9.
19. Новикова Е. Г., Шевчук А. С. Органосохраняющее лечение больных с пограничными опухолями яичников. Вопросы онкологии. 2014; 60 (3): 267–73.
20. Fauvet R, Brzakowski M, Morice P, Resch B, Marret H, Graesslin O, et al. Borderline ovarian tumors diagnosed during pregnancy exhibit a high incidence of aggressive features: results of a French multicenter study. Ann Oncol. 2012; 23 (6): 1481–7.
21. Zagouri F, Dimitrakakis C, Marinopoulos S, Tsigginou A, Dimopoulos MA. Cancer in pregnancy: disentangling treatment modalities. ESMO. 2016; 1 (3). Available from: https://www.ncbi.nlm.nih.gov/pmc/articles/PMC5070264/
22. Шевчук А. С. Повторные лапароскопические операции у больных со злокачественными опухолями яичников [диссертация]. М., 2005.
23. Kim JH, Kim TJ, Park YG. Clinical analysis of intra — operative frozen section proven borderline tumors of the ovary. J Gynecol Oncol. 2009; 20 (3): 176–80.
24. Brun JL, Cortez A, Rouzier R. Factors influencing the use and accuracy of frozen section diagnosis of epithelial ovarian tumors. Am J Obstet Gynecol. 2008; 199 (3): 241–7.
25. Du Bois A, Ewald-Riegler N, du Bois O, Harter P. Borderline tumors of the ovary — a systematic review. Geburtsh Frauenheilk. 2009; 69: 807–33.
26. Trope C, Davidson B, Paulsen T, Abeler VM, Kaern J. Diagnosis and treatment of borderline ovarian neoplasms «the state of the art». Eur J Gynecol Oncol. 2009; 30 (5): 471–82.
27. Fauvet R, Poncelet C, Boccara J. Fertility after conservative treatment for borderline ovarian tumors a French multicenter study. Fertil Steril. 2005; 83: 284.
28. Tinelli F, Tinelli R, La Grotta F. Pregnancy outcome and recurrence after conservative laparoscopic surgery for borderline ovarian tumors. Acta Obstet Gynecol Scand. 2007; 86: 81.

ULTRASONOGRAPHY FEATURES AND SCREENING OF OVARIAN MASSES IN REPRODUCTIVE-AGE WOMEN

Spiridonova NV, Demura AA ✉, Katyushina VO

Samara State Medical University, Samara, Russia

Ovarian neoplasms can develop at any age, carry a high risk for malignant transformation, reduce the reproductive potential of a woman and are an indication for surgery. The search for optimal screening algorithms for ovarian tumors is still ongoing. The aim of this study was to evaluate the prognostic efficacy of ultrasonography (US) features in differentiating between benign, malignant and borderline tumors in reproductive-age women. We examined 168 reproductive-age women with ovarian masses who underwent surgery in 2012–2015 and compared the results of histopathological examinations with pulsed-Doppler US findings. We did not establish a correlation between the size/volume of the tumor and their morphological structure. We identified the echotexture characteristics associated with malignancy, including the presence of a solid component ($p < 0.001$); septations ($p = 0.029$) and projections on the internal surface of the tumor capsule ($p < 0.001$); moderate or significant buildup of free fluid in the small pelvis ($p = 0.007$), and the nodular surface of the tumor capsule ($p = 0.008$). Solid ovarian masses were at increased (31.69-fold) risk of transformation into malignant or borderline tumors, whereas for a mixed (cystic and solid) type the risk of such transformation increased 3.46-fold. We also identified Doppler parameters that can clearly discriminate between benign and malignant growths, including the blood flow rate in the tumor over 1.85 cm/s ($p = 0.007$) and RMI over 0.16 ($p = 0.013$). The sensitivity and specificity of our diagnostic model are 87% and 68%, respectively, with a probability threshold of 0.3.

Keywords: ovarian tumors, risk of malignancy, screening, ultrasound, ovarian tumor echotexture, Doppler ultrasonography, blood flow characteristics

Acknowledgements: the authors thank Komarova MV, Cand. Sci. (Biol.) and Associate Professor at the Samara State Medical University for her invaluable help with statistical analysis

Author contribution: all authors equally contributed to the study at its every stage.

Compliance with ethical standards: the study was approved by the Ethics Committee of Samara State Medical University (Protocol № 194 dated September 12, 2018). Informed consent was obtained from all study participants.

✉ **Correspondence should be addressed:** Alina A. Demura
pr. Maslennikova, 25, Samara, 443056; lina281@ya.ru

Received: 12.02.2020 **Accepted:** 28.02.2020 **Published online:** 13.03.2020

DOI: 10.24075/brsmu.2020.016

УЛЬТРАЗВУКОВЫЕ АСПЕКТЫ И СКРИНИНГ ОПУХОЛЕЙ И ОПУХОЛЕВИДНЫХ ОБРАЗОВАНИЙ ЯИЧНИКОВ У ПАЦИЕНТОК РЕПРОДУКТИВНОГО ВОЗРАСТА

Н. В. Спиридонова, А. А. Демура ✉, В. О. Катюшина

Самарский государственный медицинский университет, Самара, Россия

Опухоли яичников возникают в любом возрасте, снижают репродуктивный потенциал женщины, имеют высокий риск малигнизации и являются показанием для оперативного лечения. На сегодняшний день продолжается поиск оптимальных алгоритмов скрининга опухолей данной нозологии. Целью работы было оценить прогностическую эффективность ультразвуковых (УЗ) признаков для дифференциальной диагностики злокачественных, доброкачественных и пограничных опухолей яичников у женщин репродуктивного возраста. Обследованы 168 пациенток репродуктивного возраста с опухолевыми и опухолевидными образованиями яичника, прооперированных с 2012 по 2015 г., и сопоставлены морфологические данные верифицированного процесса в яичниках с данными комплексного УЗИ с импульсно-волновым допплеровским режимом. В исследовании не выявлено зависимости размеров и объема образований яичников от морфологической структуры опухоли. Обнаружены эхографические особенности опухолей яичников: наличие солидного компонента ($p < 0{,}001$); наличие перегородок ($p = 0{,}029$) и разрастаний по внутренней поверхности капсулы ($p < 0{,}001$); наличие умеренного и значительного количества свободной жидкости в малом тазу ($p = 0{,}007$) и бугристая поверхность капсулы образования яичника ($p = 0{,}008$). Наличие солидного образования увеличивало вероятность появления злокачественной и пограничной опухолей в 31,69 раза, кистозно-солидной структуры образования — в 3,46 раза. Выделены значимые допплерометрические показатели, способные четко обозначить разницу между доброкачественным и злокачественным процессами, а именно превышение скорости кровотока свыше 1,85 см/с ($p = 0{,}007$) и ИР более 0,16 ($p = 0{,}013$). Чувствительность и специфичность данной диагностической модели составляют 87% и 68% при значении пороговой вероятности 0,3.

Ключевые слова: опухоли яичников, риск малигнизации, скрининг опухолей, ультразвуковое исследование, эхоструктура опухолей яичников, допплерография, особенности кровотока

Благодарности: к. б. н., доценту Самарского университета М. В. Комаровой за помощь в статистической обработке результатов исследования.

Вклад авторов: Н. В. Спиридонова, А. А. Демура, В. О. Катюшина — равнозначен на всех этапах работы и написания статьи.

Соблюдение этических стандартов: исследование одобрено этическим комитетом СамГМУ (протокол № 194 от 12 сентября 2018 г.); все участники подписали информированное согласие на участие в исследовании.

✉ **Для корреспонденции:** Алина Андреевна Демура
пр. Масленникова, д. 25, г. Самара, 443056; lina281@ya.ru

Статья получена: 12.02.2020 **Статья принята к печати:** 28.02.2020 **Опубликована онлайн:** 13.03.2020

DOI: 10.24075/vrgmu.2020.016

Ovarian neoplasms are a continuing concern for gynecologists. They can develop at any age, carry a high risk for malignant transformation, reduce the reproductive potential of a woman and are an indication for surgery. The complexity of structural and functional organization of female reproductive glands determines the vast diversity of histological types of ovarian neoplasms, especially in reproductive-age women. Mixed type tumors constituted by at least 2 histological types amplify this diversity even further. Therefore, it is important to identify the sonographic features of ovarian neoplasms that

can suggest their malignancy [1]. Some authors estimate that epithelial cancer accounts for 60% of all ovarian neoplasms and 80–90% of ovarian malignancies [2]. The rest of ovarian tumors arise from germ and stromal cells, are typically found in younger patients and their sonographic appearance can pose diagnostic difficulty for the clinician.

Because ovarian tumors are fast-growing and aggressive, about 60–70% of patients have advanced stages (III–IV) of the disease at the time of presentation [3]. The use of ultrasonography (US) and the improvement of its diagnostic efficacy may be a solution to the problem of early ovarian cancer detection. US is a noninvasive, cheap, widely available and reproducible modality introduced in 1970 [4–6]. The first ultrasound screening tests were offered to women in the 1980s; they consisted in the transabdominal examination of pelvic organs, which was not the best effective strategy, for anatomical reasons. In 1990, I. Jacobs included transvaginal scans in his screening model. Since then, US has been the primary diagnostic modality for suspected ovarian neoplasms. Over the years, better accuracy in discriminating between malignant and benign tumors has been achieved due to the use of Doppler US. The technique relies on the phenomenon of neovascularization: new capillaries start to develop in the tumor, promoting its further growth. In a malignant tumor, blood flow has a number of characteristics determined by the lack of vascular smooth muscle fibers and the presence of multiple vascular shunts increasing the rate of blood flow in the neoplasm [7].

The aim of this study was to evaluate the prognostic efficacy of some sonographic features in the differential diagnosis of benign and malignant ovarian tumors in reproductive-age women.

METHODS

The groundwork for this research was laid by the prospective study conducted in 168 reproductive-age women with a morphologically verified ovarian neoplastic process who underwent surgery at Samara Regional Oncology Center in 2012–2015. The following inclusion criteria were applied: age of 18 to 40 years; US findings suggestive of an ovarian mass; subsequent surgery and a histopathological examination of the excised tissue. Exclusion criteria: age below 18 and above 40 years; a medical history of cancer.

Pulsed-wave Doppler scans were performed using a Philips IU-22 scanner (Philips; USA).

The patients were divided into 3 groups according to the WHO classification (2013): 1) 101 (60.1%) patients with benign tumors; 2) 24 (14.3%) patients with borderline tumors; 3) 43 (25.6%) patients with malignant tumors.

The following parameters were evaluated: the size and the volume of the ovarian mass, fluid buildup in the pelvis, the type and the morphologic appearance of the tumor. The neoplastic process was evaluated based on the type of the ovarian mass (solid, cystic, mixed), the involvement of 1 or both ovaries (uni- or bilateral lesions), the size of the lesion, the presence of septations, the presence of projections on the external/internal surface of the capsule and the quality of the capsule surface itself, as well as blood flow in the tumor. We also measured the blood flow velocity in the tumor and the resistive index. Statistical analysis was carried out in SPSS21 (20130626-3; An IBM Company; USA) and Microsoft Excel (Microsoft; USA).

RESULTS

The maximum size of the tumors (Table 1) varied between 77.26 ± 6.94 mm and 97.06 ± 15.29 mm. No positive correlation was established between the size of the tumor and the stage of the disease. In the patients with benign ovarian tumors, the tumor volume was 99.06 ± 128.18 ml on average; in the patients with borderline tumors, it was 814.54 ± 358.32 ml, and in the patients with malignancies, 579.17 ± 196.37 ml ($p = 0.941$).

When analyzing the ultrasound appearance of the tumors, we assessed the involvement of one or both ovaries in the neoplastic process. We also identified a group of 15 patients who had undergone adnexa removal emergency surgery at the gynecological departments of general hospitals and had been subsequently referred to specialist centers for a postoperative US examination and a reexamination of histology slices. Unilateral lesions were more often observed in the patients with benign (81.2%) and malignant (86%) tumors than in the patients with borderline tumors (54.2%) ($p = 0.006$).

Based on their echotexture, the tumors were classified into 3 types (Fig. 1): cystic, solid and mixed, with both cystic and solid components ($p < 0.001$). Women with cystic ovarian masses made up 72.6% of the study participants. In this group of patients, the masses were round in shape, with well-circumscribed smooth margins, anechoic, with single or multiple septa and without projections along the internal capsule. Cystic masses were more typical to the patients with benign tumors (87.1%), compared to the women who had borderline (54.2%) and malignant (48.8%) tumors, respectively.

Patients with mixed type tumors (with both cystic and solid components) made up 22.6% of all study participants. In this group, the tumors were round-shaped, with fairly well-defined smooth margins, anechoic, with septations or areas of echogenicity and a solid irregular or regular-shaped component. The mixed type was more prevalent in the patients with borderline and malignant tumors (37.5 and 39.5%, respectively) than in the women with benign tumors (11.9%).

Solid tumors were observed in 4.8% of the patients. Tumors of this type were either round or irregular in shape, with fairly well-defined angular margins; they were characterized by mixed echogenicity or the presence of single anechoic round-shaped components. The solid type was observed in the participants with malignancies (11.6 %).

We also evaluated the surface of the tumor capsule (Fig. 2), which was either smooth or nodular ($p = 0.008$). In the patients with benign tumors, the capsule surface was smooth in 80 (79.2%) cases and nodular in 21 (20.8%) cases. In the group

Table 1. Sizes of ovarian tumors

	Benign	Borderline	Malignant	p_{1-2}	p_{1-3}	p_{2-3}	p
Size 1	88.10 ± 4.90	97.06 ± 15.29	91.87 ± 7.42	0.867	0.431	0.643	0.724
Size 2	77.48 ± 4.47	82.56 ± 14.00	77.26 ± 6.94	0.886	0.981	0.817	0.983
Size 3	82.79 ± 4.59	89.81 ± 14.52	84.56 ± 6.94	0.972	0.669	0.783	0.909
Tumor volume, ml	599.06 ± 128.18	814.54 ± 358.32	579.17 ± 196.37	0.965	0.727	0.844	0.941

Note: p_{1-2}, p_{1-3}, p_{2-3} — intergroup comparison; p — the Kruskal–Wallis H test.

of patients with borderline tumors, smooth capsule surface was observed in 17 (70.8%) cases, whereas nodular, in 7 (29.2%) women. In the group of patients with malignant tumors, the capsule surface was smooth in 23 (53.5%) patients, whereas nodular, in 20 (46.5%) patients. Additionally, we looked at the presence of projections on the external ($p = 0.192$) and internal ($p < 0.001$) surfaces of the capsule. We found that 40.6% of patients with benign tumors had projections on the external surface and 4% of women, on the internal surface. In the group of patients with borderline tumors, no projections were observed on the external surface of the capsule, and 79.2% had projections on the internal surface. In the groups of patients with malignant tumors, 65.1% had projections on the external surface, whereas 9.3%, on the internal surface.

Small amounts of free pelvic fluid were observed in 15.8% of women with benign tumors. In this group, there were no patients with moderate or large amounts of free fluid in the pelvis. In the borderline group, fluid buildup was observed in every third patient (33.3%), of whom 16.7% had it in moderate and large volumes. However, free pelvic fluid was discovered only in 14% of women with malignancies; of them only 1% (2.3%) had in large quantities (Kruskal–Wallis H test, $p = 0.007$).

Doppler ultrasonography can estimate blood flow in the tumor. This facilitates timely diagnosis of a neoplastic process in the ovaries and is especially important for deciding on the treatment strategy in reproductive-age women. In our study, blood flow parameters were evaluated in several steps.

Step I. The presence of blood flow within the tumor was evaluated in all patient groups ($p < 0.001$). Tumor blood flow was detected by Doppler ultrasonography in 18 (17.8%) patients with benign tumors; another 27 (26.7%) patients with benign tumors had single colored spots on the dopplergram (power Doppler). In the group of patients with borderline tumors, blood flow was registered in 9 (37.5%) women; another 9 (37.5%) had single colored spots on the dopplergram (power Doppler). Of all patients with malignancies, blood flow was detected in 23 (53.5%) women, whereas single colored spots, in 15 (34.9%) women (power Doppler).

Step II. Tumor blood flow rate and resistive index (RI) were measured (Table 2). In the patients with benign tumors, the average blood flow rate was 1.45 ± 0.4 cm/s and the RI value was the lowest. For those with borderline tumors, the average blood flow rate was 4.58 ± 1.44 cm/s and the RI value was 0.21 ± 0.05. In the patients with malignancies, the maximum values for blood flow rate and RI were 6.34 ± 1.17 cm/s and 0.26 ± 0.04, respectively. We were able to identified Doppler parameters that helped us to discriminate between benign and malignant tumors: tumor blood flow rate over 1.85 cm/s ($p = 0.007$) and RI over 0.16 ($p = 0.013$).

Using stepwise logistic regression, the US findings and the calculated blood flow rate values, we built a model for early diagnosis of ovarian cancer (Table 3). The type of tumor composition was a significant predictor: solid masses were at increased (31.69-fold) risk for malignant or borderline transformation; a mixed type with cystic and solid components increased such risk 3.46-fold. Sensitivity and specificity of this diagnostic model were 87 and 68%, respectively, with a probability threshold of 0.3.

DISCUSSION

Considering the morphologic diversity of ovarian growths and their frequently poor outcomes, the search for early

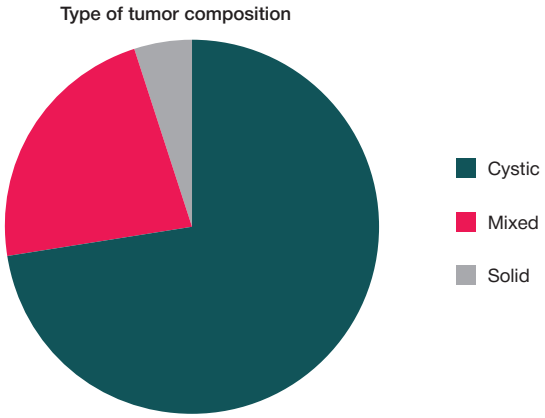

Fig. 1. The composition of tumors determined by ultrasonography

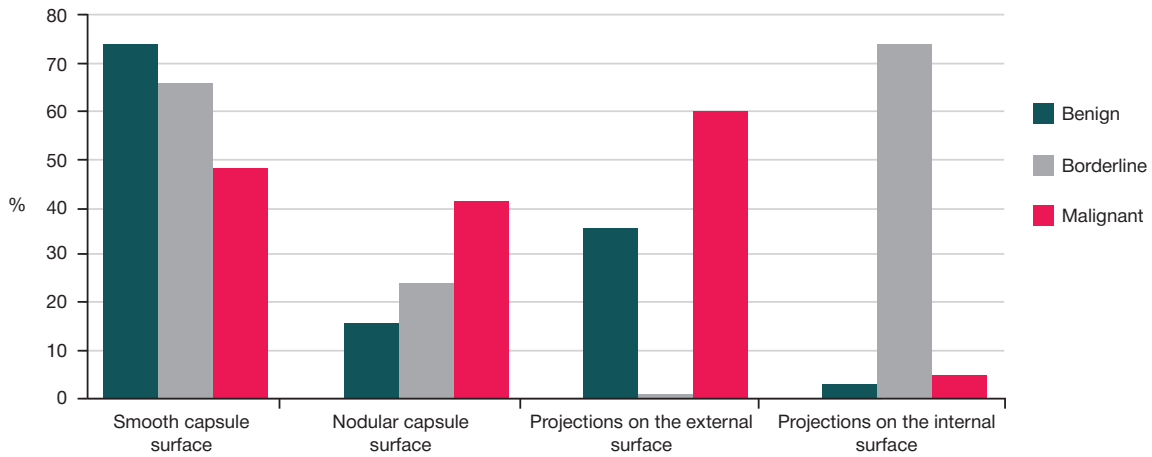

Fig. 2. Ovarian tumor capsule surface in reproductive-age patients

Table 2. Characteristics of blood flow in ovarian tumors

	Benign	Borderline	Malignant	p_{1-2}	p_{1-3}	p_{2-3}	p
v, cm/s	1.45 ± 0.40	4.58 ± 1.44	6.34 ± 1.17	0.007	< 0.001	0.261	< 0.001
RI	0.08 ± 0.02	0.21 ± 0.05	0.26 ± 0.04	0.013	< 0.001	0.319	< 0.001

Note: *v* is blood flow rate in the ovarian tumor, expressed as cm/s; RI is resistive index: p_{1-2}, p_{1-3}, p_{2-3} show intergroup differences; p is the result of the Kruskal–Wallis H test.

predictors of malignancy in reproductive-age women remains a pressing concern. Algorithms predicting the risk of malignant transformation are in continuing development, aiming at detecting cancer in its early stages and thus reducing the extent of surgery. In 1996, the risk-of-malignancy index (RMI) was first proposed. It was designed to estimate the risk of malignant transformation using a scoring system [8]. Similar to our model, it relied on US features, such the presence of septations and solid components, the involvement of 1 or both ovaries and ascites. However, unlike our model, the index also accounted for the presence of abdominal metastases, the menopausal status (premenopause/postmenopause) and the absolute values of CA 125. For the sake of convenience, each component was attributed a value (score) and the following formula was applied to calculate the index: RMI = Ultrasound features (score) · Menopausal status (premenopause/postmenopause) · Absolute values of CA 125. If the resulting RMI was below 200, the ovarian mass was assumed to be potentially benign.

The International Ovarian Tumor Analysis (IOTA) carried out in 1999–2000 aimed at formulating the guidelines and creating the models for characterizing ovarian tumors [9]. The models were developed for use by clinicians regardless of their qualifications and allowed them to better understand the etiology of ovarian cancer and the role of CA 125 and other cancer biomarkers. Later, an international team of researchers proposed 2 logistic regression models: LR1 and LR2 for differentiating between benign and malignant ovarian growths [10, 11]. According to the models, the sonographer should evaluate over 40 different clinical and US variables. The sensitivity and accuracy of the method were 96% and 90%, respectively, but the method turned to be very time-consuming and generally demanding; it did not account for the patient's medical history and laboratory test results. The researchers concluded that recognition of US features typical to an ovarian pathology by an experienced sonographer is the best method to characterize this pathology and that CA 125 does not improve the diagnostic accuracy in predicting the malignancy of the tumor [12–14]. Using statistical analysis, we were able to reduce the number of variables and thus to save time for and simplify the subsequent calculations without reducing the sensitivity and specificity of our diagnostic model (87 and 68%).

In 2011, it was demonstrated that the algorithms relying on a combination of two tumor markers (CA 125 and HE 4) and US findings should be used to identify women with indications for surgery, who should be referred to cancer centers [15].

In 2011, the international NICE clinical guideline CG 122 on the management of patients with ovarian cancer emphasized the necessity of using RMI, which accounts for 3 preoperative parameters, just like the algorithm proposed in 1996 [16]: serum CA 125, the menopausal status (M) and ultrasonography score (U). According to the guideline, US findings should be scored 1 point for each of the following characteristics: multiocular cysts, solid areas, metastases, ascites, bilateral lesions. The menopausal status should be evaluated in the following way: premenopausal women score 1 point; postmenopausal, 3 points (postmenopausal females are defined as those who have not had periods for over a year or who are older than 50 and have undergone hysterectomy). Serum CA 125 is expressed in IU/ml. Its values can vary between 0 and a few hundreds or even thousands of units. RMI is, thus, calculated using the formula: RMI = U · M · CA 125; if RMI value is above 200, the patient should be recommended additional tests.

Today, it is often reported in the literature that no significant differences can be established between benign and malignant ovarian tumors using the classic criteria for malignancy, such as irregular shape, irregular margin or large size of the tumor.

CONCLUSIONS

This study has not established a correlation between the size and volume of ovarian tumors and their morphological structure. However, the analysis of tumor echotexture allowed us to identify US characteristics associated with malignancy, including the presence of a solid component ($p < 0.001$), septations ($p = 0.029$) and projections on the internal surface of the tumor capsule ($p < 0.001$), moderate or significant buildup of free fluid in the small pelvis ($p = 0.007$) and the nodular surface quality of the tumor capsule ($p = 0.008$).

The study demonstrates that blood flow in the tumor could be a sign of possible malignant transformation ($p < 0.001$). For reproductive-age women, Doppler parameters have been identified that can clearly discriminate between benign and malignant growths: the blood flow rate over 1.85 cm/s ($p = 0.007$) and RI over 0.16 ($p = 0.013$).

The identified US features (a solid or a mixed type mass, blood flow in the tumor and increased resistance index) can be used as key parameters in differentiating between various types of ovarian tumors.

Table 3. The model for early diagnosis of ovarian cancer in reproductive-age patients

Risk factor	Risk factor grading	Regression coefficient, *b*	OR (95% CI)	*p*
Composition type	Cystic, reference	0	1	–
	Solid	3.46	31.69 (3.16–318.11)	0.003
	Mixed	1.23	3.40 (1.32–8.77)	0.011
Blood flow in the tumor	"Yes" in comparison with "no"	0.98	2.68 (1.56–4.58)	< 0.001
RI	Increment by 1	2.23	9.34 (1.92–45.49)	0.006
Constant	–	–2.35	–	< 0.001

References

1. Ashrafyan LA, Babaeva NA, Antonova IB, Ivashina SV, Lustik AV, Alyoshikova OI, et al. Ultrasound criteria for early diagnosis of ovarian cancer. Tumors of the female reproductive system. 2015; 11 (1): 53–60. Russian.
2. Urmancheeva AF, Kutusheva GF, Ulrih EA. Opuholi jaichnika (klinika, diagnostika, lechenie). Posobie dlja vrachej. SPb.: OOO «Izdatel'stvo N-L», 2012; 68 s. Russian.
3. Maksimov SYa, Khadzhimba AV, Vyshinskaya EA, Sobolev IV, Ilyin AA. Rak organov reproduktivnoj sistemy v molodom vozraste. Prakticheskaja onkologija. 2017; 18 (2): 185–96. Russian.
4. Bulanov MN. Ul'trazvukovaja ginekologija. V 3-h tomah. T. 2. M.: Vidar, 2010; 306 s.
5. Manegold-Brauer G, Bellin AK, Tercanli S, Lapaire O, Heinzelmann-Schwarz V. The special role of ultrasound for screening, staging and surveillance of malignant ovarian tumors: distinction from other methods of diagnostic imaging. Arch Gynecol Obstet. 2012; (289): 491–8.
6. Levine D, Brown DL, Andreotti RF, Benacerraf B, Benson CB, Brewster WR, et al. Management of asymptomatic ovarian and other adnexal cysts imaged at US: society of radiologists in ultrasound consensus conference statement. Radiology. 2010; 256 (3): 943–54.
7. Hachkuruzov SG. Ul'trazvukovaja simptomatika i differencial'naja diagnostika kist i opuholej jaichnikov. M.: MEDpress-inform, 2014; 288 s. Russian.
8. Gasparov AS, Zhordania KI, Payanidi YuG, Dubinskaya ED. Oncogynecological aspects of ovarian cysts. Bulletin of the RAMS. 2013; 68 (8): 9–13. Russian.
9. Higgins RV, Matkins JF, Marroum MC. Comprasion of fine-needle aspiracion cytologic findings of ovarian cysts with ovarian histologic findings. Am J Obstet gynecol. 1999; 180 (3): 550–3.
10. Campbell S. Ovarian cancer: role of ultrasound in preoperative diagnosis and population screening. Ultrasound Obstet Gynecol. 2012; (40): 245–54.
11. Kaijser J, Bourne T, Valentin L, Sayasneh A, Van Holsbeke C, Vergote I, et al. Improving strategies for diagnosing ovarian cancer: a summary of the International Ovarian Tumor Analysis (IOTA) studies. Ultrasound Obstet Gynecol. 2013; 41 (1): 9–20.
12. Fischerova D. Ultrasound scanning of the and abdomen for staging of gynecological tumors: a review. Ultrasound Obstetrics Gynecol. 2011; (38): 246–66.
13. Van Gorp T, Cadron I, Despierre E, Daemen A, Leunen K., Amant F, et al. HE 4 and CA 125 as a diagnostic test in ovarian cancer: prospective validation of Risk of Ovarian Malignancy Algorithm. Br J Cancer. 2011. (104): 863–70.
14. Valentin L, Ameye L, Franchi D, Guerriero S, Jurkovic D, Savelli L, et al. Risk of malignancy in unilocular cysts: a study of 1148 adnexal masses classified as unilocular cysts at transvaginal ultrasound and review of the literature. Ultrasound Obstet Gynecol. 2013; 41 (1): 80–89.
15. Escudero JM, Auge JM, Filella X, Torne A, Pahisa J, Molina R. Comparison of serum human epididymis protein 4 with cancer antigen 125 as a tumor marker in patients with malignant and nonmalignant diseases. Clin Chem. 2011; (57): 1534–44.
16. Ovarian cancer: recognition and initial management (CG122). National institute for health and care excellence. Clinical guideline. 2011, p. 19. Available from: https://www.nice.org.uk/terms-and-conditions#notice-of-rights.

Литература

1. Ашрафян Л. А., Бабаева Н. А., Антонова И. Б., Ивашина С. В., Люстик А. В., Алешикова О. И. и др. Ультразвуковые критерии ранней диагностики рака яичников. Опухоли женской репродуктивной системы. 2015; 11 (1): 53–60.
2. Урманчеева А. Ф., Кутушева Г. Ф., Ульрих Е. А. Опухоли яичника (клиника, диагностика, лечение). Пособие для врачей. СПб.: ООО «Издательство Н-Л», 2012; 68 с.
3. Максимов С. Я., Хаджимба А. В., Вышинская Е. А., Соболев И. В., Ильин А. А. Рак органов репродуктивной системы в молодом возрасте. Практическая онкология. 2017; 18 (2): 185–96.
4. Буланов М. Н. Ультразвуковая гинекология. В 3-х томах. Т. 2. М.: Видар, 2010; 306 с.
5. Manegold-Brauer G, Bellin AK, Tercanli S, Lapaire O, Heinzelmann-Schwarz V. The special role of ultrasound for screening, staging and surveillance of malignant ovarian tumors: distinction from other methods of diagnostic imaging. Arch Gynecol Obstet. 2012; (289): 491–8.
6. Levine D, Brown DL, Andreotti RF, Benacerraf B, Benson CB, Brewster WR, et al. Management of asymptomatic ovarian and other adnexal cysts imaged at US: society of radiologists in ultrasound consensus conference statement. Radiology. 2010; 256 (3): 943–54.
7. Хачкурузов С. Г. Ультразвуковая симптоматика и дифференциальная диагностика кист и опухолей яичников. М.: МЕДпресс-информ, 2014; 288 с.
8. Гаспаров А. С, Жордания К. И., Паяниди Ю. Г., Дубинская Е. Д. Онкогинекологические аспекты кистозных образований яичников. Вестник Российской академии медицинских наук. 2013; 68 (8): 9–13.
9. Higgins RV, Matkins JF, Marroum MC. Comprasion of fine-needle aspiracion cytologic findings of ovarian cysts with ovarian histologic findings. Am J Obstet gynecol. 1999; 180 (3): 550–3.
10. Campbell S. Ovarian cancer: role of ultrasound in preoperative diagnosis and population screening. Ultrasound Obstet Gynecol. 2012; (40): 245–54.
11. Kaijser J, Bourne T, Valentin L, Sayasneh A, Van Holsbeke C, Vergote I., et al. Improving strategies for diagnosing ovarian cancer: a summary of the International Ovarian Tumor Analysis (IOTA) studies. Ultrasound Obstet Gynecol. 2013; 41 (1): 9–20.
12. Fischerova D. Ultrasound scanning of the and abdomen for staging of gynecological tumors: a review. Ultrasound Obstetrics Gynecol. 2011; (38): 246–66.
13. Van Gorp T, Cadron I, Despierre E, Daemen A, Leunen K., Amant F, et al. HE 4 and CA 125 as a diagnostic test in ovarian cancer: prospective validation of Risk of Ovarian Malignancy Algorithm. Br J Cancer. 2011. (104): 863–70.
14. Valentin L, Ameye L, Franchi D, Guerriero S, Jurkovic D, Savelli L, et al. Risk of malignancy in unilocular cysts: a study of 1148 adnexal masses classified as unilocular cysts at transvaginal ultrasound and review of the literature. Ultrasound Obstet Gynecol. 2013; 41 (1): 80–89.
15. Escudero JM, Auge JM, Filella X, Torne A, Pahisa J, Molina R. Comparison of serum human epididymis protein 4 with cancer antigen 125 as a tumor marker in patients with malignant and nonmalignant diseases. Clin Chem. 2011; (57): 1534–44.
16. Ovarian cancer: recognition and initial management (CG122). National institute for health and care excellence. Clinical guideline. 2011, p. 19. Available from: https://www.nice.org.uk/terms-and-conditions#notice-of-rights.

EEG μ-RHYTHM REACTIVITY IN CHILDREN DURING IMITATION OF BIOLOGICAL AND NON-BIOLOGICAL MOTION

Kaida AI ✉, Mikhailova AA, Eismont EV, Dzhapparova LL, Pavlenko VB

V.I. Vernadsky Crimean Federal University, Simferopol, Russia

The development of brain-computer interfaces based on the use of EEG sensorimotor rhythms reactivity parameters and designed for the rehabilitation of people (including children) with impaired motor functions is currently relevant. The study was aimed to analyse the EEG μ-rhythm in the individual frequency range in children during imitation of biological and non-biological motion. EEG was recorded at frontal, central and parietal cortical regions in 136 normally developing right-handed children aged 4–15, at rest and during the execution and imitation of movements using the computer mouse. When the children moved the computer mouse on their own ($F_{1, 132}$ = 31.17; p < 0.001) and executed the concentric moving of the coloured circle ($F_{1, 132}$ = 90.34; p < 0.001), the μ-rhythm desynchronization developed in the frontal, central and parietal neocortical regions. The μ-rhythm synchronization was detected during the non-biologocal motion imitation ($F_{1, 132}$ = 12.65; p < 0.001), compared to the task on the autonomous movement execution. The μ-rhythm desynchronization was observed during the biologocal motion imitation in relation to autonomous movement execution ($F_{1, 132}$ = 9.58; p = 0.002). The described effects had their own features in the groups of children aged 4–6, 7–9, 10–12 and 13–15. The study results demonstrate the desirability of taking into account the μ-rhythm reactivity age-related features and the visual stimuli nature when developing software for the brain-computer interfaces.

Keywords: children; EEG; μ-rhythm; imitation; biological motion; non-biological motion

Funding: the study was performed as a part of the project “Development of a complex of exoskeleton, hands and procedures for the rehabilitation of children with cerebral palsy” supported by the Ministry of Science and Higher Education of Russian Federation (RFMEFI60519X0186).

Author contribution: Kaida AI — data acquisition and analysis, manuscript writing; Mikhailova AA — data analysis, manuscript writing; Eismont EV — research planning, data acquisition and analysis, manuscript writing; Dzhapparova LL — data acquisition, manuscript writing; Pavlenko VB — research planning, data analysis, manuscript writing.

Compliance with ethical standards: the study was approved by the Ethics Committee of V.I. Vernadsky Crimean Federal University (protocol № 12 dated June 14, 2016). Informed consent to participation in the study was obtained from the parents.

✉ **Correspondence should be addressed:** Anna I. Kaida
Angarskaya, 38, Simferopol, 295001; kaydaanna@gmail.com

Received: 01.04.2019 **Accepted:** 15.04.2020 **Published online:** 16.04.2020

DOI: 10.24075/brsmu.2020.019

РЕАКТИВНОСТЬ μ-РИТМА ЭЭГ У ДЕТЕЙ ПРИ ИМИТАЦИИ ДВИЖЕНИЙ ВИЗУАЛЬНЫХ ОБРАЗОВ БИОЛОГИЧЕСКОГО И НЕБИОЛОГИЧЕСКОГО ПРОИСХОЖДЕНИЯ

А. И. Кайда ✉, А. А. Михайлова, Е. В. Эйсмонт, Л. Л. Джаппарова, В. Б. Павленко

Крымский федеральный университет имени В. И. Вернадского, Симферополь, Россия

В настоящее время актуальна разработка интерфейсов мозг-компьютер, основанных на использовании параметров реактивности сенсомоторных ритмов ЭЭГ и предназначенных для реабилитации людей с нарушениями двигательных функций, в том числе детей. Целью работы было проанализировать реактивность μ-ритма ЭЭГ в индивидуально определенном частотном диапазоне у детей при имитации движений визуальных образов биологического и небиологического происхождения. ЭЭГ регистрировали во фронтальных, центральных и париетальных областях коры у 136 нормально развивающихся детей-правшей 4–15 лет в состоянии двигательного покоя, а также при самостоятельном выполнении и имитации движений с помощью компьютерной мыши. При выполнении детьми самостоятельных движений компьютерной мышью ($F_{1, 132}$ = 31,17; p < 0,001) и при осуществлении концентрических перемещений цветного круга ($F_{1, 132}$ = 90,34; p < 0,001) развивается десинхронизация μ-ритма во фронтальных, центральных и париетальных областях неокортекса. При имитации движений визуальных образов небиологического происхождения, по сравнению с заданием на выполнение самостоятельных движений, была выявлена синхронизация μ-ритма ($F_{1, 132}$ = 12,65; p < 0,001). При подражании движениям визуальных образов биологического происхождения относительно самостоятельных движений выявлена десинхронизация μ-ритма ($F_{1, 132}$ = 9,58; p = 0,002). Данные эффекты имели свои особенности в группах детей 4–6, 7–9, 10–12 и 13–15 лет. Результаты исследования показывают целесообразность учета возрастных особенностей реактивности μ-ритма и характера предъявляемых зрительных стимулов при разработке программного обеспечения интерфейсов мозг-компьютер.

Ключевые слова: дети; ЭЭГ; μ-ритм; имитация; биологическое движение; небиологическое движение

Финансирование: исследования выполнены в рамках темы: «Разработка комплекса экзоскелета кисти с внешним программным управлением и биологической обратной связью для процедуры реабилитации детей с синдромом ДЦП» при финансовой поддержке Министерства науки и высшего образования Российской Федерации (RFMEFI60519X0186).

Вклад авторов: А. И. Кайда — набор и обработка данных, написание статьи; А. А. Михайлова — обработка данных, написание статьи; Е. В. Эйсмонт — план исследований, набор и обработка данных, написание статьи; Л. Л. Джаппарова — набор данных, написание статьи; В. Б. Павленко — план исследований, обработка данных, написание статьи.

Соблюдение этических стандартов: исследование одобрено этическим комитетом ФГАОУ ВО «Крымский федеральный университет им. В. И. Вернадского» (протокол № 12 от 14 июня 2016 г.). Получено добровольное информированное согласие родителей на участие детей в эксперименте.

✉ **Для корреспонденции:** Анна Ивановна Кайда
ул. Ангарская, д. 38, г. Симферополь, 295001; kaydaanna@gmail.com

Статья получена: 01.04.2019 **Статья принята к печати:** 15.04.2020 **Опубликована онлайн:** 16.04.2020

DOI: 10.24075/vrgmu.2020.019

The human’s ability to understand the goal of action and imitate is necessary for effective integration into the social environment, allowing one to master various types of activities and norms of behavior in society. The mirror neuron system (MNS)

is important for recognition of movements and associated intentions. Mirror neurons are neurons able to activate in a similar way, both when executing actions, and when watching other individuals executing similar actions [1, 2]. It has been suggested that MNS plays an important role in the complex forms of social interaction. [3].

Desynchronization of the EEG sensorimotor rhythm, the μ-rhythm, is considered to be a marker of MNS activation [4]. Since modulations of the α-rhythm in the occipital region can overlap the effects of μ-rhythm desynchronization [5], to determine the individual frequency range and reactivity, the following features are taken into account: unlike the occipital α-rhythm, the μ-rhythm is most pronounced in the fronto-parietal regions; the μ-rhythm amplitude decreases when the subject moves, imagines movement or watches the other subjects' movement, but does not change significantly when the subject opens or closes the eyes [6, 7].

Sensorimotor rhythm amplitude depression during the biological motion watching is more pronounced than during watching the non-biological motion [8], which is also characteristic of watching social actions, compared to actions outside the social context [9]. Regarding the movement imitation, it is assumed that imitation is associated with the activation of human MNS, and is the result of the comparison of the observed action and the internal motor plan for the execution of action [10].

The study of MNS and μ-rhythm reactivity is of special interest in a view of new methods development for rehabilitation of patients with various motor impairments using brain-computer interfaces [11, 12]. In particular, in the treatment of adult patients, the synchronous interfaces are used, based on the analysis of the EEG sensorimotor rhythms reactivity when representing the movement in response to the signal presented [13, 14]. Recently, such methods are beginning to be used for rehabilitation of children with cerebral palsy [15]. Symbols or text commands are reported to be used as the signals presented to patients. However, the concept of MNS suggests that stimuli visually representing movements and requiring the simulation of movements could be more effective for triggering reactions in the EEG μ-rhythm range. It should be noted that when working with children it is preferable to use the actions that are in the child's motor repertoire for more effective task execution [16]. The study was aimed to analyse the EEG μ-rhythm under conditions of biological and non-biological motion imitation in children aged 4–15 using the computer pointer device, the mouse. Now, even the preschool children are familiar with the computer mouse operation.

METHODS

Characteristics of a sample

The study was performed at the Center for Collective Use of Scientific Equipment "Experimental physiology and biophysics" of V.I. Vernadsky Crimean Federal University.

The study included 136 righ-handed children aged 4–15 (69 boys and 67 girls). Inclusion criteria: normal (or corrected to normal) vision and hearing; preferred right hand when operating the computer mouse; sufficient degree of cognitive development (IQ at least 80 points according to the Wechsler scale, variants WPPSI and WISC). Exclusion criteria: taking the CNS affecting drugs; severe chronic somatic diseases. The children were divided into four age groups: 4–6 years (30 people), 7–9 years (46 people), 10–12 years (30 people) and 13–15 years (30 people).

EEG recording

EEG recording was performed using the Neuron-Spectrum-3 EEG System (Neurosoft; Russia). Data were obtained using the WinEEG version 2.8 software (available for free). Independent component analysis was used for the artifacts correction. The 19 monopolar EEG electrodes were used in accordance with the 10–20 system. In our study, the frontal, central and parietal neocortical regions were the area of concern (F3, F4, Fz, C3, C4, Cz, P3, P4, Pz loci). Paired electrodes attached to the the ear lobes were the reference electrode. Cut-off frequencies of the high and low pass filters were 1.5 and 35 Hz, respectively, EEG digitization rate was 250 Hz.

EEG recording was performed while the children performed a queue of sequential tasks, the duration of each task was 30 s. EEG segments were processed using the Fast Fourier Transform with the 4 epoch of analysis and 50% mutual overlapping of epochs.

To imitate the non-biological motion, the following tasks were used:

1) gaze fixation on the video of the computer mouse (baseline);

2) concentric moving of the coloured circle on the monitor screen using the computer mouse (Mn.1) (Fig. 1A);

3) imitation of the other coloured circle's motion (imitation of non-biological motion, ImNB) (Fig. 1B).

When imitating the biological motion, the subject and the researcher were located at the tables next to each other (the researcher on the right), each of tables had a monitor and a computer mouse on it. Using the webcam, the working plane of the researcher's table with the mouse on it was demonstrated on the monitor in front of the subject. The tasks queue was as follows:

1) gaze fixation on the video of the computer mouse (baseline);

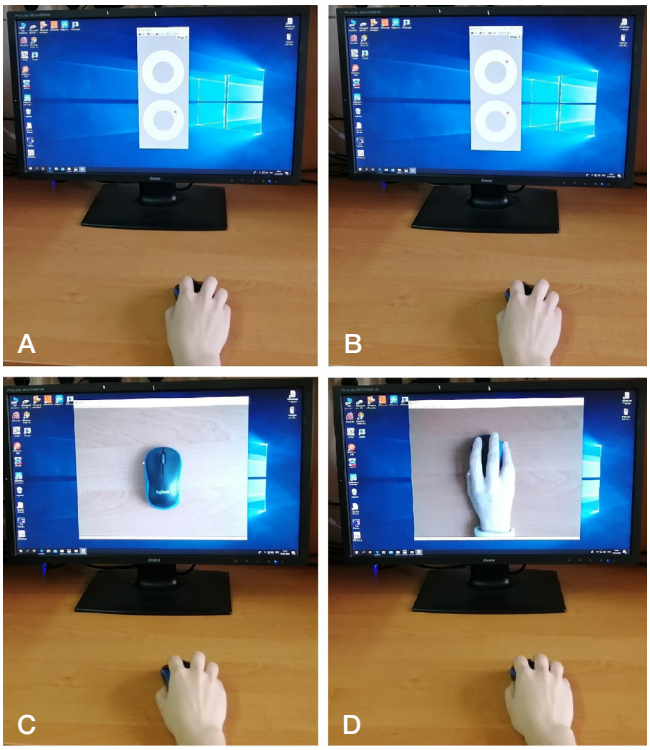

Fig. 1. Task queue. **A**. Concentric colored circle moving on the monitor screen using the computer mouse (Mn.1). **B**. Imitation of other colored circle's movement (ImNB). **C**. Children move the computer mouse in circle on their own (Mn.2). **D**. Children imitate the researcher's movements (ImB)

2) moving the computer mouse in a circle by children on their own (Mn.2) (Fig. 1C);

3) imitation of the researcher's movements by the children (imitation of biological motion, ImB) (Fig. 1D).

EEG was analysed in the individual μ-rhythm frequency range defined when the subject moved his right hand on his own (C3). The full frequency range of the μ-rhythm (6–13 Hz) was divided into segments of 1 Hz. As an individual frequency range, two adjacent segments were taken with maximum desynchronization in relation to baseline [17]. The μ-rhythm amplitude within the individual frequency range was calculated for each experimental situation. Log transformation was used for normalization of the amplitude values distribution.

Reactivity indices were used for comparison of μ-rhythm parameters under conditions of biological and non-biological movement imitation. These indices were calculated according to the generally accepted scheme [18] using the following formula: k = ln (B/A), where k is the sensorimotor rhythm reactivity index, B is the sensorimotor rhythm amplitude in the major situation, and A is the sensorimotor rhythm amplitude in the initial reference situation (baseline or subjects' moving on their own). Positive reactivity index values corresponded to synchronization of the sensorimotor rhythm, and negative values corresponded to desynchronization.

Statistical analysis

Statistical analysis was performed using the STATISTICA 12.0 software (StatSoft Inc.; USA). To describe the non-normal distributions, median and interquartile range were used, the differences between the groups were evaluated using the Mann–Whitney U-test. For normal data distribution, the mean and standard error of the mean were used. The differences of the amplitude and reactivity indices of the μ-rhythm recorded in different experimental situations were evaluated by the repeated measures ANOVA. The 4×2×9 scheme was used for assessment of the one intersubjective factor (age group, AGE) and two intrasubjective factors (situation, SIT, and locus, LOC) influence. To calculate the statistical significance of the sensorimotor rhythm differences in relation to each of the nine EEG derivations within each age group, the ad-hoc analysis method (F-distribution estimation) was used.

RESULTS

μ-rhythm frequency parameters

The median values of the individual μ-rhythm range lower boundary were 9 Hz (8.5; 10), the extreme values were 6 and 11 Hz. The median values of the individual μ-rhythm range upper boundary were 11 Hz (10.5; 12), and the extreme values were 8 and 13 Hz. The differences between the age groups were not significant.

EEG μ-rhythm amplitude at rest and under condition of motion execution and imitation

The μ-rhythm amplitude differences analysis of variance in the Mn.1 situation in relation to baseline taking into account the age group and EEG locus revealed the sifnificant influence of the SIT ($F_{1, 132}$ = 90.34; p < 0.001), AGE ($F_{3, 132}$ = 10.18; p < 0.001) and LOC ($F_{8, 1056}$ = 73.06; p < 0.001) factors, as well as the SIT×LOC interaction ($F_{8, 1056}$ = 41.28; p < 0.001). Compared to Mn.1, in the ImNB situation the SIT ($F_{1, 132}$ = 12.65; p < 0.001), AGE ($F_{3, 132}$ = 14.67; p < 0.001) and LOC ($F_{8, 1056}$ = 39.43; p < 0.001) factors significantly affected the μ-rhythm amplitude changes.

The μ-rhythm amplitude differences analysis of variance in the Mn.2 situation in relation to baseline taking into account the age group and EEG locus revealed the sifnificant influence of the SIT ($F_{1, 132}$ = 31.17; p < 0.001), AGE ($F_{3, 132}$ = 6.46; p < 0.001) and LOC ($F_{8, 1056}$ = 71.55; p < 0.001), factors, as well as the SIT×LOC ($F_{8, 1056}$ = 28.32; p < 0.001) and SIT×AGE ($F_{3, 132}$ = 6.35; p < 0.001) interactions. Evaluation of the μ-rhythm amplitude changes in the ImB situation in relation to Mn.2 revealed the significant influence of the SIT ($F_{1, 132}$ = 9.58; p = 0.002), AGE ($F_{3, 132}$ = 18.63; p < 0.001) and LOC ($F_{8, 1056}$ = 54.08; p < 0.001) factors, as well as the SIT×LOC ($F_{8, 1056}$ = 3.28; p = 0.001) and SIT×AGE ($F_{3, 132}$ = 6.2; p = 0.001) interactions.

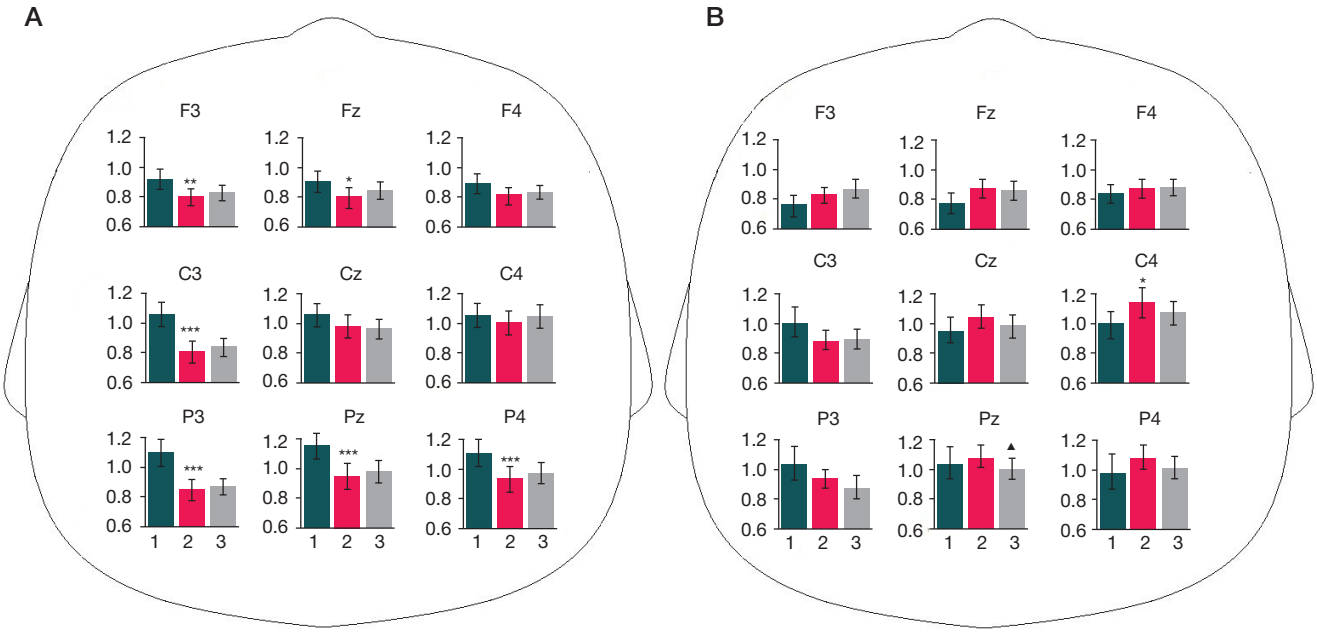

Fig. 2. EEG μ-rhythm amplitude (A, Ln μV) in children aged 4–6 during imitation of non-biological (**A**) and biological (**B**) motion. 1 — baseline, 2 — autonomous movements' execution at arbitrary speed, 3 — motion imitation. Amplitude differences between baseline and autonomous movements' execution: * — p < 0.05; ** — $p \le 0.01$; *** — $p \le 0.001$; when executing autonomous movements and imitating: ▲ — p < 0.05

In children aged 4–6 executing the concentric moving of the coloured circle, the significant EEG μ-rhythm desynchronization was detected (Mn.1 in relation to baseline) in most studied regions. The μ-rhythm amplitude changes in children imitating the coloured circle movement (ImNB in relation to Mn.1) were not significant (Fig. 2A). When the children of that age moved the computer mouse on their own, the significant EEG μ-rhythm amplitude increase (Mn.2 in relation to baseline) was detected in the the right hemisphere central locus (C4). When the children imitated the researcher's movements, the sensorimotor rhythm desynchronization (ImB in relation to Mn.2) was registered in the в mid-parietal locus (Pz) (Fig. 2B).

In the group of children aged 7–9, the significant depression of μ-rhythm in the Mn.1 situation was observed in most studied regions. In the ImNB situation (in relation to Mn.1) the μ-rhythm amplitude changes were not significant (Fig. 3A). In the Mn.2 situation the significant sensorimotor rhythm desynchronization was detected in the central (C3 and Cz) and all parietal loci. In the ImB situation (in relation to Mn.2) there were no significant μ-rhythm amplitude changes (Fig. 3B).

In children aged 10–12, in the Mn.1 sitiation the significant μ-rhythm suppression was detected in most studied loci. During the coloured circle movement imitation the significant sensorimotor rhythm synchronization (ImNB in relation to Mn.1) was detected in the mid-frontal locus (Fig. 4A). In the Mn.2 situation the significant decrease in μ-rhythm amplitude was observed in the central (C3 и Cz) and all parietal loci. In the ImB situation (in relation to Mn.2) there were no significant sensorimotor rhythm amplitude changes (Fig. 4B).

In the group of teenagers aged 13–15, in the Mn.1 sitiation the significant μ-rhythm suppression was observed in most studied loci. During the non-biological motion imitation (ImNB in relation to Mn.1) the significant sensorimotor rhythm

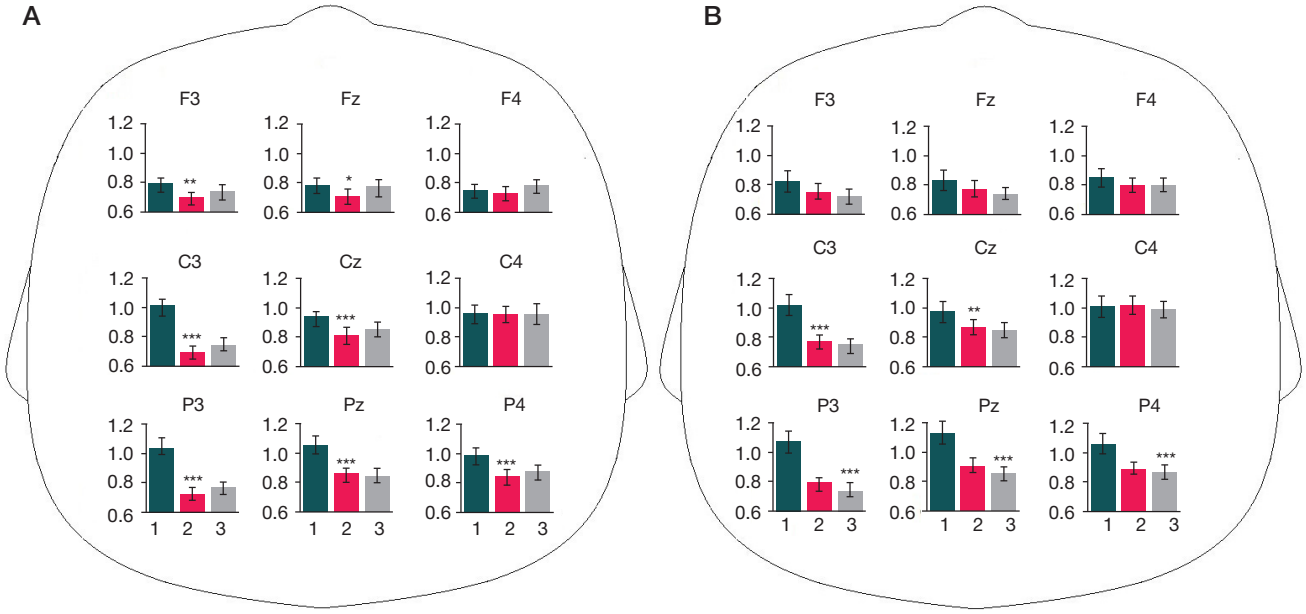

Fig. 3. EEG μ-rhythm amplitude (A, Ln μV) in the group of children aged 7–9 during imitation of non-biological (**A**) and biological (**B**) motion. The remaining notation is the same as in Fig. 2

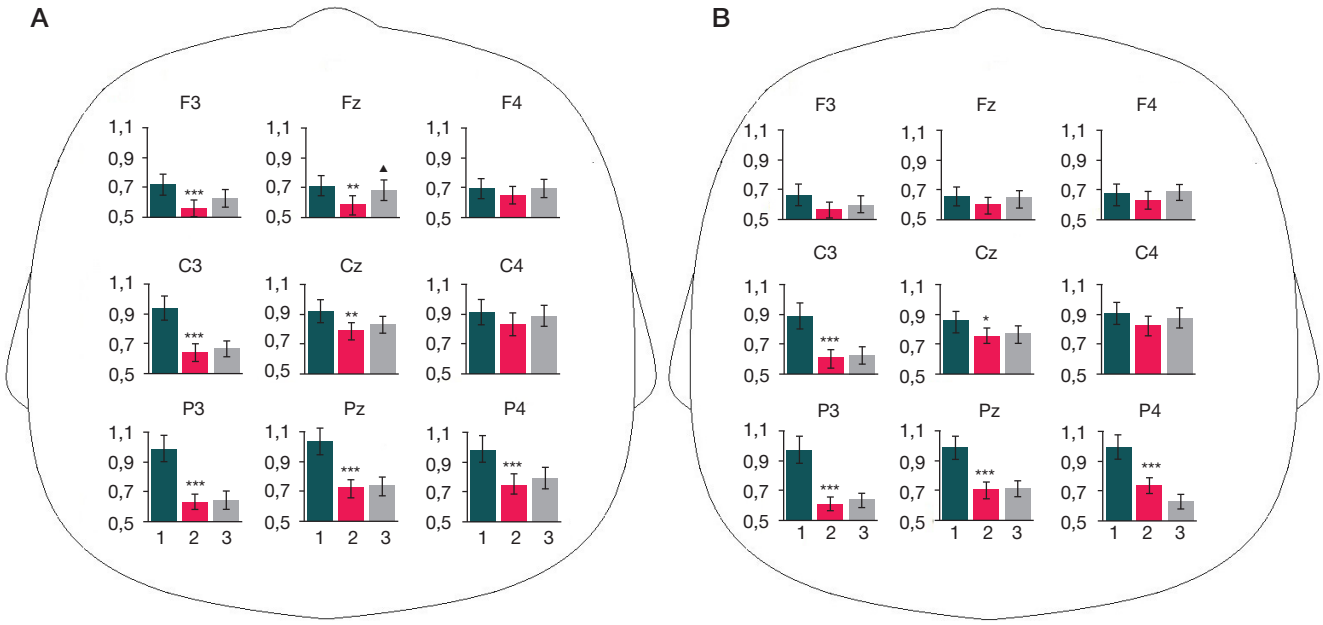

Fig. 4. EEG μ-rhythm amplitude (A, Ln μV) in the group of children aged 10–12 during imitation of non-biological (**A**) and biological (**B**) motion. The remaining notation is the same as in Fig. 2

synchronization was detected in most studied regions (Fig. 5A). When the subjects moved the computer mouse on their own, significant sensorimotor rhythm desynchronization (Mn.2 in relation to baseline) was registered in all studied regions. In the ImB situation, the additional (compared to previous task) μ-rhythm desynchronization was observed that was significant in all loci (Fig. 5B).

EEG μ-rhythm reactivity comparison under conditions of biological and non-biological motion imitation

To evaluate the differences of μ-rhythm reactivity in the ImNB and ImB situations (compared to execution of movements by children on their own at arbitrary speed), the reactivity indices analysis of variance was performed taking into account the age group and EEG locus. The mean μ-rhythm reactivity index values for children of four age groups are presented in Tables 1 and 2. The significant impact of SIT ($F_{1, 132}$ = 21.85; $p < 0.001$) and LOC ($F_{8, 1056}$ = 3.95; $p < 0.001$) factors, as well as the SIT×AGE interaction ($F_{3, 132}$ = 5.52; p = 0.001) was revealed. In the group of pre-school children, the significant μ-rhythm reactivity indices differences in the ImNB and ImB situations were detected in the parietal loci Pz and P4 (p = 0.03). In children aged 7–9, the significant differences were observed in the locus Fz (p = 0.04). In children aged 10–12, no significant μ-rhythm reactivity indices differences were detected. In the group of teenagers aged 13–15, the differences were significant in all studied regions ($p \leq 0.001$).

DISCUSSION

According to the study results, the individual sensorimotor rhythm frequency ranges of the 4–15 years old children vary widely, and there are no significant differences in the mean values between different age groups. In the other authors's paper [19] reporting the EEG μ-rhythm reactivity analysis in the selected frequency range in children aged 4–11, the average sencorimotor rhythm band was 9–11 Hz. High sensorimotor rhythm parameters variability among the individuals and no association with the children's age were detected. These indicate the need to determine the children's individual frequency range when studying the sensorimotor rhythm reactivity, as well as when attempting the correction using the μ-rhythm parameters (EEG based neurofeedback training, correction using the brain-computer interface).

Analysis of the μ-rhythm amplitude changes demonstrated that in 4–6 years old children arbitrarily moving the coloured circle (Mn.1) the significant EEG μ-rhythm desynchronization in the frontal and central loci of left hemisphere, as well as in the median frontal and all parietal loci (F3, Fz, C3, P3, Pz, P4) could be detected. The results of our study are consistent with the literature data on the sensorimotor rhythm desynchronization during the voluntary movements' execution [20]. When the children moved the computer mouse on their own (Mn.2), no significant μ-rhythm amplitude decrease was observed. It is possible that for children of this age, the task of relatively simple circular movements' execution with a computer mouse was simpler than the task of capturing and moving a colored circle using the computer mouse left button, and it did not require any special motor control. During the task execution, the significant EEG μ-rhythm amplitude increase in the locus C4 was registered, which could be due to inhibition of the ipsilateral hemisphere (in relation to the hand used) [21].

In the groups of children aged 7–9 and 10–12 executing the movements on their own, the μ-rhythm desynchronization was detected in most studied regions. The concentric coloured circle moving (Mn.1) unlike the mouse moving in a circle (Mn.2) was also associated with the sensorimotor rhythm desynchronization in the frontal loci (F3, Fz). It is known that the frontal cortical regions are responsible for planning and preparation of complex movements [22]. It is also assumed that more complex motor actions are accompanied by a more widespread μ-activity desynchronization [23]. Presumably, moving the color circle in the group of 7–12 years old children, as well as in the group of younger children, required considerable effort, which led to the involvement of the cerebral cortex frontal region.

The situations of biological and non-biological motion imitation in children aged 4–6, 7–9 and 10–12 were associated with almost no additional modulation of the μ-rhythm in relation to the arbitrary movements' execution. This may indicate that in children of said age the required for processing

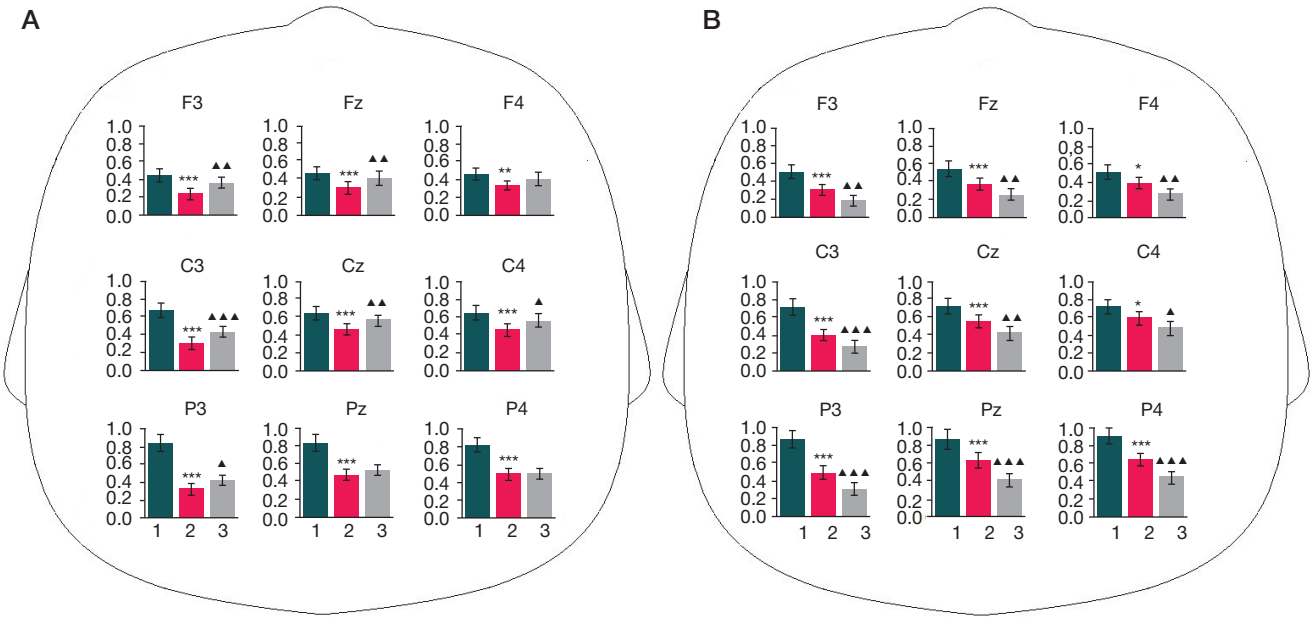

Fig. 5. EEG μ-rhythm amplitude (A, Ln μV) in the group of children aged 13–15 during imitation of non-biological (**A**) and biological (**B**) motion. Amplitude differences when executing autonomous movements and imitating: ▲▲ — $p \leq 0.01$; ▲▲▲ — $p \leq 0.001$. The remaining notation is the same as in Fig. 2

Table 1. Reactivity indices mean values (together with standard error of the mean) obtained during imitation of non-biological motion

Group	EEG electrodes								
	F3	Fz	F4	C3	Cz	C4	P3	Pz	P4
4–6 years	0.03 ± 0.04	0.04 ± 0.04	0.03 ± 0.03	0.03 ± 0.04	–0.02 ± 0.04	0.04 ± 0.03	0.02 ± 0.04	0.03 ± 0.04	0.04 ± 0.04
7–9 years	0.05 ± 0.03	0.06 ± 0.03	0.05 ± 0.03	0.05 ± 0.03	0.04 ± 0.03	0.00 ± 0.05	0.04 ± 0.03	–0.01 ± 0.03	0.03 ± 0.03
10–12 years	0.06 ± 0.04	0.09 ± 0.04	0.05 ± 0.04	0.03 ± 0.04	0.04 ± 0.03	0.06 ± 0.03	0.01 ± 0.04	0.01 ± 0.04	0.05 ± 0.05
13–15 years	0.11 ± 0.04	0.11 ± 0.05	0.07 ± 0.04	0.12 ± 0.03	0.10 ± 0.03	0.11 ± 0.04	0.09 ± 0.03	0.05 ± 0.03	0.01 ± 0.03

Note: positive reactivity index values correspond to sensorimotor rhythm synchronization, negative values correspond to desynchronization.

Table 2. Reactivity indices mean values (together with standard error of the mean) obtained during imitation of biological motion

Group	EEG electrodes								
	F3	Fz	F4	C3	Cz	C4	P3	Pz	P4
4–6 years	0.04 ± 0.04	–0.01 ± 0.05	0.01 ± 0.05	0.01 ± 0.04	–0.07 ± 0.05	–0.07 ± 0.06	–0.06 ± 0.05	–0.09 ± 0.05	–0.06 ± 0.06
7–9 years	–0.03 ± 0.03	–0.04 ± 0.03	0.00 ± 0.03	–0.03 ± 0.02	–0.03 ± 0.03	–0.03 ± 0.04	–0.04 ± 0.04	–0.06 ± 0.03	–0.03 ± 0.03
10–12 years	0.04 ± 0.05	0.04 ± 0.04	0.06 ± 0.04	0.03 ± 0.03	0.01 ± 0.03	0.06 ± 0.04	0.03 ± 0.03	0.01 ± 0.04	0.05 ± 0.03
13–15 years	–0.11 ± 0.03	–0.12 ± 0.03	–0.11 ± 0.03	–0.14 ± 0.03	–0.12 ± 0.04	–0.11 ± 0.04	–0.18 ± 0.03	–0.21 ± 0.04	–0.20 ± 0.03

multimodal information additional neocortical resources are not sufficiently involved under the conditions of imitation.

In the group of teenagers aged 13–15, the significant sensorimotor rhythm desynchronization during the autonomous movements' execution was detected in all studied regions. The μ-rhythm amplitude decrease above the frontal, central and parietal loci in elder children may be due to development of connections between the neocortical regions involved. During the non-biological motion imitation a smaller drop in the sensorimotor rhythm amplitude was observed than during the autonomous movements execution and biological motion imitation (which is especially pronounced in the frontal and central loci). It can be assumed, that the need to imitate the movements of another object (colored circle) led to the shift of attention to its perception and, as a result, to weakening of one's own movements' motor control. In children of this age, in the ImB situation, the additional (compared to the observed during the Mn.2 task execution) significant μ-rhythm desynchronization in all loci was detected. The more pronouced reaction in the parietal loci is noteworthy. It is known, that parietal cortical regions are involved into the information processing during watching the human's motion (compared to watching the non-biological objects' motion) [24]. The sensorimotor rhythm modulation, revealed by us in the described regions during the biological motion imitation, may be due to involvement of the parietal cortex MNS components responsible for coding of goals underlying the watched movements [25]. The mirror neurons are associated with the cognitive integration of visual, auditory and motor stimuli needed for social interaction in children [26] and adults [27]. Thus, it can be assumed, that the additional μ-rhythm desynchronization during the other man's movements imitation is caused precisely by the social context to which the MNS is sensitive.

Comparison of the μ-rhythm reactivity indices for imitation tasks revealed that the biological motion imitation in elder children was associated with the greater desynchronization, compared with the situation of color circle movements' imitation. As already noted, similar features of the sensorimotor rhythm reactivity during watching the biological and non-biological objects movements were detected in adult volunteers [8].

A sensorimotor rhythm reactivity patterns comparative analysis in children of different ages allows us to come to a number of conclusions. In the group of youngest children (4–6 years), the most pronounced activation of the frontal, central and parietal cortical regions, manifested in the μ-rhythm amplitude decrease (more pronounced in the left hemisphere), is observed during computer mouse operation associated with a non-biological motion (coloured circle) (Mn.1). Random rhythm computer mouse movements' execution (Mn.2) does not lead to the significant decrease in the μ-rhythm amplitude, and the biological motion imitation (the other person's hand movement) is not associated with any additional activation in most loci. Thus, in the described experimental situation, in pre-school children, the cortical center of motor analyzer is especially sensitive to manipulations with biological objects. In elder children (7–9 and 10–12 year), a similar neocortical activation pattern was revealed during execution of movements associated with non-biological objects, computer mouse moving and biological object (researcher's hand) motion imitation. Unlike the previously described groups, the children aged 13–15 demonstrate the significant μ-rhythm desynchronization in the frontal, central and parietal cortical regions of both hemispheres during imitation of the other person's motion.

It stands to reason, that processes of perception and other person's movement imitation in younger children are in their infance, and in teenagers, these processes are rather developed and similar to those in adults. In teenagers, the pronounced μ-rhythm desynchronization in all studied regions during moving on their own or imitating the biological visual images motion may be due to maturation of motor, sensorimotor and associative cortical regions involved in the execution and imitation of movements [28]. The revealed age-related sensorimotor rhythm reactivity features may be used for improvement of existing rehabilitation techniques based on the EEG-controlled robotic systems for children with cerebral palsy [15].

CONCLUSION

When children aged 4–15 move the computer mouse on their own, the μ-rhythm desynchronization develops in the frontal, central and parietal neocortical regions, which is more pronounced in the left hemisphere. When the children aged 4–6, 7–9 and 10–12 imitate the biological and non-biological motion no significant additional μ-rhythm modulation is revealed, compared to the execution of movements on their own. In children aged 13–15, the highest sensorimotor rhythm desynchronization is observed during the resercher's hand

motion imitation. When developing the software for brain-computer interfaces designed for motor function impairment correction, elements of the non-biological objects' movement may be used as visual stimuli, but the older the children, the more effective the presentation of moving biological objects can be for neocortical activation.

References

1. Rizzolatti G, Fogassi L. The mirror mechanism: recent findings and perspectives. Philos Trans R Soc Lond B Biol Sci. 2014; 369 (1644): 20130420.
2. Hardwick RM, Caspers S, Eickhoff SB, Swinnen SP. Neural correlates of action: Comparing meta-analyses of imagery, observation, and execution. Neurosci Biobehav Rev. 2018; (94): 31–44.
3. Lebedeva NN, Zufman AI, Mal'cev VJu. Sistema zerkal'nyh nejronov mozga: kljuch k obucheniju, formirovaniju lichnosti i ponimaniju chuzhogo soznanija. Uspehi fiziologicheskih nauk. 2017; 48(4): 16–28.
4. Fox NA, Bakermans-Kranenburg MJ, Yoo KH, Bowman LC, Cannon EN, Vanderwert RE, et al. Assessing human mirror activity with EEG mu rhythm: A meta-analysis. Psychol Bull. 2016; 142 (3): 291–313.
5. Hobson HM, Bishop DVM. Mu suppression — a good measure of the human mirror neuron system? Cortex. 2016; (82): 290–310.
6. Gundlach C, Muller MM, Nierhaus T, Villringer A, Sehm B. Modulation of Somatosensory Alpha Rhythm by Transcranial Alternating Current Stimulation at Mu-Frequency. Front Hum Neurosci. 2017; (11): 432.
7. Bimbi M, Festante F, Coude G, Vanderwert RE, Fox NA, Ferrari PF. Simultaneous scalp recorded EEG and local field potentials from monkey ventral premotor cortex during action observation and execution reveals the contribution of mirror and motor neurons to the mu-rhythm. Neuroimage. 2018; (175): 22–31.
8. Ulloa ER, Pineda JA. Recognition of point-light biological motion: mu rhythms and mirror neuron activity. Behav Brain Res. 2007; 183 (2): 188–94.
9. Oberman LM, Pineda JA, Ramachandran VS. The human mirror neuron system: a link between action observation and social skills. Soc Cogn Affect Neurosci. 2007; 2 (1): 62–66.
10. Wohlschlager A, Gattis M, Bekkering H. Action generation and action perception in imitation: an instance of the ideomotor principle. Philos. Trans. R Soc. Lond., B Biol Sci. 2003; (358): 501–15.
11. Frolov AA, Bobrov PD. Interfejs mozg-komp'juter: nejrofiziologicheskie predposylki i klinicheskoe primenenie. Zhurnal vysshej nervnoj dejatel'nosti. 2017; 67(4): 365–376.
12. Levickaja OS, Lebedev MA. Interfejs mozg-komp'juter: budushhee v nastojashhem. Vestnik Rossijskogo Gosudarstvennogo Medicinskogo Universiteta. 2016; (2): 4–16.
13. Lopez-Larraz E, Escolano C, Montesano L, Minguez J. Reactivating the Dormant Motor Cortex After Spinal Cord Injury With EEG Neurofeedback: A Case Study With a Chronic, Complete C4 Patient. Clin EEG Neurosci. 2019; 50 (2): 100–10.
14. Liburkina SP, Vasilev AN, Kaplan AJa, Ivanova GE, Chukanova AS. Pilotnoe issledovanie ideomotornogo treninga v konture interfejsa mozg-komp'juter u pacientov s dvigatel'nymi narushenijami. Zhurnal nevrologii i psihiatrii. 2018; 9 (2): 63–68.
15. Larina NV, Korsunskaja LL, Vlasenko SV. Kompleks «Jekzokist'-2» v reabilitacii verhnej konechnosti pri detskom cerebral'nom paraliche s ispol'zovaniem neinvazivnogo interfejsa «mozg-komp'juter». Nervno-myshechnye bolezni. 2019; 9 (4): 44–50.
16. Cannon EN, Yoo KH, Vanderwert RE, Ferrari PF, Woodward AL, Fox NA. Action experience, more than observation, influences mu rhythm desynchronization. PLoS One. 2014; 9 (3): e92002.
17. Mahin SA, Kaida AI, Eismont EV, Mihailova AA, Pavlenko VB; FGAOU VO «Krymskij federal'nyj universitet imeni V.I. Vernadskogo», patentoobladatel'. Sposob opredelenija individual'nogo chastotnogo diapazona mju-ritma JeJeG. Patent RF № 2702728. 09.10.2019.
18. Raymaekers R, Wiersema JR, Roeyers H. EEG study of the mirror neuron system in children with high functioning autism. Brain research. 2009; (1304): 113–21.
19. Lepage JF, Théoret H. EEG evidence for the presence of an action observation-execution matching system in children. Eur J Neurosci. 2006; 23 (9): 2505–10.
20. Lebedeva NN, Karimova ED, Karpychev VV, Malcev VJu. Zerkal'naja sistema mozga pri nabljudenii, vypolnenii i predstavlenii motornyh zadach — nejrofiziologicheskoe otrazhenie vosprijatija chuzhogo soznanija. Zhurnal vysshej nervnoj dejatel'nosti. 2018; 68 (2): 204–15.
21. Hummel F, Andres F, Altenmüller E, Dichgans J, Gerloff C. Inhibitory control of acquired motor programmes in the human brain. Brain. 2002; 125 (2): 404–20.
22. Brown MN, Staines WR. Differential effects of continuous theta burst stimulation over left premotor cortex and right prefrontal cortex on modulating upper limb somatosensory input. Neuroimage. 2016; (127): 97–109.
23. Thorpe SG, Cannon EN, Fox NA. Spectral and source structural development of mu and alpha rhythms from infancy through adulthood. Clin Neurophysiol. 2016; 127 (1): 254–69.
24. Saygin AP, Stadler W. The role of appearance and motion in action prediction. Psychol Res. 2012; (76): 388–94.
25. Bonini L, Rozzi S, Serventi FU, Simone L, Ferrari PF, Fogassi L. Ventral premotor and inferior parietal cortices make distinct contribution to action organization and intention understanding. Cereb Cortex. 2010; (20): 1372–85.
26. Filippi CA, Cannon EN, Fox NA, Thorpe SG, Ferrari PF, Woodward AL. Motor system activation predicts goal imitation in 7-month-old infants. Psychol Sci. 2016; (27): 675–84.
27. Yin J, Ding X, Xu H, Zhang F, Shen M. Social Coordination Information in Dynamic Chase Modulates EEG Mu Rhythm. Sci Rep. 2017; 7 (1): 4782.
28. Segalowitz SJ, Santesso DL, Jetha MK. Electrophysiological changes during adolescence: a review. Brain Cogn. 2010; 72 (1): 86–100.

Литература

1. Rizzolatti G, Fogassi L. The mirror mechanism: recent findings and perspectives. Philos Trans R Soc Lond B Biol Sci. 2014; 369 (1644): 20130420.
2. Hardwick RM, Caspers S, Eickhoff SB, Swinnen SP. Neural correlates of action: Comparing meta-analyses of imagery, observation, and execution. Neurosci Biobehav Rev. 2018; (94): 31–44.
3. Лебедева Н. Н., Зуфман А. И., Мальцев В. Ю. Система зеркальных нейронов мозга: ключ к обучению, формированию личности и пониманию чужого сознания. Успехи физиологических наук. 2017; 48 (4): 16–28.
4. Fox NA, Bakermans-Kranenburg MJ, Yoo KH, Bowman LC, Cannon EN, Vanderwert RE, et al. Assessing human mirror activity with EEG mu rhythm: A meta-analysis. Psychol Bull. 2016; 142 (3): 291–313.
5. Hobson HM, Bishop DVM. Mu suppression — a good measure of the human mirror neuron system? Cortex. 2016; (82): 290–310.
6. Gundlach C, Muller MM, Nierhaus T, Villringer A, Sehm B. Modulation of Somatosensory Alpha Rhythm by Transcranial Alternating Current Stimulation at Mu-Frequency. Front Hum

Neurosci. 2017; (11): 432.
7. Bimbi M, Festante F, Coude G, Vanderwert RE, Fox NA, Ferrari PF. Simultaneous scalp recorded EEG and local field potentials from monkey ventral premotor cortex during action observation and execution reveals the contribution of mirror and motor neurons to the mu-rhythm. Neuroimage. 2018; (175): 22–31.
8. Ulloa ER, Pineda JA. Recognition of point-light biological motion: mu rhythms and mirror neuron activity. Behav Brain Res. 2007; 183 (2): 188–94.
9. Oberman LM, Pineda JA, Ramachandran VS. The human mirror neuron system: a link between action observation and social skills. Soc Cogn Affect Neurosci. 2007; 2 (1): 62–66.
10. Wohlschlager A, Gattis M, Bekkering H. Action generation and action perception in imitation: an instance of the ideomotor principle. Philos. Trans. R Soc. Lond., B Biol Sci. 2003; (358): 501–15.
11. Фролов А. А., Бобров П. Д. Интерфейс мозг-компьютер: нейрофизиологические предпосылки и клиническое применение. Журнал высшей нервной деятельности. 2017; 67 (4): 365–76.
12. Левицкая О. С., Лебедев М. А. Интерфейс мозг-компьютер: будущее в настоящем. Вестник Российского Государственного Медицинского Университета. 2016; (2): 4–16.
13. Lopez-Larraz E, Escolano C, Montesano L, Minguez J. Reactivating the Dormant Motor Cortex After Spinal Cord Injury With EEG Neurofeedback: A Case Study With a Chronic, Complete C4 Patient. Clin EEG Neurosci. 2019; 50 (2): 100–10.
14. Либуркина С. П., Васильев А. Н., Каплан А. Я., Иванова Г. Е., Чуканова А. С. Пилотное исследование идеомоторного тренинга в контуре интерфейса мозг-компьютер у пациентов с двигательными нарушениями. Журнал неврологии и психиатрии. 2018; 9 (2): 63–68.
15. Ларина Н. В., Корсунская Л. Л., Власенко С. В. Комплекс «Экзокисть-2» в реабилитации верхней конечности при детском церебральном параличе с использованием неинвазивного интерфейса «мозг-компьютер». Нервно-мышечные болезни. 2019; 9 (4): 44–50.
16. Cannon EN, Yoo KH, Vanderwert RE, Ferrari PF, Woodward AL, Fox NA. Action experience, more than observation, influences mu rhythm desynchronization. PLoS One. 2014; 9 (3): e92002.
17. Махин С. А., Кайда А. И., Эйсмонт Е. В., Михайлова А. А., Павленко В. Б.; ФГАОУ ВО «Крымский федеральный университет имени В. И. Вернадского», патентообладатель. Способ определения индивидуального частотного диапазона μ-ритма ЭЭГ. Патент РФ № 2702728. 09.10.2019.
18. Raymaekers R, Wiersema JR, Roeyers H. EEG study of the mirror neuron system in children with high functioning autism. Brain research. 2009; (1304): 113–21.
19. Lepage JF, Théoret H. EEG evidence for the presence of an action observation-execution matching system in children. Eur J Neurosci. 2006; 23 (9): 2505–10.
20. Лебедева Н. Н., Каримова Е. Д., Карпычев В. В., Мальцев В. Ю. Зеркальная система мозга при наблюдении, выполнении и представлении моторных задач — нейрофизиологическое отражение восприятия чужого сознания. Журнал высшей нервной деятельности. 2018; 68 (2): 204–15.
21. Hummel F, Andres F, Altenmüller E, Dichgans J, Gerloff C. Inhibitory control of acquired motor programmes in the human brain. Brain. 2002; 125 (2): 404–20.
22. Brown MN, Staines WR. Differential effects of continuous theta burst stimulation over left premotor cortex and right prefrontal cortex on modulating upper limb somatosensory input. Neuroimage. 2016; (127): 97–109.
23. Thorpe SG, Cannon EN, Fox NA. Spectral and source structural development of mu and alpha rhythms from infancy through adulthood. Clin Neurophysiol. 2016; 127 (1): 254–69.
24. Saygin AP, Stadler W. The role of appearance and motion in action prediction. Psychol Res. 2012; (76): 388–94.
25. Bonini L, Rozzi S, Serventi FU, Simone L, Ferrari PF, Fogassi L. Ventral premotor and inferior parietal cortices make distinct contribution to action organization and intention understanding. Cereb Cortex. 2010; (20): 1372–85.
26. Filippi CA, Cannon EN, Fox NA, Thorpe SG, Ferrari PF, Woodward AL. Motor system activation predicts goal imitation in 7-month-old infants. Psychol Sci. 2016; (27): 675–84.
27. Yin J, Ding X, Xu H, Zhang F, Shen M. Social Coordination Information in Dynamic Chase Modulates EEG Mu Rhythm. Sci Rep. 2017; 7 (1): 4782.
28. Segalowitz SJ, Santesso DL, Jetha MK. Electrophysiological changes during adolescence: a review. Brain Cogn. 2010; 72 (1): 86–100.

CIRCADIAN RHYTHMS OF LEUKEMIA INHIBITORY FACTOR IN THE BLOOD OF PATIENTS WITH ESSENTIAL HYPERTENSION

Radaeva OA[1] ✉, Simbirtsev AS[2], Gromova EV[1], Iskandiarova MS[1], Belyaeva SV[3]

[1] Institute of Medicine, National Research Mordovia State University, Saransk, Russia

[2] State Research Institute of Highly Pure Biopreparations, FMBA, Saint Petersburg, Russia

[3] North Caucasus Health Center, Pyatigorsk, Russia

Leukemia inhibitory factor (LIF) exerts multidirectional effects in the setting of essential hypertension (EH). There is a mounting body of evidence refuting the postulate about identical STAT3 signaling in cardiomyocytes and endothelial/smooth muscle cells, which is important in the situation of extended exposure to gp 130 ligands (LIF in particular). At the same time, there are no reports on the circadian dynamics of peripheral blood LIF concentrations and possible secondary changes to the pathophysiological effects of this cytokine. This study aimed to analyze the circadian dynamics of LIF concentrations in the peripheral blood serum measured at 5 different time points in patients with stage II EH in the presence/absence of antihypertensive therapy and their relationship with the frequency of complications developing within a 5-year follow-up. Blood serum LIF was measured in 60 patients with stage II EH using ELISA at 8:00, 14:00, 20:00, 2:00, and 8:00 o'clock before putting the patients on antihypertensive therapy and one year after its onset. The identified patterns of diurnal LIF concentrations (a rise by ≥15% at 20:00, $p < 0.001$; a further rise by ≥22% peaking at 2:00, $p < 0.001$ relative to the values at 8:00) can be regarded as pathologic; their persistence after one year of antihypertensive therapy is a sign of EH progression and puts the patients at 6-fold risk for cardiovascular complications, including myocardial infarction and acute cerebrovascular events.

Keywords: LIF, leukemia inhibitory factor, cytokine circadian rhythms, essential hypertension

Author contribution: Radaeva OA designed the study, analyzed the results, formulated the conclusions and wrote the manuscript; Simbirtsev AS formulated the objective of the study, revised its conclusions and the manuscript itself; Gromova EV designed the study, carried out laboratory tests, and contributed to writing the manuscript; Iskandiarova MS analyzed the literature, supervised blood collection, followed up with the patients, contributed to writing the manuscript; Belyaeva SV analyzed the literature, supervised blood collection, followed up with the patients.

Compliance with ethical standards: the study was approved by the Ethics Committee of National Research Mordovia State University (Protocol No. 12 dated December 14, 2008). Written informed consent was obtained from all study participants. Blood samples were collected in compliance with the Declaration of Helsinki (2008), the protocol of European Convention on Human Rights and Biomedicine (1999) and the additional protocol to the Convention on Human Rights and Biomedicine concerning Biomedical Research (2005).

✉ **Correspondence should be addressed:** Olga A. Radaeva
Ulianova, 26a, Saransk, 430000; vtlbwbyf_79@mail.ru

Received: 11.03.2020 **Accepted:** 25.03.2020 **Published online:** 28.03.2020

DOI: 10.24075/brsmu.2020.017

ИЗМЕНЕНИЕ СУТОЧНОГО РИТМА СОДЕРЖАНИЯ ИНГИБИРУЮЩЕГО ЛЕЙКЕМИЮ ФАКТОРА В КРОВИ БОЛЬНЫХ ЭССЕНЦИАЛЬНОЙ ГИПЕРТЕНЗИЕЙ

О. А. Радаева[1] ✉, А. С. Симбирцев[2], Е. В. Громова[1], М. С. Искандярова[1], С. В. Беляева[3]

[1] Медицинский институт Национального исследовательского Мордовского государственного университета имени Н. П. Огарева, Саранск, Россия

[2] Государственный научно-исследовательский институт особо чистых биопрепаратов Федерального медико-биологического агентства, Санкт-Петербург, Россия

[3] Санаторно-курортный комплекс «Северокавказский», Пятигорск, Россия

Ингибирующий лейкемию фактор (LIF) обладает неоднозначными физиологическими эффектами при эссенциальной артериальной гипертензии (ЭАГ). Опровергается постулат об идентичности STAT3-сигнализации в клетках миокарда и эндотелиальных/гладкомышечных клетках, что значимо при длительном воздействии цитокинов-лигандов gp 130 (в частности LIF). При этом отсутствуют данные о суточных характеристиках содержания LIF в крови с потенциальными вторичными изменениями его патофизиологических эффектов. Целью исследования было проанализировать особенности суточных ритмов содержания LIF в сыворотке периферической крови больных ЭАГ II стадии, определенного в пяти временны́х точках в зависимости от применения гипотензивной терапии и частоты развития осложнений в последующие 5 лет наблюдения. У 60 больных ЭАГ II стадии иммуноферментным методом определяли уровни LIF в сыворотке периферической крови в 8.00, 14.00, 20.00, 2.00, 8.00 ч до и после года гипотензивной терапии. Выявленные закономерности суточного ритма содержания LIF в сыворотке крови больных ЭАГ II стадии в виде увеличения в 20.00 ч на 15% ($p < 0,001$) и выше с максимальным ростом в 2.00 ч на 22% ($p < 0,001$) и более при сравнении с индивидуальным уровнем в 8.00 ч можно характеризовать как патологические, а их сохранение после года гипотензивной терапии служит признаком прогредиентного течения гипертензии с повышением риска развития сердечно-сосудистых осложнений (инфаркт миокарда, острое нарушение мозгового кровообращения) в 6 раз.

Ключевые слова: LIF, ингибирующий лейкемию фактор, суточный ритм цитокинов, эссенциальная гипертензия

Вклад авторов: О. А. Радаева — разработка дизайна исследования, анализ результатов, формулировка выводов, оформление рукописи; А. С. Симбирцев — формулирование цели исследования, корректирование выводов и итогового варианта рукописи; Е. В. Громова — разработка дизайна исследования, проведения лабораторного этапа исследования, оформление рукописи; М. С. Искандярова — работа с литературой, контроль забора материала, динамическое наблюдение за пациентами, работа над первым вариантом рукописи; С. В. Беляева — работа с литературой, контроль забора материала и участие в наблюдении за пациентами.

Соблюдение этических стандартов: исследование одобрено этическим комитетом Мордовского государственного университета имени Н. П. Огарева (протокол № 12 от 14 декабря 2008 г.). Все пациенты подписали добровольное информированное согласие. Получение биологического материала для исследования (кровь) производили с учетом положений Хельсинской декларации ВМА (2008 г.) и протокола Конвенции Совета Европы о правах человека и биомедицине (1999) с учетом дополнительного протокола к Конвенции по правам человека и биомедицине в области биомедицинских исследований (2005).

✉ **Для корреспонденции:** Ольга Александровна Радаева
ул. Ульянова, д. 26а, г. Саранск, 430000; vtlbwbyf_79@mail.ru

Статья получена: 11.03.2020 **Статья принята к печати:** 25.03.2020 **Опубликована онлайн:** 28.03.2020

DOI: 10.24075/vrgmu.2020.017

Leukemia inhibitory factor (LIF) exerts a vast variety of physiological effects through specific LIF receptors located on the membranes of endothelial cells, monocytes, neurons and other cells [1] in physiologically relevant quantities [2]. Although LIF signaling pathways through JAK/STAT (Janus kinase/signal transducer and activator of transcription), MAPK (mitogen-activated protein kinases) and PI3K (phosphoinositide 3-kinases) are stable, the effects LIF induces in different cell types can be opposite, including both stimulation and inhibition of cell differentiation and survival. There is a lot of debate as to how LIF affects the arterial wall in patients with essential hypertension (EH) since the mechanism underlying STAT3 activation is redox-sensitive [3] and its directionality changes in the setting of chronically elevated blood pressure, distorting LIF effects. There is a growing body of evidence refuting the postulate about identical STAT3 signaling in cardiomyocytes and endothelial/smooth muscle cells, which is important in the situation of extended exposure to gp 130 ligands (LIF in particular) [4]. Research has demonstrated that factors implicated in EH progression and the risk of EH complications are dependent on time of day [5], proving the significance of investigating both the levels of cytokines involved and diurnal variations in their concentrations.

The aim of this study was to analyze the circadian rhythms of LIF concentrations in the peripheral blood serum measured at 5 different time points (8:00, 14:00, 20:00, 2:00, and 8:00 o'clock) in patients with stage II EH in the presence/absence of antihypertensive therapy and their relationship with the frequency of complications developing within a 5-year follow-up.

METHODS

In 2008 through 2019, a study called *Cytokines in the pathogenesis of essential hypertension* was carried out at the Institute of Medicine (National Research Mordovia State University) and the Regional Vascular Center (Republican Clinical Hospital № 4).

As part of the study, a group of 60 patients with stage II EH (30 men and 30 women) was formed to explore how LIF production changed over a 24-hour cycle. The following inclusion criteria were applied: individuals with stage II EH, born in 1955–1956, who had a 10- to 14-year history of the disease, were not receiving any antihypertensive therapy at the beginning of the study but were subsequently put on therapy (ACE inhibitors ± diuretics) to achieve a target blood pressure, as recommended by the Russian guidelines on the diagnosis and treatment of hypertension (2010) [6], which they did within a year that followed; total cholesterol < 5.0 mmol/L, LDL < 3.0 mmol/L, HDL > 1.0 mmol/L, triglycerides < 1.7 mmol/L, glucose < 5.5 mg/dl, BMI < 30 kg/m^2; comparable risk of developing EH-related complications. Patients with hypertension-associated comorbidities, types 1 or 2 diabetes mellitus, autoimmune disorders, allergies, or symptomatic hypertension were excluded from the study. The control group consisted of 30 seemingly healthy individuals (15 men and 15 women) with systolic BP of 100 to 130 mmHg and diastolic BP of 70 to 89 mmHg; the groups were comparable in terms of age and blood biochemistry.

Blood samples (2 ml) were collected prior to the onset of antihypertensive therapy (2014) and one year after the start of treatment (2015) at 8:00, 14:00, 20:00, 2:00, and 8:00 o'clock (the fasting period was at least 6 hours). The time points were selected based on the results of our pilot study (blood samples had been collected from 7 individuals at 7:00, 8:00, 10:00, 12:00, 14:00, 16:00, 18:00, 20:00, 22:00, 00:00, 2:00, 4:00, 6:00, 7:00, and 8:00 o'clock). Time elapsed from sample collection to sample freezing was 60 min. Serum LIF concentrations were measured using ELISA kits (Bender MedSystems; USA).

Follow-up phone interviews were conducted annually (2014–2019) to obtain information about possible complications, such as myocardial infarction (MI), acute cerebrovascular events (ACVE) and transient ischemic attacks (TIA), which were subsequently confirmed by clinical and diagnostic tests, including ECG, echocardiography, troponin tests, brain CT scans.

The obtained data were processed in Statistica 10.0 (Stat Soft; USA). Normality of data distribution was analyzed using the one-sample Kolmogorov–Smirnov test. Based on the obtained results, we used the paired t-test to compare the results of pre-treatment blood tests taken at 8:00, 14:00, 20:00, 2:00, and 8:00 o'clock in the group of patients with stage II EH; the Wilcoxon test was applied to compare the data in the group of patients on antihypertensive therapy one year after its onset and also in healthy controls. Intergroup comparison was carried

Table 1. LIF concentrations (pg/ml) in the peripheral blood serum in patients with stage II EH at 8:00, 14:00, 20:00, 2:00, and 8:00 o'clock (next day) in the absence/presence of antihypertensive therapy in patients with or without cardiovascular complications developed in the 5-year follow-up period (Me (Q25%–Q75%))

Groups		8.00 (day 1)	14.00 (day 1)	20.00 (day 1)	2.00 (day 2)	8.00 (day 2)
Patients with EH (before therapy), $n = 60$	*a*	7.51 [6.58–8.34]	7.58 [6.47–8.41]	9.02 [7.52–9.73] *8.00. 14.00	10.1 [9.44–11.8] *8.00. 14.00. 20.00	7.53 [6.65–8.22] *20.00. 2.00
Healthy controls, $n = 30$	*b*	1.41 [1.02–1.83]	1.38 [1.04–1.79]	1.45 [1.06–1.78]	1.42 [1.03–1.81]	1.37 [0.99–1.79]
		$p(b–a) < 0.001$	$p(b–a) < 0.001$	$p(b–a) < 0.001$	$p(b–a) < 0.001$	$p(b–a) < 0.001$
Patients with EH (one year in treatment), $n = 60$, of them:	*c*	7.54 [6.57–8.38]	7.61 [6.53–8.44]	8.95 [7.63–9.58] *8.00. 14.00	7.62 [6.84–8.63] '8.00 *20.00	7.58 [6.62–8.31] *20.00
		$p(c–a) > 0.05$ $p(c–b) < 0.001$	$p(c–a) > 0.05$ $p(c–b) < 0.001$	$p(c–a) > 0.05$ $p(c–b) < 0.001$	$p(c–a) < 0.001$ $p(c–b) < 0.001$	$p(c–a) < 0.05$ $p(c–b) < 0.001$
5-year follow-up — MI, ACVE, $n = 15$	*c*1	7.66 [6.68–8.22]	7.59 [6.49–8.37]	9.01 [7.56–9.61] *8.00. 14.00	9.69 [8.91–9.98] *8.00. 14.00. 20.00	7.72 [6.71–8.17] *20.00. 2.00
5-year follow-up — no complications, $n = 45$	*c*2	7.58 [6.52–8.41]	7.62 [6.5–8.42]	8.79 [7.98–9.62] *8.00. 14.00	7.55 [6.93–8.21] *20.00	7.36 [6.51–8.24] *20.00
		$p(c2–c1) > 0.05$	$p(c2–c1) > 0.05$	$p(c2–c1) > 0.05$	$p(c2–c1) < 0.001$	$p(c2–c1) > 0.05$

Note: significant for comparisons with the specified time of blood collection or the group (*a*, *b*, *c*, *c*1, *c*2); * — $p < 0.001$; ^ — $p < 0.01$; ' — $p < 0.05$. The paired t-test was applied for intragroup comparison of pretreatment results obtained at 8:00, 14:00, 20:00, 2:00 and 8:00 o'clock. The Wilcoxon test was applied for intragroup comparison in the group of patients after one year of treatment and in the healthy controls. The Mann–Whitney U test was applied to compare independent samples. The Wilcoxon test was applied to compare dependent samples.

out using the Mann–Whitney U (for independent samples) and the Wilcoxon test (for dependent samples). Below, the data are presented as a median (Me) and percentiles (Q0.25–Q0.75). When comparing the subgroups, the Bonferroni correction for multiple comparisons was applied, ensuring the reliability of the statistical data. We calculated the absolute and relative risks of developing MI and ACVE, 95% CI, sensitivity and specificity. The analysis was aided by Fisher's exact test (φ) and Pearson's correlation coefficient (C') were used.

RESULTS

The analysis revealed significant qualitative and quantitative differences in the circadian rhythms of blood serum LIF between the control group and the patients with stage II EH and a 10–14-year history of the disease who were not on antihypertensive therapy at the beginning of the study. In patients with stage II EH, LIF levels measured at 8:00, 14:00, 20:00 and 2:00 o'clock were 5–7.5 times higher ($p < 0.001$) than in the healthy individuals (Table 1). In the group of patients with EH, a significant increase in LIF levels relative to 8:00 measurements (by 20.1% (16.7–24.3%); $p < 0.001$) was observed at 20:00, peaking at 2:00 (an increase by 34% (25.7–43%); $p < 0.001$). Importantly, in the group of healthy controls, LIF levels did not change at 14:00, 20:00 and 2:00 o'clock relative to their initial values at 8:00 ($p > 0.05$). After being on antihypertensive therapy for one year, the patients with stage II EH who had achieved their target blood pressure demonstrated no decline in LIF concentrations at 8:00, 14:00 and 20:00 o'clock in comparison with pretreatment values ($p < 0.01$), but the circadian rhythm of the cytokine was different. In the patients who had been receiving antihypertensive therapy and had achieved the desired blood pressure, blood serum LIF peaked at 20:00; measurements taken at 2:00 showed a decline in LIF concentrations (Table 2) in comparison with the pretreatment period. In the group of patients undergoing treatment, the distribution of data differed from Gauss–Laplace distribution, which prompted us to analyze LIF circadian rhythms for each individual patient in order to identify the criteria for heterogeneity. We found that 22 patients undergoing antihypertensive therapy who had achieved the target blood pressure had the same circadian rhythms of blood serum LIF as before therapy (a rise at 20:00 with a peak at 2:00 and a decline at 8:00; see Table 2).

The analysis of data obtained during the follow-up observation from the patients undergoing antihypertensive therapy who had partially recovered normal LIF dynamics (a decline in LIF concentrations at 2:00) revealed that only 4 of 42 patients had developed ACVE or MI within a 5-year follow-up period (the absolute risk of complications was 9.5% (0.63–18.4%)). In the group of patients with persisting pathological diurnal rhythms of serum LIF (a rise at 20:00, a peak at 2:00 and a return to morning levels at 8:00), 11 of 18 patients had developed complications (ACVE, MI); in this group, the absolute risk of complications was 61.1% (38.6–83.6%). The risk ratio between these two groups was 6.41 (2.35–17.5%); specificity, 0.84; sensitivity, 0.73; $\varphi = 0.0000$ ($p < 0.05$), C' = 0.67 (the correlation was very strong).

DISCUSSION

The rise in serum LIF concentrations observed in the patients with stage II EH relative to the healthy controls can be explained by impaired integration of LIFR/CD118 and gp130 signaling under oxidative stress accompanying EH, which affects the catalytic activity of JAK [7] and can stimulate LIF secretion. The elevation of LIF levels at 20:00 o'clock, with a further rise peaking at 2:00 observed in the study participants prior to antihypertensive therapy and also in some patients who had reached the desired blood pressure and were still on antihypertensive drugs is pathogenically relevant: there are

Table 2. The percentage of deviations of blood serum LIF (pg/ml) measured at 14.00, 20.00, 2.00 and 8.00 o'clock (next day) from the initial concentrations measured at 8:00 of the first day in patients with stage II EH in the absence/presence of antihypertensive therapy with or without cardiovascular complications developed in the 5-year follow-up period (Me (Q25%–Q75%))

Groups		8.00 (day 1)	14.00 (day 1)	20.00 (day 1)	8.00 (day 2)
Patients with EH (before therapy), $n = 60$	*a*	0.91 [–1.67–2.54]	20.1 [16.7–24.3] *14.00	34 [25.7–33] *14.00. 20.00	1.06 [–1.05–3.65] *20.00. 2.00
Healthy controls, $n = 30$	*b*	–1.08 [–2.03–1.19]	2.81 [1.93–3.22]	0. 98 [–0.13–2.03]	1.03 [–1.72–2.56]
		$p(b–a) > 0.05$	$p(b–a) < 0.001$	$p(b–a) < 0.001$	$p(b–a) > 0.05$
Patients with EH (one year in treatment), $n = 60$, of them	*c*	0.93 [–0.61–2.03]	18.9 [15.9–24.1] *14.00	6.32 [2.08–14.4] *14.00. 20.00	0.76 [–0.45–2.21] *20.00. 2.00
		$p(c–a) > 0.05$ $p(c–b) > 0.05$	$p(c–a) > 0.05$ $p(c–b) < 0.001$	$p(c–a) < 0.001$ $p(c–b) < 0.05$	$p(c–a) > 0.05$ $p(c–b) > 0.05$
5-year follow-up — MI, ACVE, $n = 15$	*c*1	–0.91 [–2.83–1.8]	19.9 [15.1–23.8] *14.00	26.5 [22.3–28.1] *14.00. 20.00	0.22 [–1.35–2.33] *20.00. 2.00
		$p(c1–a) > 0.05$ $p(c1–b) > 0.05$	$p(c1–a) > 0.05$ $p(c1–b) < 0.001$	$p(c1–a) > 0.05$ $p(c1–b) < 0.001$	$p(c1–a) > 0.05$ $p(c1–b) > 0.05$
5-year follow-up — no complications, $n = 45$	*c2*	0.52 [–0.47–1.67]	18.1 [14.8–23.8] *14.00	2.29 [–0.35–5.44] '14.00 *20.00	0.92 [–0.62–2.13] *20.00. 2.00
		$p(c2–c1) > 0.05$ $p(c2–b) > 0.05$ $p(c2–a) > 0.05$	$p(c2–c1) > 0.05$ $p(c2–b) < 0.001$ $p(c2–a) > 0.05$	$p(c2–c1) < 0.001$ $p(c2–b) < 0.05$ $p(c2–a) < 0.001$	$p(c2–c1) > 0.05$ $p(c2–b) > 0.05$ $p(c2–a) > 0.05$

Note: significant for comparisons with the specified time of blood collection or the group (*a*, *b*, *c*, *c*1, *c*2). * — $p < 0.001$; ^ — $p < 0.01$; ' — $p < 0.05$. The paired t-test was applied for intragroup comparison of pretreatment results obtained at 8:00, 14:00, 20:00, 2:00 and 8:00 o'clock. The Wilcoxon test was applied for intragroup comparison in the group of patients after one year of treatment and in the healthy controls. The Mann–Whitney U test was applied to compare independent samples. The Wilcoxon test was applied to compare dependent samples.

reports that LIF-dependent stimulation of STAT3 in endothelial cells triggers the inflammatory cascade [8] and IL1 activation; in turn, this causes a more pronounced EH progression in the evening (20:00) and at night (2:00), when proinflammatory activity of IL1ra and IL10 is low, through the activation of protein arginine methyltransferase and the inhibition of dimethylarginine, leading to an imbalance in the NO synthesis system. Previously [9], we reported an increased left ventricular mass index, a low mean fiber shortening fraction and a reliable association with pronounced concentric left ventricular hypertrophy in patients with EH and elevated LIF (>7.5 pg/ml). The observed pathophysiological process led us to hypothesize that patients whose LIF levels were growing between 20:00 and 2:00 in the setting of antihypertensive therapy were at increased risk for cardiovascular complications. The hypothesis was confirmed in the course of this study. LIF-induced cardiac hypertrophy can be characterized by an early reduction in myocardial contractility resulting from the transmural changes in cardiomyocytes [10, 11]. In the early stages of the pathology, elevated LIF serves as a mechanism of compensatory adaptation that stimulates contractility of cardiomyocytes by increasing the activity of T-type Ca^{2+}-channels [12]. Besides, elevated LIF could be potentially protective against the inflammation-induced loss of axons and also promotes survival of oligodendrocytes by stimulating the expression of IGF-1 (insulin-like growth factor 1) [13]. However, the further rise in LIF levels and its circadian fluctuations reported in this study promote poor outcomes in patients with stage II EH, including potential damage to the myocardium or the brain.

CONCLUSIONS

The identified patterns of circadian rhythms of blood serum LIF in patients with stage II EH, namely the rise by 15% at 20:00 and the further rise by 22% peaking at 2:00, relative to LIF levels at 8:00, can be regarded as pathologic. Their persistence in the setting of antihypertensive therapy could contribute to the progression of hypertension and put the patient at increased risk for cardiovascular complications, in spite of seemingly clinically favorable course of the disease and the success in achieving the target blood pressure. Our findings might lay the groundwork for further research into the role of LIF aimed at establishing a personalized approach to interpreting its dynamics in individual patients. The analysis of LIF circadian rhythms is a candidate diagnostic approach for the assessment of occult progression of the disease in patients with essential hypertension who have managed to achieve their target blood pressure.

References

1. Mathieu M-E, Saucourt C, Mournetas V, Gauthereau X, Theze N, Praloran V, et al. LIF-Dependent Signaling: New Pieces in the Lego. Stem Cell Rev. 2012; 8 (1): 1–15.
2. Nicola NA, Babon JJ. Leukemia Inhibitory Factor (LIF). Cytokine & growth factor reviews. 2015; 26 (5): 533–44.
3. Wu J, Xia S, Kalionis B, Wan W, Sun T. The Role of Oxidative Stress and Inflammation in Cardiovascular Aging. BioMed Research International. [Internet] 2014: 615312. Available from: https://doi.org/ 10.1155/2014.
4. González GE, Rhaleb N-E, D'ambrosio MA, Nakagawa P, Liu Y, Leung P, Dai X, Yang XP, Peterson EL, Carretero OA. Deletion of interleukin-6 prevents cardiac inflammation, fibrosis and dysfunction without affecting blood pressure in angiotensin II-high salt-induced hypertension. J Hypertens. 2015; (33): 144–52.
5. Bennardo M, Alibhai F, Tsimakouridze E, Chinnappareddy N, Podobed P, Reitz C, et al. Day-night dependence of gene expression and inflammatory responses in the remodeling murine heart post-myocardial. Am J Physiol Regul Integr Comp Physiol. 2016; 311 (6): 1243–1254.
6. Chazova IE, Ratova LG, Bojcov SA, i dr. Diagnostika i lechenie arteria'noj gipertonii. Sistemnye gipertenzii. 2010; (3): 5–26. Russian.
7. Zgheib C, Zouein FA, Kurdi M, Booz GW. Differential STAT3 Signaling in the Heart: Impact of Concurrent Signals and Oxidative Stress. JAK-STAT. 2012; 1 (2): 101–10.
8. Fujio Y, Maeda M, Mohri T, Obana M, Iwakura T, Hayama A, et al. Glycoprotein 130 cytokine signal as a therapeutic target against cardiovascular diseases. J Pharmacol Sci. 2011; 117 (4): 213–22.
9. Radaeva OA, Simbirtsev AS. Izmenenie urovnya faktora, ingibiruyushchego lejkemiyu, v syvorotke perifericheskoj krovi svyazano s progressirovaniem essencialnoj arterialnoj gipertenzii. Medicinskij akademicheskij zhurnal. 2015; 15 (1): 34–42. Russian.
10. Zouein FA, Kurdi M, Booz GW. Dancing rhinos in stilettos: The amazing saga of the genomic and nongenomic actions of STAT3 in the heart. JAKSTAT. 2013; 2 (3): 101–10.
11. Jia D, Cai M, Xi Y, Du S, Zhenjun T. Interval exercise training increases LIF expression and prevents myocardial infarction-induced skeletal muscle atrophy in rats. Life Sci. 2018; (193): 77–86.
12. Dey D, Shepherd A, Pachuau J, Migue M. Leukemia inhibitory factor regulates trafficking of T-type Ca2+ channels. Am J Physiol Cell Physiol. 2011; 300 (3): 576–87.
13. Xu L, Long J, Shi C, Zhang N, Lv Y, Feng J, et al. Effect of leukocyte inhibitory factor on neuron differentiation from human induced pluripotent stem cell-derived neural precursor cells. Int J Mol Med. 2018; 41 (4): 2037–49. https://doi.org/10.3892/ijmm.2018.3418.

Литература

1. Mathieu M-E, Saucourt C, Mournetas V, Gauthereau X, Theze N, Praloran V, et al. LIF-Dependent Signaling: New Pieces in the Lego. Stem Cell Rev. 2012; 8 (1): 1–15.
2. Nicola NA, Babon JJ. Leukemia Inhibitory Factor (LIF). Cytokine & growth factor reviews. 2015; 26 (5): 533–44.
3. Wu J, Xia S, Kalionis B, Wan W, Sun T. The Role of Oxidative Stress and Inflammation in Cardiovascular Aging. BioMed Research International. [Internet] 2014: 615312. Available from: https://doi.org/ 10.1155/2014.
4. González GE, Rhaleb N-E, D'ambrosio MA, Nakagawa P, Liu Y, Leung P, Dai X, Yang XP, Peterson EL, Carretero OA. Deletion of interleukin-6 prevents cardiac inflammation, fibrosis and dysfunction without affecting blood pressure in angiotensin II-high salt-induced hypertension. J Hypertens. 2015; (33): 144–52.
5. Bennardo M, Alibhai F, Tsimakouridze E, Chinnappareddy N, Podobed P, Reitz C, et al. Day-night dependence of gene expression and inflammatory responses in the remodeling murine heart post-myocardial. Am J Physiol Regul Integr Comp Physiol. 2016; 311 (6): 1243–1254.
6. Чазова И. Е., Ратова Л. Г., Бойцов С. А., и др. Диагностика и лечение артериальной гипертонии. Системные гипертензии. 2010; (3): 5–26.
7. Zgheib C, Zouein FA, Kurdi M, Booz GW. Differential STAT3 Signaling in the Heart: Impact of Concurrent Signals and Oxidative Stress. JAK-STAT. 2012; 1 (2): 101–10.
8. Fujio Y, Maeda M, Mohri T, Obana M, Iwakura T, Hayama A, et al.

Glycoprotein 130 cytokine signal as a therapeutic target against cardiovascular diseases. J Pharmacol Sci. 2011; 117 (4): 213–22.
9. Радаева О. А., Симбирцев А. С. Изменение уровня фактора, ингибирующего лейкемию, в сыворотке периферической крови связано с прогрессированием эссенциальной артериальной гипертензии. Медицинский академический журнал. 2015; 15 (1): 34–42.
10. Zouein FA, Kurdi M, Booz GW. Dancing rhinos in stilettos: The amazing saga of the genomic and nongenomic actions of STAT3 in the heart. JAKSTAT. 2013; 2 (3): 101–10.
11. Jia D, Cai M, Xi Y, Du S, Zhenjun T. Interval exercise training increases LIF expression and prevents myocardial infarction-induced skeletal muscle atrophy in rats. Life Sci. 2018; (193): 77–86.
12. Dey D, Shepherd A, Pachuau J, Migue M. Leukemia inhibitory factor regulates trafficking of T-type Ca2+ channels. Am J Physiol Cell Physiol. 2011; 300 (3): 576–87.
13. Xu L, Long J, Shi C, Zhang N, Lv Y, Feng J, et al. Effect of leukocyte inhibitory factor on neuron differentiation from human induced pluripotent stem cell-derived neural precursor cells. Int J Mol Med. 2018; 41 (4): 2037–49. https://doi.org/10.3892/ijmm.2018.3418.

PREVENTIVE PHARMACOTHERAPY OF TYPE 2 DIABETES MELLITUS IN PATIENTS WITH EARLY CARBOHYDRATE METABOLISM DISORDERS: LONG-TERM EFFICACY AND CLINICAL OUTCOMES

Boeva VV[1] ✉, Zavyalov AN[2]

[1] Federal Clinical Center of High Medical Technologies, FMBA, Khimki, Moscow region, Russia

[2] Pirogov Russian National Research Medical University, Moscow, Russia

Prevention of type 2 diabetes mellitus (T2DM) in prediabetic patients is a pressing concern due to its increasing prevalence. The aim of this study was to evaluate the efficacy of preventive pharmacotherapy in delaying progression of incident impaired glucose tolerance (IGT) and impaired fasting glycemia (IFG) to T2DM. The participants of the study (1,136 subjects) found healthy by a regular annual checkup underwent repeat screening for T2DM. Blood samples were processed following the guidelines for good preanalytical sample preparation. Patents with incident IGT/IFG were prescribed medication therapy with metformin or/and acarbose. The rate of IGT/IFG conversion to T2DM was evaluated in years 3 and 10 of observation. Carbohydrate metabolism disorders were detected in 18.5% (n = 210) of the re-screened patients: 5.0% had T2DM, 5.5% had IGT, 8.0% had IFG. Patients with incident T2DM were prescribed blood sugar lowering therapy and they were excluded from further analysis. Patients with IGT/IFG (n = 151) were given recommendations on lifestyle modification and prescribed metformin (77%) or a combination of metformin and acarbose (23%). Three years after the start of observation, the rate of conversion to T2DM was 6.8% in patients undergoing monotherapy with metformin and 11.4% in patients undergoing combination therapy with metformin and acarbose. After the active follow-up phase was over, the majority of the patients (n = 85) decided to discontinue preventive therapy without consulting their physicians. Ten years after the active follow-up phase, the rate of NGT/IFG conversion to T2DM was 38.8% in patients who had discontinued their treatment and 0% in patients still taking metformin ($p < 0.01$). Long-term therapy with metformin prevented progression to T2DM in the long run in 83.3% ($p < 0.05$).

Keywords: type 2 diabetes mellitus, impaired fasting glucose, impaired glucose tolerance, screening, metformin, acarbose, prevention, fasting plasma glucose

Author contribution: Boeva VV planned the study; analyzed the literature; collected, analyzed and interpreted study results; wrote the manuscript; Zavyalov AN analyzed the literature; analyzed and interpreted study results; wrote the manuscript.

Compliance with ethical standards: the study was approved by the Ethics Committee of Pirogov Russian National Research Medical University (Protocol № 176 dated June 25, 2018). Informed consent was obtained from all study participants.

✉ **Correspondence should be addressed:** Valentina V. Boeva
Ivanovskaya, 15A, Khimki, Moscow region, 141435; boevaVV@yandex.ru

Received: 09.01.2020 **Accepted:** 08.02.2020 **Published online:** 06.03.2020

DOI: 10.24075/brsmu.2020.014

МЕДИКАМЕНТОЗНАЯ ПРОФИЛАКТИКА САХАРНОГО ДИАБЕТА 2-ГО ТИПА У ПАЦИЕНТОВ С РАННИМИ НАРУШЕНИЯМИ УГЛЕВОДНОГО ОБМЕНА: ЭФФЕКТИВНОСТЬ И КЛИНИЧЕСКИЕ ИСХОДЫ ПРИ ДЛИТЕЛЬНОМ НАБЛЮДЕНИИ

В. В. Боева[1] ✉, А. Н. Завьялов[2]

[1] Федеральный клинический центр высоких медицинских технологий Федерального медико-биологического агентства России, Химки, Московская область, Россия

[2] Российский национальный исследовательский медицинский университет имени Н. И. Пирогова Минздрава России, Москва, Россия

Актуальность профилактики сахарного диабета (СД) 2-го типа у пациентов с предиабетом увеличивается из-за неуклонного распространения заболевания. Целью работы было оценить эффективность медикаментозной профилактики в замедлении темпов конверсии впервые выявленных нарушенной толерантности к глюкозе и нарушенной гликемии натощак (НТГ/НГН) в СД 2-го типа. Участникам исследования (1136 человек), считавшимся здоровыми после диспансеризации, повторно провели скрининг СД 2-го типа с соблюдением правил преаналитической подготовки образцов крови. Пациентам с впервые выявленными НТГ/НГН была назначена терапия метформином и/или акарбозой, частоту конверсии НТГ/НГН в СД 2-го типа оценивали через 3 и 10 лет наблюдения. У 18,5% (n = 210) обследованных выявили различные категории нарушения углеводного обмена: СД 2-го типа — у 5,0%, НТГ — у 5,5%, НГН — у 8,0%. Пациентам с впервые выявленным СД 2-го типа была назначена сахароснижающая терапия, они были исключены из последующего наблюдения. Пациентам с НТГ/НГН (n = 151) рекомендовали изменение образа жизни и назначили терапию метформином (77%) или метформином и акарбозой (23%). Частота конверсии СД 2-го типа в течение 3 лет активного наблюдения составила 6,8% на фоне монотерапии метформином и 11,4% — на фоне комбинированной терапии метформином и акарбозой. По окончании периода активного наблюдения большинство пациентов (n = 85) самостоятельно прекратили терапию. Частота конверсии НТГ/НГН в СД 2-го типа через 10 лет после окончания активного наблюдения в группе без медикаментозной профилактики составила 38,8% и 0% — в группе принимающих метформин ($p < 0,01$). Показано, что длительное применение метформина предупредило развитие СД 2-го типа в отдаленном периоде у 83,3% ($p < 0,05$).

Ключевые слова: сахарный диабет 2-го типа, нарушенная гликемия натощак, нарушенная толерантность к глюкозе, скрининг, метформин, акарбоза, профилактика, глюкоза венозной плазмы натощак

Вклад авторов: В. В. Боева — планирование исследования, анализ литературы, сбор, анализ и интерпретация данных, подготовка черновика рукописи; А. Н. Завьялов — анализ литературы, анализ и интерпретация данных, подготовка черновика рукописи.

Соблюдение этических стандартов: исследование одобрено этическим комитетом РНИМУ имени Н. И. Пирогова (протокол № 176 от 25 июня 2018 г.). Все пациенты подписали добровольное информированное согласие на участие в исследовании.

✉ **Для корреспонденции:** Валентина Владимировна Боева
ул. Ивановская, д. 15А, г. Химки, Московская область, 141435; boevaVV@yandex.ru

Статья получена: 09.01.2020 **Статья принята к печати:** 08.02.2020 **Опубликована онлайн:** 06.03.2020

DOI: 10.24075/vrgmu.2020.014

Type 2 diabetes mellitus (T2DM) imposes a huge burden on society. This disease has a high, steadily rising prevalence and increases the risk of disabilities and early death in the affected individuals. It was reported that 4.1 million people in Russia were living with T2DM in 2018 [1, 2]. But according to epidemiologic surveillance, the actual number of such patients could be as high as at least 8 million. Based on extrapolation from the NATION study data, it is estimated that about 20.7 million Russians with prediabetes are undiagnosed [3] and, therefore, do not receive therapy or counseling on lifestyle modification.

Currently, it is not mandatory for healthcare providers to report patients who test positive for impaired glucose tolerance and impaired fasting glycemia (IGT/IFG); such patients are overlooked by statistical reports and are not followed up, so the actual prevalence of prediabetes remains understudied.

The primary cause of delay in the diagnosis of T2DM and detection of carbohydrate metabolism disorders in their early stages is preanalytical errors, specifically failure to comply with standard procedures for blood sample collection and handling aimed at inhibiting glycolysis in the sample. Upon sample collection, blood cells in the test tube undergo glycolysis, which causes glycose levels to decline and thus skews the result of the test. This is the reason why screening tests reveal normal glycose levels in some patients with carbohydrate metabolism disorders (18.5% in our study); as a result, such patients are not followed up by their physicians.

Primary care physicians do not always attach due importance to IGT/IFG. They give their patients some perfunctory advice on lifestyle modification and do not prescribe any preventive pharmacotherapy; in turn, the patients do not find it necessary to follow the recommendations. Importantly, the efficacy of medication therapy in prediabetic individuals has already been confirmed by multiple studies [4–7] and meta-analyses [8].

Today, there is a need for implementing effective strategies for active case-finding of early carbohydrate metabolism disorders and their treatment. The aim of this study was to assess the long-term efficacy of preventive pharmacotherapy in delaying conversion of incident IGT/IFG to T2DM in the real clinical setting.

METHODS

Study participants

The study enrolled 1,136 adult residents of Tambov region presenting at Tambov Central Regional Hospital for an annual medical checkup under the annual health screening program in 2007. All patients were found to be healthy. Inclusion criteria: no history of carbohydrate metabolism disorders; no history of glucose-lowering therapy. Patients who screened positive for types 1 or 2 DM were excluded from the study.

Study phases

In the first phase, individuals found healthy after the annual medical checkup were screened for carbohydrate metabolism disorders; preventive pharmacotherapy was prescribed to those at risk for T2DM; the rate of IGT/IFG conversion to T2DM or normoglycemia within 3 years of follow-up was evaluated.

In the second phase, long-term outcomes were analyzed, i.e. the rate of IGT/IFG conversion to T2DM or normoglycemia within 10 years after active follow-up (Fig. 1).

The first phase is essentially a nonrandomized continuous prospective interventional study; the second phase should be regarded as a non-randomized retrospective observational controlled study.

Study duration

The active follow-up phase, which included preventive pharmacotherapy for T2DM, lasted for 3 years. Some patients continued their therapy for as long as 13 years. Its long-term efficacy was evaluated 10 years after the active follow-up phase was over.

Description of medical intervention

Disorders of carbohydrate metabolism were identified based on the screening data, including the results of the oral glucose tolerance test (OGTT). Patients with IGT/IFG received

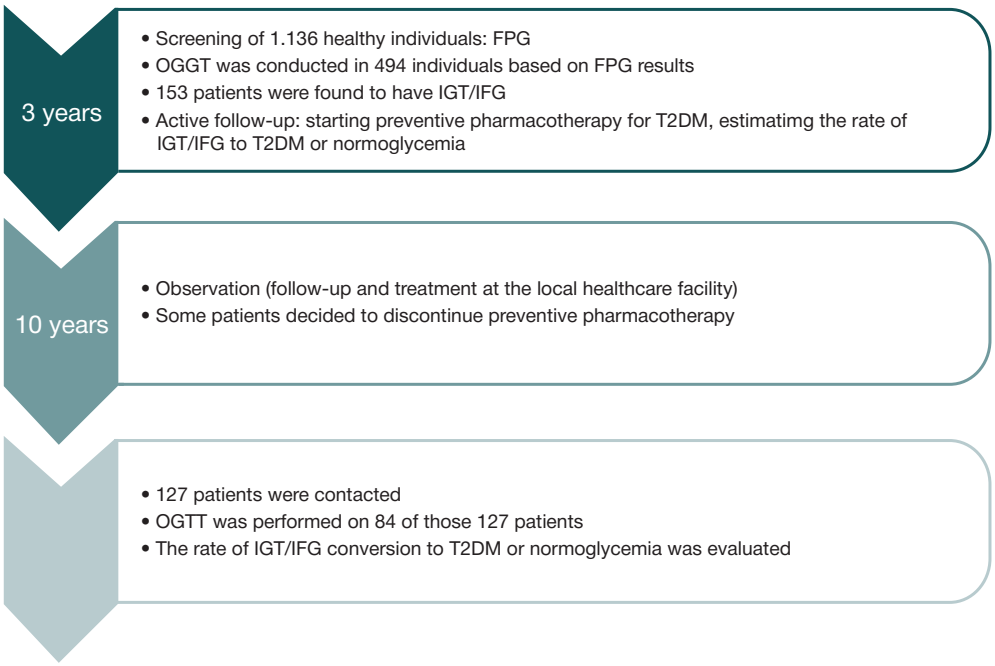

Fig. 1. A study plan. FPG — fasting plasma glucose test; OGTT — 75-gram oral glucose tolerance test

counseling on lifestyle modification and were prescribed medication therapy. Ten years after the active follow-up phase, the patients we were able to contact were re-examined (n = 115). The primary focus was on the rates of IGT/IFG conversion to T2DM or normoglycemia during the active follow-up phase in the setting of preventive pharmacotherapy (3 years) and in the 10 years that had followed.

Analysis of subgroups

In the screening stage, the participants were stratified in groups by the presence of the metabolic syndrome and risk factors for T2DM.

In 10 years, the outcomes for metabolic syndrome were stratified by adherence to long-term T2DM prevention therapy. The patients available for the analysis (n = 115) were divided into 2 subgroups: subgroup 1 had discontinued their medications without consulting their physicians (n = 85), subgroup 2 had been taking metformin throughout the entire observation period (n = 30).

Evaluation of outcomes

Disorders of carbohydrate metabolism were diagnosed and classified following WHO guidelines published in 1999. Carbohydrate metabolism was evaluated using a conventional 2-hour 75-gram OGTT. For all samples, glucose measurements were conducted at the laboratory of Tambov Central Regional Hospital. Blood samples were collected into test tubes containing sodium fluoride. Sample preparation was performed following a standardized analytical technique.

Statistical analysis

The obtained data were processed in Statistica 6.1 (TIBCO; USA). For the analysis, we used nonparametric statistics, Pearson's χ^2, Fisher's exact test, and Yates' correction for contingency tables. Differences were considered significant at $p < 0.05$.

RESULTS

Initial screening was conducted in 1,136 individuals who denied any health complaints. The fasting plasma glucose test (FPG) revealed plasma glucose levels ≥ 7.0 mmol/l in 73 (6.4%) individuals. The test was repeated in those patients, confirming T2DM in 37 cases. They were prescribed medication therapy and excluded from further observation. The remaining 36 patients had glycemia ranging from 6.1 to 6.9 mmol/l. Those 36 patients and other 181 subjects (of 1,136 study participants) who tested positive for blood glucose in the same range underwent OGTT.

In 882 of 1,136 (77.6%) subjects, FPG was below 6.1 mmol/l, which WHO interprets as normal and does not recommend testing for DM in the short run. However, according to IDF guidelines (2005), OGTT should be performed on all patients with the metabolic syndrome (MS) whose fasting blood sugar levels are ≥ 5.6 mmol/l. Of all examined study participants, 430 had FPG within the normal range (5.6–6.0 mmol/l). Of them, MS signs were detected in 169 (39.3%) individuals, who subsequently underwent OGTT, as recommended by IDF. The rest 261 subjects had not developed a full clinical picture of MS, but 108 still had risk factors for T2DM and underwent OGTT (Fig. 2). In total, OGTT was performed on 494 people.

OGTT revealed that 20 participants (4.0%) had T2DM, 62 participants (12.6%) had impaired glucose tolerance, 91 participants (18.4%) had impaired fasting glucose, and 321 participants (65.0%) had normal glucose tolerance.

Characteristics of the patients included in the study were previously published in [9].

Of 153 prediabetic patients, 2 (1.3%) had counterindications for metformin and 26 (16.9%) refused to take acarbose because of its high cost. Thus, in the first year of active follow-up, there

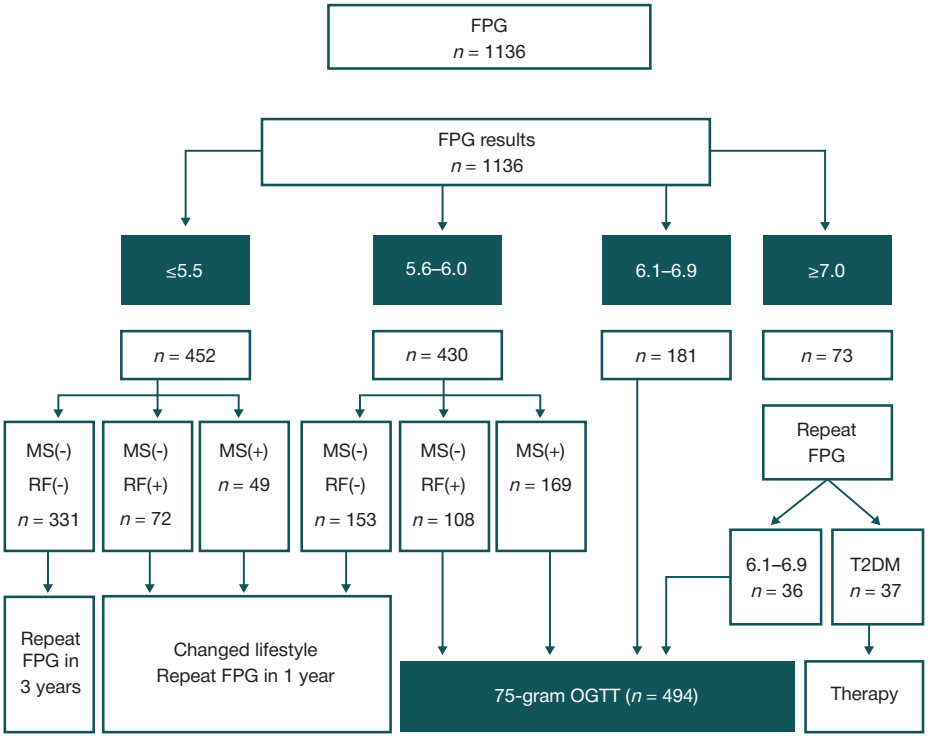

Fig. 2. Stratification of patients based on screening data for further T2DM diagnostic tests. FPG — fasting plasma glucose test; MS — metabolic syndrome; OGTT — 75-gram oral glucose tolerance test; RF — risk factors for T2DM

were 90 patients with IFG undergoing therapy with metformin (500 mg/day), 26 patients with IGT undergoing therapy with metformin (500 mg/day), 35 patients with IGT undergoing combination therapy with metformin (500 mg/day) and acarbose (titrated from 50 mg to a maximum dose of 150 mg following the titration scheme provided by the manufacturer). OGTT was repeated in prediabetic patients and those with normal glucose tolerance in years 2 and 3 of active follow-up. In year 3, T2DM was detected by OGTT in 4 subjects (1.4%) with previously normal glucose tolerance; in 1 patient (1.1%) with IFG undergoing therapy with metformin; in 2 patients (8.7%) with IGT undergoing treatment with metformin; in 2 patients (6.1%) with IGT undergoing treatment with metformin and acarbose. By the end of year 3, there were a total of 156 people with IGT/IFG (Fig. 3).

When the active follow-up phase, which included visits to the endocrinologist, was over, the majority of the patients discontinued their medications, in spite of having been recommended not to.

Of 156 patients with IGT/IFG, the analysis of long-term (10 years) outcomes of preventive pharmacotherapy for T2DM was done in 115 individuals. Causes for not including some patients in the analysis are shown in Fig. 4.

Of 115 people available for the analysis, 30 (26.1%) were still taking 500 mg/day metformin at the time of data collection for our study (2018). Eighty-five patients had chosen to terminate their treatment; of them 74 did it almost immediately after 3 years of active follow-up. Distribution of patients by type and duration of preventive pharmacotherapy after the end of the active follow-up phase is shown in Fig. 5.

Causes of poor adherence to treatment were not analyzed in detail in our study, but it should be noted that the patients reported not only health-related factors affecting their adherence but also organizational and financial issues. For example, the most common cause of non-compliance was the fact that the patients had not been followed up by their local endocrinologists and as a result had been refused prescriptions for preventive medications at their local healthcare facilities.

Results of preventive pharmacotherapy

During the active observation phase, 12 (7.9%) of 151 prediabetic patients progressed from a carbohydrate metabolism disorder to T2DM.

In the setting of preventive therapy, OGTT was repeated in years 2 and 3 of active follow-up. In the IFG group undergoing treatment with metformin, significant positive outcomes were achieved by the patients with initial FPG of 5.6–6.0 mmol/l who were able to normalize their carbohydrate metabolism in 47.8% cases in year 2 and in 72.9% of cases in year 3 of observation (χ^2 = 6,195; p = 0.013). Outcomes of preventive pharmacotherapy for T2DM in the IFG group achieved during the active follow-up phase are detailed in [9].

In the IGT group, the patients undergoing combination therapy with metformin and acarbose demonstrated better results than the group undergoing treatment with metformin: normal glucose tolerance was observed in the majority of patients in combination therapy in year 3 of active follow-up (χ^2 = 7.222; p = 0.007). Of 115 individuals available for the analysis 10 years later, 30 (26.1%) were still taking metformin

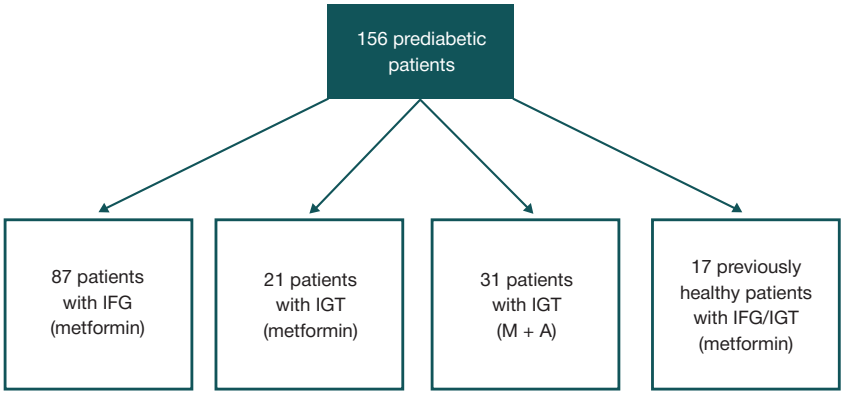

Fig. 3. Stratification of patients by the initial state of carbohydrate metabolism and prescribed therapy. M+A – therapy with metformin and acarbose

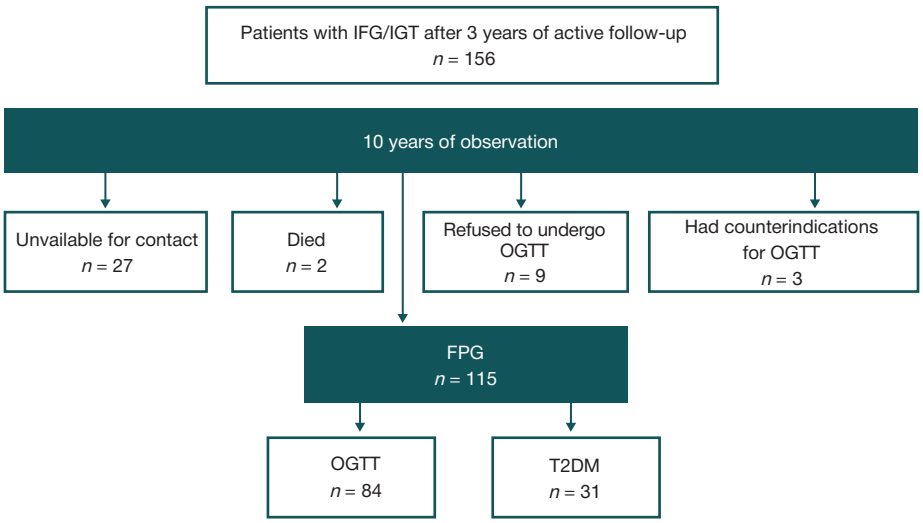

Fig. 4. Stratification of patients with IGT/IFG 10 years after the end of the active follow-up phase

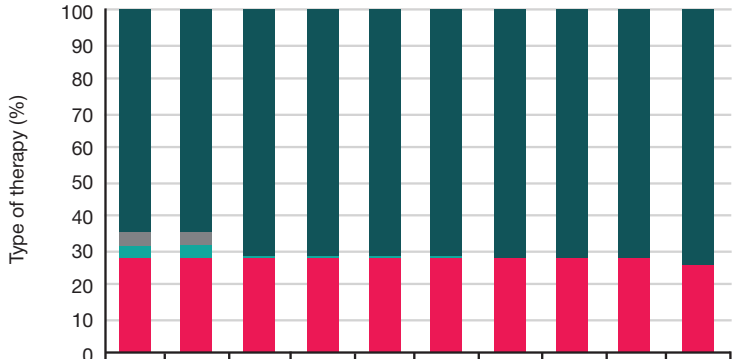

	1	2	3	4	5	6	7	8	9	10
Without therapy	74	74	82	82	82	82	83	83	83	85
Metformin + acarbose	5	5	0	0	0	0	0	0	0	0
Acarbose	4	4	1	1	1	1	0	0	0	0
Metformin	32	32	32	32	32	32	32	32	32	30

Fig. 5. Distribution of patients by type and duration of preventive pharmacotherapy after the end of the active follow-up phase (years 1 through 10)

(500 mg a day) at the time of data collection for this study (2018); the duration of acarbose intake was much shorter (Table 1).

Importantly, patients who had been taking metformin continuously did not progress to T2DM in the long run and were able to normalize their blood sugar in comparison with those who had not been taking preventive pharmacotherapy ($p < 0.05$). Ten years after the active follow-up phase, the rate of IFG/IGT conversion to T2DM was 38.8% in the group without preventive treatment and 0% in the metformin group ($p < 0.01$).

Metformin was equally effective in preventing progression of any type of carbohydrate metabolism disorders into T2DM: no statistically significant differences in terms of outcomes were observed between the patients with IFG/IGT undergoing long-term preventive pharmacotherapy with metformin (Table 2).

Even short-term (in the active follow-up period, i.e. 3-year long) preventive pharmacotherapy against T2DM can affect the long-term outcome (10 years after the start of observation) (Table 3).

The long-term efficacy of short-term preventive pharmacotherapy turned to be higher for patients with IFG than for patients with IGT ($p = 0.012$ for achieving normal blood sugar; $p = 0.004$ for progression to T2DM), which might be linked to a high rate of metformin prescription, in comparison with acarbose.

Adverse effects

No unpredicted adverse effects of preventive pharmacotherapy against T2DM were observed during the study. The analysis of other adverse events was beyond the scope of this study and was not implied by the study design.

Limitations of the study

The study had some limitations related to its design. The study was observational and the use of only routine medical interventions did not allow us to form positive and negative control groups. The patients had been undergoing diagnostic procedures and receiving medical care at their local healthcare facilities and not under the supervision of the study authors, meaning that we were unable to fully rule out the impact of external factors on the study outcomes.

DISCUSSION

The issue of adherence to preventive pharmacotherapy is closely linked to screening issues. The lack of motivation for early detection of carbohydrate metabolism disorders on part of healthcare providers leads to the lack of awareness on part of patients and results in noncompliance with prescribed medication therapy.

According to ADA standards of medical care (2019) [10, 11], the use of metformin, α-glucosidase inhibitors, orlistat, GLP-1 agonists, and thiazolidinediones helps to reduce the incidence of T2DM, but so far, prediabetes is not an approved indication for any of these drugs. The protocol of the SiMePred study intended to evaluate the efficacy of sitagliptin (a DPP-4 inhibitor) in preventing T2DM has already been published but the results of the study are not available yet [12]. ADA experts believe that metformin should be a preferred drug for secondary prevention of T2DM. For other drugs listed above, the risks and benefits should be thoroughly considered in each individual case [10]. However, IDF guidelines formulated in 2019 recommend both metformin and acarbose (an α-glucosidase inhibitor) for T2DM prevention in patients with early stages of carbohydrate metabolism disorders [13]. In Russia, information leaflets for metformin and acarbose list prediabetes as an indication for use [14, 15].

In 2005, the Diabetes mellitus state-funded program was launched in the Russian Federation under the nationwide Health project [16]. The key parameters it focused on were: life expectancy of patients with diabetes mellitus and the rate of complications in these patients, i.e. tertiary prevention. The existing electronic state registry of diabetes mellitus can also be regarded as a tool for tertiary prevention, but there is still a dearth of data on its long-term efficacy.

In our opinion, regular medical checkups and screening tests are the key measure for primary T2DM prevention [17]. Regular checkups help to identify risk factors for T2DM and subsequently take measures to reduce the contribution of modifiable risk factors to the development of the disease. Screening should be used both for regular checkups and in patients with identified risk factors. In screening tests, preanalytical errors are not rare, leading to the underdiagnosis of carbohydrate metabolism disorders. According to WHO report (2006), the whole blood sample collected from a patient

Table 1. Long-term outcomes in patients who had and had not been receiving preventive pharmacotherapy

Carbohydrate metabolism	Number of re-examined patients $n = 115$				χ^2	p
	Preventive pharmacotherapy $n = 30$		No preventive pharmacotherapy $n = 85$			
	abs.	%	abs.	%		
Normal	25	83.3	22	25.8	30.28	< 0.05
IFG	1	3.3	13	15.2	3.0	SI
IGT	4	13.3	17	20.0	0.66	SI
T2DM	0	0	33	38.8	16.3	< 0.01

Note: SI — statistically insignificant.

Table 2. Long-term results of OGTT in patients with different disorders of carbohydrate metabolism undergoing long-term preventive pharmacotherapy

OGTT results in 10 years	Initial condition of patients in the long-term pharmacotherapy group ($n = 30$)		χ^2	p
	IFG	IGT		
Normal	21	4	0.250	> 0.05
IFG	1	0	1	> 0.05
IGT	2	2	0.169	> 0.05
T2DM	0	0	–	–

Table 3. Long-term results of OGTT in patients with different disorders of carbohydrate metabolism who did not have long-term preventive pharmacotherapy

OGTT results in 10 years	Initial condition of patients in the group without preventive pharmacotherapy ($n = 85$)		χ^2 (with Yates' correction)	p
	IFG	IGT		
Normal	17 (20.0%)	5 (5.9%)	6.4	0.012
IFG	9 (10.5%)	4 (4.8%)	1.14	0.28
IGT	8 (9.4%)	9 (10.5%)	0.027	0.82
T2DM	10 (11.8%)	23 (27.1%)	8.6	0.004

should be placed in a blood collection tube containing a glycolysis inhibitor (collection tubes with gray caps) if immediate plasma separation is not possible. The collection tube should be kept on ice until plasma separation or the test itself. The cap color has been approved by the International Organization for Standardization (2000) [18].

Secondary prevention of T2DM includes early detection of the disease, as well as measures for slowing conversion of the initial pathology to T2DM. Secondary prevention is closely related to primary prevention: for patients with one or more risk factors for T2DM who have been covered by primary prevention, secondary prevention should consist in screening tests. Currently, there is no state-funded program on secondary prevention of T2DM (progression of prediabetes to diabetes) in Russia. Secondary prevention with pharmacotherapy has demonstrated its long-term efficacy both in this research work and in international studies [19, 20] and could be a cost-effective way of reducing the burden of early stage carbohydrate metabolism disorders and T2DM.

CONCLUSIONS

1. Currently, healthcare providers are not required to report patients with early disorders of carbohydrate metabolism; these patients are not followed up, which results in the underestimating the danger of IGT/IFG, delayed diagnosis of type 2 DM and poor adherence to treatment. 2. We have demonstrated that metformin can significantly delay progression to type 2 DM in the actual clinical setting. 3. Recommendation on active case-finding of IGT/IFG and early start of preventive pharmacotherapy should be included in the diagnostic algorithms and healthcare standards used in clinical routine. 4. In the absence of counterindications, all patients with early disorders of carbohydrate metabolism should be prescribed long-term medication therapy with metformin.

References

1. State Diabetes Register. Professional All-Russian Resource on Diabetes Nosology under the auspices of Endocrinology Research Center. Available from: http://diaregistry.ru/content/o-proekte.html#content. Verified on May 28, 2018. Russian.
2. Dedov II, Shestakova MV, editors. Algorithms of Specialized Medical Care for Diabetes Mellitus Patients. 9th ed. Moscow, 2019. Russian.
3. Dedov II, Shestakova MV, Galstyan GR. Prevalence of Type 2 Diabetes Mellitus in Adult Russian Population (NATION study). Diabetes Mellitus. 2016; 19 (2): 104–12. Russian.
4. Ametov AS. Saharnyj diabet 2-go tipa. Problemy i reshenija. M.: GEOTAR-Media, 2017; s. 125–144. Russian.
5. Barry E. Efficacy and effectiveness of screen and treat policies in prevention of type 2 diabetes: systematic review and meta-analysis of screening tests and interventions. BMJ. 2017 Jan 4; (356): i6538.
6. Ametov AS, Krivosheyeva AA. Prevention of type 2 diabetes mellitus. Endocrinology. 2017; (4): 14–25.
7. Chazova IE, Mychka VB, Belenkov YuN. Osnovnye rezul'taty Rossijskoj programmy ''APREL'' (jeffektivnost' primenenija akarbozy u pacientov s narushennoj tolerantnost'ju k gljukoze i arterial'noj gipertoniej). Consilium medicum. 2005; (2): 18–22. Russian.
8. Madsen KS, Chi Y, Metzendorf MI, Richter B, Hemmingsen B. Metformin for prevention or delay of type 2 diabetes mellitus and its associated complications in persons at increased risk for the development of type 2 diabetes mellitus. Cochrane Database of Systematic Reviews. 2019; (12): CD008558

9. Demidova IYu, Boeva VV. Early diagnosis and treatment of the initial stages of carbohydrate metabolism disorders. Bulletin of The Russian State Medical University. 2013; (1): 9–13.
10. Diabetes Care. 2019; 42 (Suppl. 1): 29–33.
11. Ametov AS, Krivosheyeva AA. Prospects of early pharmacological intervention at the stage of prediabetes. Endocrinology. 2018; 7 (3): 75–87.
12. Naidoo P, et al. Effect of Sitagliptin and Metformin on prediabetes progression to type 2 diabetes — a randomized, double-blind, double-arm, multicenter clinical trial: protocol for the sitagliptin and metformin in prediabetes (SiMePreD) study. JMIR Res Protoc. 2016; 5 (3): e145.
13. International Diabetes Federation. Clinical Practice Recommendations for managing Type 2 Diabetes in Primary Care, 2017.
14. Gosudarstvennyj reestr lekarstvennyh sredstv. Instrukcija po primeneniju lekarstvennogo preparata dlja medicinskogo primenenija gljukofazh, izmenenie # 4 k P N014600/01-140812 ot 6.07.2016 g. S. 3. Data pereoformlenija: 04.04.2018 g. Russian.
15. Gosudarstvennyj reestr lekarstvennyh sredstv. Instrukcija po medicinskomu primeneniju preparata gljukobaj. Registracionnyj nomer P N012033/01 ot 24.06.2005 g. S. 2. Data pereoformlenija: 24.08.2017 g. Russian.
16. Dedov II, Shestakova MV, redaktory. The results of the implementation of the “Diabetes mellitus” subprogram of the Federal target program “Prevention and Control of Socially Significant Diseases 2007–2012”. Diabetes; 2013; (2): 2–48.
17. Prikaz Minzdrava Rossii ot 3 dekabrja 2012 g. # 1006n. Available from: https://normativ.kontur.ru/document?moduleId=1&documentId=212999. Russian.
18. Dolgov VV, Selivanova AV, i dr. Laboratornaja diagnostika narushenij obmena uglevodov. Metabolicheskij sindrom. Saharnyj diabet. M.-Tver': Triada, 2006; 128 s. Russian.
19. Chiasson J-L, Josse RG, Gomis R, Hanefeld M, Karasik A, Laakso M, et al. Acarbose for prevention of type 2 diabetes mellitus: the STOP-NIDDM randomised trial. Lancet. 2002 Jun 15; 359 (9323): 2072–7.
20. Wenying Y, Lixiang L, Jinwu Q. The preventive effect of acarbose and metformin on the progression to diabetes mellitus in the IGT population: 3-year multicenter prospective study. Chin J Endocrin Metab. 2001; (17): 131–6.

Литература

1. Государственный регистр сахарного диабета. Профессиональный Всероссийский ресурс по нозологиям диабета под эгидой Эндокринологического Научного Центра. Доступно по ссылке: http://diaregistry.ru/content/o-proekte.html#content (проверено 28.05.18).
2. Дедов И. И., Шестакова М. В., редакторы. Алгоритмы специализированной медицинской помощи больным сахарным диабетом. 9-е изд. М., 2019.
3. Дедов И. И., Шестакова М. В., Галстян Г. Р. Распространенность сахарного диабета 2-го типа у взрослого населения России (исследование NATION). Сахарный диабет. 2016; 19 (2): 104–12.
4. Аметов А. С. Сахарный диабет 2-го типа. Проблемы и решения. М.: GEOTAR-Media, 2017; с. 125–44.
5. Barry E. Efficacy and effectiveness of screen and treat policies in prevention of type 2 diabetes: systematic review and meta-analysis of screening tests and interventions. BMJ. 2017 Jan 4; (356): i6538.
6. Аметов А. С., Кривошеева А. А. Профилактика развития сахарного диабета типа 2. Эндокринология. 2017; (4): 14–25.
7. Чазова И. Е., Мычка В. Б., Беленков Ю. Н. Основные результаты Российской программы АПРЕЛЬ (эффективность применения акарбозы у пациентов с нарушенной толерантностью к глюкозе и артериальной гипертонией). Consilium medicum. 2005; (2): 18–22.
8. Madsen KS, Chi Y, Metzendorf MI, Richter B, Hemmingsen B. Metformin for prevention or delay of type 2 diabetes mellitus and its associated complications in persons at increased risk for the development of type 2 diabetes mellitus. Cochrane Database of Systematic Reviews. 2019; (12): CD008558
9. Демидова И. Ю., Боева В. В. Ранняя диагностика и лечение начальных стадий нарушений углеводного обмена. Вестник Российского государственного медицинского университета. 2013; (1): 9–13.
10. Diabetes Care. 2019; 42 (Suppl. 1): 29–33.
11. Аметов А. С., Кривошеева А. А. Перспективы ранней фармакологической интервенции на этапе предиабета. Эндокринология. 2018; 7 (3): 75–87.
12. Naidoo P, et al. Effect of Sitagliptin and Metformin on prediabetes progression to type 2 diabetes — a randomized, double-blind, double-arm, multicenter clinical trial: protocol for the sitagliptin and metformin in prediabetes (SiMePreD) study. JMIR Res Protoc. 2016; 5 (3): e145.
13. International Diabetes Federation. Clinical Practice Recommendations for managing Type 2 Diabetes in Primary Care, 2017.
14. Государственный реестр лекарственных средств. Инструкция по применению лекарственного препарата для медицинского применения глюкофаж, изменение № 4 к П N014600/01-140812 от 6.07.2016 г. С. 3. Дата переоформления: 04.04.2018 г.
15. Государственный реестр лекарственных средств. Инструкция по медицинскому применению препарата глюкобай. Регистрационный номер П N012033/01 от 24.06.2005 г. С. 2. Дата переоформления: 24.08.2017 г.
16. Дедов И. И., Шестакова М. В., редакторы. Результаты реализации подпрограммы «Сахарный диабет» Федеральной целевой программы «Предупреждение и борьба с социально значимыми заболеваниями 2007–2012 годы». Сахарный диабет. 2013; (2): 2–48.
17. Приказ Минздрава России от 3 декабря 2012 г. № 1006н. Доступно по ссылке: https://normativ.kontur.ru/document?moduleId=1&documentId=212999.
18. Долгов В. В., Селиванова А. В. и др. Лабораторная диагностика нарушений обмена углеводов. Метаболический синдром. Сахарный диабет. М.-Тверь: Триада, 2006; 128 с.
19. Chiasson J-L, Josse RG, Gomis R, Hanefeld M, Karasik A, Laakso M, et al. Acarbose for prevention of type 2 diabetes mellitus: the STOP-NIDDM randomised trial. Lancet. 2002 Jun 15; 359 (9323): 2072–7.
20. Wenying Y, Lixiang L, Jinwu Q. The preventive effect of acarbose and metformin on the progression to diabetes mellitus in the IGT population: 3-year multicenter prospective study. Chin J Endocrin Metab. 2001; (17): 131–6.